Synthesis and Characterisation of Basic Magnesium Carbonate

by

Adelé Botha

submitted in partial fulfilment of the requirements for the degree

Philosophiae Doctor

Chemistry

in the Faculty of Natural and Agricultural Sciences

University of Pretoria

Pretoria

July 2002

Synthesis and Characterisation of Basic Magnesium Carbonate

by

Adelé Botha

submitted in partial fulfilment of the requirements for the degree

Philosophiae Doctor
Chemistry

in the Faculty of Natural and Agricultural Sciences
Department of Chemistry
University of Pretoria
Pretoria

July 2002

Supervisor: Professor C.A. Strydom

Abstract

Hydromagnesite, the most stable of the basic magnesium carbonates, can be obtained by mining or by synthesis. Existing synthetic procedures have certain drawbacks which include, undesirable environmental effluents or high pressure and/or temperature requirements. Due to the lack of information in the literature, the aim of this study was to develop a cost effective procedure for the synthesis of basic magnesium carbonate from $Mg(OH)_2$, not hampered by the above mentioned drawbacks.

Following an extensive investigation into various parameters that influenced the final product, a simple procedure, based on sparging CO_2 through a slurry of magnesium hydroxide in water until the pH reached 7.5–8.5, was developed. The solid portion of the slurry is dried at 80 or 120°C to deliver an unidentified basic magnesium carbonate

and hydromagnesite respectively. The products were characterised by XRD, TG-DTA, surface area determination, SEM and FT-IR. The rehydration characteristics of the products were also investigated. By combining the information obtained by each technique, valuable information could be obtained.

The synthesised products were evaluated for flame retardant application, due to the demand for mineral flame retardants which could compete with $Mg(OH)_2$ and $Al(OH)_3$. Compared to the traditionally used halogenated flame retardants, the mineral flame retardants deliver non-toxic, non-corrosive decomposition products and contributes in suppressing the emission of smoke in a fire. Results indicated that the basic magnesium carbonates compared favourably to $Mg(OH)_2$ and $Al(OH)_3$ and presented several advantages in terms of flame retardant applications. Further tests will be necessary to accurately assess the flame retardant effect of the basic magnesium carbonates. The possibilities however seem promising.

Sintese en Karakterisering van Basiese Magnesium Karbonaat

deur

Adelé Botha

voorgelê ter vervulling van 'n deel van die vereistes vir die graad

Philosophiae Doctor
Chemie

in die Fakulteit Natuur- en Landbouwetenskappe
Departement Chemie
Universiteit van Pretoria
Pretoria

Julie 2002

Promotor: Professor C.A. Strydom

Samevatting

Hidromagnesiet, die mees stabiele basiese magnesium karbonaat, kan of gemyn of gesintetiseer word. Bestaande sintetiese prosedures het spesifieke nadele, naamlik uitvloeisels wat nadelig is vir die omgewing of hoë druk en/of temperatuur vereistes. As gevolg van die tekort aan inligting in die literatuur, was die doel van die studie om 'n koste effektiewe prosedure te ontwikkel, vir die sintese van 'n basiese magnesium karbonaat vanaf $Mg(OH)_2$, wat nie aan die bogenoemde nadele onderhewig is nie.

Na 'n uitgebreide ondersoek van verskeie parameters wat die finale produk kan beinvloed, kon 'n eenvoudige prosedure, waar CO_2 deur 'n magnesium hidroksied suspensie in water geborrel word tot 'n pH van 7.5–8.5, voorgestel word. Die soliede deel van die suspensie is by 80 of 120°C gedroog om 'n onbekende basiese

magnesium karbonaat en hidromagnesiet respektiewelik te lewer. Die produkte is gekarakteriseer deur XRD, TG-DTA, oppervlakarea bepaling, SEM en FT-IR. Die rehidrasie karakteristieke van die produkte is ook ondersoek. Deur die inligting wat van die onderskeie tegnieke verkry is te kombineer, kon waardevolle inligting verkry word.

Die gesintetiseerde produkte is geëvalueer as vlamvertragers, as gevolg van die vraag na vlamvertragers wat op dieselfde vlak kan kompeteer as $Mg(OH)_2$ en $Al(OH)_3$. Vergeleke met die tradisionele halogeneerde vlamvertragers, lewer die minerale vlamvertragers nie-toksiese, nie-korrosiewe ontbindings produkte en dra by tot die onderdrukking van rookvorming in 'n vuur. Die resultate het aangetoon dat die basiese magnesium karbonate gunstig vergelyk met $Mg(OH)_2$ en $Al(OH)_3$ en dat dit verskeie voordele as vlamvertragers bied. Verdere toetse sal nodig wees om die vlamvertragings effek van die basiese magnesium karbonate akkuraat te evalueer. Die moontlikhede lyk egter belowend.

Acknowledgements

I would like to express my deepest gratitude towards the following people and institutions that contributed in making this study possible:

- To Him who has all the power to grant us more than we could ever ask for, unto Him the glory! Without the Lord our God, none of this would ever have been possible.

- I would like to sincerely thank my supervisor, Professor C.A. Strydom, for always willing to help where she could as well as giving valuable advice, support and encouragement. It was my privilege to be a part of her research group.

- My husband André deserves special recognition. Thank you for al the moral support, encouragement and patience that you've given me, as well as for proofreading my thesis and for fruitful discussions relating to my research.

- My parents for al their love, support and encouragement always. They contributed immensely in the success of my studies.

- NRF and the University of Pretoria for financial support.

- Liezel van der Merwe and Liana Swanepoel for their friendship, support and encouragement.

- Dr. Sabine Verryn for doing the XRD analysis and interpretation of the results.

- Linda Prinsloo for providing assistance with the FT-IR analyses and useful discussions.

- Alan Hall and Chris van der Merwe at the Lab for Microscopy and Micro-analysis at the University of Pretoria, for providing valuable assistance with the SEM analyses.

- Retha Bezuidenhout for providing me with the glassware and instruments I needed to conduct some of the experimental work.

- Professor W. Focke at the Institute of Applied Materials at the University of Pretoria, for providing valuable assistance with the compounding of the synthesised products into the EVA polymer and for useful discussions.

- Johan Labuschagne, a fellow-student at the Institute of Applied Materials at the University of Pretoria, for always willing to help and for fruitful discussions.

- Sandy Marais at the Rubber and Plastics division of the SABS, for conducting the LOI tests.

- My family and friends for their constant encouragement and support throughout my studies.

Table of contents

Chapter 1

Aim of the basic magnesium carbonate study

1.1 Introduction

There is a continued interest in the development of new procedures of synthesis for various commercially available products. By developing new synthesis procedures for existing commercial products, new applications are created for the starting materials that may be used for the synthesis, that formerly only had limited application. Existing procedures of synthesis for a specific product differ with respect to the starting materials that are required as well as the experimental parameters that needs to be employed to obtain the required product. When a new starting material is to be used for the synthesis of a product, it becomes necessary for development of a new procedure that is optimised specifically for the starting material used.

The basic magnesium carbonates can either be mined as the mineral or it can be manufactured synthetically. The purity of the naturally occurring basic magnesium carbonates are quite variable. The disadvantages associated with the mined mineral, is the large range of additional minerals that occurs with it in certain instances. This results in a need for various separation procedures to isolate the required product. Selective mining practices can produce a relatively good quality of industrial-grade basic magnesium carbonate. The cost of mining the product as well as a possible complicated separation process, could result in a costly procedure that might reduce the viability of the procedure. In addition to this, the problem exists that the purity of the mined product could still be insufficient.

A synthetically manufactured basic magnesium carbonate, presents the possibility of obtaining a relatively pure compound that complies to the set requirements since experimental conditions are controllable. It is important in this instance that the starting material be of high purity to prevent unnecessary side reactions taking place. Variations in the experimental conditions could result in various phases of the basic magnesium carbonate being obtained. It is necessary to characterise the products obtained to determine the success rate of the attempted procedures. When the

required product is finally obtained and possibly other phases thereof as well, it is necessary to fully characterise their physical and chemical properties. Characterisation presents valuable information relating to the possible application of the respective obtained products.

The primary aim of this study was the synthesis of a basic magnesium carbonate via a newly developed procedure, using a starting material not commonly used and optimising the experimental parameters for this starting material. The various products that were obtained were characterised by various techniques, in order to identify the chemical and physical characteristics of each. As a secondary objective to this study, the newly synthesised products' flame retardant efficiency was compared to well known flame retardants.

1.2 $MgO\text{-}CO_2\text{-}H_2O$ system

Chemical reactions in the system $MgO\text{-}CO_2\text{-}H_2O$ result in a series of normal carbonates which include the following mineral species: magnesite, barringtonite, nesquehonite and lansfordite. These reactions also produce a series of basic, i.e. hydroxyl-containing magnesium carbonates having the general formula $xMgCO_3 \cdot yMg(OH)_2 \cdot zH_2O$ (Jackson *et al.*, 1995). This basic carbonate series includes: artinite, dypingite, giorgiosite, hydromagnesite, pokrovskite and an unnamed octahydrate. The molecular composition of these minerals are summarised (Jackson *et al.*, 1995; Gaines *et al.*, 1997) in Table 1.1.

Table 1.1 Summary of the normal and basic magnesium carbonates and their molecular formula

Mineral	Molecular formula
Normal magnesium carbonates :	
Magnesite	$MgCO_3$
Barringtonite	$MgCO_3 \cdot 2H_2O$
Nesquehonite	$MgCO_3 \cdot 3H_2O$
Lansfordite	$MgCO_3 \cdot 5H_2O$
Basic magnesium carbonates :	
Artinite	$Mg_2(CO_3)(OH)_2 \cdot 3H_2O$
Dypingite	$Mg_5(CO_3)_4(OH)_2 \cdot 5H_2O$
Giorgiosite	$Mg_5(CO_3)_4(OH)_2 \cdot 6H_2O$
Hydromagnesite	$Mg_5(CO_3)_4(OH)_2 \cdot 4H_2O$
Pokrovskite	$Mg_2(CO_3)(OH)_2 \cdot 0.5H_2O$
Unnamed octahydrate	$Mg_5(CO_3)_4(OH)_2 \cdot 8H_2O$

Hydromagnesite is the most stable of the basic carbonates at ambient temperatures, usual humidities and ambient partial pressures of CO_2.

Only two of the basic magnesium carbonates that have been described in literature are of geologic importance. These are the minerals hydromagnesite and artinite. The absence of other similar species in natural environments strongly suggests that they are unstable (Langmuir, 1965).

1.3 Properties of the magnesium carbonates

The physical properties of the normal magnesium carbonates are given in Table 1.2, and in Table 1.3 for the basic magnesium carbonates.

Table 1.2 Physical properties of the normal magnesium carbonates (Jackson *et al.*, 1995)

Parameter	Magnesite	Barringtonite	Nesquehonite	Lansfordite
mol wt	84.32	120.35	138.37	174.4
crystal system	hexagonal	triclinic	monoclinic	monoclinic
space group	R3c		$P2_1/n$	$P2_1/n$
lattice constants, nm				
a	0.46332	0.9115	1.2112	
b		0.6202	0.539	
c	1.5015	0.6092	0.77697	
angle, degree				
α		94.00		
β		95.53	90.42	
γ		108.87		
Z	6	4	4	
density, calculated, g/cm^3	3.009	2.825	1.837	1.730
hardness, Mohs'	3.5–5.0		2.5	2.5
color	white	colorless	colorless to white	white
melting point, °C	402–480			
index of refraction	1.510, 1.700	1.458, 1.473, 1.501	1.412, 1.501, 1.526	1.456, 1.476, 1.502
heat of formation, ΔH_{298}, kJ/mol	–1095.8			
free energy of formation, ΔG_{298}, kJ/mol	–1012.1		–1726.3	–2199.5

Table 1.3 Physical properties of the basic magnesium carbonates (Jackson *et al.*, 1995)

Parameter	Artinite	Hydromagnesite	Dypingite	Octahydrate
mol wt	196.70	467.67	485.69	539.74
crystal system	monoclinic	monoclinic	monoclinic	
space group	C_2 or C_2/M	$P2_1/C$		
lattice constants, nm				
a	1.656	1.011		
b	0.315	0.894		
c	0.622	0.838		
angle, β degree	99.15	114.58		
Z	2	2		
density, calculated, g/cm^3	2.039	2.254		
hardness, Mohs'	2.5	3.5		
color	white	white	white	white to gray
index of refraction	1.488, 1.534, 1.556	1.458, 1.473, 1.501	1.412, 1.501, 1.526	1.456, 1.476, 1.502

The relatively high solubility of magnesium bicarbonate, $Mg(HCO_3)_2$, at low temperature and high partial pressures of CO_2 permits the separation of magnesium compounds from impurities. Normal, hydrated and the basic magnesium carbonates react with acids to yield salts which can be recovered by crystallisation.

1.4 Occurrence of hydromagnesite

Hydromagnesite occurs widespread in nature, sometimes in deposits having economic significance, as an alteration of serpentine or other magnesian rocks. It is found in veinlets in serpentines and altered magnesium-rich rocks with opal, calcite, dolomite, magnesite, artinite, deweylite and pyroaurite. Hydromagnesite occurs in old chrome mines (e.g. Wood's mine, near the town of Texas and Cedar Hill quarry, State Line district southern Lancaster County, Pennsylvania); in serpentine rock (e.g. Sulfur Creek area, Colusa Co., and at New Idria district, California); with magnesite (e.g. in valley bottoms in the Caribou, Atlin and Kamloops districts, Canada); as an alteration product of brucite in marble-serpentinites (e.g. Kraubat, Styria, Austria); in chromite mines in Serbia; as the alteration product in the periclase marbles (e.g. Predazzo, southern Tyrol

and Viu, Lombardy, Italy) (Gaines *et al.*, 1997).

Hydromagnesite is also found in caves as a very unusual cave formation called "bubbles" (Figure 1.1). The bubbles look like chewing gum bubbles and are caused by magnesium rich fluids being forced into the opening of the cave and encountering a viscous film that is pushed outward forming the bubble. The film is a plastic-like, carbonaceous liquid called "moonmilk" that when it eventually dries will crack open and reveal the hydromagnesite precipitate within (http://mineral.galleries.com).

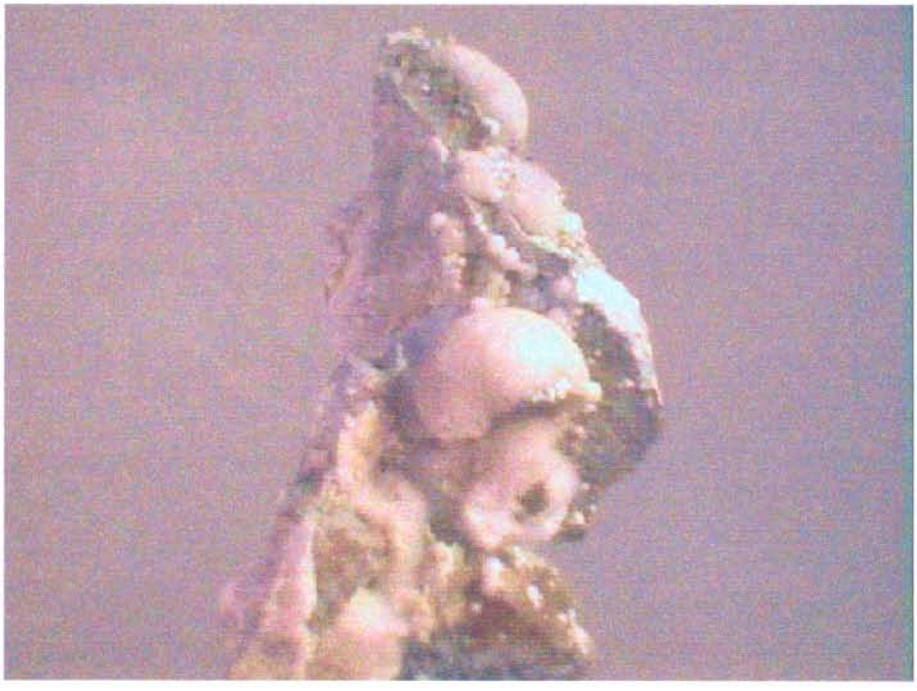

Figure 1.1 Hydromagnesite "bubbles" in caves

The physical characteristics of hydromagnesite (Roberts *et al.*, 1990) are:

Cleavage: {010} perfect. Brittle.
Habit: Crystals acicular or bladed, elongated along c-axis and flattened on {100}. Large crystals vertically striated on {100} by repetition of {110} and {100} forms. As sprays, rosettes or crusts. Also massive, powdery or chalklike. Twinning on {100} very common. Also found as concretions and encrustations.

Colour-luster: Colourless, white. Transparent. Crystals vitreous. Aggregates pearly, silky or dull.

Other characteristics: Fluorescent green in shortwave UV and bluish white in longwave UV light.

1.5 Uses of basic magnesium carbonate

Two forms of magnesium carbonate are essentially used - light and heavy - the difference being the number of water molecules that are included in the compound. Light magnesium carbonate has the empirical formula $Mg_5(CO_3)_4(OH)_2 \cdot 4H_2O$ and heavy magnesium carbonate $Mg_5(CO_3)_4(OH)_2 \cdot 5H_2O$. The light and heavy magnesium carbonates are hydrated basic magnesium carbonates containing the equivalent of 40 to 45% of MgO. Magnesium carbonate (US Pharmacopeia [USP]) is a basic hydrated magnesium carbonate or a normal hydrated magnesium carbonate containing the equivalent of 40.0 to 43.5% of MgO (Reynolds *et al.*, 1993).

The magnesium carbonates have various applications. USP-grade magnesium carbonate is used as an inert vehicle and an adsorbent, in pharmaceuticals. Heavy magnesium carbonate is used in concentrations up to 45% in tablets as an inert material to aid in drug delivery. Light magnesium carbonate can be used in concentrations of 0.5 to 1.0% as a liquid absorbent, particularly for flavourings in tablets. One of its most visible uses is as an antacid (Kramer, 1998). Magnesium carbonate is also the preferred starting material in the preparation of magnesium citrate solutions and of the purer grades of magnesium salts.

Magnesium carbonate is also used in cosmetic manufacturing. Due to its fine texture and high absorbency, light magnesium carbonate is an excellent carrier and retainer of perfumes. It can also be added to loose powders to provide fluffiness. In most cases it is blended with talc in quantities from 1–5%. The USP-grade of magnesium carbonate is used as an additive to table salt to keep it free flowing and to avoid caking in the containers.

Magnesium carbonate is used in the rubber industry as a reinforcing agent. It is also used as a smoke suppressant in rubber and some plastic compounds to replace some of the alumina trihydrate that is traditionally used. Replacing approximately 12.5% of the alumina trihydrate with magnesium carbonate, increases the quantity of char that

is formed in a fire. It also decreases the rate of flame spreading and the quantity of smoke generated (Kramer, 1998). Technical grades of magnesium carbonate find use in the manufacturing of flooring and polishing compositions and as fillers for paper, plastics, paints and varnishes. A large portion of the production of basic magnesium carbonate goes into the manufacture of heat-insulating compositions (Gloss, 1952).

Magnesium carbonate also finds use as an extender for titanium dioxide in paint, in lithographing inks and as a precursor for other magnesium-based chemicals. The basic magnesium carbonates are calcined to produce magnesia having surface areas of ~200 $m^2 g^{-1}$. These high surface area magnesias are used as thickening agents in the sheet molding of rubber and as scorch retarders in chloroprene rubbers (Jackson *et al.*, 1995).

1.6 Basic magnesium carbonate as flame retardant

Polymeric materials have entered almost every part of our daily life. Fire resistance of these materials is an extremely important subject, as most commercial plastics burn fairly easily even under moderate conditions. Therefore it's common practice to use flame retardants for improving the fire resistance performance and reducing the tendency for smoke emission. A variety of different flame retardants are available on the market for various applications. The addition of a few percent of the traditionally organic flame retardants, containing elements such as chlorine, bromine, phosphorus, nitrogen and antimony, is sufficient to improve the fire retardancy behaviour significantly. Although they are very effective, some of them cause serious trouble in case of a fire. The combination of, for instance, halogen and antimony oxide has come under certain pressure due to environmental issues such as the evolution of smoke and toxic gases. The threat from toxic flame retardants is becoming an increasingly debated subject. Toxic and bioaccumulative flame retardants, which are widely used in electronic equipment and other manufacturing processes, have been reported to enter the marine food chain and were accumulating in deep sea whales (Jones, 1998). The need for environmentally safe flame retardants is evident.

The metal hydroxides have been established to substitute critical organic flame retardants in applications where human life is directly threatened in a fire. The halogen- and acid-free character of these substances in combination with halogen-free plastics is promoting the trend to use environmentally benign products.

Magnesium hydroxide, aluminium hydroxide, huntite/hydromagnesite and hydromagnesite (alone) present safer alternatives for application as flame retardants, since they don't evolve toxic or corrosive gases as well as suppressing the emission of smoke. The relatively high processing temperatures that are used in certain instances for polymer processing, necessitates the use of flame retardants with a high thermal stability. The use of aluminium hydroxide is limited by its relatively low decomposition temperature. Magnesium hydroxide presents an alternative for polymers processed at high temperatures.

It is evident that there is a need for a mineral flame retardant with a higher thermal stability than aluminium hydroxide and which could compete at the level of magnesium hydroxide, but being more cost-effective. This reasoning supports the decision to evaluate the flame retardant characteristics of the basic magnesium carbonate products that were synthesised in this study.

Chapter 2

Theoretical background on flame retardants

2.1 Introduction

Despite extensive fire precaution regulations for buildings, transportation, electrical engineering, etc., fires still occur frequently all over the world. Fires cause huge monetary losses for the economy and loss of life. In our daily life we are increasingly surrounded by non-flame retarded plastics. The importance of additional chemical protection that can contribute to fire prevention is thus evident. The use of synthetic polymers has grown dramatically and along with it, growth in the use of flame retardants of all types.

The aim of this chapter is to highlight the aspects relating to the use of flame retardants. The range of flame retardants available is quite extensive, although there are certain risks associated with the use of some flame retardants. It will be shown that mineral flame retardants present several advantages in terms of smoke generation, toxicity and environmental aspects, compared to the traditionally used halogenated flame retardants.

The fact that all organic materials will burn is a given. The extent and rate of combustion is a function of the composition, density and configuration of the materials, as well as of the intensity and duration of the ignition source. The oxidant concentration of the surrounding atmosphere also determines the combustibility of the materials involved.

A variety of adjectives are used to describe a product that has an apparent low contribution to a fire. Terms such as fireproof, flameproof, self-extinguishing, non-burning and noncombustible are just a few of the nonquantitative words that exist. This results in a lot of confusion regarding the relative fire safety of different materials. A clear definition regarding the term “flame retardant (FR)” is thus required.

Flame retardation is a process by which the normal degradation or combustion processes of polymers have been altered by the addition of certain chemicals. The polymers will thus exhibit resistance to decomposition by thermal stress when measured by standard tests. A *fire-retardant chemical* is a compound or a mixture of compounds that, when added to or incorporated chemically into a polymer, serves to slow or hinder the ignition or growth of fire. A *flame-retarded material* can thus be formulated to be more resistant to ignition than non-flame-retarded materials, or to have slower rates of flame spread in a major fire that is initiated by some other source. It is however important to note that the flame retarded article will ultimately burn (Sutker, 1988; Gann, 1993).

2.2 Components of combustibility

In order to understand polymer combustibility as a whole, it is necessary to understand the component of combustion. Fires can usually be depicted as having five components or phases. The components are:

1. Ignition
2. Fire growth
3. Full fire (steady state)
4. Smoke and toxic gases
5. Extinction/suppression

A brief description of each component and the means to minimise it (Petrella, 1992) follows. The time-temperature profile of a fire is depicted in Figure 2.1.

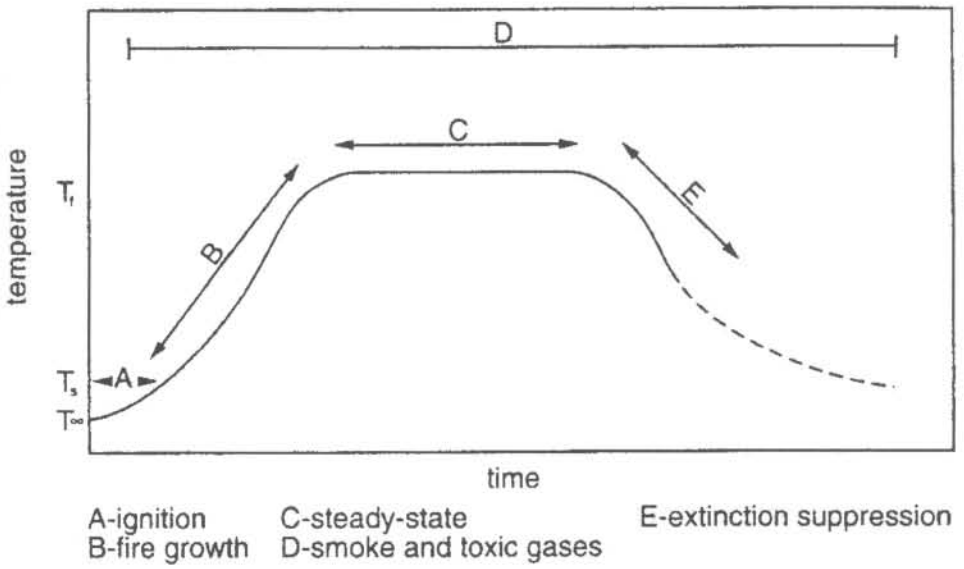

Figure 2.1 A generalised time-temperature profile of a fire (Petrella, 1992)

2.2.1 Ignition

Sources of ignition may be as insidious as slow-oxidation of oily rags or as violent as a gas explosion. Ignition is usually controlled by increasing the rate at which heat is dissipated away from the source of ignition at the polymer surface. The so-called heat sink FR's, such as alumina trihydrate (ATH), calcium carbonate and magnesium hydroxide function best during the ignition phase of combustion. These materials decompose endothermically to water or CO_2, thereby dissipating heat that would otherwise raise the temperature of the polymer surface to its ignition point (T_s).

2.2.2 Fire growth

Fire growth begins at relatively low temperatures (200–400°C) and reaches the temperatures at which steady-state full combustion dominates (800–1900°C) quickly, if unsuppressed. At this stage a fire grows from the point of initial ignition to rapidly engulf the whole surface of the fuel. FR's are most effective in suppressing a fire during this stage. This is especially true of halogenated FR's.

2.2.3 Full fire (steady state)

This stage defines the rate at which a full-scale fire consumes fuel to release heat, combustion gases and smoke at the maximum rate. This is the stage at which flash-over occurs, in confined spaces. A fire spends most of its life in this stage. FR's are least effective at this stage of a fire, because heat and reactive species are being released at the maximum rate. When exposed to the high temperatures or heat fluxes, many FR agents actually add to the burning rate and intensity of a fire.

2.2.4 Smoke and toxic gases

The combination of smoke and toxic gases accounts for a large number of fire deaths. Increased toxic gas levels (primarily carbon monoxide), usually accompanies increased smoke. As a rule, FR agents tend to increase the levels of smoke produced in a fire. The gaseous products of combustion can also be affected by the presence of FR's, as the latter tend to inhibit the combustion process. The result is that the intermediate products of combustion (smoke, CO and oxygenated species such as aldehydes and ketones) are produced in larger amounts.

2.2.5 Extinction / suppression

Extinction marks the natural end of a fire due to the unavailability of fuel or air (usually fuel). Suppression is the cessation of a flame due to external factors (i.e. water, FR agent and loss of air) while a sufficiency of fuel is still available. FR's act to suppress a flame by changing the chemistry of the flame through modification of the flame process by chemical and/or physical means.

All fires proceed through the various stages described above. The relative time/temperature values for each component in a particular fire are influenced by a number of factors, including the chemical and physical nature of the substrate and the presence of FR's.

2.3 Model for polymer combustion

The combustion of a solid polymer is a complicated phenomenon involving chemical kinetics, heat and mass transfer and fluid flow. Figure 2.2 depicts a simple model for polymer combustion.

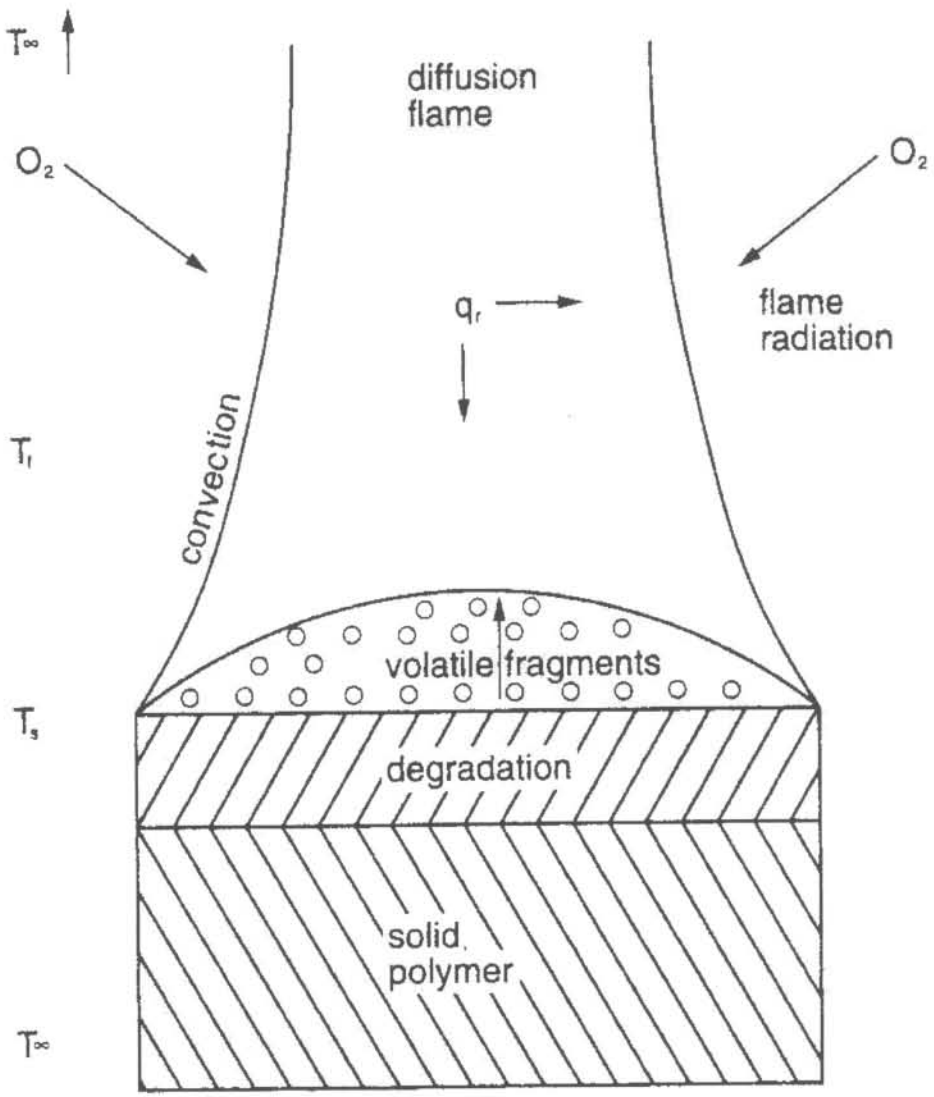

Figure 2.2 Model for polymer combustion (Petrella, 1992)

The model involves (Petrella, 1992):

1. Degradation of fuel to volatile species which diffuse away from the surface as heat from the ignition source is absorbed.

2. Oxygen diffuses toward the fuel surface and volatiles diffuses away from it. The diffusion flame is established at a fuel/oxygen ratio of about 1. For the flame to stabilise and continue existence, fuel and oxygen must be supplied continually.

3. Heat of combustion of the polymer is released in and near the diffusion flame. The actual flame is not in contact with the pyrolysing surfaces, but hovers above it, approaching closest to the surface at its edges. The radiation from the flame impinges on the fuel surfaces and causes further degradation which perpetuates the flame. Once the flame is established, it will continue to burn as long as fuel and air are available. The speed and severity with which the fire will continue to burn is determined by the availability of fuel and air.

Polymeric combustion is by and large a heterogeneous degradation process followed immediately (in both time and distance) by a rapid series of homogeneous processes resulting in the production of heat and light.

The combustion of a polymeric material can also be visualised as seen in Figure 2.3. This schematic simply shows the major features of Figure 2.2. The flame front has been removed from the pyrolysing fuel to show the temperature and species profile in greater detail. This figure can be thought of as the previous figure rotated 90°.

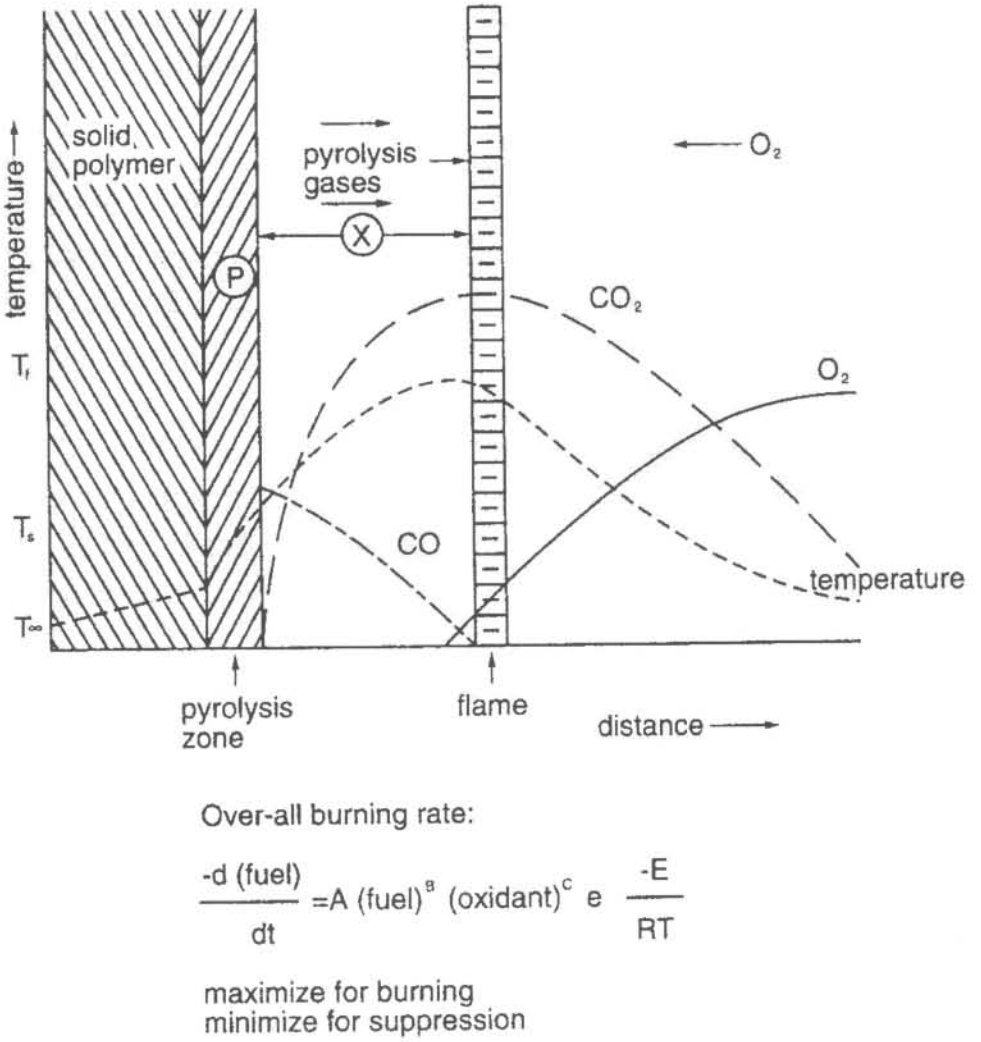

Figure 2.3 Combustion of polymeric materials (Petrella, 1992)

Figure 2.3 shows that the temperature of the solid polymer increases from ambient (for thick fuel beds) or near-ambient (for thin fuel beds) to the decomposition temperature of the particular fuel as the surface is approached. The temperature increases rapidly in this pyrolytic zone until the surface burning (T_s) temperature is attained. The major degradation of the polymer occurs in this zone. The fuel-rich pyrolytic gases diffuse toward the flame front where they are admixed with increasing amounts of oxygen from the ambient atmosphere. Air is entrapped into the combustion zone by the buoyancy and convection currents resulting from the flame. At some point, the appropriate

combination of fuel gases, air and temperature causes the flame to be established at a short distance above the fuel surface. The flame front oscillates back and forth above the surface until a quasisteady state is achieved.

The maximum temperature is reached just inside of the visible flame (T_F). The oxidation of CO to CO_2 (via the hydroxyl [OH] radical) is minimal at the surface and only becomes significant as the flame front is approached, since little oxygen penetrates the flame front. Figure 2.3 also shows that as the species diffuse away from the flame front into the ambient atmosphere, their concentration and temperature decrease.

The zone in which halogen FR's function, is indicated by the (X), between the pyrolysing polymer surface and the flame front, in Figure 2.3. Halogen flame retardants are most effective in the gas phase. Phosphorus or boron-based FR's function best in the condensed phase in the pyrolysis zone as indicated by the (P) in Figure 2.3.

From a heuristic point of view the over-all burning rate of a polymeric system can be expressed by the equation below Figure 2.3. Factors which maximise the right-hand side of the equation increase the burning rate, while the factors which minimises the right-hand side suppress combustion. The equation indicates that combustion can be controlled by (Petrella, 1992):

1. Changing the amount of fuel sustaining the flame.
2. Varying the amount of air reaching the flame.
3. Changing the relative values of diffusion and heat of combustion.
4. Modifying the activation energy for the over-all combustion process.

FR's are generally thought to operate via steps 1, 2 and 3. Water and CO_2 fire extinguishers operate by steps 2 and 4.

2.4 The role of flame retardants

The materials of attention in promoting fire safety are generally organic polymers, both natural (e.g. wood and wool) and synthetic (e.g. nylon, vinyl and rubber). Less fire prone products generally have either inherently more stable polymeric structures or fire-retardant additives (Gann, 1993). Flame retardancy can be imparted to plastics by incorporating elements such as bromine, chlorine, antimony, tin, molybdenum, phosphorus, aluminium and magnesium, either during the manufacture or when the plastics are compounded into some useful product (Touval, 1993). The type and amount of FR added to a particular substrate is largely determined by the degradation chemistry and high-temperature melt-flow properties of the substrate. FR's generally effect either lower ignition susceptibility or, once ignited, lower flammability.

A basic understanding of the different theories by which FR's function is essential for identifying and selecting the optimum material for any given situation. FR's function by their interaction or interference with one of the three required components of a fire (Sutker, 1988):

1. A combustible substance or fuel
2. Heat, supplied either externally or from the combustion process itself
3. An oxidising gas, primarily oxygen

There are several mechanistic descriptions by which FR's modify flammability. Each FR actually functions by a combination of mechanisms.

2.4.1 Dilution

Reducing the total quantity of combustible matter improves overall flame retardation. For example, adding fillers, such as clays, to polymer systems (often 50–200 parts by weight per 100 parts of polymer) reduces flammability. In some cases however, such as glass fiber reinforced composites, the glass fiber stiffens the polymer. On exposure to heat or a flame, the glass may prevent the polymer from melting away from the flame; thus, the material burns. In addition, the glass can act as a heat sink so that less energy input is required to ignite the polymer on a second exposure to heat. The FR thus acts as a thermal sink, increasing the heat capacity of the polymer or reducing the fuel content to a level below the lower limit of flammability.

2.4.2 Generation of noncombustible gases

When heated, some materials decompose to generate noncombustible gases. These gases lower the oxygen concentration at the front of the flame and often result in flame snuffing because of lack of oxygen. This result is transitory because once the material decomposes the residual matter acts as an incombustible diluent of the polymer matrix. An example of this type of FR is calcium carbonate which decomposes at 825°C to generate the solid, calcium oxide and the gas, carbon dioxide (Sutker, 1988). These products do not support combustion.

Some materials decompose to produce water vapour as the noncombustible gas. Heat is absorbed because of decomposition as well as vaporisation of liquid water. Aluminium oxide trihydrate ($Al_2O_3 \cdot 3H_2O$) begins decomposition at 230°C with the release of 34.5 wt% of its original mass as water vapour. Magnesium hydroxide begins decomposition at 340°C with the release of 31 wt% of the original mass as water. For processing polymers at elevated temperatures, the higher decomposition temperature of magnesium hydroxide makes it preferable to hydrated alumina. Typically, 50–100 parts by weight of these compounds are required per 100 parts of polymer to achieve flame retardation (Sutker, 1988).

Azo compounds are used in forming foam polymer systems. These materials liberate nitrogen . Although effective in producing foams, their cost effectiveness compared to that of other compositions has eliminated their use as FR's.

2.4.3 Gas-phase, free-radical inhibition

Combustion of hydrocarbons creates highly active fragments in the solid or condensed phase. These fragments vaporise, react with oxygen and form free radicals. Free-radical formation is highly exothermic resulting in volatilisation of additional active fragments from the condensed phase. The process continues unless free-radical formation is interrupted and stable species are produced. Some of the reactions that may occur are as follows (Sutker, 1988):

$$HO\cdot + CO \rightarrow CO_2 + H\cdot \qquad \text{Highly exothermic}$$

$$H\cdot + O_2 \rightarrow HO\cdot + O\cdot \qquad \text{Chain branching}$$

$O\cdot + HBr \rightarrow HO\cdot + Br\cdot$ Chain transfer

$HO\cdot + HBr \rightarrow H_2O + Br\cdot$ Chain termination

The HBr from decomposing brominated compounds is very effective in deactivating free radicals in the vapour phase. The FR dissociates into radical species that compete with chain propagating and branching steps in the combustion process. The formation of new radicals is also reduced as less heat is generated and the entire combustion process is slowed. Chlorinated compounds function in the same manner. Compounds containing iodine are known, but are of limited use as FR's because of their poor thermal stability. Fluorine containing compounds generally exist as functional polymers instead of as materials added to other polymeric systems to provide flame retardation. These polymers are very stable and decompose only at a high temperature.

Antimony oxide (Sb_2O_3) is generally used as a synergist in conjunction with halogen FR's. Antimony oxide reacts with the halogen to form antimony oxyhalides which then re-release halogen to the flame.

The efficiency of the halogens can also be enhanced by the addition of inorganic FR's, resulting in the overall reduction of FR additive package and minimising the adverse effects of the retardants.

The effectiveness of halogens in inhibiting radical formation is often a function of the organic structure to which it is attached. Typically, halogenated compounds used in applications of FR's contain either 40–70 wt% chlorine or 45–80 wt% bromine. From 20–40 parts of chlorinated compound or 5–30 parts of brominated compound would be used per 100 parts of polymer, depending on the FR requirements. Antimony oxide use is typically 25–50% that of the halogenated material (Sutker, 1988).

There is no doubt that halogenated systems make the ignition of plastics more difficult and they slow down the propagation of a fire. The high level of activity allows these additives to be used at relatively low loadings, translating to a greater retention of the physical properties of the base polymer. In the case of a fire, halogenated systems used in combination with antimony trioxide have serious drawbacks. The breakdown products of the initiated uncomplete combustion lead to an increase in smoke density which is more toxic and corrosive. The incomplete burned substances that are produced include black smoke (soot particles) and toxic CO. The presence of CO

disturbs the body's respiration process immediately as it blocks the oxygen transport of the blood.

Besides CO formation, halogens may support the formation of other highly toxic substances such as dioxins and furans in fire conditions. These compounds, in most cases, do not directly kill people, but it is time consuming and expensive to get buildings cleaned and decontaminated from such substances after a fire. The acids formed in a fire with halogen containing FR's or with halogen containing polymers like PVC can cause secondary damage to electronic equipment, which may be much more severe than the damage by the fire itself (Weber, 2000).

2.4.4 Solid-phase char formation

Several different types of FR's form insulating or minimally combustible chars on polymer surfaces exposed to external heat sources. This char reduces volatilisation of active fragments and absorbs and dissipates heat. The effectiveness of the FR is specific for each polymer.

In the presence of heat and oxygen, phosphorus compounds decompose to form water vapour and phosphorus oxides. The phosphorus oxides subsequently react with the polymer matrix and dehydrate it, reforming phosphoric acids. These acids again decompose to form water vapour and phosphorus oxides. Ultimately as the water available from normal combustion of hydrocarbons diminishes, the phosphorus oxides react with hydrocarbon fragments to produce a very high melting point char at the interface between the polymer and the heat source. The chars, which contain phosphorus, rapidly dissipate heat energy and lose their "glow". This antiglow property of phosphorus contributes to its effectiveness as a FR. Typically, 1–10 parts of contained phosphorus is used per 100 parts of polymer.

2.4.5 Thermal quenching

Endothermic degradation of the FR results in thermal quenching. The polymer surface temperature is lowered and the rate of pyrolysis is decreased. Metal hydroxides and carbonates act in this way (Pettigrew, 1993).

2.5 Smoke

Smoke is the result of incomplete combustion of organic materials. It is a dispersion of the liquids and solids carried aloft by the convection currents of the gaseous combustible products and unreacted air in the fire. The composition of the constituents of smoke varies from material to material. The composition of the smoke from a given material also varies as the fire progresses. The composition is a sensitive function of the heat flux from the flame to the surface, the aspiration rate of the fire and the chemical composition of the fuel. Smoke is first produced just after ignition and continues to be produced after the visible flame ceases to exist.

The liquid portion of the smoke consists primarily of partially oxygenated combustion products (e.g. alcohols, aldehydes and ketones and organic acids). The liquid portion of the smoke is responsible for its toxic and corrosive nature. The solid components of smoke are ash, inorganic salts and solid carbonaceous particles which condense to form soot. Carbon monoxide and hydrogen cyanide (when nitrogen-containing materials are burned) are not components of smoke. They are though among the combustion gases which carry the smoke aloft and are very toxic (Petrella, 1992).

Dense, black smoke hinders vision and prevents people escaping from a fire, especially in unfamiliar surroundings. FR's that interfere with the normal combustion process change the rate of smoke evolution and the amount and composition of the smoke. Smoke is formed of relatively large carbon-rich particles which issue from polycyclic aromatic hydrocarbons. First, nuclei are formed, which grow and then agglomerate to give smoke. Its suppression can be due to (Delfosse *et al.*, 1989) either:

- the formation of products of more complete oxidation, leading to CO, CO_2 and H_2O,
- or to a decrease of the number of nuclei,
- or to the hindrance of agglomeration.

It has been suggested that halogen compounds promote formation of polycyclic aromatic hydrocarbons and hence smoke nuclei, thus increasing smoke and soot yields (Hornsby and Watson, 1986). Actually, much of the smoke is produced because the fuel is already in the gas phase and the combustion process is interrupted by the halogen scavengers that removes fuel from the burning process leaving the carbon products suspended in the gas phase.

It has been shown that the addition of ATH, magnesium hydroxide (Hornsby and Watson, 1986) and huntite/hydromagnesite (Kirschbaum, 1999) as FR's to polymers, contributes in reducing smoke generation. Less smoke allows individuals more time to safely exit from confined areas.

The smoke inhibition effect of the mineral FR's is attributed to the catalytic properties of the oxides, upon the oxidation of the char residue. Mineral FR's are active smoke suppressants because of the large activated surface areas of the oxides created during the decomposition reaction. Such materials will readily adsorb many species. Considerable quantities of carbon are deposited on residual ash during combustion of polymers. This subsequently volatilises on exposure to oxygen (Hornsby and Watson, 1990). The appearance of incandescence is an obvious result of this more complete oxidation. Thus production of more degraded oxidation products decreases the amount of smoke precursors (Delfosse *et al.*, 1989).

It is thus evident that the mineral FR's present a viable solution in contributing to a decrease in the evolution of smoke in a fire.

2.6 Mineral flame retardants

The disadvantages associated with halogenated FR's, can be reduced or overcome by using the mineral flame retardants aluminium hydroxide or magnesium hydroxide. The mineral FR's are usually used alone because they are not synergistic with the halogens. These compounds act both in the condensed and gas phase as FR's. The FR effect of ATH and magnesium hydroxide is based on the endothermic decomposition into aluminium (magnesium) oxide and water. During decomposition, considerable quantities of heat are consumed and hence withdrawn from the combustion, contributing in retarding the rate of thermal degradation.

$$2\ Al(OH)_3 \xrightarrow{> 200^\circ C} Al_2O_3 + 3\ H_2O \qquad 1051\ J.g^{-1} \tag{2.1}$$

$$Mg(OH)_2 \xrightarrow{> 340^\circ C} MgO + H_2O \qquad 1316\ J.g^{-1} \tag{2.2}$$

Only non-toxic and non-corrosive decomposition products are formed during this process. As a result, the plastic is protected from a rapid thermal decomposition and the formation of combustible breakdown products is inhibited. The water vapour which is formed displaces the oxygen (thus diluting the fuel supply present in the gas phase) and functions as a protective gas. The heat capacities of the FR additives and inert decomposition products further reduce the thermal energy available to degrade the substrate. A heat resistant covering layer is formed on the surface of the plastic, consisting of carbonised products and aluminium (magnesium) oxide. This inhibits further combustion. This ceramic layer also reduces smoke density by adsorbing soot particles (Weber, 2000).

ATH starts decomposition at about 200°C and can be used in all kinds of polymers that are processed at temperatures at these levels. At higher processing temperatures, ATH becomes impractical due to problems of premature decomposition. For polymers which are processed at higher temperature levels, magnesium hydroxide can be used. Magnesium hydroxide is stable up to 340°C that allows processing with a wide variety of thermoplastics. It should be noted that modern trends towards faster, more economic processing of all polymers creates compounding situations in which certain polymers, that were usually processed at temperatures at which ATH could be incorporated as FR, are processed at temperatures that exceed the decomposition temperature of ATH (Weber, 2000).

Huntite [$Mg_3Ca(CO_3)_4$] and hydromagnesite [$Mg_5(CO_3)_4(OH)_2 \cdot 4H_2O$] formulations have also found use in the polymer industry. Similarly to ATH and magnesium hydroxide, both minerals decompose during endothermic reactions. The decomposition products are calcium- and magnesium oxide, water and carbon dioxide. The main advantage compared with ATH lies in the higher thermal stability of huntite/hydromagnesite, that allows a processing temperature up to 250°C. Combinations with ATH and magnesium hydroxides have also shown good performance by extending the effective temperature range (Kirschbaum, 1999). Because of its high decomposition temperature huntite alone is not a very effective FR. Hydromagnesite though has been shown to be effective as a FR on its own (Rigolo and Woodhams, 1992).

Owing to the reaction mechanisms described, mineral flame retardants offer distinctive advantages compared to traditional (halogen-containing) solutions. These advantages include (Weber, 2000):

- being non-corrosive to processing equipment
- low smoke generation
- no acid gas emission
- halogen free
- environmentally safe
- recyclable
- no combustion gas corrosion
- no limitation in colouring
- low combustion gas toxicity

One challenge of the mineral FR's is the loading levels of 50–65% necessary to achieve the required flame retardancy standards. The high filler content has the advantage that it acts as a solid phase diluent. The high loading levels do though cause problems during compounding and processing and often compromise the mechanical properties of the resultant composites. Consequently only polymers which can incorporate high percentages of additives without loss of mechanical or viscosity properties can be fireproofed in this way. To retain the mechanical properties of the polymer, good bonding at the interface must be obtained.

The mineral FR's also act as catalysts for the oxidation of the carbonaceous residues reducing the CO/CO_2 ratio. This results in an incandescence phenomenon. Its propagation, which continues after the extinction of the flame, causes temperature rises which aid the pyrolysis of fresh material. Accumulation of gases can then give rise to re-ignition.

2.7 System development

Flaming can be retarded by incorporation of the FR molecule into the polymer itself (reactive approach) or by admixture of the FR with the polymer (additive approach). Reactive FR's contain functional groups which allow the retardant to be incorporated into the polymer molecule. The functional group usually is the hydroxyl (–OH) group, although other groups can also be present. The major advantage of the reactive approach is the nonmigratory nature of the FR. Because the FR is an integral part of the polymer backbone bleeding out of the polymer and blooming are prevented. The volatility of the FR is also minimised. Another advantage of the reactive approach is the ability to produce optimum polymer properties by using the proper balance of reactive

material and other monomers. Reactive FR's are more expensive than additive FR's due to the additional cost associated with the increased cost of manufacture of the former. Reactive systems may not be as effective as additive systems because of the more controlled availability of the FR. The ability of FR's to melt and migrate to the flame front in the heat of a fire is often desirable; such movement is restricted if the FR is part of the polymer backbone.

Additive FR's are usually incorporated into the polymers following the polymerisation process. Their main use is in thermoplastics, where they may have a plasticiser or filler effect upon the host polymer. Additive FR's generally reduce some property, such as impact resistance or heat resistance (Sutker, 1988; Petrella, 1992).

2.8 General rules for the use of flame retardants

Not all FR's are equally effective in all polymer systems and not all FR's are equivalent in a given polymer. Experience and familiarity with a polymer system do not always lead to the best choice of FR's for that system. Experience does however, make one aware of certain trends which can lead to a judicious use of FR's. The following items seem to work for Petrella (1992):

1. FR's should decompose at a temperature slightly lower than the ignition temperature of the polymer system it is to protect, to be effective. The decomposition temperature must however, exceed the highest processing temperature.

2. Polymer systems, that melt and gasify easily, should be treated with halogen FR's.

3. Polymers that produce hydrogen upon pyrolysis can be protected by FR's that produce either halogen or hydrogen halides (HCl or HBr).

4. Polymers that produce little or no hydrogen should use a FR that produces hydrogen halide rather than the free halogen.

5. Polymers which form char upon pyrolysis are most often treated with a phosphorus-containing FR.

6. Polymers which gasify to a small extent and give rise to small blue flames (gas-solid reactions) should be treated with phosphorus-based FR's.

The above considerations are general observations and are not a guarantee to success.

An ideal FR polymer system should have (Pearce, 1986):

- high resistance to ignition and flame propagation
- a low rate of combustion
- a low rate and amount of smoke generation
- low combustibility and toxicity of combustion gases
- no change in flammability during use
- performance of the base material should be fairly close to the original and there should not be a difference in appearance
- the economic penalty should be acceptable

2.9 Selection criteria of flame retardants

Identification of the *flammability test requirements* is the initial criterion for selection of the appropriate FR. In some cases, changing part design or construction material obviates the need for FR's.

Establishing the desired *cost-performance parameters* is the second key criterion. The properties and costs of systems containing high loadings of FR are vastly different from those at low loadings.

The third criterion is *environmental exposure requirements* of the finished article. For example, ethylene bis(tetrabromophthalimide) has superior resistance to UV light in styrenic polymers compared with halogenated diphenyl oxides. However, television cabinets and computer components are often painted to mask colour changes resulting from fluorescent or UV light exposure in preference to using FR's with good light resistance. Optical clarity and corrosion resistance are other environmental exposure criteria.

Compounding (or reacting) of the FR must take into account the stability of the FR, the matrix in which it is suspended and the effect of the FR or its degradation products on processing or compounding equipment. Thermal gravimetric analysis is typically used to evaluate the decomposition or volatilisation of FR's and to aid in selection of the most cost-effective material (Sutker, 1988).

2.10 Fire hazard test methods

Fire test methods attempt to provide correct information on the fire contribution of a product by exposing a small sample to conditions expected in a fire scenario. Methods can be viewed in two ways: the first entails the strategy of the fire test, ignition resistance or low flammability once ignited. The second addresses the test specimen, a sample representative of the product or a sample of a material that might be used in the product (Gann, 1993).

The material's behaviour, the "flammability" of the compound, is a first hint that a finished product which uses this material may survive a real fire attack. Such material behaviour is generally and easily checked by loss on ignition (LOI). LOI tests determine the oxygen concentration which is needed to keep a sample of material burning. The main problem with testing conditions is that an oxygen concentration is used which is higher than the usual oxygen concentration in the air. Keeping in mind that oxygen is needed and used during a fire, the oxygen content of the air surrounding a burning plastic part will in any case be lower than the standard amount. The LOI test might be used as a quick test for development purposes in the laboratory. Here it can differentiate between samples created under similar conditions by slightly changing type and amount of ingredients (Schmidt, 1999).

Small-scale fire tests do not however indicate how the tested products will behave in actual fires and should not be considered as a valid indication of full-scale fire behaviour. Full scale tests are used to check finished products by simulating potential practical fire attacks. Full-scale tests are necessary since configuration affects flammability results.

Test procedures can be grouped as follows (Schmidt, 1999):

- fire propagation
- fire resistance
- fire gases
- integrity of service

A real system test would not only include the fire retarded product, such as the cable, but also all other system parts like adhesives, paints, joints or repair kits. Test methods have been developed that vary in complexity. These methods may evolve on the basis of particular requirements of a country or industrial group. A few of the fire hazard test methods (Schmidt, 1999) that are used in the USA and Europe, are summarised in Table 2.1

Table 2.1 Fire hazard test methods

Fire hazard criteria	USA	Europe
Ignitability	Oxygen Index (ASTM D–2863)	IEC 332–3 Appendix A
Propagation	Vertical Tray UL 1581	IEC 332–3
Smoke	NBS Chamber (ASTM E–662)	3 Metre Cube (IEC 220(CO) 178
Toxicity	New York State (University of Pittsburgh)	ISO Guide TR 9122
Corrosivity	ASTM Copper Mirror Test	IEC 754–1

Several test methods exist for assessing the flammability of materials. These range in severity from small-scale measures of the ignitability of a material to actual testing in a full-scale fire. The list of fire tests available is too long and varied to be fully recorded here. Instead a few of the tests are shortly discussed below (Pettigrew, 1993), to indicate the types of measurements that are involved.

2.10.1 Material tests

Material tests measure some property of the polymer or plastic as opposed to measuring the flammability of the final product which contains the plastic.

2.10.2 Limiting oxygen index

The minimum concentration of oxygen in an O_2 / N_2 mixture that supports combustion of a vertically mounted test specimen is called the limiting oxygen index. This test is reproducible which makes it useful for quality control. The main disadvantage is that the results rarely correlate with the results of other fire tests.

2.10.3 Specific tests

Federal (United States) Motor Vehicle Safety Standard (MVSS) 302 is used to measure the burning behaviour of materials used in automobile interiors.

The Underwriters Laboratory UL 94 Standard for Safety measures the ignitability of plastics by a small flame. This test rates materials on the basis of their ability to resist combustion on repeated application of a flame. It also rates materials for their resistance to dripping with subsequent ignition of a combustible substance (cotton) from the resulting drips. Materials are classified on the basis of after-flame time and ignition of the cotton caused by flaming drips. The flammability is classified as: V–0, V–1 and V–2.

2.10.4 Heat release calorimeters

There are three principal types of heat release calorimeters. The Cone calorimeter measures the rate of heat release of a burning specimen. Additional parameters that may be measured include total heat released, mass loss, time to ignition, critical heat flux and smoke production. The heat released is calculated based on oxygen consumption. The advantage of this test is that materials can be subjected to heat fluxes similar to those encountered in real fires. The results must though correlate with large-scale testing before they are useful.

The OSU (Ohio Sate University) calorimeter differs from the Cone calorimeter in that it is a true adiabatic instrument which measures heat released during burning of polymers by measurement of the temperature of the exhaust gases.

The Factory Mutual flammability apparatus allows the measurement of flame spread as well as heat release and smoke. It uses oxygen concentrations higher than ambient to simulate back radiation from the flames of a large-scale fire.

2.10.5 Product tests

Product tests are tests in which the finished article is subjected to a more or less realistic fire. A few examples follows:

Tunnel test: This test is used to test the flame spread potential of building products such as electrical cable and wall coverings. During the test, the maximum flame spread, temperature and smoke evolved is measured.

Factory mutual corner test: This is a large-scale corner test used to test building products. In order to pass this test, no flame can propagate to any extremity of the walls or ceiling.

CAL 133: California Technical Bulletin 133 is a test of the fire hazard associated with upholstered furniture. Smoke, heat and toxic gas emissions are measured during the test.

Chapter 3

Theoretical background on the synthesis and characterisation of the basic magnesium carbonates

3.1 Introduction

Various procedures have been described in literature relating to the preparation of the basic magnesium carbonates. These procedures used various approaches to obtain the required product. Each specific approach is dependant on the raw materials that are available for synthesis of the basic magnesium carbonate. The various methods of synthesis can be summarised in terms of the raw materials used to prepare the product namely,

1. Preparation using MgO
2. Preparation by addition of a precipitating agent to a magnesium salt solution, using basic reagents such as sodium or potassium carbonates or bicarbonates
3. Preparation using $Mg(OH)_2$
4. Preparation using $MgCO_3 \cdot 3H_2O$

Basic magnesium carbonates can be obtained either by mining or by preparing it synthetically. The aim of this discussion is to highlight the procedures that currently exist for preparation of a basic magnesium carbonate and the techniques that have been applied successfully for the characterisation thereof. By weighing up the advantages and disadvantages associated with each procedure, a decision could be made regarding the basis of the procedure that was to be followed in following chapters. The most favourable techniques for investigating the physical and chemical properties of the products that were to be synthesised, could also be identified.

3.2 Phase and stability relations in the system $MgO-CO_2-H_2O$

Various parameters influence the relationship between the compounds in the $MgO-CO_2-H_2O$ system. This includes ionic strengths in aqueous solution, relative humidities of water vapour, CO_2 pressures and temperature. It is necessary to be aware of the influence of these factors when synthesising a specific compound in this system.

Figure 3.1 depicts the probable phase relations in the $MgO-CO_2-H_2O$ system at 25°C and 1 atm total pressure. The indicated compatibilities are consistent with free-energy values as derived by Langmuir (1965). The phases in the interior of the diagram are supposedly highly metastable. Lansfordite is metastable with respect to nesquehonite and water and artinite probably metastable relative to hydromagnesite, brucite and water at 25°C (Langmuir, 1965).

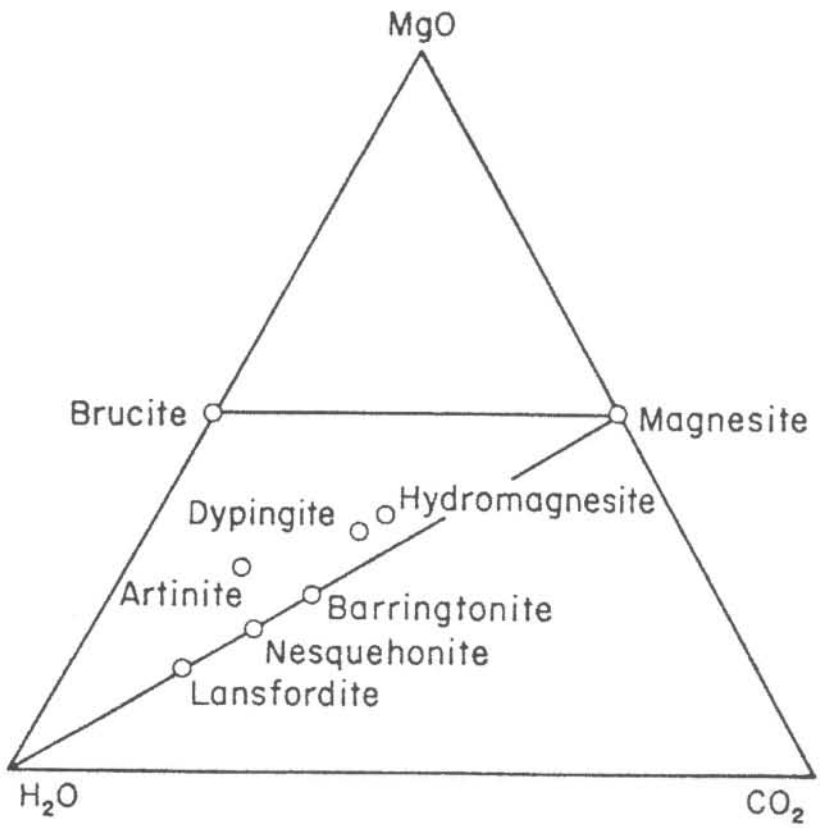

Figure 3.1 Probable phase relations in the system $MgO-CO_2-H_2O$ at 25°C and 1 atm total pressure. Mineral formulas are plotted in mole per cent (Hill *et al.*, 1982)

Probable phase relations in the system MgO-CO_2-H_2O between 0 and 100°C as a function of log P_{CO_2}, and assuming aH_2O = 1, is depicted in Figure 3.2. The diagram has not been extended to high CO_2 pressures since solubilities in this system become sufficiently great under such conditions to reduce the activity of water significantly below unity. At 25°C and $P_{CO_2} \leq 1$ atm, $aH_2O \geq 0.99$, so that in general within the diagram the assumption of aH_2O = 1 is largely justified. The only stable phases in the diagram, if Stout and Robie's free energy for magnesite is used, are brucite and magnesite with a calculated CO_2 pressure of $10^{-6.2}$ atm for the brucite-magnesite equilibrium at 25°C. The lansfordite-nesquehonite and nesquehonite-magnesite boundaries must be horizontal since they represent dehydration equilibria and are thus independent of P_{CO_2}.

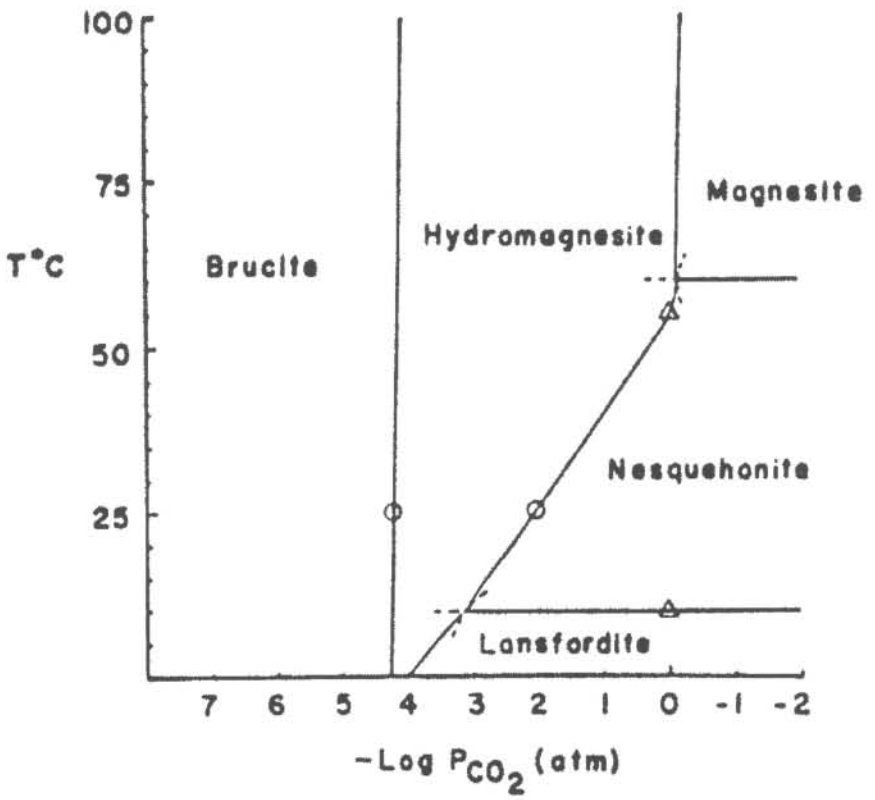

Figure 3.2 **Probable stability relations in the system MgO-CO_2-H_2O between 0 and 100°C as a function of P_{CO_2} and assuming aH_2O = 1 (Langmuir, 1965)**

The dependence of magnesite stability on the activity of water at 25°C and 1 atm total pressure is depicted in Figure 3.3. According to the diagram, magnesite should not form unless the relative humidity is less than 70% at 25°C. Comparison of this and Figure 3.2 suggests that for temperatures approaching 60°C, magnesite should become stable in the presence of increasing activities of water. The broken lines (Figure 3.3) represent phase relations among magnesite, periclase and brucite assuming a free energy of -246 030 cal mol^{-1} for magnesite. As is indicated by the other diagrams as well, this stability for magnesite would indicate that all other carbonate phases in the system $MgO-CO_2-H_2O$ are metastable at 25°C and 1 atm total pressure (Langmuir, 1965).

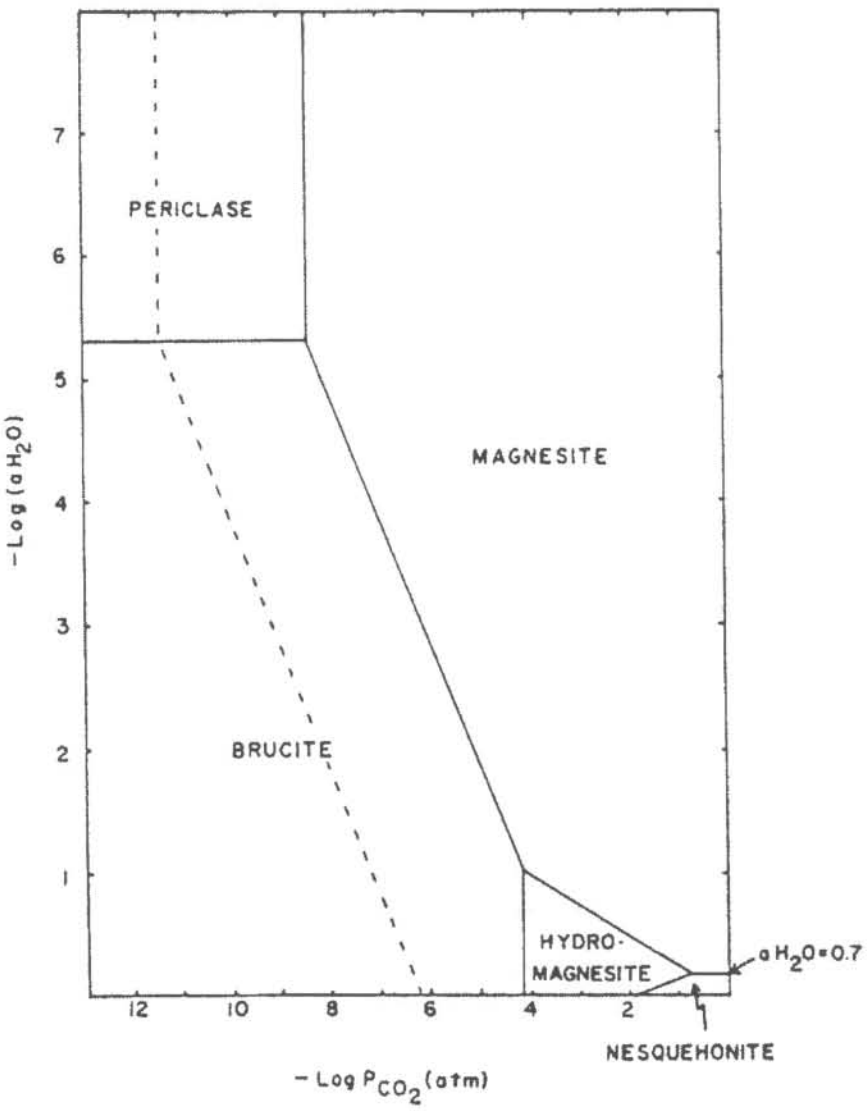

Figure 3.3 Probable stability relations in the system MgO-CO_2-H_2O at 25°C and 1 atm total pressure as a function of P_{CO_2} and aH_2O (Langmuir, 1965)

3.3 Synthesis procedures

In the following discussion the various procedures that have been investigated regarding the synthesis of basic magnesium carbonate, are summarised. Each procedure has certain advantages and disadvantages associated with the specific method of synthesis. These advantages and disadvantages were taken into account when deciding on the most appropriate procedure to build upon. Various aspects determine the choice of the most suitable method. These include availability of the raw material, experimental requirements (e.g. temperature, pressure, additional reagents, etc.), environmental impact and economic viability.

The following discussion on the various procedures has been structured with respect to different starting reagents. This seems to be a logical method of categorising existing preparation procedures.

3.3.1 Preparation using MgO

Canterford and Moorrees (1985) showed that the temperature and rate of sparging to remove carbon dioxide, determined the rate of precipitation and the chemical and physical properties of hydrated magnesium carbonates precipitated from clarified magnesium bicarbonate liquors derived from crude magnesia. At temperatures above 55°C, the product was largely in the form of hydromagnesite. Between 15 and 55°C, the major product was nesquehonite, although partial hydromagnesite precipitation could be induced by a high rate of aeration. It was preferable to precipitate hydromagnesite rather than nesquehonite due to reduced time required to bring about greater than 95% magnesium precipitation. The higher MgO content of the hydromagnesite product, the ease of product recovery from the precipitation vessel and the lower energy requirement for thermal decomposition of the precipitate to magnesia were also contributing factors. They found that the magnesia produced from hydromagnesite was somewhat more reactive than that formed from nesquehonite.

The manufacturing of basic magnesium carbonate by mixing a basic magnesium carbonate suspension and a magnesium oxide suspension, while bubbling with CO_2, was described by Morie *et al.* (1986).

The Pattison process (McMichael, 1989) is a well known process for precipitating magnesium hydroxide carbonate. Dolomite and magnesium limestone were burned at 1000°C to produce magnesium oxide and calcium oxide. The oxides were hydrated to form hydroxides and carbon dioxide. The CO_2 was used to carbonate the hydroxide mixture and in the first step of a double stage process insoluble calcium carbonate was precipitated. Step two of the double stage process involved the application of higher CO_2 pressure, which resulted in the formation of magnesium hydrogene carbonate and CO_2.

Cosic *et al.* (1994) described different stoichiometries of the basic magnesium carbonates obtained by varying the experimental conditions for carrying out the hydrothermal decomposition.

The carbonation of calcined dolomite and further heating of the magnesium bicarbonate solution that was formed after the filtration thereof, was described by Rosa (1996).

While studying the separation of magnesium/calcium carbonates from dolomite using partial thermal decomposition followed by hydration and recarbonation, Cáceres and Attiogbe (1997) recovered pure hydromagnesite from the aqueous residue. The liquid that was obtained after recarbonation and filtration was heated to 100°C under atmospheric conditions, until all the water was driven off. The solids that came out of the aqueous solution were collected and dried at 120°C. X-ray analysis of the precipitated solid showed the presence of hydromagnesite.

The formation of a $Mg(HCO_3)_2$ solution by carbonation of a MgO-containing residue slurry and further precipitation of hydromagnesite by addition of pure magnesium oxide as the precipitating agent, was described by Fernández *et al.* (2000). This procedure was done at room temperature and the final pulp heated at 55°C to successfully obtain hydromagnesite. The optimum parameters for precipitation were established and the kinetic data were examined according to the equation for diffusive control. The kinetics of the reaction, as well as the purity of the product, are strongly influenced by the magnesium oxide used. By using a reactive, high-purity MgO, a high-purity hydromagnesite could be obtained. The process allowed the production of hydromagnesite without the introduction of foreign ions and therefore, the water effluents generated could be discharged or reused to obtain the magnesium bicarbonate solution.

3.3.2 Preparation by addition of a precipitating agent to a magnesium salt solution

Preparation by addition of a precipitating agent to a magnesium salt solution using basic reagents such as sodium or potassium carbonates or bicarbonates has also been described in the literature. Black and Bergmann (1939) described a method of preparation that included the addition of a magnesium sulphate solution to a sodium carbonate solution. Both these solutions were heated separately to 70°C before they were added together. The resulting precipitate was boiled at approximately 95°C and then filtered and washed. The precipitate was dried at 150°C. Hydromagnesite was obtained as the final product. Other methods were also described using different magnesium salts (e.g. $MgCl_2$, $Mg(NO_3)_2$) and carbonate salts (e.g. $(NH_4)_2CO_3$, NH_4HCO_3, K_2CO_3, $KHCO_3$, Na_2CO_3).

A high pressure technique was employed by Choudhari *et al.* (1972), to prepare the heavy basic magnesium carbonate. A solution of magnesium chloride and sodium chloride was heated at 130°C in a reaction vessel containing aqueous sodium carbonate at a pressure of 2.8 kg cm^{-2}.

Choudhary *et al.* (1994) prepared basic magnesium carbonate samples for thermal analysis by precipitation, using different magnesium salts (magnesium nitrate, sulphate, chloride and acetate) and precipitating agents (viz. sodium carbonate and bicarbonate and potassium carbonate and bicarbonate) at different concentrations of magnesium salt (0.005–2.0 M), temperatures (0–100°C) and pH 9–11 using different modes of mixing in the precipitation and also by ageing the precipitate for different periods (0.5–96 h). Choudhary *et al.* (1995) found that the chemical composition of basic magnesium carbonate and the surface properties and carbon dioxide content of MgO, were strongly influenced by the aforementioned preparation conditions of basic magnesium carbonate.

3.3.3 Preparation using $Mg(OH)_2$

Prakash and Gupta (1987) formed magnesium carbonate trihydrate by carbonation of $Mg(OH)_2$ slurries and then, by boiling the pulp, formed the basic magnesium carbonate. This procedure was also described by Gloss (1952) who indicated that the procedure was followed in one sea-water plant where the starting material was relatively pure

magnesium hydroxide. Flue gases with a low carbon dioxide content could be utilised in this case, because the separation step was eliminated and the hydroxide was converted directly into solid-phase $MgCO_3 \cdot 3H_2O$ or $5MgO \cdot 4CO_2 \cdot 6H_2O$, depending on the temperature of carbonation.

Pond and Heneghan (1965) prepared a hydrated magnesium carbonate by forming a slurry of magnesium hydroxide in water. CO_2 was introduced into the slurry until the pH was between 7.5 and 9.0 (more specifically between 8.0 and 8.6). At this point the solid portion of the slurry was separated from the liquid portion and dried below 75°C. The magnesium hydroxide suspension contained approximately 5 g of magnesium hydroxide per 125 ml of solution, although the amount was limited by what may conveniently be handled in the suspension. The CO_2 may be introduced into the magnesium hydroxide-water slurry by sparging with gas mixtures containing CO_2 or by introducing solid CO_2 therein. Flue gas containing about 10% CO_2 was found suitable for this purpose. The rate of gas sparging was not critical.

Jackson *et al.* (1995) described the production of synthetic hydromagnesite by the following procedure. The carbonation of magnesium hydroxide slurry at 345–517 kPa and at temperatures below 50°C, formed a more soluble bicarbonate which was then separated from the other reaction products by means of filtration with subsequent crystallisation. The trihydrate form was recovered from the filtrate by decarbonation under vacuum or by filtration. Boiling the bicarbonate solution or drying the trihydrate precipitate at approximately 100°C produced a basic magnesium carbonate.

3.3.4 Preparation using $MgCO_3 \cdot 3H_2O$

It was shown by Davies and Bubela (1973), that nesquehonite, synthesised in the laboratory, could readily be altered to hydromagnesite via an intermediate phase. This procedure was based on the biological and abiological preparation of nesquehonite from saturated $Mg(HCO_3)_2$ solutions below 52°C. Hydromagnesite is the stable hydrate above this temperature. Nesquehonite crystals were placed in three vessels: (1) in the dry state; (2) with distilled water; and (3) with the mother liquor from which the crystals were precipitated. The vessels were sealed and placed in a water bath, kept at a constant temperature of 52°C for three days. The nesquehonite crystals completely disappeared and were replaced by hydromagnesite in the first experiment. Nesquehonite formed the major component in the third experiment. The second

experiment was rerun for another week after which a mixture of hydromagnesite and an intermediate phase were obtained.

3.3.5 Advantages and disadvantages of various procedures

It is evident that each procedure that was mentioned above, presents certain advantages and disadvantages. There are certain aspects that needs to be considered when choosing the most appropriate procedure. The availability of the starting reagent is an important aspect. Whether the starting reagent has to be prepared, bought or mined and the subsequent purity thereof, are important aspects. This could influence the purity of the basic magnesium carbonate product, that in turn could influence its characteristics and application. If the starting reagent is a mixture of different compounds, which is sometimes the case when mined, additional procedures will be necessary to separate the required reagent from the rest of the mined compounds, before attempting the preparation of the basic magnesium carbonate.

Other aspects that could be important is whether the procedure requires elevated temperatures. Elevated temperatures increase the processing costs that could result in a procedure becoming uneconomical. The use of high pressure systems are also not desirable.

Another obstacle that could arise is the production of effluents that could pose environmental problems. The procedures that requires magnesium nitrate, sulphate, chloride or acetate falls in this category. These reagents result in effluents that could be harmful to the environment. A lot of emphasis is currently placed on conducting environmentally safe processes. It is of course advantageous if the effluents could be reused or recycled back into the process.

3.4 Characterisation techniques

The basic magnesium carbonates have been characterised by various techniques. Each of these techniques aimed at highlighting a specific characteristic of these compounds. By characterising the products it is possible to obtain valuable information relating to the physical and chemical aspects of the basic magnesium carbonates. In the following discussion the various approaches of characterisation will be mentioned.

A decision on the most suitable techniques for characterisation of the basic magnesium carbonate will follow from this discussion.

Rajeswara Rao and Chohan (1995) studied the thermal decomposition of hydromagnesite using thermogravimetric analysis. The experiments were conducted in a nitrogen atmosphere with pellets of hydromagnesite in the range 300–550°C and also with powder samples under non-isothermal conditions at a heating rate of 10°C min^{-1}. They found that the reaction proceeded in two stages: dehydration (between 100 and 300°C) followed by decomposition (between 320 and 550°C). The dehydration reaction is controlled by external mass transfer whilst the decomposition reaction is controlled by both external and internal mass transfer.

Khan *et al.* (2001) investigated the thermal analysis of basic magnesium carbonate by thermogravimetry, derivative thermogravimetry and differential thermal analysis. The thermal analysis was carried out in nitrogen, carbon dioxide and air at different heating rates and the origin of the exothermic peak studied. Generally, the decomposition peaks were endothermic, but a persistent exothermic peak was noted, always accompanied by a very sharp drop in the thermogravimetric curve and the weight loss in this region may be significant. The exothermic differential thermal analysis peak was found to be strongly influenced by the rate at which the samples were heated, sample size and atmospheric conditions.

The thermal decomposition of precipitated basic magnesium carbonate and the surface area of the resulting solid product MgO, were shown by Choudhary *et al.* (1994) to be strongly influenced by the preparation conditions (magnesium salt and precipitating agent used) and the precipitation conditions (concentration of magnesium salt, pH, temperature, mode of mixing of magnesium salt and precipitating agents and ageing period of the precipitate) of basic magnesium carbonate. The thermal analysis was carried out in the temperature range 30–600°C. The exothermic differential thermal analysis peak, attributed to recrystallisation of solid product, was not found for all the samples.

The surface area, total basicity and base strength distribution (weak, strong and intermediate strength basic sites) of magnesium oxide obtained from basic magnesium carbonate (by its decomposition at 873 K) prepared by precipitation using different magnesium salts, precipitating agents and conditions (viz. magnesium salt concentration, pH, temperature, mode of mixing and ageing period), was investigated

by Choudhary *et al.* (1995).

Cáceres and Attiogbe (1997) analysed the precipitated solid that was obtained from the aqueous residue after separation of magnesium/calcium carbonates from dolomite, using partial thermal decomposition followed by hydration and recarbonation, by X-ray analysis. The presence of hydromagnesite in the precipitated solid was shown.

Fernández *et al.* (2000) used X-ray diffraction to analyse the solids that were obtained in the procedure to obtain hydromagnesite from a MgO-containing residue. Scanning electron microscopy was also used to view the crystals of basic magnesium carbonate that formed on the particle surface. Elementary analysis of C and H was done by chromatography and thermogravimetric analysis.

Canterford and Moorrees (1985) used X-ray diffraction, optical microscopy and differential thermal and thermogravimetric analysis to investigate the products that were obtained. Differential thermal and thermogravimetric analysis in a static air atmosphere, showed that the precipitates dehydrated in several distinct stages, being complete at about 350°C. Carbon dioxide evolution also took place in several stages, but were less distinct than the dehydration stages. A sharp exotherm was observed at 505–510°C prior to a pronounced endotherm corresponding to the major weight loss associated with carbon dioxide evolution. Decomposition was complete at 570°C.

Scanning electron microscopy, X-ray diffraction and optical microscopy were used by Davies and Bubela (1973) to examine the crystals that were obtained during the investigation of the transformation of nesquehonite into hydromagnesite. Differential thermal analysis and thermal gravimetric analysis were used to investigate the decomposition characteristics of these products.

Sawada *et al.* (1978) studied the thermal decomposition of hydromagnesite by comparing the structural changes under two typical experimental conditions; the condition in which the exothermic phenomenon at ~520°C was absent (P_{CO_2} = 0.00 atm) and the one in which it was present (P_{CO_2} = 0.50 atm). The specimens were heated in the apparatus of differential thermal gas analysis in flowing helium-carbon dioxide mixed atmospheres and quenched from various temperatures for analysis. Differential thermal analysis and thermogravimetry, powder X-ray diffraction analysis and infrared spectrum analysis were used to study the decomposition behaviour of hydromagnesite at the various conditions. An amorphous phase including a lower carbonate

intermediate was formed after dehydration (~300°C) was completed. At P_{CO_2} = 0.00 atm, decarbonation proceeded and MgO was formed at ~500°C. At P_{CO_2} = 0.50 atm, crystallisation of $MgCO_3$, the evolution of heat and a rapid evolution of carbon dioxide took place at ~520°C. The $MgCO_3$ was decomposed at higher temperatures.

Infrared characterisation of water and the hydroxyl ion in the basic magnesium carbonate minerals was investigated by White (1971). The infrared spectrum is particularly sensitive to hydrogen bonding and was expected to provide a valuable supplement to less sensitive diffraction methods. The mid-infrared region of the basic magnesium carbonate minerals was dominated by the vibrational modes of the carbonate ion. The various bands in the 3000 cm^{-1} range were all due to O-H stretching motions of water or hydroxyl. No additional features could be observed in the near-infrared region. The CO_3^{2-} internal vibrations were sharp in hydromagnesite and broad and diffuse in artinite and nesquehonite. The OH^- stretching region contained a sharp band indicative of a weak, well defined hydrogen bond in all three minerals. Hydromagnesite was also characterised by two sharp intense bands not present in the other two minerals.

Raade (1970) utilised X-ray powder data, infrared absorption analysis and differential thermal and thermogravimetric analysis to characterise dypingite, a newly discovered basic magnesium carbonate. The results were compared to hydromagnesite to identify differences and similarities between these two basic magnesium carbonates. It was shown that by heating at 150°C, dypingite was converted to hydromagnesite. The infrared absorption spectrum and differential thermal analysis curve of dypingite was very similar to those of hydromagnesite. The X-ray powder pattern of dypingite only slightly resembled that of hydromagnesite and was clearly different.

The nature of the heavy basic magnesium carbonate, prepared from magnesium chloride and soda ash solution was investigated by Choudhari *et al.* (1972). X-ray diffraction, thermal and infrared data were employed for this investigation. The results for the heavy product were compared with those of light basic magnesium carbonate.

It is evident from this discussion that various techniques exist by which the basic magnesium carbonates have been successfully characterised. In short, five techniques are generally used: X-ray diffraction, microscopy, infrared analysis and thermogravimetric and differential thermal analysis.

X-ray diffraction is used to identify the product obtained by fitting diffraction patterns from the XRD database to the diffraction pattern obtained for the synthesised products. This approach makes it possible to determine the exact identity of the product obtained.

The physical appearance of the products can be assessed by using microscopy. This technique gives the opportunity to compare physical characteristics of a product to results obtained elsewhere. This can be done since each basic magnesium carbonate has certain inherent physical characteristics relating to its crystal form and shape.

Problems relating to the structural arrangement of inorganic substances have been successfully resolved with infrared spectroscopy. This approach is possible because mechanical vibrations of molecules from which infrared spectra originate, are governed by molecular symmetry in such a way that specific sets of vibrations can be correlated with specific symmetry operations.

The thermal decomposition of products have been successfully studied by using thermogravimetric and differential thermal analysis. Thermogravimetry measures the change in weight of a sample as a function of temperature. Differential thermal analysis is a technique in which the difference in temperature between the sample and an inert reference material is measured as a function of temperature. From the differential thermal analysis results, it is possible to determine whether the processes that are observed are exothermic or endothermic in nature.

3.5 Conclusion

The previous discussion has highlighted various procedures that exist for the preparation of a basic magnesium carbonate. It became evident that there are various factors that influence the choice of the most suitable procedure. The starting material, experimental conditions that needs to be employed (e.g. heating, pressure), additional reagents, effluents and cost, are just some of the factors that could influence the choice of a procedure.

It was also shown that various techniques could be employed to characterise the products that were synthesised. The choice of a specific technique will depend on the information that is required. The work of previous authors indicated mainly five techniques that are generally used to characterise the basic magnesium carbonate

products. This included X-ray diffraction, microscopy, infrared analysis and thermogravimetric and differential thermal analysis. Both physical and chemical information, relating to the inherent characteristics of the respective basic magnesium carbonates, can be obtained by combining these techniques.

The information presented here forms the basis for the development of a procedure of synthesis of a basic magnesium carbonate. The respective techniques employed to characterise the basic magnesium carbonates will be used to study the synthesised products.

Chapter 4

Theoretical background on experimental techniques

4.1 Introduction

The aim of this chapter is to highlight the important aspects relating to the various experimental techniques that were applied in this study. Since it was necessary to study various properties of the synthesised products, to evaluate the attempted experimental procedures and products, various techniques needed to be applied to obtain the relevant information. The techniques that were chosen needed to highlight the appropriate aspects of the products. The physical properties of the synthesised products were studied with X-ray diffraction (XRD), surface area determination and scanning electron microscopy (SEM). The chemical properties were studied with thermogravimetric analysis (TG), differential thermal analysis (DTA) and Fourier transform infrared (FT-IR). The flame retardant behaviour of the synthesised products were evaluated with the limiting oxygen index (LOI).

The following discussion will highlight the theoretical aspects relating to each technique, as well as the importance of experimental conditions on the respective techniques.

4.2 X-ray diffraction

X-ray crystallography encompasses a group of techniques which utilise the wave properties of X-rays. A wealth of information is provided by the positions and intensities of the X-rays diffracted by a crystalline solid. This includes crystal structure, composition of a solid, particle size, evidence of decomposition, polymorphism, preferred orientation, disorder and so on.

"Single crystals" are the classical objects investigated by crystallography. Single-crystal structure analysis (the determination of the structure of the asymmetric unit of a crystal)

is so far the only analytical method that can yield direct and unambiguous information about the three-dimensional atomic structure of a substance.

The diffraction of X-rays from a fine grained crystalline powder, is based on the principle that a beam of X-rays that strikes a crystal will pass through it, but with scattering or diffraction of the photons in the beam. Since the particles in the crystal are in a regular or symmetrical arrangement, the X-rays will be scattered in a regular pattern.

4.2.1 Generation of X-rays

X-rays are produced when high speed electrons are suddenly stopped by a solid object. To generate X-rays the following is needed:

- a source of electrons
- a means of accelerating them
- a target to stop them.

An X-ray tube is the modern device used to generate X-rays. Two varieties are in current use, known as the side window tube and the end window tube. Only the side window X-ray tube will be discussed, since they are very similar with respect to their integral components, only differing with respect to geometry.

Figure 4.1 shows a schematic diagram of a side window tube. The electrons are produced by an electrically heated tungsten filament. The electrons are accelerated towards the target by applying a large potential difference (voltage), e.g. 60 kV, between the filament and the target. To allow free flight of the electrons, the X-ray tube is evacuated to produce a very high vacuum.

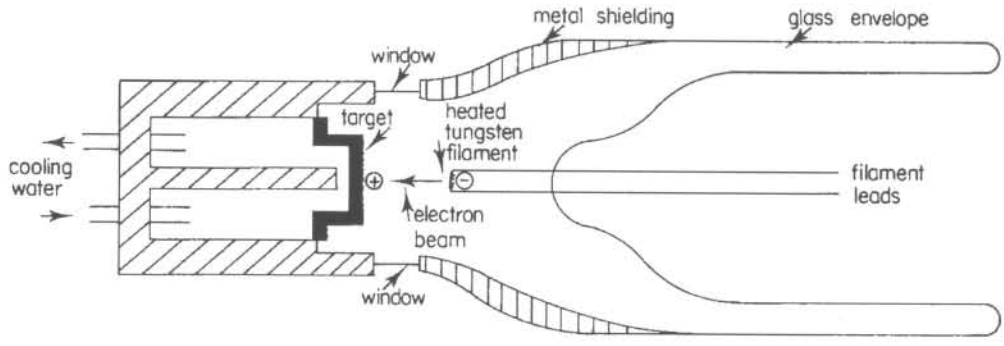

Figure 4.1 Schematic diagram of a side-window X-ray tube (Whiston, 1987)

The high speed electrons are stopped by the atoms of the target resulting in X-rays being produced in all directions from the surface of the target. The tube is partly clad with a heavy absorbing material such as lead. The X-rays are allowed to leave the tube through one or more windows, these being made of a thin light metal such as aluminium or beryllium.

Only a fraction (~ 1%) of the total energy supplied to the tube is converted to X-rays. Most of the energy is transferred into heat. The target is cooled from behind by running water to prevent it from melting. The target material must be made of a high melting material which has good thermal conductivity. To produce high intensity X-rays a target element should have a high atomic number. Typical target materials are pure transition metals such as Mo, W, Cu, Cr etc. (Whiston, 1987).

4.2.2 Characteristic radiation

Characteristic radiation arises from the rearrangement of the orbital electrons of the target element following the ejection of one or more electrons in the excitation process. The final resting place of the transferred electron determines the type of radiation.

If the high speed electrons from the X-ray tube have sufficient kinetic energy to cause internal ionisation of the atoms in the anode (target), a small part of the energy released

is consumed in ejecting electrons from the K-shell of the atoms. The vacant energy levels are filled, chiefly by electrons from the L shell (L III and L II levels) and also from the M-shell (M III level). The energy thus gained is emitted as X-rays (Figure 4.2) (Paulus and Gieren, 1994), a photon of definite wavelength. If the vacancy in the K-shell is filled by an M electron then the photon produced is called a $K\beta_1$ X-ray. If the vacancy is filled by an L electron then a $K\alpha_1$ or a $K\alpha_2$ X-ray is produced, depending on the subshell of the electron involved in the transition. A mixture of $K\alpha_1$ and $K\alpha_2$ radiation can be used for most diffraction studies. The $K\beta_1$ is removed by a filter or a crystal monochromator.

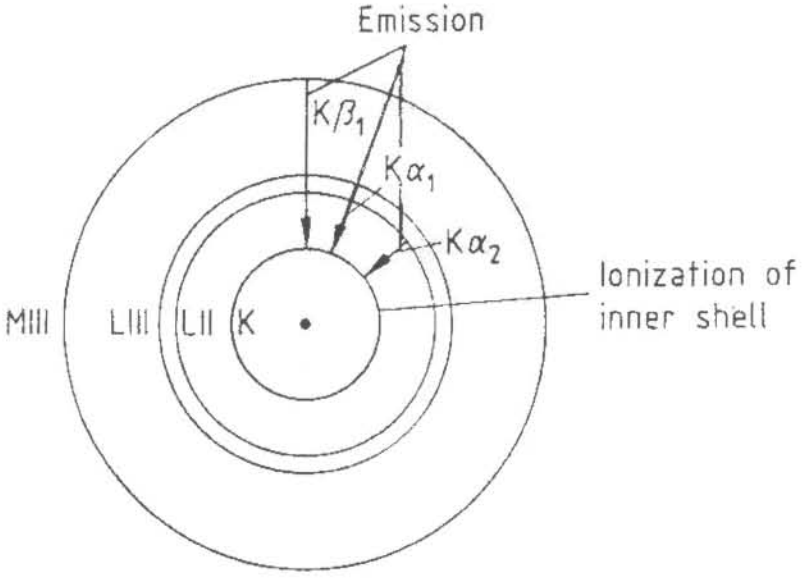

Figure 4.2 Generation of X-rays (Paulus and Gieren, 1994)

4.2.3 Principle of X-ray diffraction

The phenomenon of X-ray diffraction is an interaction of X-rays and crystals. X-rays penetrate atomic layers, but are also reflected by them. Measuring distances (d) between units in crystals by X-ray diffraction is done by the Bragg method. The units in each Bragg plane act as the X-ray scattering sources and the X-ray beam striking the crystal will act as if it had been reflected from these evenly spaced planes. This will also give rise to reinforcement of the beam at certain angles and destruction at others,

so that the spacing between the planes can be determined. The condition for reinforcement is that λ, the wavelength of the X-ray and d, the distance between planes, are related to the angle of incidence (and "reflection") by the Bragg equation 4.1 (Verryn, 2000). W.L. Bragg devised a simple approach to consider X-ray diffraction, based on the reflection of X-rays by planes of atoms. It was concluded that the condition for X-ray diffraction is

$$2d \sin \theta = n\lambda \qquad (4.1)$$

where n is an integer (1,2,3 etc.) called the order of reflection. If a single crystal is placed in a monochromatic X-ray beam, then diffraction would only occur if the Bragg equation was being obeyed for a particular family of planes. Although the crystal contains a number of families of planes it would be mere chance that a particular family was at the correct angle θ to satisfy the Bragg condition. If the crystal is rotated, then sooner or later a position would be reached when a particular family of planes was satisfying the Bragg condition and a reflection would "shoot out". Since the maximum value of sin θ is unity, then for a given wavelength of X-rays, there is a lower limit to the spacing, d, that can give observable diffraction lines, viz., $d_{min} = \lambda / 2$ (Whiston, 1987).

By powdering a crystal, the crystal structure is not destroyed but millions of very small crystals pointing in all possible directions are produced. Thus if the powdered crystal is placed in a monochromatic X-ray beam, then for any particular family of planes, there will be at least a few having those planes satisfying the Bragg equation, compared to a single crystal (Whiston, 1987).

4.2.4 The powder diffractometer

The layout of a typical powder diffractometer is given in Figure 4.3. A flat specimen is mounted on a turntable around which moves a detector. As the sample rotates, so the angle θ between the incident beam and the sample changes. Whenever the Bragg condition is fulfilled, X-rays are reflected to the detector. The detector is connected to the specimen table and geared in such a way that when the table rotates through θ degrees, the detector rotates through 2θ degrees. This results in the detector always being in the correct position to receive rays reflected by the sample.

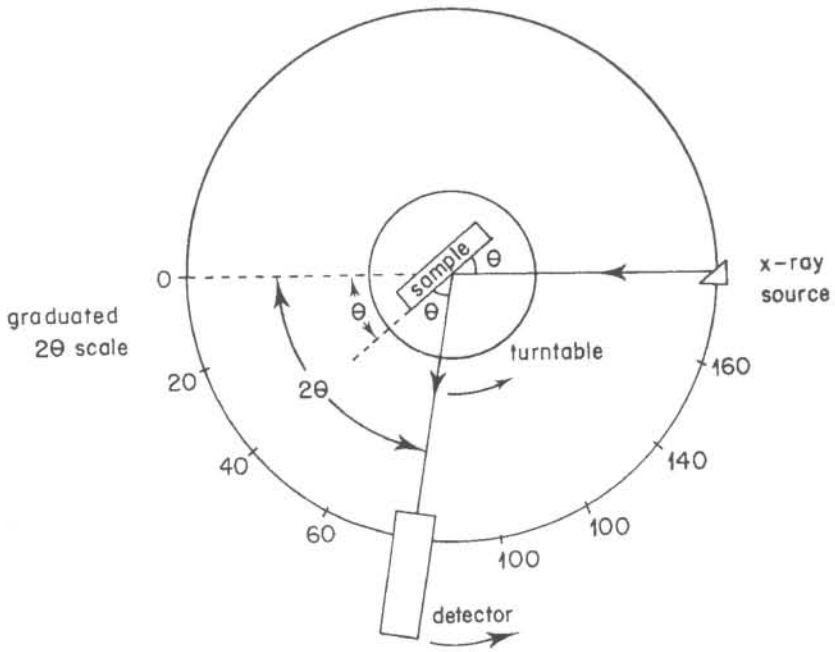

Figure 4.3 Layout of powder diffractometer (Whiston, 1987)

To record a diffraction pattern, the detector is positioned at or near 0° on the graduated 2θ scale and then driven by a motor at constant speed, e.g. 2° per minute. Alternatively, the detector may be driven clockwise from about 170°. The X-rays reaching the detector are registered and displayed on a recorder as a series of peaks on top of background due to white radiation.

Figure 4.4 depicts the powder diffractometer in detail. In practice a divergent beam of X-rays is produced from the source (A). The X-rays diffracted by the sample (B) converge to a focus at the slit (C) and enter the detector (D). E and F are slit systems which define and collimate the incident and diffracted beam respectively. The detector is an electronic device called a counter. It converts the X-rays diffracted by the sample into electrical pulses in the circuit to which they are connected. The number of pulses produced is directly proportional to the intensity of the beam entering the counter. The particular circuit used depends on whether the diffractometer is being used in the scanning mode (ratemeter circuit), for line profile studies, or in the stationary mode (scaler-timer circuit), for accurate intensity measurement.

The powder diffractometer uses a proportional counter or scintillation counter. The counter depends on the ability of X-rays causing atoms to ionise: either of a gas (proportional) or of a solid (scintillation). The counter rotates at twice the speed of the specimen to detect X-rays. The reflections are recorded as a series of peaks together with a scale of 2θ. Bragg angles are simply read of the diffractometer trace and rough values of relative intensity are derived from peak heights above background (Whiston, 1987).

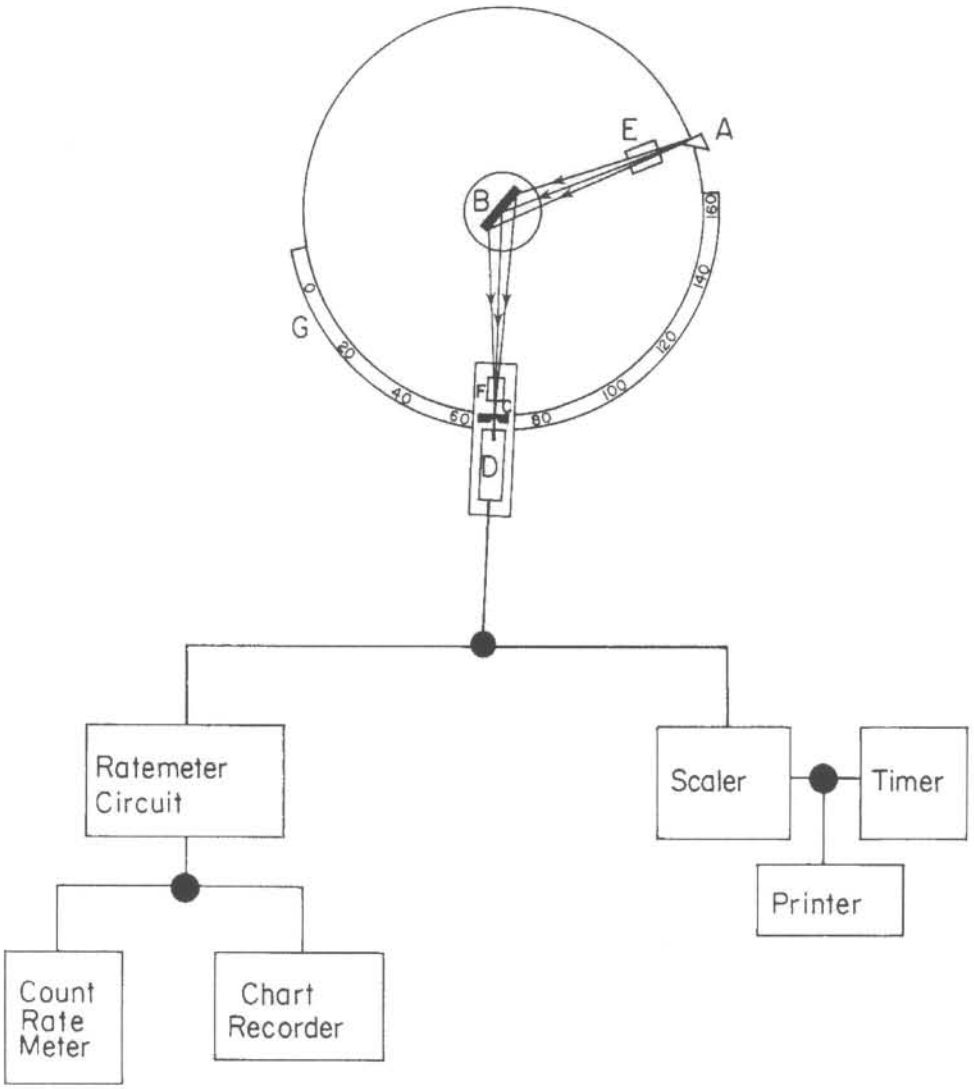

Figure 4.4 Layout of powder diffractometer and detector circuits (Whiston, 1987)

4.2.5 Sample preparation for XRD analysis

A crystalline powder must meet certain specifications in order to obtain a satisfactory powder pattern. The important factors requiring attention in sample preparation (Verryn, 2000) are:

- crystallite- or grain size,
- sample thickness,
- preferred orientation,
- sample homogeneity,
- strain- or cold-working (mainly in metals) and
- surface planarity.

4.2.5.1 Preparation of powders

The number of crystallites contributing to each reflection must be large enough to generate signals of reproducible intensity. Samples should be ground to a crystallite size of < 15 μm, or even better < 5 μm. The surface area of the sample irradiated also influences the counting statistics. A sample can also be ground to fine, making it amorphous to X-ray diffraction.

4.2.5.2 Sample thickness

The sample thickness required is closely linked to the depth of X-ray penetration. Considering a flat specimen, the thickness of the sample must be great enough to give maximum diffracted intensity. A criterion for this condition is:

$$\mu t \geq 3.2 \, (\rho / \rho') \sin \theta \qquad (4.2)$$

where t is the sample thickness in centimetres, μ and ρ are, respectively the linear absorption coefficient and the density of the solid material composing the powder, and ρ' is the density of the powder including interstices (Verryn, 2000).

4.2.5.3 Preferred orientation

Each grain in a polycrystalline aggregate usually has a crystallographic orientation different from that of its neighbours. Considered as a whole, the orientations of all the grains may be randomly distributed in relation to some selected frame of reference, or they may tend to cluster about some particular orientation. Any aggregate characterised by such a condition is said to have "preferred orientation". This can be greatly reduced through the reduction of the crystallite size. The method of mounting the sample and procedures such as back and side filling can be followed to reduce preferential orientation.

4.2.5.4 Small samples

Sample support and position become very important when extremely small quantities of sample are to be analysed. Single crystals (e.g. fluorite, calcite, MgO, Si, quartz) are effective sample supports. The sample must then be placed in the centre of the X-ray beam. This is called the Zero Background Holder (ZBH) technique and can be used on samples as small as 1.0 mg.

4.2.5.5 Special samples

Slightly reactive, hygroscopic materials, slurries and liquids can be sealed by placing them in a sample holder and covering them with a thin film or even cellophane tape (the diffraction pattern of the sealing material must be recorded and subtracted from the sample).

4.2.6 Qualitative phase analysis

It is possible to identify an unknown solid from its unique powder pattern. Every crystalline substance has a unique X-ray powder pattern because line position depends on unit cell size and line intensity depends on the type of atoms present and on their arrangement in the crystal. A characteristic set of d and I/I_1 values can be derived from the unique X-ray powder diffraction pattern of every crystalline substance. These values are used to identify materials in conjunction with the JCPDS Powder Diffraction

File (PDF). The PDF is a collection of single-phase X-ray powder diffraction patterns in the form of tables of interplanar spacings (d) and relative intensities (I/I_1). Most known crystalline phases are recorded here.

This approach will not work well with multi-component mixtures due to overlapping reflections and phases occurring in low concentrations since only a few of their lines will show up. A mixture of two or more substances gives a diffraction pattern made up of the superimposed patterns of the individual components. A number of quantitive methods exist to distinguish between the individual substances. One method requires an internal standard, another requires an external standard and another does not require a standard at all (Whiston, 1987). These will not be discussed in detail since the qualitative method of analysis was mainly used in this study.

4.3 Thermogravimetric and Differential thermal analysis

Thermogravimetry (TG) is a technique in which the weight of a sample is measured as a function of temperature, whilst it is subjected to a controlled heating programme. TG especially examines reactions under participation of volatile components. Evaporation- and decomposition processes are typical examples of reactions which involve a mass loss. An increase in mass can be observed for oxidation reactions. TG provides quantitative information on weight change processes and enables the stoichiometry of a reaction to be followed directly (Dodd and Tonge, 1987), e.g.,

$$\text{Reactant}_{(\text{solid})} \rightarrow \text{Product}_{(\text{solid})} + \text{Gas} \qquad (4.3)$$

or,

$$\text{Gas} + \text{Reactant}_{(\text{solid})} \rightarrow \text{Product}_{(\text{solid})} \qquad (4.4)$$

Differential thermal analysis (DTA) is a technique in which the difference in temperature (ΔT) between the sample and an inert reference material, is measured as a function of temperature. A controlled thermal programme is operative. When a material undergoes a change in its physical state, or when it reacts chemically, heat is either absorbed or liberated. This corresponds to endothermic or exothermic changes respectively. DTA is particularly useful for investigating such thermal energy changes. The DTA peak area is related to both the energy change and the sample size according

to the relationship (Warrington and Höhne, 1994):

$$\Delta H \cdot m = K \int \Delta T \cdot dt \qquad (4.5)$$

where ΔH = enthalpy of reaction
m = sample mass
K = proportionality constant (temperature-dependent)
ΔT = $T_{sample} - T_{reference}$

DTA curves are useful both qualitatively and quantitatively since the positions and profiles of the peaks are characteristic of the sample. The curve may be thought of then, as a kind of "thermal fingerprint". The appearance though of DTA curves is markedly influenced by experimental factors.

4.3.1 Simultaneous TG-DTA

Thermal methods are dynamic techniques in which heating (or cooling) is applied to a sample. The recorded curve depends not only on the nature of the sample, but also on the experimental conditions employed. These include, e.g. heating/cooling rate, atmosphere, sampling characteristics, etc. It is therefore often difficult to correlate the results of two different sets of thermal measurements. The use of simultaneous thermal measurements are preferable, because the thermal measurements are directly comparable to one another (Dodd and Tonge, 1987). They follow similar regimes of heating and atmosphere control and should show the thermal events in a complementary manner. Simultaneous execution means, that both measuring techniques will be applied at the same time and on the same sample.

The NETZSCH STA 409 simultaneous TG-DTA instrument was used in this investigation. Most thermal analysis systems consists of four major parts:

- the electrobalance and its controller,
- the furnace and temperature sensors,
- the programmer or computer and
- the recorder, plotter or data acquisition device.

Figure 4.5 depicts the measuring part of the NETZSCH STA 409. It consists of a casing in which the sample carrier system and the balance are housed and a furnace with a hoisting device.

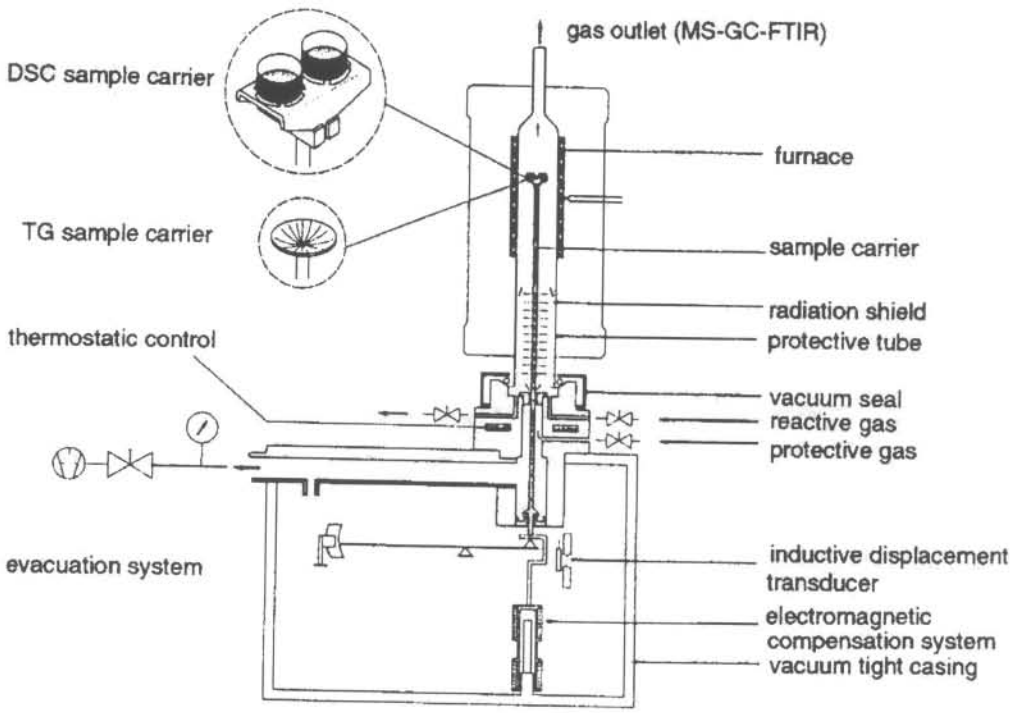

Figure 4.5 Structure of the measuring part of the Netzsch STA 409 simultaneous TG-DTA (Haines, 1995)

4.3.1.1 The balance

The balance transmits a continuous measure of the mass of the sample to the recording system (computer). The STA 409 contains a high-sensitive analytical balance for measuring the mass change of the sample as a function of temperature or of time. It works according to the principle of the substitution beam balance (Netzsch-Gerätebau). As a change in weight occurs and the balance beam starts to deviate from its normal position, a sensor detects the deviation and triggers the restoring force to bring the balance beam back to the null position (Dodd and Tonge, 1987).

4.3.1.2 Sample carrier system

The sample carrier system is connected to the balance. It contains the thermocouples to measure the temperature and the temperature difference. If both thermocouple beads at the sample crucible and the reference crucible, respectively are at different temperatures, a voltage proportional to the temperature difference will occur. The reference is used to measure the temperature because the sample temperature does not increase linearly during a thermal effect.

4.3.1.3 Furnace

The furnaces used are generally non-inductively wound electrical resistance heaters, that ensures linear heating rates over a wide temperature range and an isothermal mode of operation. The furnace should have a zone of uniform temperature which is considerably longer than the sample plus holder. The tube furnace of the STA 409 produces maximum temperatures of approximately 1400°C. It is heated with a resistance wire coil. For regulation of the furnace temperature a control thermocouple (Pt10%Rh-Pt), that is chemically inert at high temperatures, is built in (Netzsch-Gerätebau).

4.3.1.4 Programmer

The programmer is directly linked to the furnace and remains in control of the furnace throughout the experiment. A furnace programmer normally supports a wide range of heating and cooling rates, as well as precise isothermal control. The signal from the furnace (or control) thermocouple is transmitted to the programmer and the temperature it represents is compared with that required by the programme set by the operator. If the temperature is too low, the system must respond by supplying more power to the furnace, and if too high, by reducing the power. The response times of the controller and of the furnace govern the thermal lag of the instrument and hence the range of heating rates that is achievable.

4.3.1.5 Data acquisition

The computer makes the collection, interpretation, storage and retrieval of instrumental data easier. During data acquisition the sample weight as a function of temperature, is continuously recorded. The computer allows the user to calculate the results of an experiment easy and accurately (Haines, 1995; Dodd and Tonge, 1987).

4.3.2 Factors affecting TG curves

The shape of TG curves yields useful information about weight losses and about the temperature range over which a particular sample appears to be stable or unstable. It is vital to appreciate that the actual experimental conditions under which thermogravimetry is performed can profoundly affect the characteristics of the corresponding TG curve. It is important not to attach undue importance to the temperatures at which reactions involving weight changes appear to commence, or finish, on a TG curve. The term "procedural decomposition temperature" is often used in literature. It indicates that a decomposition temperature does not have a fixed value, but depends on the experimental procedure employed to investigate it.

The following factors affects TG curves (Dodd and Tonge, 1987; Warrington and Höhne, 1994):

4.3.2.1 Heating rate

It has been found experimentally that the degree of decomposition of a material at a given temperature, increases with decrease in heating rate. Slower heating rates give more time for decomposition to occur. The shape of the TG curve will thus be influenced by the heating rate. More specifically the procedural decomposition temperature (T_i) and also T_f (the procedural final temperature) will decrease with decrease in heating rate. Slower heating rates are useful to resolve inflections in a TG curve into a plateau.

4.3.2.2 Sample size

The greater the mass of sample, the poorer the resolution of the TG record will be. This is due to the significant temperature gradient within a large sample and also the greater difficulty of volatile products escaping from a large sample. This tends to increase the temperature at which sample decomposition occurs. Small samples and a thin layer of powder are thus preferred. Particle size effects and the degree to which a sample is packed can also influence the TG results.

4.3.2.3 Crucible shape

The sample container must not react chemically with the sample. A shallow container is preferred since it allows a better exchange between the sample and its gaseous environment, than a deeper crucible shape would.

4.3.2.4 Ambient atmosphere

By changing the ambient atmosphere, the procedural decomposition temperature could be moved. The reaction taking place can also be altered completely by changing the ambient atmosphere around the sample. For example, organic materials undergo oxidation when heated in air and pyrolysis in the absence of oxygen, i.e. under nitrogen or other inert atmospheres.

4.3.2.5 Self generated atmosphere

When a sample produces volatiles as a result of decomposition, the atmosphere in immediate contact with the sample is constantly changing. If these volatiles have difficulty in escaping from immediate contact with the sample, then their presence will slow down further decomposition.

It can be concluded that the optimum conditions (Dodd and Tonge, 1987) for normal TG investigations are:

- a small amount of sample (e.g. a few mg),
- a thin layer of sample,
- an open sample container,
- the sample must not react with the material of the sample container,
- a flow of inert gas (e.g. dry nitrogen) and
- a slow heating rate.

4.3.3 Factors affecting DTA curves

As with thermogravimetric studies the effects of variations in experimental conditions on resultant DTA curves, are numerous, complex and often interactive. The experimental factors that could influence the DTA curves can be divided into two sets:

- sample factors
- instrumental factors

4.3.3.1 Sample factors

a. Amount of sample

In general, large samples lead to an increase in sensitivity (owing to higher heat change) but with a corresponding decrease in resolution. Small samples offers the advantage of sharper peaks and more resolution between the peaks, coupled to a distinct reduction in base-line drift (Pope and Judd, 1977).

b. Particle size

Most DTA experiments are carried out on powdered samples if possible. It is not possible to be absolutely specific about the effect of particle size on the record, since the effect depends upon the type of chemical reaction taking place. For surface reactions and diffusion controlled reactions, changes in particle size may lead to changes in peak temperature, with decreasing peak temperature as the particle size is reduced. The effect of particle size is generally minimal on decomposition reactions which proceed via a mechanism other than diffusion control and for phase transitions.

Fine powders are generally preferable. Samples of similar particle size characteristics should be used when making comparisons between materials (Pope and Judd, 1977).

c. Sample packing

Significant effects on thermal records may be expected when the sample interacts with the atmosphere surrounding it, since tight packing will impede the interaction of sample and atmosphere. The ease of escape of volatiles may also be influenced. It is desirable to have a reproducible method of packing the sample.

d. Heat capacity and thermal conductivity

Heat capacity and thermal conductivity also affect the thermal behaviour of a sample. It varies with the physical state or chemical constitution of the sample as it is exposed to a temperature programme. These two properties will also be affected by the way in which the sample is packed.

e. Diluents

These are materials (which will not react with the sample) that are sometimes employed in thermal analysis to modify some property of the sample. It may be necessary to "bulk up" a small sample in order to fill the container to an acceptable degree, or to reduce the peak area associated with the sample. Glass beads, powdered alumina, iron filings, etc. have been used for such purposes (Dodd and Tonge, 1987).

4.3.3.2 Instrumental factors

a. Heating rate

An increase in heating rate increases the procedural temperature and often increases peak areas to a small degree. It can also decrease the resolution between two adjacent peaks, so slower heating rates are preferable, i.e. between 0.1 and 10 °C min^{-1}.

b. *Sample holder materials*

Glass, ceramic or metal containers are used in DTA. Both the material and the geometrical design of the sample container can affect the subsequent thermal record.

c. *Thermocouples*

The DTA design is usually so that the sample and reference containers are in direct contact with the thermocouples. In such a design the thermocouple location is constant and it is easier to reproduce the results of the DTA experiments.

d. *Atmosphere around sample*

This may be chosen to be static or flowing, active or inert. A flowing gas is normally preferable to a "static" atmosphere, which is liable to change slightly as soon as sample degradation or decomposition occurs. In such cases, it is easier to maintain control via a flowing atmosphere which will sweep away volatile by-products. In general the atmosphere is chosen to be compatible with the process under investigation.

4.4 Surface area

The specific surface area of a solid is one of the first things that must be determined if any detailed physical and chemical interpretation of its behaviour as an adsorbent is to be possible. Each method for surface area determination involves the measurement of some property that is observed qualitatively to depend on the extent of surface development and that can be related by means of theory to the actual surface area (Adamson, 1990).

The most important methods for specific surface area analysis of solids are based on adsorption. The following two assumptions are made (Mikhail and Robens, 1983):

a. It is possible to determine the quantity of adsorbate required for complete coverage of the substrate surface by a monolayer.

b. The cross-sectional area of an adsorbed molecule is known and independent of the substrate (adsorbent)

Adsorption (strictly, physical adsorption) is defined as the enrichment (i.e. positive adsorption or simply adsorption) or depletion (i.e. negative adsorption) of one or more components in an interfacial layer. Adsorption is brought about by the forces acting between the solid and the molecules of the gas. These forces are of two main kinds - physical and chemical - and they give rise to physical (or "van der Waals") adsorption and chemisorption respectively. The adsorption of a gas by a solid can, in principle, be made to yield valuable information as to the surface area and pore structure of the solid (Gregg and Sing, 1982).

4.4.1 BET theory

Brunauer, Emmett and Teller (BET), made a significant advance in the interpretation of the physical adsorption process. Starting with the basic concepts of Langmuir, these authors assumed that the rate of evaporation from the *n*th adsorbed layer was equal to the rate of condensation of the (*n*–1)th layer. From this assumption it proved possible to derive the BET equation (Hair, 1967).

One form of the well-known BET equation that describes the adsorption of a gas upon a solid surface (Micromeritics Instruction manual, 1985; Mikhail, 1983) is:

$$\frac{\left(\frac{P}{P_0}\right)}{V\left[1-\left(\frac{P}{P_0}\right)\right]} = \frac{1}{V_m C} + \left[\frac{(C-1)}{V_m C}\right]\left(\frac{P}{P_0}\right) \qquad (4.6)$$

where V = the volume (at standard temperature and pressure, STP) of gas adsorbed at pressure P

P_0 = the saturation pressure which is the vapour pressure of liquified gas at the adsorbing temperature

V_m = the volume of gas (STP) required to form an adsorbed monomolecular layer

C = a constant related to the energy of adsorption

The BET method is applied to the calculation of specific surface area, S ($m^2\ g^{-1}$), giving the monolayer adsorbed gas volume, V_m (STP), using the relation (Micromeritics Instruction manual, 1985):

$$S = \frac{V_m A N}{M} \tag{4.7}$$

where A = Avogadro's number (6.023×10^{23} molecules mol^{-1})

N = the area of each adsorbed gas molecule

M = the molar volume of the gas

In this study the FlowSorb 2300 was used for the measurement of surface area of the samples. This instrument measures surface area of granulated and powdered solids or porous materials, by determining the quantity of a gas that adsorbs as a single layer of molecules, a so-called monomolecular layer, on a sample. This adsorption is done at or near the boiling point of the adsorbate gas. Under specific conditions, the area covered by each gas molecule is known within relatively narrow limits. The area of the sample is thus directly calculable from the number of adsorbed molecules, which is derived from the gas quantity at the prescribed conditions and the area occupied by each. For a nitrogen and helium mixture of 30 volume % nitrogen, conditions most favourable for the formation of a monolayer of adsorbed nitrogen are established at atmospheric pressure and the temperature of liquid nitrogen (Micromeritics Instruction manual, 1985).

Of the large number of readily available gases, the proportion that is suitable for surface area determination is quite small, because a number of conditions have to be met. These include that the adsorptive must be chemically inert towards the solid; the saturation vapour pressure, P_0, at the working temperature must be large enough to allow the accurate measurement of the relative pressure over a reasonably wide range ($\sim 0.001 < P / P_0 < \sim 0.5$); but, for reasons of experimental convenience, P_0 should not exceed 1 to 2 atmospheres. In addition, the working temperatures tend to be limited to those which can be obtained with the common refrigerants (e.g. nitrogen, oxygen,

carbon dioxide slush and melting ice). It is also desirable that the shape of the adsorbate molecule shall not be far removed from spherical symmetry, so as to minimise the uncertainty in a_m (molecular area of the adsorbate, i.e. the area occupied by an adsorbate molecule in the completed monolayer) arising from the different possible orientations on the surface. These rather exacting requirements explain why only five adsorptives are suitable enough for surface area determinations. These include nitrogen, argon, krypton, n-butane and benzene. The most commonly used one is nitrogen at its boiling point, 77 K (Gregg and Sing, 1982).

Surface area measurement can be accomplished either by a simplified, single point procedure or by the more conventional multipoint BET technique.

The single point determination method was used in this investigation. In single point surface area determinations, the constant C of equation 4.6 is typically a relatively large number, i.e. C>>1, from which equation 4.6 reduces to

$$\frac{\left(\frac{P}{P_0}\right)}{V\left[1-\left(\frac{P}{P_0}\right)\right]} = \left(\frac{1}{V_m}\right)\left[\left(\frac{1}{C}\right)+\left(\frac{P}{P_0}\right)\right] \tag{4.8}$$

If $P/P_0 >> 1/C$, then equation 4.8 can be changed and rearranged to equation 4.9

$$V_m = V\left[1-\frac{P}{P_0}\right] \tag{4.9}$$

By substituting equation 4.9 into equation 4.7 the following equation is obtained

$$S = \frac{VAN\left[1-\frac{P}{P_0}\right]}{M} \tag{4.10}$$

from which the sample surface area is readily determined once the volume V of gas adsorbed is measured and appropriate values for the other terms are incorporated.

For nitrogen gas adsorbed from a mixture of 30 mol % nitrogen and 70 mol % helium using a liquid nitrogen bath, the values are arrived at as follows:

- The volume (V) of gas with which the Flowsorb 2300 is calibrated is injected at room temperature and the prevailing atmospheric pressure. This volume must be multiplied by the ratio

$$\frac{273.2}{\text{Room temperature } (^{\circ}\text{K})} \times \frac{\text{Atmospheric pressure (mm Hg)}}{760} \qquad (4.11)$$

  to convert it to standard conditions (0 °C and 760 mm Hg).

- Avogadro's number (A) is 6.023×10^{23} molecules mol^{-1}
- Molar volume (M) of a gas at standard conditions is 22414 cm^3 mol^{-1}
- The accepted value for the area N of a solid surface occupied by an adsorbed nitrogen molecule is 16.2×10^{-20} m^2
- Adsorption takes place at atmospheric pressure, thus the pressure P is

$$P = \frac{\%N_2}{100} \times \text{Atmospheric pressure (mm Hg)} \qquad (4.12)$$

- P_0, the saturation pressure of liquid nitrogen is typically a small amount greater than atmospheric due to thermally induced circulation, dissolved oxygen and other factors. With relatively pure liquid nitrogen, the saturation pressure is typically about 15 mm Hg greater than atmospheric pressure.

When these values, for a 30% N_2 / 70% He mixture adsorbed at liquid nitrogen temperature when room temperature is 22 °C and atmospheric pressure is 760 mm Hg, are substituted into equation 4.10 the surface area obtained is 2.84 x V m^2. For calibration purposes, this means that a syringe injection of V = 1.00 cm^3 of nitrogen (at 22 °C and 760 mm Hg) should produce an indicated surface area of 2.84 m^2 (Micromeritics Instruction manual, 1985).

4.4.2 Accuracy

A high degree of accuracy is out of the question where evaluation of specific surface from adsorption data is concerned. A divergence of at least ±10% from the actual area of the solid must be reckoned with, owing to theoretical factors as yet not susceptible of accurate quantitative assessment. The attainment of this level of accuracy is a notable achievement in a field where, prior to the development of the BET method, even the order of magnitude of the specific surface of highly disperse solids was in doubt. The adsorption method still provides the only means of determining the specific surface of a mass of non-porous powder or of a porous solid large enough to constitute a representative sample (Gregg and Sing, 1982).

4.5 Scanning electron microscopy

The scanning electron microscope (SEM) is one of the most versatile instruments available for the examination and analysis of the microstructural characteristics of solid objects. SEM permits the observation and characterisation of heterogeneous organic and inorganic materials and surfaces on such a local scale. The signals obtained from specific emission volumes within the sample can be used to examine many characteristics of the sample, e.g. composition, surface topography, crystallography, etc. The primary reason for the SEM's usefulness is the high resolution that can be obtained when bulk objects are examined (Goldstein *et al.*, 1992). Another important feature of the SEM is the three-dimensional appearance of the specimen image, a direct result of the large depth of field, as well as to the shadow-relief effect of the secondary and backscattered electron contrast.

The scanning electron microscope utilises a focused beam of high energy electrons that systematically scans across the surface of the specimen. The interaction of the beam with the specimen produces a large number of signals at or near the specimen surface. These interactions include lower energy electrons, termed secondary electrons. The low energy of the secondary electrons makes them a conveniently collected signal for scanning electron microscopy since they can be easily drawn to a positively biased detector system. The electron signal is eventually converted to an electronic signal which is portrayed on a cathode ray tube (essentially a television screen) (Postek *et al.*, 1980).

4.5.1 Operating principles of the SEM

The following section provides a brief outline of the basic operating principles of the scanning electron microscope.

Electron lenses produce a small spot: The electron column consists of an electron gun and two or more electron lenses, operating in a vacuum. A source of electrons is produced by the electron gun, which is accelerated to an energy in the range 1–40 keV. The beam diameter produced directly by the conventional electron gun is too large to generate a sharp image at high magnification. Electron lenses are used to reduce the diameter of this source of electrons and place a small, focused electron beam on the specimen as shown schematically in Figure 4.6.

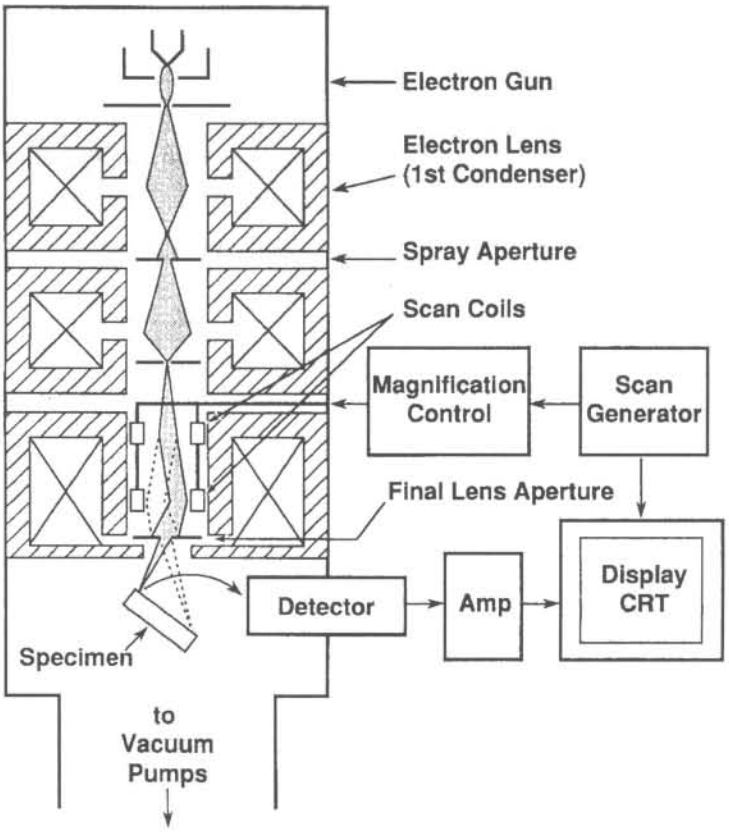

Figure 4.6 Schematic drawing showing the electron column, the deflection system and the electron detectors (Goldstein *et al.*, 1992)

In most SEMs, the electron beam emerges from the final lens into the specimen chamber, where it interacts with the near-surface region of the specimen to a depth of approximately 1 μm and generates signals used to form an image. The actual formation of an image requires a scanning system to construct the image point by point.

Deflection system controls magnification: In order to produce contrast in an image, the signal intensity from the beam-specimen interaction must be measured from point to point across the specimen surface. The function of the deflection system is to scan the beam along a line and then displaces the line position for the next scan so that a rectangular raster is generated on both the specimen and the viewing screen. Two pairs of electromagnetic deflection coils (scan coils) are used to control the raster of the beam. The first pair bends the beam off the optical axis of the microscope and the second pair bends the beam back onto the axis at the pivot point of the scan (Figure 4.6). The magnification *M* of the specimen image is the ratio of the linear size of the viewing screen, known as the cathode ray tube (CRT), to the linear size of the raster on the specimen. Thus, increased magnification may be obtained by exciting the scan coils less strongly so that the beam deflects a smaller distance on the specimen.

Electron detectors collect the signal: The interaction of the electron beam with the specimen causes the generation of many signals, which may be used to modulate the intensity of the viewing CRT and produce an image. The two signals most often used to produce images are secondary electrons (SEs) and backscattered electrons (BSEs) (Figure 4.7.a).

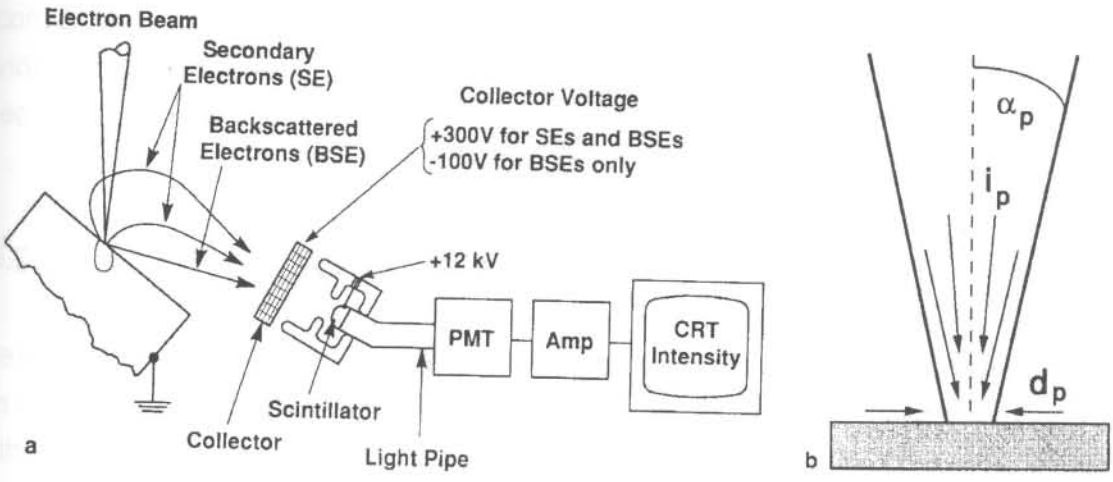

Figure 4.7 **a.** **Diagram showing backscattered and secondary-electron emission and Everhart-Thornley (E-T) detector**

b. **Diagram showing the point where the electron beam meets the specimen. The three major electron-beam parameters are defined: electron probe diameter d_p, electron probe current i_p and electron probe convergence α_p (Goldstein *et al.*, 1992)**

Secondary and backscattered electrons are collected by the Everhart-Thornley (E-T) electron detector. This detector consists of a scintillator, a light pipe and a photomultiplier tube. The E-T detector has a wire mesh screen in front of it at a potential of about +300 V. This positively charged screen draws the low-energy secondary electrons into the detector from anywhere in the specimen chamber, but to form a high quality SEM image the strongest source of SEs should be located at the point where the beam enters the specimen surface.

All electrons entering the E-T detector are accelerated by a voltage of +12 kV placed on the aluminium coating of the scintillator. The now-energetic SEs strike the scintillator material and produce light that travels down a light pipe to the photomultiplier tube (PMT), which converts the light to an amplified electrical signal. Variations in signal occurring as the beam moves over the specimen surface provide the intensity changes that are seen on the viewing screen as an image. It should be clear that any signal collected and suitably amplified may be used to form an image in the SEM.

Camera records the image: Most SEMs have a separate CRT viewed by a camera to record slow-scan images on Polaroid or conventional wet-processed film. Alternatively, a video printer may be used to convert the record CRT signal to a positive image on special printing paper.

4.5.2 Specimen preparation

The most critical part of SEM is adequate preparation of the specimen. The procedures can vary greatly from the simple preparation of inert geological or metallurgical samples to the complex methods used for many biological tissues. Specimen preparation is often the factor limiting the quality of a micrograph. In the following section the various aspects relating to specimen preparation (Postek *et al.*, 1980) will be discussed.

4.5.2.1 Specimen selection

A variety of factors limits the selection of a sample material to be viewed by SEM. All of the factors that determine proper specimen selection manifest themselves when the investigator determines the size and number of the samples to be observed. A first important consideration in determining specimen size is the preparatory procedure. A small specimen is generally desirable, but a small specimen that has been separated from a much larger one can result in a second problem. The properties of the smaller portion characterised by a scanning electron microscope study may not be representative of the bulk of the material. This can be overcome by selecting a large number of samples at random from the bulk material.

The size of the specimen is also compromised by the capacity of the instrument. The surface on which the specimen is to be mounted and the space in which it will reside during viewing are two major limitations.

A final factor which deserves consideration during specimen selection is the magnification range to be used during observation. Magnification, resolution and depth of field are determined in part by the working distance and proper specimen positioning relative to the final lens and the signal detector. Such specimen manipulations may be limited by the sample or stub size.

4.5.2.2 Surface preparation

In view of the fact that SEM is often used to view the detailed surface structure of a specimen, consideration must be given to the state of the specimen surface before it is viewed. Several types of surface preparation techniques have been in use to prepare the surface of a specimen for analysis. These metallurgical techniques are designed to expose areas of interest within the specimen for analysis. These include grinding and polishing techniques, etching techniques of several types and fracture techniques, some of which have been adapted to biological research. Such techniques are useful in revealing substructure within a specimen (particularly fracturing), however some are also useful in preparing very smooth surfaces for elemental analysis.

4.5.2.3 Fixation

In order for the structural integrity of the specimen to be maintained, fixation is necessary. The aim of fixation is to preserve the fine structure of the biological cells and to make them immune to alteration or distortion during subsequent preparatory treatments. Two distinct types of fixation may be differentiated, namely chemical and mechanical. Chemical fixation relies upon chemical means to kill and fix the tissue, whereas mechanical fixation relies upon rapid freezing for structural stability.

4.5.2.4 Dehydration

When specimens to be observed contain water or reside in an aqueous environment, it is difficult to examine them in an evacuated column at temperatures above freezing, since water is volatile. Water loss from the specimen can result in both contamination of the column, as well as tremendous damage to the topography of the sample. A variety of methods have been utilised to remove water from materials, with emphasis placed on minimising the distortion of the material surface during the procedure. Critical point drying is the most commonly used method for specimen dehydration, although it has some drawbacks. Dehydration without structural damage remains, therefore, a major problem in the preparation of wet samples for observation.

4.5.2.5 Mounting

The specimen stub is the support for the sample material. It may be fashioned from a section of polished metal rod or more elaborately machined metallic material. The sample must be securely attached to the stub so that during manipulations inside the specimen chamber it will not fall off. Additionally, the stub is made out of conductive material (often aluminum or brass) to conduct current produced by the electron beam away from the specimen. In order to optimise image quality, several factors need be taken into consideration before the specimen is mounted on a stub: the material the stub is made of; the signal to be detected from the sample; the stub size; the adhesive used to attach the specimen to the stub surface; and the orientation of the sample inside the specimen chamber.

4.5.2.6 Coating non-conductive specimens

Materials that do not naturally conduct electricity and heat cause problems in the scanning electron microscope unless they can be made conductive by some method. Problems include the effects known as "charging" (imparts a negative charge to an insulated surface that cannot be dissipated) and "beam damage" (damage caused by heating, which may appear as cracks in the specimen surface). Coating specimens with a thin layer of a conductive material helps to overcome these problems. An additional advantage of coating may be an improvement in the strength of the secondary electron signal from the specimen surface.

The choice of an appropriate coating material and method for its application must take into account several factors. These include the type of observation to be made (e.g. secondary electron imaging versus x-ray microanalysis). The type of coating material may determine the method of application (e.g. vapour deposition of a metal versus chemical deposition). Properties of the sample such as molecular weight and susceptibility to heat damage will also determine the type of coating material and the method of deposition.

4.6 Infrared spectroscopy

Spectroscopic techniques in general have been the most useful tool ever made available to chemists for the investigation of atoms and molecules. Thus, the study of molecular spectra gives information not only of the dimension of molecules but also of molecular vibrational, rotational and electronic states.

Infrared spectroscopy is based on the interaction of an oscillating electromagnetic field with a molecule. This is only possible if the dipole moment of the molecule changes as a result of a molecular vibration. The infrared absorption spectrum of a compound may be regarded as a sort of "fingerprint" of that compound. It also furnishes a more definitive test for functional groups than does chemical analysis. In addition to the characteristic nature of the absorption, the magnitude of the absorption due to a given species is directly relatable to the concentration of that species.

4.6.1 Theory of infrared absorption

If two quantised energy levels E_1 and E_2 are placed in an electromagnetic field and the difference in energy between the two states is equal to a constant multiplied by the frequency of the incident radiation ν, a transfer of energy between the field and the molecule can occur. Thus,

$$\Delta E = h\nu \qquad (4.13)$$

where h = Planck's constant (6.626×10^{-34} J.s)

All spectra arise from the absorption or emission of radiation that occurs between definitely quantised energy levels when the above condition is satisfied. When ΔE is positive, the molecule absorbs radiation and an absorption spectrum is obtained. When ΔE is negative, radiation is emitted during the energy transfer and an emission spectrum is obtained. When the energetics of equation 4.13 are satisfied (in conjunction with certain quantum-mechanical selection rules) a spectrum unique to the molecule under investigation is obtained. This spectrum is usually represented as a plot of the light intensity against the frequency and a peak occurs whenever the conditions of equation 4.13 are satisfied (Hair, 1967).

Both atoms and molecules give rise to spectra. The difference between the atomic and molecular spectra lies in the different energy levels involved in the transitions. In the atom the absorptions represent transitions between the different allowed energy levels for the orbital electrons. In the case of a molecule, the atoms within the molecule vibrate and the molecule as a whole rotates and thus the total energy contributions are represented by the equation:

$$E_{total} = E_{electronic} + E_{vibrational} + E_{rotational} + E_{translational} \qquad (4.14)$$

The separate energy levels are quantised and only certain transitions of electronic, vibrational and rotational energy are possible. Translational energy is usually sufficiently small to be ignored. Transitions between vibrational levels in the same electronic state give absorption in the infrared region of the spectrum.

4.6.2 Vibrational spectra

Infrared spectra originate from the different modes of vibration and rotation of a molecule. The symmetry and bond strengths of the molecule as a whole determine the number and frequency of the vibrations. At wavelengths above 400 cm^{-1}, the radiation has sufficient energy to cause changes in the vibrational (and also the rotational) levels of the molecule. If the simple case of a diatomic molecule, which can be treated as a harmonic oscillator, is considered, the order of vibrational frequencies can be determined. It can be shown that the frequency of the simple harmonic vibration is given by classical mechanics (Hair, 1967; Vogel, 1961) and it is:

$$\bar{\nu} = \frac{1}{2\pi c}\sqrt{\frac{k}{\mu_m}} \qquad (4.15)$$

where $\bar{\nu}$ = wavenumber (cm^{-1})

k = standard-type force constant

c = velocity of light (3×10^{10} cm s^{-1})

μ_m = reduced mass

The reduced mass of the system (μ_m) is defined by the relationship:

$$\mu_m = \frac{m_1 x m_2}{m_1 + m_2} \qquad (4.16)$$

where m_1 and m_2 are the relative masses of the atoms.

For a vibrational mode to appear in the infrared spectrum and therefore absorb energy from the incident radiation, it is essential that there be a change in dipole moment during the vibration. For a polyatomic molecule a series of absorptions will take place, as radiation is absorbed each time the radiation frequency is in resonance with the natural frequency of a fundamental mode, which is capable of dipolar interaction.

The true internal motions of the molecule, which constitute its vibrational spectrum, are composed of the normal vibrations as a coupled system of these independent inharmonic oscillators. Thus, a molecule is unambiguously characterised by its vibrational spectrum.

4.6.3 Fourier transform infrared technique

All IR spectrometers, whether simple or sophisticated, have certain elements in common. They are the source, optical system, detector and amplifier. The basis of Fourier transform infrared (FT-IR) spectroscopy is the two-beam interferometer designed by Michelson in 1891 and shown schematically in Figure 4.8.A.

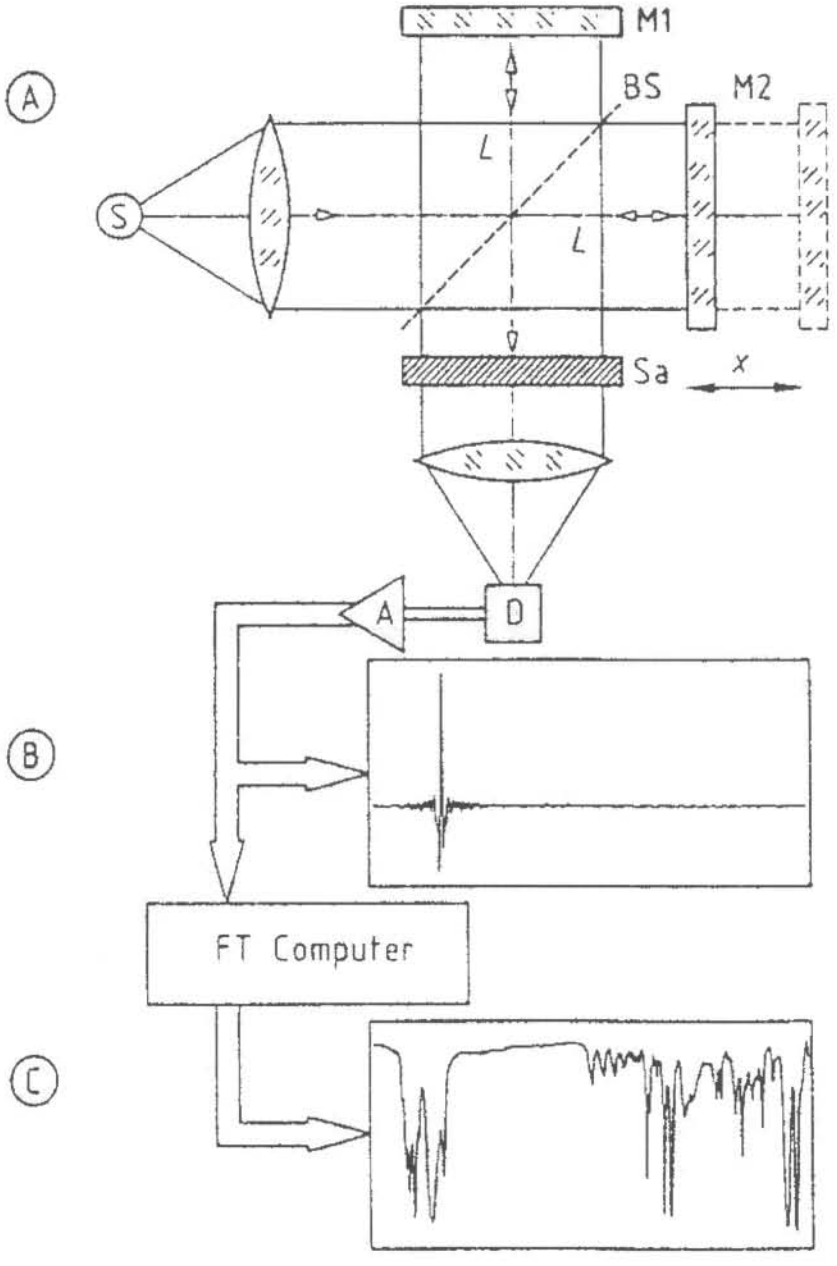

Figure 4.8 A. Schematic diagram of a Michelson interferometer
B. Signal registered by the detector D, the interferogram
C. Spectrum obtained by Fourier transform of the interferogram

S = Radiation source; Sa = Sample cell; D = Detector;
A = Amplifier; M1 = Fixed mirror; M2 = Movable mirror;
BS = Beam splitter; *x* = Mirror displacement (Gremlich, 1994)

The most commonly used source for IR spectroscopy is one that radiates a continuous spectrum approximating a blackbody. In the region 100–4000 cm^{-1} the most popular sources are the Globar, which is a bonded silicon carbide rod and the Nernst glower, which is a mixture of zirconium, thorium and yttrium oxides (Smith, 1979).

The broadband infrared radiation emitted by a thermal source (globar, metal strips, Nernst glower), falls onto a beam splitter which, in the ideal case, transmits half the radiation and reflects the other half. The reflected half, after traversing a distance *L*, falls onto a fixed mirror M1. The radiation is reflected by M1 and, after traversing back along distance *L*, falls onto the beam splitter again. The transmitted radiation follows a similar path and also traverses distance *L*. The mirror M2 of the interferometer can however be moved very precisely along the optical axis by an additional distance *x*. Hence, the total path length of the transmitted radiation is $2(L + x)$.

On recombination at the beam splitter the two beams possess an optical path difference of $\Delta = 2x$. Since they are spatially coherent, the two beams interfere on recombination. The beam, modulated by movement of the mirror, leaves the interferometer, passes through the sample cell and is finally focused on the detector. The signal registered by the detector , the interferogram, is thus the radiation intensity $I(x)$, measured as a function of the displacement *x* of the moving mirror M2 from the distance *L* (Figure 4.8.B). The mathematical transformation, a Fourier transform, of the interferogram, performed by computer, initially provides a so-called single-beam spectrum. This is compared with a reference spectrum measured without the sample to obtain a spectrum analogous to that measured by conventional dispersive methods. This spectrum is stored digitally in the computer, from which it can be retrieved for further use (Figure 4.8.C) (Gremlich, 1994).

A detector must have adequate sensitivity to the radiation arriving from the sample over the entire spectral wavenumber region. Two major kinds of detector are used in mid-infrared FT-IR spectrometers. The deuterated triglycine sulfate (DTGS) pyroelectric detector, due to its good response to a wide range of IR frequencies and radiation intensities. The mercury cadmium telluride (MCT) photodetector responds more quickly and is more sensitive than the DTGS detector, but it operates at liquid-nitrogen temperature and has a limited frequency and dynamic range.

4.6.4 Transmission spectroscopy

When light strikes a body, it can undergo one of three transitions. It can be reflected and scattered, it can be absorbed or it can be transmitted. In this study the transmission and reflection spectra of the compounds were obtained.

Transmission spectroscopy is generally used for routine spectral measurements on all kinds of samples. The sample is placed in the light beam of an infrared spectrometer and the intensity of the incident beam is compared with that transmitted by the sample. According to the fundamental relation governing the absorption of radiation as a function of transmittance, parameters that can be determined in transmission spectroscopy are the thickness or the concentration of the sample.

If I_0 is the intensity of monochromatic radiation entering a sample and I is the intensity transmitted by the sample, then the ratio I / I_0 is the transmittance T of the sample. If the sample cell has thickness b and the absorbing component has concentration c, then the fundamental relation governing the absorption of radiation as a function of transmittance is (Gremlich, 1994):

$$T = \frac{I}{I_0} = 10^{-abc} \qquad (4.17)$$

The constant a is called the absorptivity and is characteristic of a specific sample at a specific wavelength.

Transmission spectroscopy requires only simple accessories, such as infrared-transparent windows (e.g. potassium bromide, sodium chloride or thallium bromoiodide) for gases and liquids or a sample holder for solids.

4.6.5 Diffuse reflection spectroscopy

Also known as diffuse reflectance infrared Fourier transform (DRIFT) spectroscopy. Many substances in their natural state, especially powders, but also any solid with a rough surface, e.g. dyed textiles and printed papers, exhibit diffuse reflection. With diffuse reflection incident light is scattered in all directions.

The sample to be analysed is diluted with a nonabsorbing powder such as KBr that ensures deeper penetration of the incident beam and therefore, an increased contribution of transmission and internal reflection components to the DRIFT spectrum. The diffuse reflectance spectrum is usually calculated as the ratio of sample and reference reflectance, with the pure diluent being taken as reference.

Diffuse reflectance accessories have been developed that pay special attention to the optimal reduction of the disturbing specular component, that produces inverted bands. The Praying Mantis diffuse reflectance attachment depicted in Figure 4.9, uses an off-line collection angle incorporating two 6:1 90° off-axis ellipsoidal mirrors. One ellipsoidal mirror focuses the incident beam on the sample, while the radiation diffusely reflected by it is collected by the other. Both ellipsoidal mirrors are tilted forward; therefore the specular component is deflected behind the collecting ellipsoid, permitting the diffusely reflected component to be collected (Gremlich, 1994).

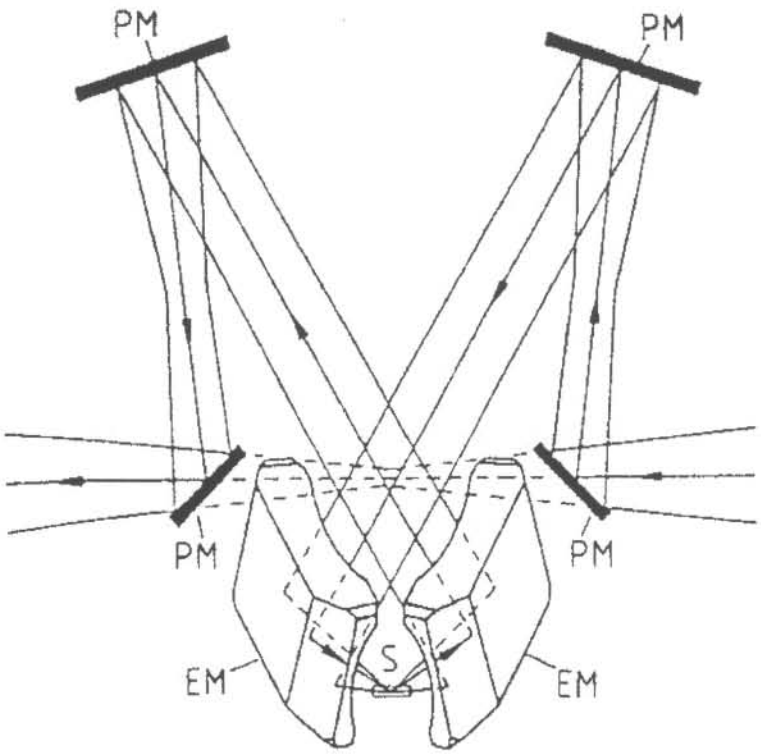

Figure 4.9 Ray diagram of the Praying Mantis diffuse reflectance attachment. EM = Ellipsoidal mirror; PM = Planar mirror; S = Sample (Gremlich, 1994)

4.6.6 Sampling techniques

In infrared spectroscopy, it is relatively easy to obtain spectra from a variety of samples. This includes solids, liquids, gases and polymer films. A choice of sampling techniques exists for all states of matter. The one chosen depends on the application. The sample is contained in a cell having a path which is transparent to the incident infrared radiation. The sample is placed in this path. The parts of the cell in the beam must be constructed of materials that do not themselves absorb radiation. These "windows" are normally alkali halides.

Liquid films is the quickest method for preparing a sample. A small drop of the liquid is placed on a sodium chloride plate and a second plate placed on top. The liquid will spread out to form a thin film. This is then mounted in a cell-holder and placed in the front beam (sample beam) of the instrument.

The sample can also be dissolved in a suitable solvent to form a solution. A cell of known path-length is filled and placed in the spectrometer. The concentration is usually in excess of 0.01 mol dm^{-3}. A suitable solvent should dissolve the compound, be non-polar, should not strongly absorb infrared radiation, be volatile and not be viscous.

Mulls and alkali halide discs are the methods used to prepare solids for analysis. With mulls, the solid is first grinded to reduce the crystal size, then suspended in 1–2 drops of the mulling agent (Nujol (liquid paraffin), Voltalef 3S oil (a halogenated hydrocarbon) or hexachlorobuta-1,3-diene), followed by further grinding until a smooth paste is obtained. The most commonly used alkali halide is potassium bromide which is completely transparent in the commonly scanned region. Here, the solid (a few mg) is mixed with the dry alkali halide (100–200 mg), ground and subjected to pressure in an evacuated die. This sinters the mixture and produces a clear transparent disc (George and McIntyre, 1987).

Gases are analysed with special gas cells. The cells have two taps and can be filled by flushing if the sample is plentiful or by attachment to a vacuum manipulation line.

4.6.7 Spectrum interpretation

The complexity of practical infrared spectroscopy is simplified by three factors:

- the frequencies of many vibrations lie outside the normal scanning range of instruments.
- by no means all vibrations give rise to strong absorption and some vibrations are infrared inactive.
- some bands have very similar frequencies and coalesce.

It has been shown that certain vibrations are confined to one bond, while others could be referred to as coupled and involves many atoms. The first type can be relied on to appear in the spectrum at the same frequency (to a few cm^{-1}) in different molecules, while the second type varies in frequency with small changes in molecular structure. The first type is referred to as a group frequency. Group frequencies are very useful, since the presence of an absorption band at a particular frequency can be interpreted as the presence of a particular functional group. These groups absorb at very nearly the same wavelengths regardless of the molecule in which they are found. Group frequencies represent a rapid, unambiguous means of confirming the presence or absence of the chemical moiety responsible for the absorption.

At frequencies corresponding to values greater than 1500 cm^{-1}, it is possible to assign each absorption band in an infrared spectrum. This is possible since the various regions of the infrared spectrum can be associated with certain fundamental vibrations. Correlation charts that contain the characteristic group absorptions in the infrared region is a useful aid for spectrum interpretation. These charts show the most probable range of absorption frequencies found when a certain group is known to be present. The assignment of each absorption band is no longer true below 1500 cm^{-1}. This region is referred to as "the fingerprint region", since very similar molecules give different absorption patterns at these frequencies. That is, a characteristic pattern is found for individual molecular species. The most important rule in spectral interpretation is to look at the whole spectrum, not to spot a band and jump to conclusions (George and McIntyre, 1987).

4.7 Limiting oxygen index

The limiting oxygen index (LOI) is a test method that may be used to measure and describe the properties of materials, products or assemblies in response to heat and flame under controlled laboratory conditions. It may not be used to describe or appraise the fire hazard or fire risk of materials, products or assemblies under actual fire conditions. Results of this test may be used as elements of a fire risk assessment which take into account all of the factors which are pertinent to an assessment of the fire hazard of a particular end use.

LOI determines the minimum oxygen concentration at which sustained combustion occurs in a flowing mixture of oxygen and nitrogen, using a vertically mounted specimen ignited at the upper end. The test is performed at room temperature. Results are expressed as (Sutker, 1988):

$$LOI = \left[\frac{V_{O_2}}{(V_{O_2} + V_{N_2})} \right] x100\% \qquad (4.18)$$

The LOI test is simple and reproducible and is used to guide development work.

4.7.1 Test method

A standard test method described by the American Society for Testing and Materials (ASTM D2863), for measuring the minimum oxygen concentration to support candle-like combustion of plastics, was followed. The test was conducted by the South African Bureau of Standards (SABS).

A small test specimen is supported vertically in a mixture of oxygen and nitrogen flowing upwards through a transparent chimney. This is depicted in Figure 4.10. The upper end of the specimen is ignited, when burning is supported by the whole of the top end of the specimen. After ignition, the period for which burning continues or the length of specimen burnt, with specified limits for each burning, is measured. If the relevant limits are not exceeded, then the oxygen concentration was not sufficient to sustain burning and the oxygen concentration has to be increased for the following run. If the relevant

limits are exceeded the flame is extinguished. In this case the oxygen concentration exceeded the concentration to sustain burning. The oxygen concentration has to be decreased for the following run. By testing a series of specimens in different oxygen concentrations, the minimum oxygen concentration is determined.

The test specimen dimensions are ±150 mm in length, ±10 mm in width and ±4 mm in thickness for molding materials. Detailed specimen specifications are set out in the standard test method.

The burning characteristics of the material must also be noted during the test. This includes dripping, charring, erratic burning, glowing combustion or after-glow.

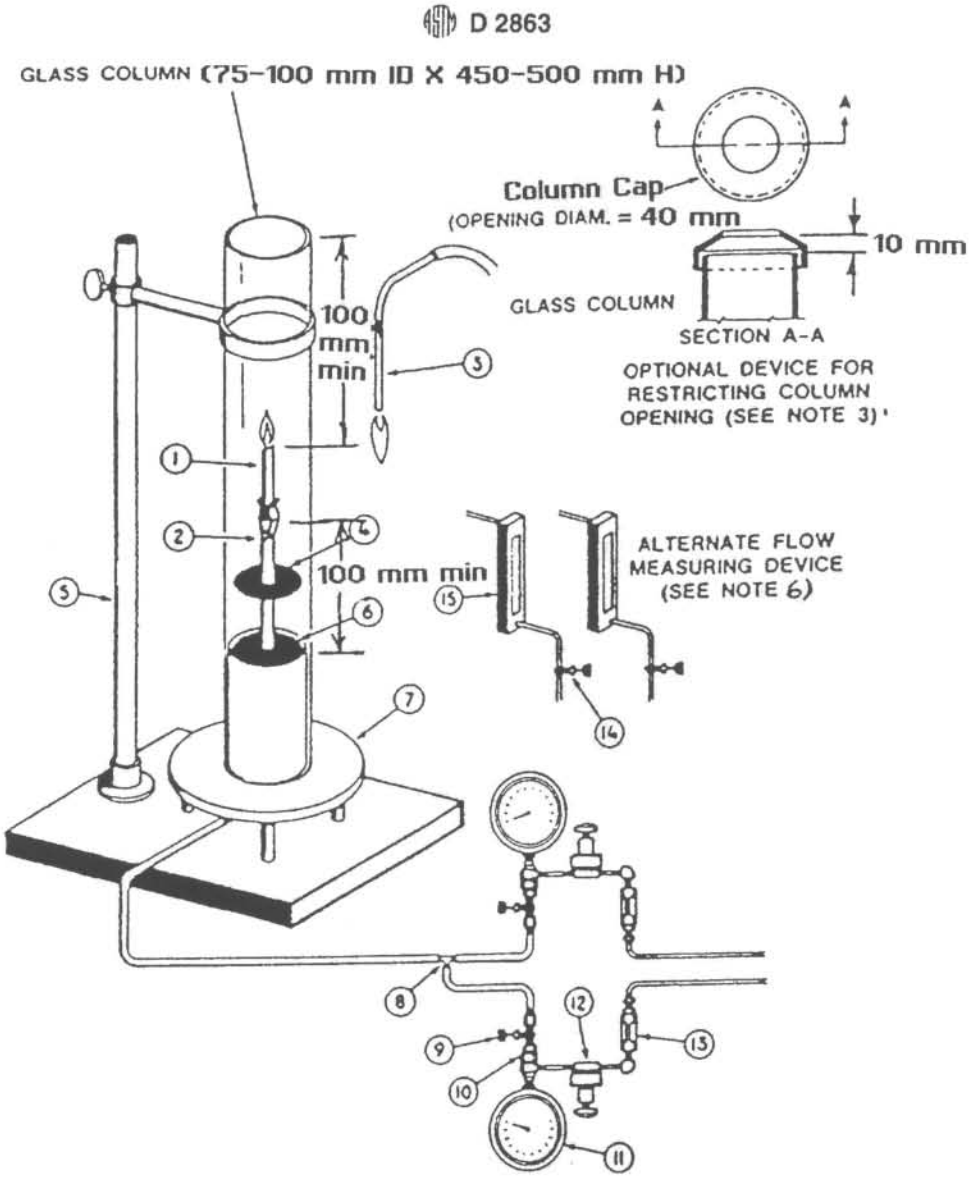

1. Burning Specimen
2. Clamp with Rod Support
3. Igniter
4. Wire Screen
5. Ring Stand
6. Glass Beads in a Bed
7. Brass Base
8. Tee
9. Cut-Off Valve
10. Orifice in Holder
11. Pressure Gage
12. Precision Pressure Regulator
13. Filter
14. Needle Valve
15. Rotameter

Figure 4.10 Typical equipment layout for measuring LOI (ASTM D2863)

Chapter 5

Experimental procedures for the synthesis of a basic magnesium carbonate

5.1 Introduction

In chapter 3, various procedures have been discussed by which a basic magnesium carbonate could be synthesised. It was evident from the discussion that most of the suggested procedures concentrated on either the use of MgO as precursor for the suggested synthesis or the addition of a precipitating agent to a magnesium salt solution using basic reagents such as sodium or potassium carbonates or bicarbonates. In the following discussion the synthesis of a basic magnesium carbonate, with $Mg(OH)_2$ as precursor, will be discussed (Botha and Strydom, 2001). This approach was followed due to the lack of information in the literature relating to the synthesis of basic magnesium carbonate from $Mg(OH)_2$.

The discussion will outline the various procedures that have been followed in an attempt to synthesise a basic magnesium carbonate. The aim of this discussion is to clearly indicate the path followed in obtaining the required product. It will be shown that various experimental conditions influence the product that formed, and by manipulating these conditions, a specific required product could be obtained.

The synthesis of a basic magnesium carbonate from $Mg(OH)_2$ is based on the procedure suggested by Pond and Heneghan (1965). This procedure is based on the introduction of CO_2 into a magnesium hydroxide-water slurry, by either sparging with gas mixtures containing CO_2 or by introducing solid CO_2, until the pH of the slurry is between 7.5 and 9.0. No mention is made of whether the slurry should be heated or not. The solid portion of the slurry is then separated from the liquid portion and dried at less than 75°C. This approach was subsequently investigated.

5.2 Experimental

5.2.1 Experimental setup

The experimental setup that was used in the various procedures is given in Figure 5.1 and 5.2 The system consisted of a:

- pH meter and a pH electrode
- magnetic stirrer
- gas inlet (fabricated in-house) for the CO_2 gas, consisting of a glass tube connected to a PVC pipe
- flowmeter
- temperature regulator (for elevated temperature applications)
- heating mantle with magnetic stirrer

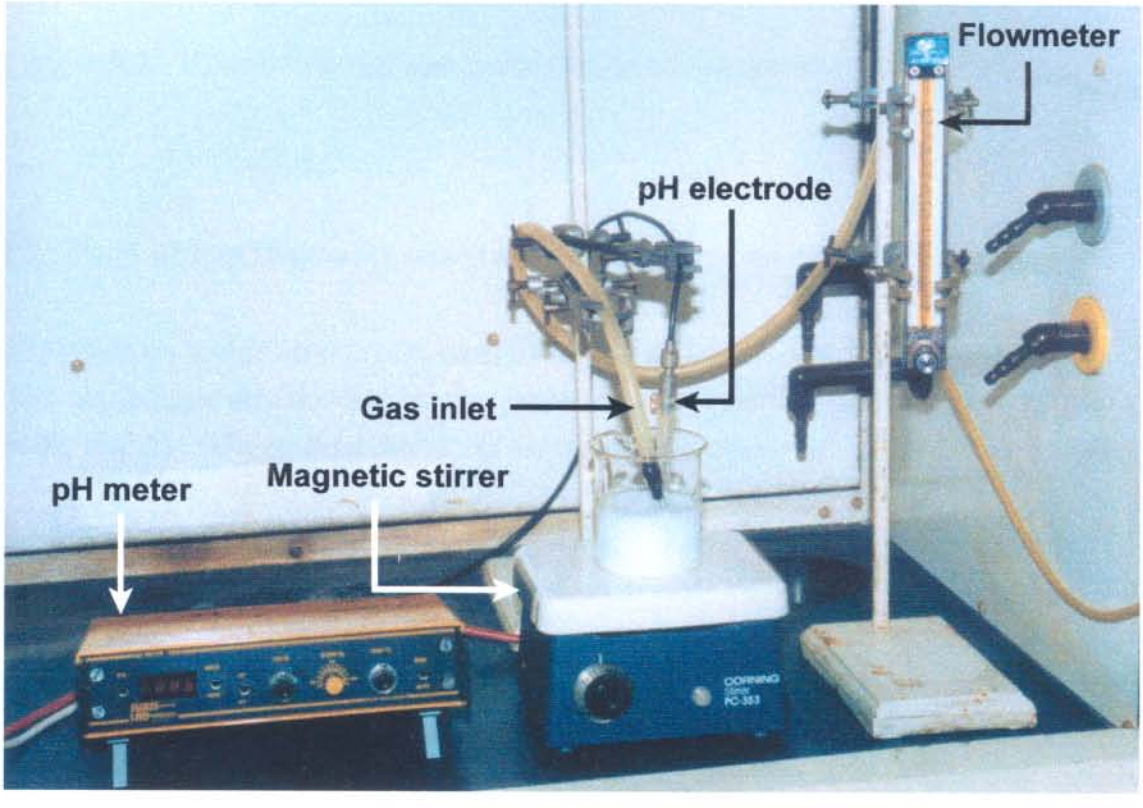

Figure 5.1 Standard experimental setup

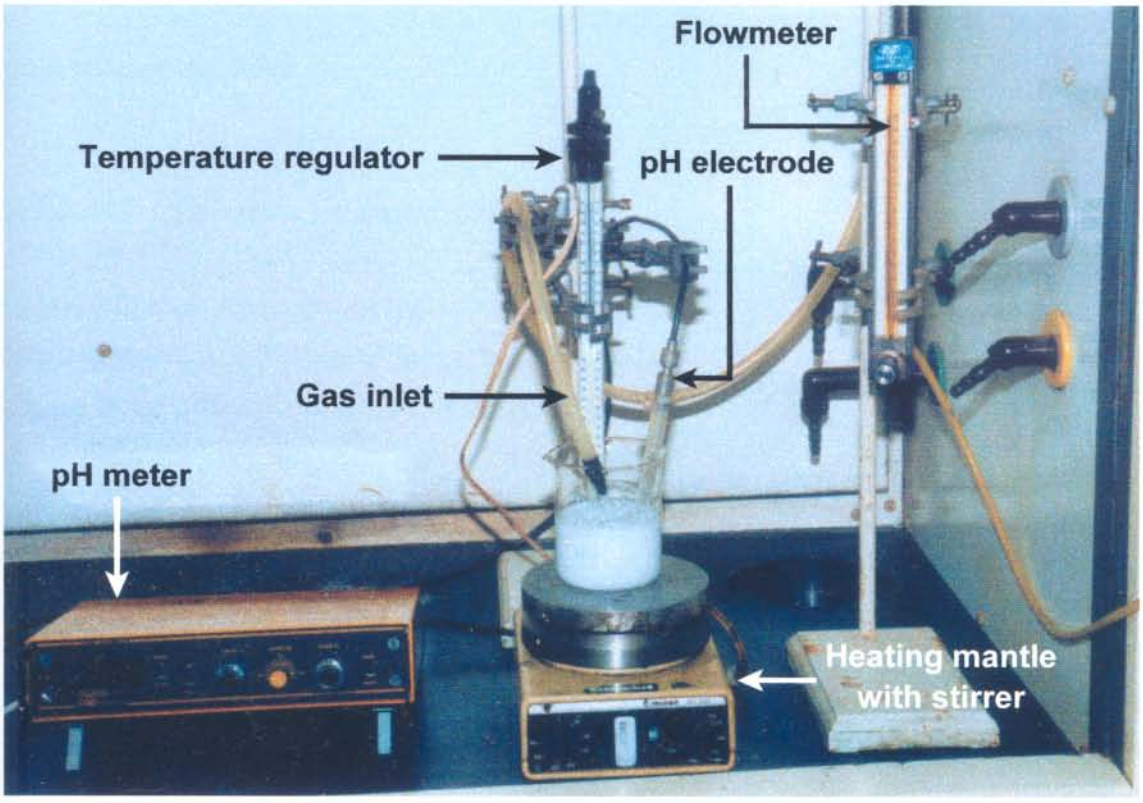

Figure 5.2 Experimental setup for elevated temperature applications

5.2.2 Experimental procedure with $Mg(OH)_2$ as reagent

In all instances a standard procedure, as stated (5.2.2.1), was followed except for one or two variations depending on the experimental conditions employed to achieve specific results. These deviations will be discussed under the appropriate heading.

5.2.2.1 Standard procedure

A $Mg(OH)_2$ slurry was obtained by suspending approximately 5.0 g $Mg(OH)_2$ (CP from UniLAB, Saarchem (Pty) Ltd) in 125 mL deionised water. The suspension was agitated vigorously with a magnetic stirrer and the pH measured before sparging with CO_2 (HP compressed gas from Air Products, South Africa). The CO_2 gas was sparged through the solution at a flow rate of ~190 mL min^{-1} while stirring continuously. The final pH of the slurry was obtained by stopping the CO_2 gas flow at the desired pH between 7.5–9.0. The slurry was then filtered and the solid product washed with deionised water

and dried for approximately 20 h at the desired temperature. The solid product was then analysed by XRD.

5.2.2.2 Variation of slurry pH

The influence of slurry pH on the resulting product was investigated by preparing three slurry solutions, at 20°C, with a final pH of 9.3; 8.2 and 7.3 respectively. After filtration all three solid products were dried at 60°C.

5.2.2.3 Variation of slurry temperature

The influence of the temperature of the $Mg(OH)_2$ slurry was investigated by preparing two slurries. The one was heated to 40°C and the other to 65°C before CO_2 gas was sparged through the slurry. The addition of CO_2 was continued until the slurry pH stabilised despite the continued addition of CO_2. At this point the CO_2 gas-flow was stopped and the slurry cooled down to measure the pH at ambient temperature. During the process of cooling to ambient temperature, an increase in pH was observed. This increase is consistent with the temperature dependance of pH measurements. No other physical changes were observed when cooling the slurry to ambient temperature. After filtration both products were dried at 60°C.

5.2.2.4 Addition of HCl at elevated temperatures

Two $Mg(OH)_2$ slurries were prepared and heated to 65°C before the addition of CO_2. The CO_2 was sparged through the suspensions until the pH stabilised despite the continued addition thereof. At this point 0.1 M HCl was added to the one suspension to lower the pH further while continuing sparging with CO_2. After the pH was lowered satisfactory, the CO_2 flow was stopped and the suspension cooled down.

The pH of the other suspension was lowered similarly by the addition of 1 M HCl so that a lower final pH than the aforementioned suspension could be obtained. The CO_2 flow was then stopped and the suspension cooled down. The pH of both suspensions, 9.1 (0.1 M HCl) and 8.3 (1 M HCl), were measured at ambient temperature before filtration. The solid products were washed thoroughly with deionised water to ensure that all the

chloride ions were removed. The solids were then dried at 60°C.

5.2.2.5 Variation of drying temperature

1. Five $Mg(OH)_2$ slurries were prepared at 20°C with a final pH between 7.5–9.0, after which the solid products were dried at 20, 80, 90, 100 and 120°C respectively.

2. $MgCO_3 \cdot 3H_2O$ was prepared as described in 5.2.2.2 (pH ~7.8). The product obtained was then divided into three parts and dried at 80, 100 and 120°C.

3. The influence of drying temperature was also evaluated on the product obtained for 1 M HCl in 5.2.2.4. The product was divided into three parts and dried at 20, 60 and 120°C.

5.2.2.6 Variation of drying time

The drying time was evaluated for two $Mg(OH)_2$ slurries prepared at 20°C with a final pH between 7.5–9.0. After filtration the products were dried at 80 and 120°C respectively. Samples were removed from the oven after 1, 3, 6, 9, 12, 24, 52 h for the product dried at 80°C. Samples were removed after 15, 30, 45 minutes, 1, 3, 6, 9, 12 and 24 h of drying for the 120°C product.

5.2.3 Experimental procedure with $MgCO_3 \cdot 3H_2O$ as reagent

$MgCO_3 \cdot 3H_2O$ was prepared as described in 5.2.2.2. The product was then suspended in deionised water and heated to 90°C. The pulp was then cooled down and the pH measured at ambient temperature after which the solid was filtered and dried at 65°C.

5.2.4 Experimental procedure with MgO as reagent

Exactly the same procedure was followed as discussed for $Mg(OH)_2$ in the standard procedure (5.2.2.1), except that MgO instead of $Mg(OH)_2$ was used. The MgO was

prepared by heating $Mg(OH)_2$ (CP from UniLAB, Saarchem (Pty) Ltd) for 2.5 h at 800°C. A MgO slurry was prepared at 20°C with a final pH between 7.5–9.0, after which the solid product was divided into three parts and dried at 20, 80 and 120°C.

5.2.5 Experimental procedure with $MgSO_4 \cdot 7H_2O$ and Na_2CO_3 as reagents

The procedure described by Black and Bergmann (1939) was followed. A $MgSO_4 \cdot 7H_2O$ (GR, Pro Analysi, Merck, South Africa) solution was prepared by dissolving 20.5 g in 80 mL deionised water and a Na_2CO_3 (GR, Pro Analysi, Merck, South Africa) solution by dissolving 10.0 g in 80 mL deionised water. Both solutions were heated to 70°C, after which the $MgSO_4 \cdot 7H_2O$ solution was added to the Na_2CO_3 solution and an additional 40 mL of deionised water to obtain a final volume of 200 mL. The resulting suspension was heated to 90°C after which it was allowed to cool down before filtration of the formed precipitate. The precipitate was thoroughly washed with deionised water to remove any traces of sulphate. The precipitate was then dried at 160°C.

5.2.6 X-ray diffraction analysis

X-ray powder diffraction analyses were performed on a Siemens D501 diffractometer using Cu K_α radiation. The PDF-2 database from ICDD volume 1–45 was used to analyse the data (JCPDS, 1995). In order to avoid confusion when comparing more than one XRD pattern of different compounds on the same graph, less lines were used to represent each compound. This was accomplished by selecting the strongest lines for each compound under consideration to constitute the XRD pattern of the compound.

The unidentified compound that will be referred to, could not be matched with any of the compounds in the XRD database. It was decided to compile an XRD pattern for the unidentified compound, by selecting the strongest lines of the diffraction pattern. This pattern was used to identify the unidentified compound that was obtained by the various procedures.

5.3 Results and Discussion

The emphasis of the following discussion will be on the synthesis of a basic magnesium carbonate from $Mg(OH)_2$. Various experimental conditions were investigated for each of the precursors, in order to determine the most favourable conditions for synthesis of a basic magnesium carbonate. XRD was used to identify the products that were synthesised at each procedure. The products that were obtained from the respective procedures are summarised in Table 5.1 and 5.2 at the end of the discussion.

5.3.1 $Mg(OH)_2$ as reagent

5.3.1.1 Influence of slurry pH

The initial approach was to investigate the influence of slurry pH on the resulting product. The method followed by Pond and Heneghan (1965) suggested that the final pH of the slurry should be between 7.5 and 9.0 to obtain the basic magnesium carbonate. Langmuir (1965) also indicated that naturally occurring hydromagnesite precipitates in water with a pH of approximately 8.9. It was however not specified in the procedure of Pond and Heneghan (1965) whether the slurry was to be heated or not. Initially it was decided to perform the procedure at ambient temperature. Figure 5.3 (a) illustrates the preliminary testing. Three slurries were prepared with different slurry pH's (9.3; 8.2 and 7.3) and dried below 75°C as suggested by Pond and Heneghan (1965).

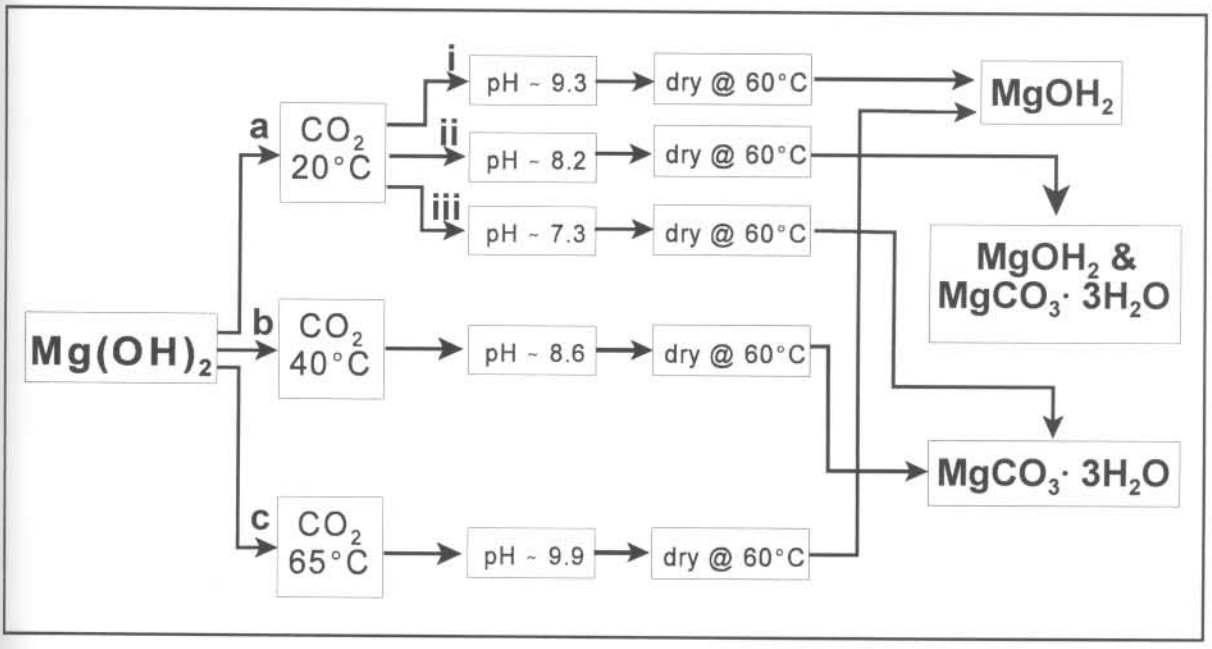

Figure 5.3 Influence of pH and slurry temperature on $Mg(OH)_2$ and CO_2 reaction

From the XRD results obtained (Figure 5.4) it is evident that this procedure did not result in the formation of a basic magnesium carbonate. At a pH of 9.3 it seemed that the reaction was either incomplete or not occurring, due to the presence of only $Mg(OH)_2$ in the product. This incomplete reaction can be ascribed to an inadequate amount of time and CO_2 allowed to react with the $Mg(OH)_2$ slurry.

A pH of 7.3 also seemed to be insufficient in forming the required product. Only $MgCO_3 \cdot 3H_2O$ (nesquehonite) was obtained by the aforementioned approach. The formation of nesquehonite at ambient temperature is well known (Langmuir, 1965). The transition between nesquehonite and hydromagnesite occurs at 55–65°C with nesquehonite the stable phase below 55°C. A mixture of $Mg(OH)_2$ and $MgCO_3 \cdot 3H_2O$ were obtained at pH 8.2. This clearly indicates an incomplete reaction with respect to $Mg(OH)_2$ due to its presence in the product mixture.

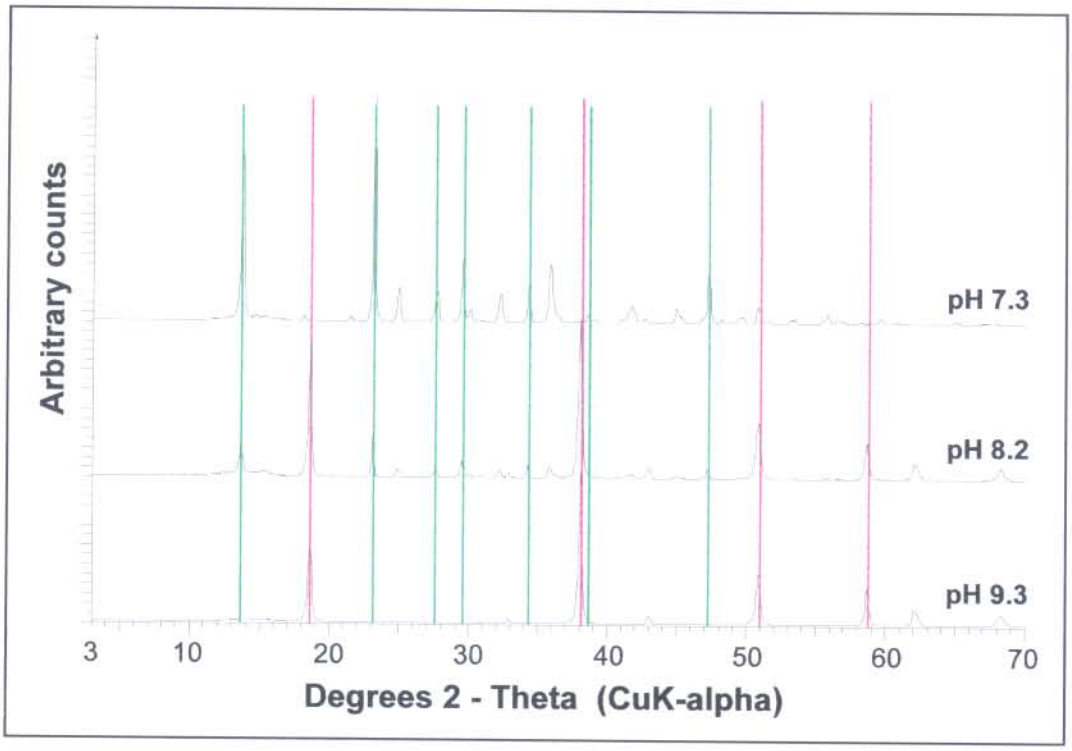

Figure 5.4 **XRD patterns of products obtained for different slurry pH's of $Mg(OH)_2$ and a slurry temperature of 20°C (— nesquehonite; — $Mg(OH)_2$)**

The influence of time on pH was evaluated when sparging CO_2 gas through the $Mg(OH)_2$ slurry at ambient temperature. This is depicted in Figure 5.5. This graph clearly indicates the change in pH of the slurry during the continuous addition of CO_2. The pH versus time graph was characterised by a rapid decrease in pH with the initial addition of CO_2. This was followed by a steady increase in pH and then stabilisation of the pH for a specific time after which the pH slowly decreased again. The rapid initial decrease in pH was ascribed to the acidic nature of dissolved CO_2.

$$CO_{2\,(g)} + H_2O_{(l)} \rightleftharpoons CO_{2\,(aq)}$$

$$CO_{2\,(aq)} + H_2O_{(l)} \rightleftharpoons H^+_{(aq)} + HCO_3^-{}_{(aq)}$$

The hydration of CO_2 predominates at a pH below 10 (Smithson and Bakhshi, 1973). The stabilisation of the pH possibly corresponded to the consumption of HCO_3^- by the Mg^{2+} that formed during the dissolution of $Mg(OH)_2$. The surface layer of $Mg(OH)_2$ can react with either H^+ or $CO_{2\,(aq)}$. Since H^+ is produced in the hydration of $CO_{2\,(aq)}$, its availability will depend on the rate of this reaction.

$$Mg(OH)_{2\,(s)} + 2\,CO_{2\,(aq)} \rightleftharpoons Mg^{2+}{}_{(aq)} + 2\,HCO_3^-{}_{(aq)}$$

$$Mg(OH)_{2\,(s)} + 2\,H^+{}_{(aq)} \rightleftharpoons Mg^{2+}{}_{(aq)} + 2\,H_2O_{(l)}$$

When most of the available Mg^{2+} has been consumed by HCO_3^-, the pH decreased again due to the sole hydration of $CO_{2\,(aq)}$. The increase in pH when the CO_2 flow was ceased was ascribed to the CO_2 gas which has not yet entered the aqueous phase and which was subsequently removed from the slurry during agitation. The slurry had to be agitated until a stable pH was obtained.

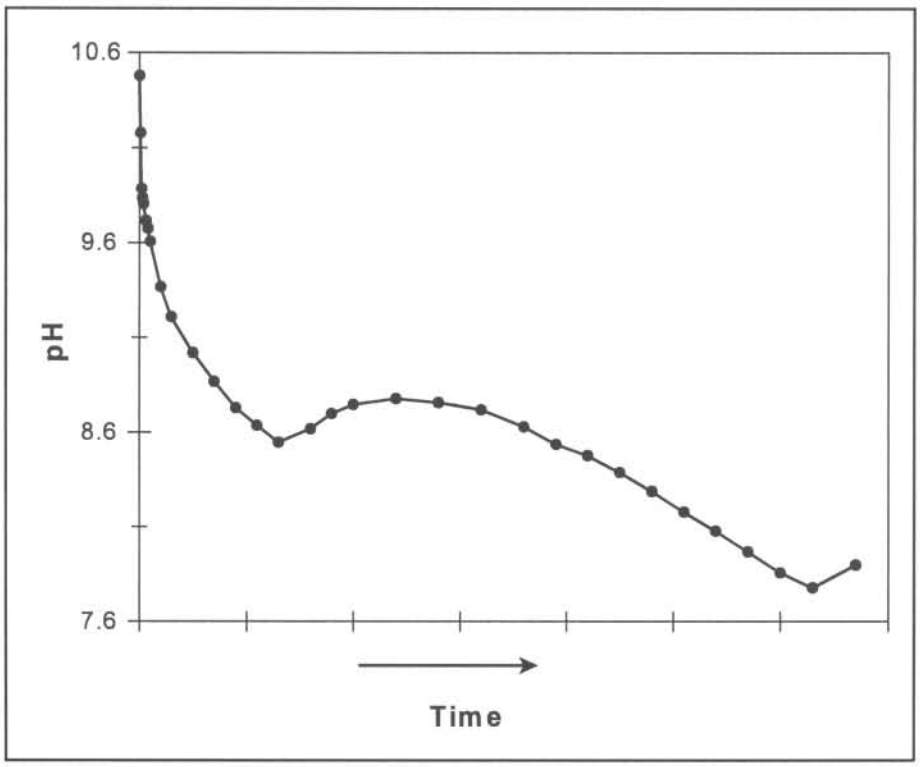

Figure 5.5 pH change with time for $Mg(OH)_2$ and CO_2 reaction at 20°C

It is evident from the experimental results in Figure 5.4, that pH alone was not sufficient to ensure formation of the basic magnesium carbonate. Either the slurry had to be heated or a different drying temperature had to be used in order to obtain the required product.

5.3.1.2 Influence of slurry temperature

The following attempt involved heating the slurry (Figure 5.3 b and c) in an attempt to obtain reaction conditions which could result in the formation of a basic magnesium carbonate. An inherent problem that occurs at elevated temperatures is a decrease in the solubility of CO_2 gas in water (Pierantozzi, 1993). This resulted in a difficulty in obtaining a slurry pH between 7.5 and 9.0 which is the pH range which is suitable for the formation of a basic magnesium carbonate (Pond and Heneghan, 1965).

It is clear from the XRD results in Figure 5.6 that no significant reaction took place between $Mg(OH)_2$ and CO_2 at a slurry temperature of 65°C and that the $Mg(OH)_2$ remained unchanged. This is probably due to the high temperature of the slurry resulting in very little of the CO_2 dissolving in the slurry and being available for reaction with the $Mg(OH)_2$. An aqueous solution of CO_2 is required in order for the CO_2 to participate in the reactions taking place at the $Mg(OH)_2$ interface. The formation of hydromagnesite is expected to be successful at 65°C since its formation above 55°C is favoured above that of nesquehonite (Langmuir, 1965). The XRD results showed the presence of hydromagnesite at a slurry temperature of 65°C, though it was evident that reaction of the $Mg(OH)_2$ was not completed.

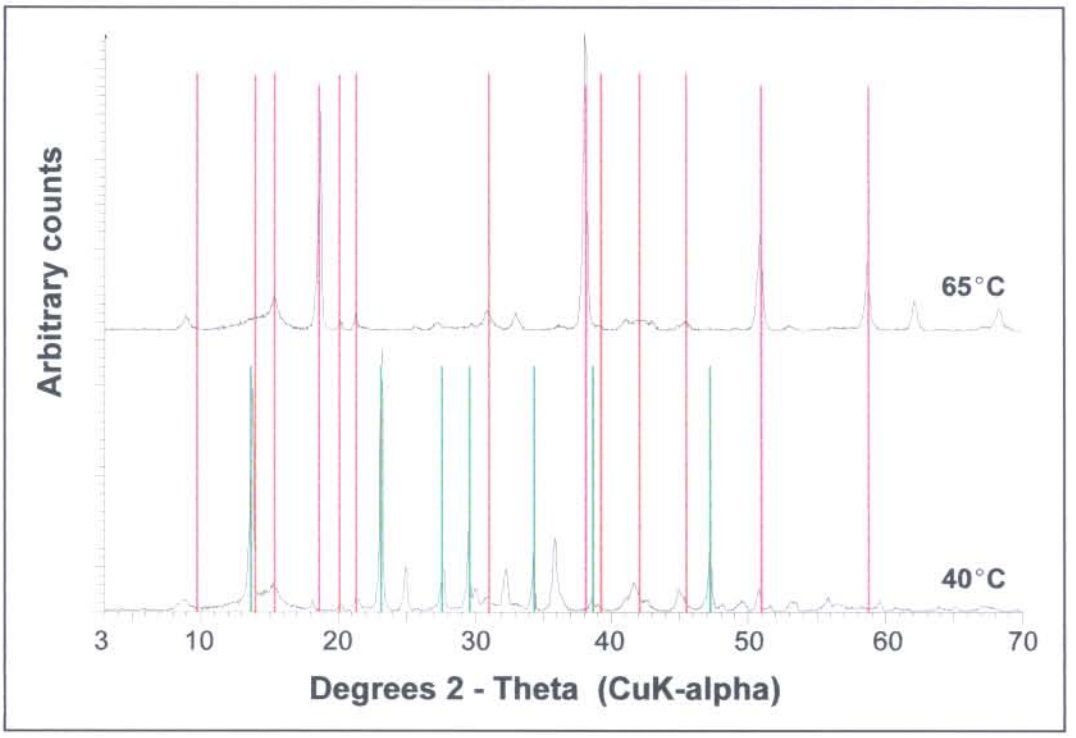

Figure 5.6 XRD patterns of products obtained for different $Mg(OH)_2$ slurry temperatures (— nesquehonite; — $Mg(OH)_2$; — hydromagnesite)

At a slurry temperature of 40°C the $Mg(OH)_2$ reacted to form $MgCO_3 \cdot 3H_2O$. This complies with the expected formation of nesquehonite below 55°C. If the reaction is to be performed above 55°C, where the successful preparation of hydromagnesite is to be expected, an alternative approach will be required.

5.3.1.3 Influence of HCl addition at elevated temperatures

The next approach was to determine whether it could be possible to obtain hydromagnesite by heating the formed suspension. As already mentioned it was difficult to obtain a low end pH when heating the suspension. An attempt was made to lower the slurry pH through the addition of HCl at a slurry temperature of 65°C. This procedure is depicted in Figure 5.7 (a & b.ii). Initially 0.1 M HCl was used to lower the slurry pH at 65°C. This proved to be inefficient since a relatively large volume of the 0.1 M acid was necessary to lower the pH significantly. It was then decided to

investigate the influence of adding 1 M HCl in an attempt to lower the slurry pH more efficiently. A slurry pH of 9.1 and 8.3 were obtained through the addition of the 0.1 and 1 M HCl respectively.

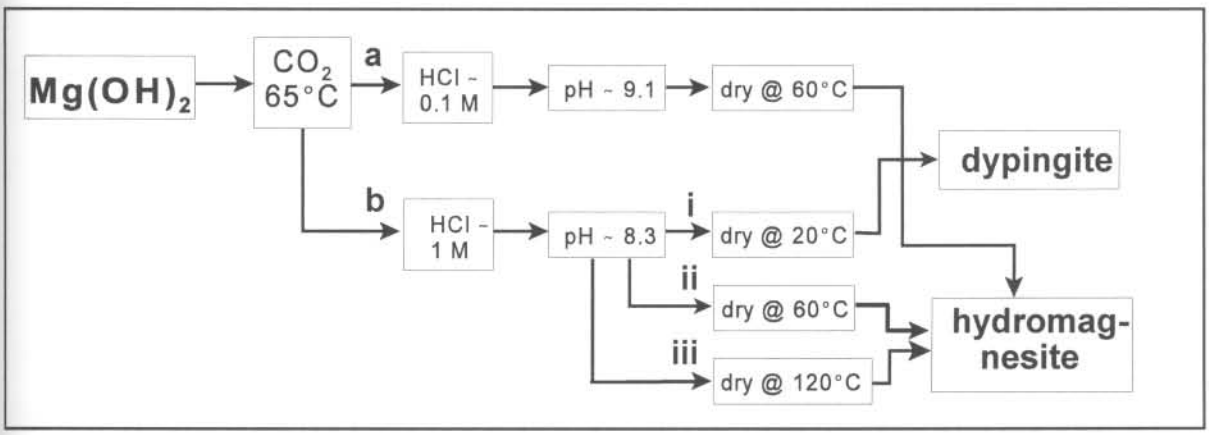

Figure 5.7 Influence of different HCl concentrations and drying temperatures on $Mg(OH)_2$ and CO_2 reaction and a slurry temperature of 65°C

The product that was obtained in both instances is hydromagnesite (Figure 5.8). It would seem that the addition of the acid had a significant influence on the reaction mechanism between $Mg(OH)_2$ and CO_2. A possible explanation is that the acid contributed in an increased dissolution of the $Mg(OH)_2$ that subsequently resulted in a more complete reaction with the CO_2. Since a more complete reaction could be obtained, it was possible to form hydromagnesite above 55°C as expected.

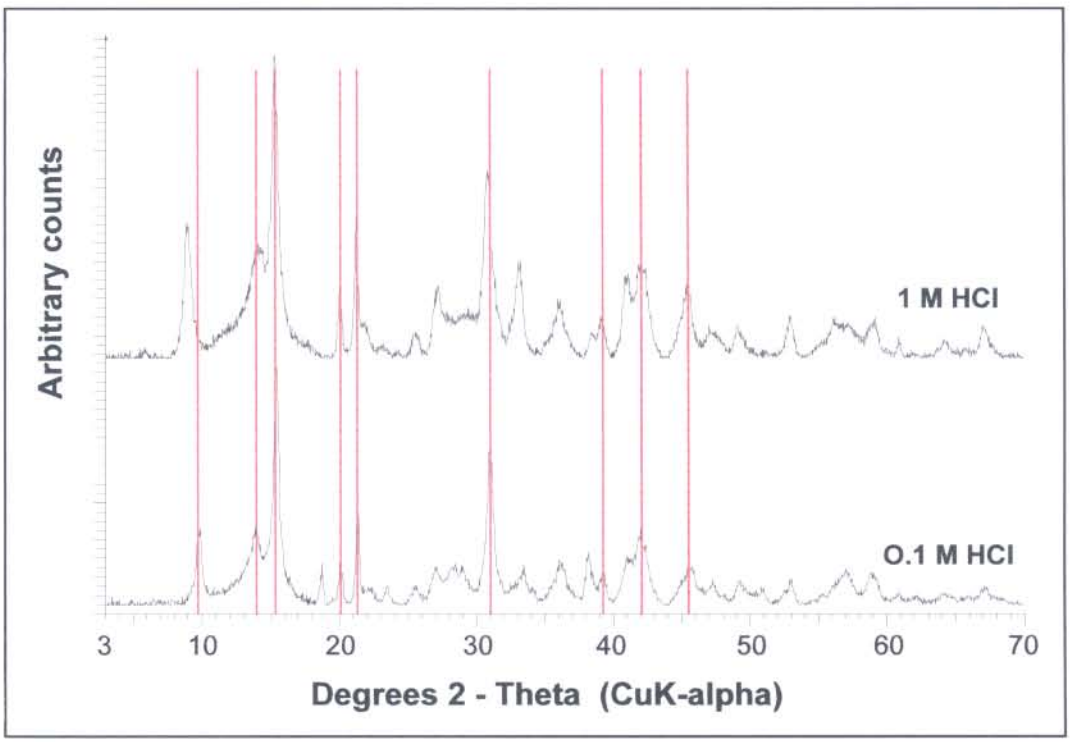

Figure 5.8 XRD patterns of products obtained for different HCl concentrations at a 65°C slurry temperature and 60°C drying temperature (— hydromagnesite)

5.3.1.4 Influence of drying temperature

The next approach was to evaluate the influence of drying temperature. Up to this point the product was dried below 75°C. The reason for this was that the basic magnesium carbonate that was synthesised by Pond and Heneghan (1965), started to decompose above about 75°C. It was decided to dry the solid at an elevated temperature in an attempt to obtain a basic magnesium carbonate. Since an increase in slurry temperature resulted in a decrease in solubility of CO_2, it was decided to perform the reaction at ambient temperature, although the formation of nesquehonite is more likely at ambient temperature. Drying temperatures of 90 and 100°C (Figure 5.9 a) were first evaluated. Since the 100°C drying temperature delivered hydromagnesite, three additional temperatures (20, 80 and 120°C) were investigated (Figure 5.9 b).

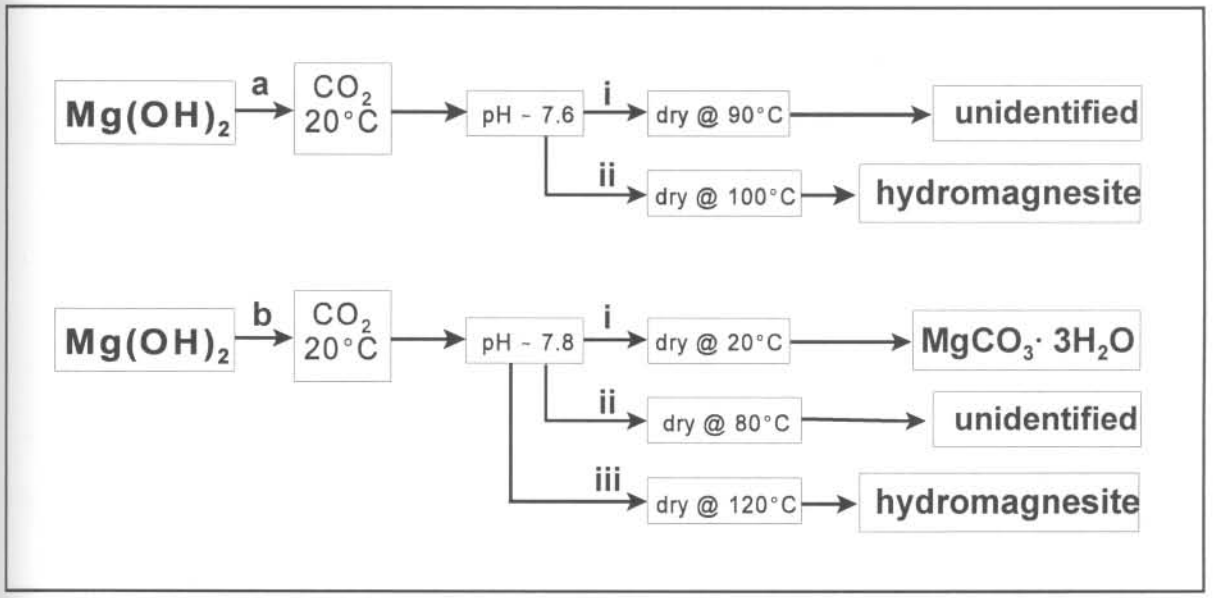

Figure 5.9 Influence of drying temperature on $Mg(OH)_2$ and CO_2 product

The formation of hydromagnesite at 100 and 120°C as well as the formation of an unidentified crystalline structure at 80 and 90°C is evident from Figure 5.10. The XRD pattern of the unidentified compound could not be matched to any of the compounds in the XRD database. It is very similar though to that obtained at 30°C by Fernández *et al.* (2000). At 20°C, $MgCO_3 \cdot 3H_2O$ was formed. Since nesquehonite was formed at ambient temperature from the same slurry as the hydromagnesite product that was formed at 120°C drying temperature, it was questioned whether it might be possible to obtain hydromagnesite by heating nesquehonite at elevated temperatures. This was subsequently investigated.

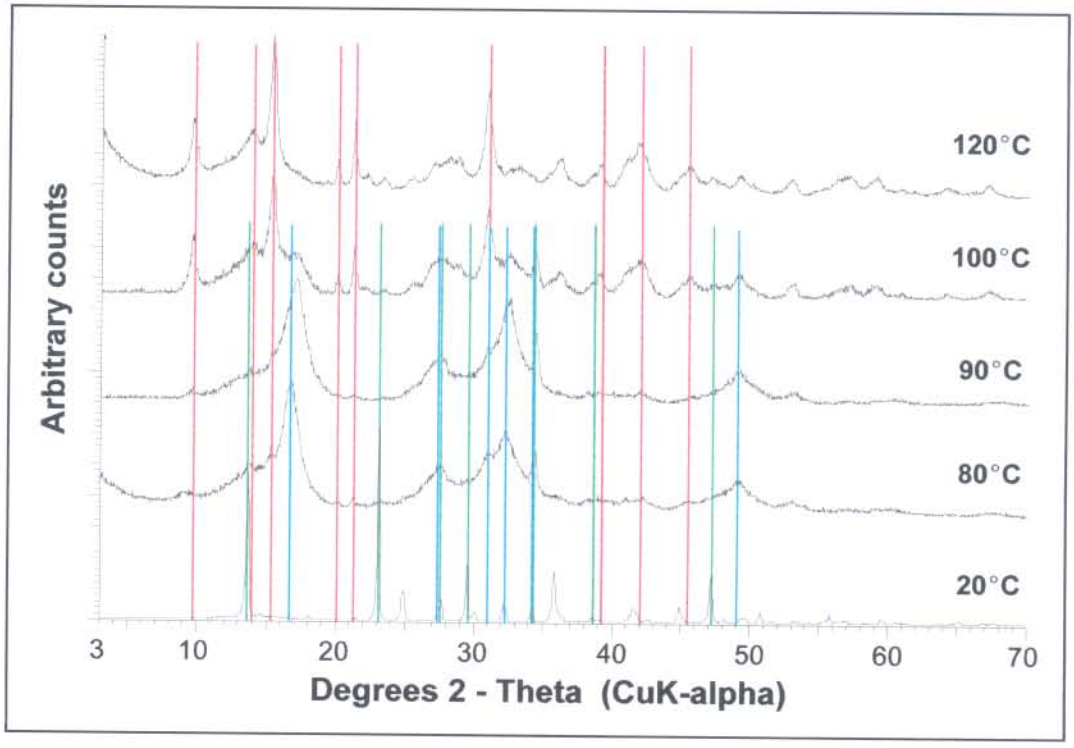

Figure 5.10 XRD patterns of products obtained at different drying temperatures for $Mg(OH)_2$ and CO_2 product (— nesquehonite; — hydromagnesite; — unidentified)

Heating $MgCO_3 \cdot 3H_2O$ at 80, 100 and 120°C did not result in the formation of hydromagnesite as expected. Only the unidentified product could be obtained at the respective drying temperatures depicted in Figure 5.11. The XRD results (Figure 5.12) supported the expected conversion of nesquehonite to the unidentified product. An alternative mechanism possibly existed by which nesquehonite is converted to hydromagnesite.

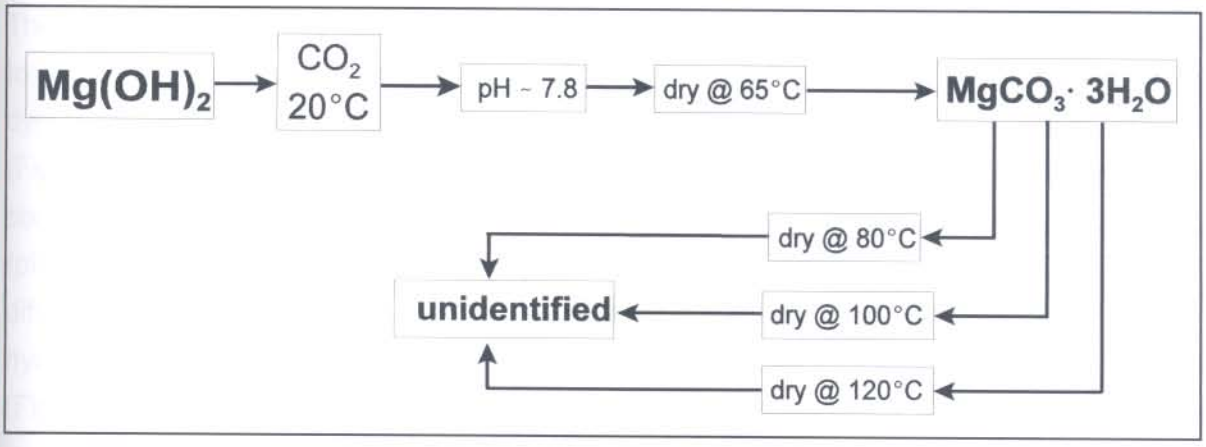

Figure 5.11 Influence of drying temperature on product obtained from $MgCO_3 \cdot 3H_2O$ as reagent

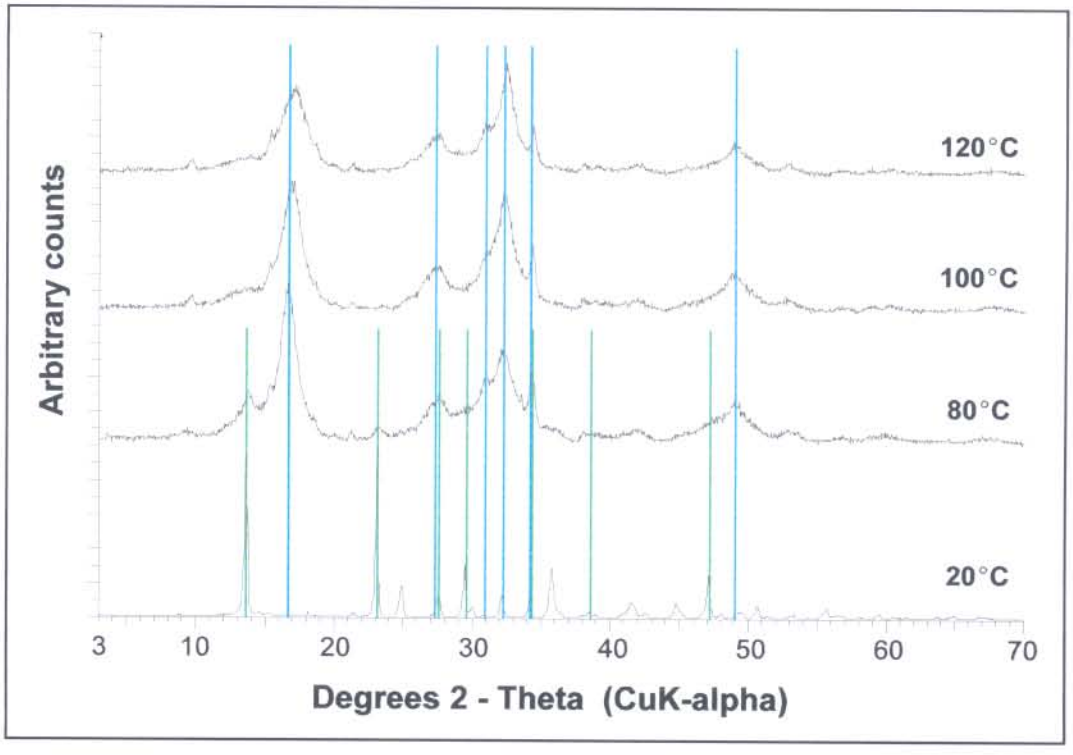

Figure 5.12 XRD patterns of products obtained at different drying temperatures for $MgCO_3 \cdot 3H_2O$ as reagent
(— nesquehonite; — unidentified)

The influence of drying temperature was also investigated for the addition of 1 M HCl to the $Mg(OH)_2$ and CO_2 reaction at 65°C (Figure 5.7 b). At ambient temperature dypingite was formed while hydromagnesite formed at 60 and 120°C. These results (Figure 5.13) are in contrast with those obtained in Figure 5.10 where the product consisted entirely of hydromagnesite at 100 and 120°C, as well as the results at 60°C (pH 7.3) where the product consisted entirely of nesquehonite (Figure 5.4). This difference was ascribed to a slurry temperature of 65°C (Figure 5.7 b) at which hydromagnesite is formed preferentially compared to an ambient slurry temperature (Figure 5.9). The formation of dypingite at ambient temperature, after being left open in air for approximately 10 days to dry (Figure 5.13), supported the theory that hydromagnesite is formed from dypingite. It was evident that the product was not yet dry enough, after 10 days of drying, to favour the conversion of dypingite to hydromagnesite.

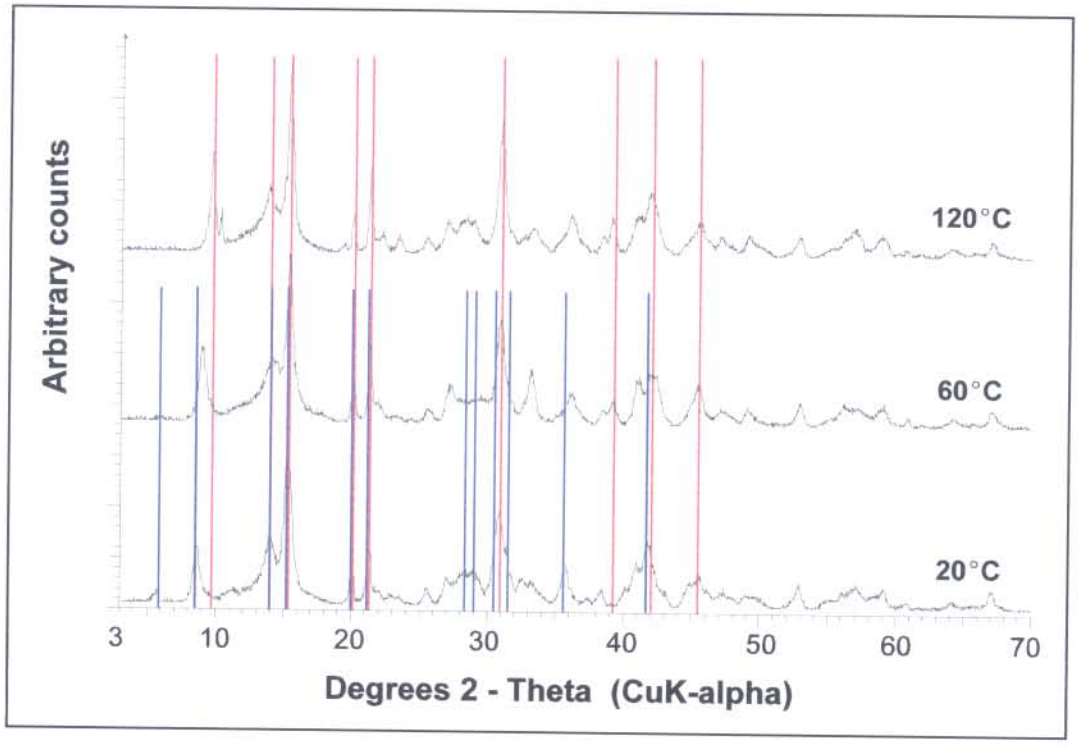

Figure 5.13 XRD patterns of products obtained at different drying temperatures for $Mg(OH)_2$ + 1 M HCl + CO_2 reaction (— hydromagnesite; — dypingite)

5.3.1.5 Influence of drying time

Up to the previous investigations the products obtained were dried for a minimum of 20 h. It was decided to investigate the influence of shorter drying times. This investigation was done for the products formed at 80 and 120°C (Figure 5.9). The results are depicted in Figure 5.14 for the product formed at 120°C.

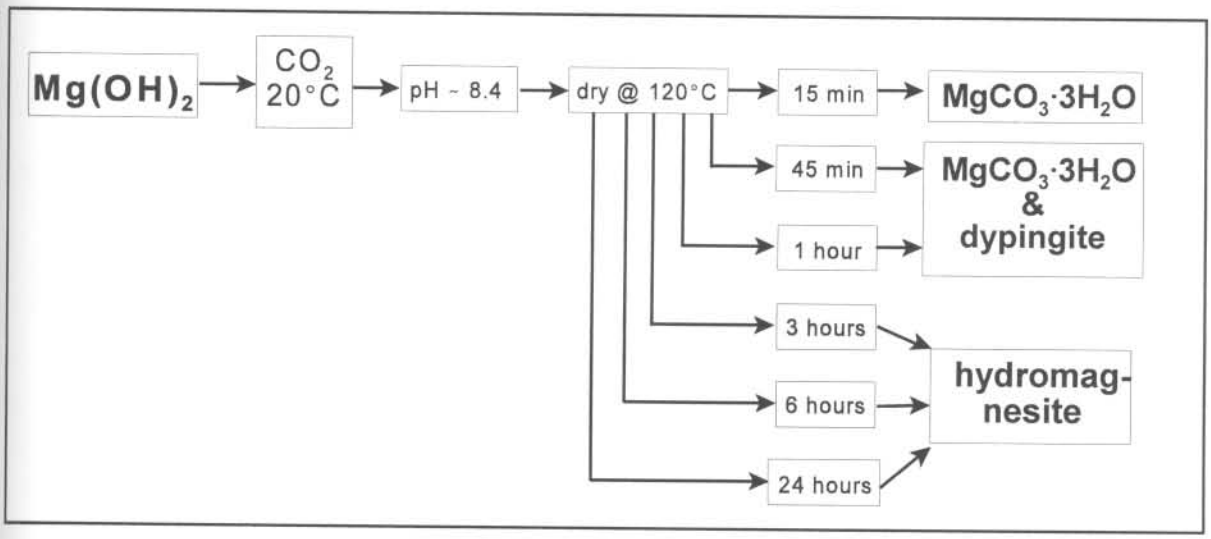

Figure 5.14 Influence of drying time on $Mg(OH)_2$ and CO_2 product obtained at 120°C

The XRD results for the product dried at 120°C are given in Figure 5.15. The formation of hydromagnesite at 120°C was preceded by the formation of nesquehonite after 15 minutes drying time. As time progressed, nesquehonite converted to dypingite between 1 and 3 h drying and finally to hydromagnesite after 3 h. This confirmed the conversion of nesquehonite to dypingite and ultimately to hydromagnesite. Since hydromagnesite and dypingite only differ with respect to dypingite having one water molecule more than hydromagnesite, it is clear that the formation of hydromagnesite using a longer drying time would be feasible. No further changes were observed between 6 and 24 h. It could be concluded that if the drying time did not exceed 3 h, the final product would not have been hydromagnesite.

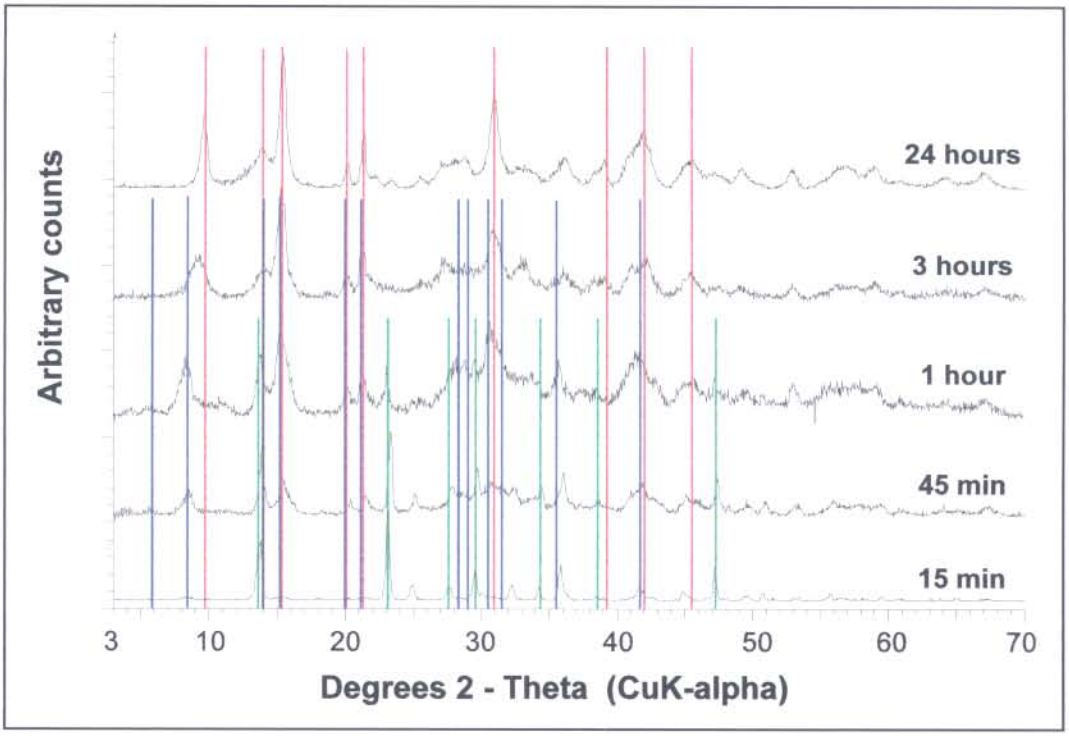

Figure 5.15 XRD patterns of products obtained at different drying times for $Mg(OH)_2$ and CO_2 product obtained at 120°C (— nesquehonite; — hydromagnesite; — dypingite)

The formation of the unidentified product at 80°C also delivered interesting results for the various drying times depicted in Figure 5.16. The XRD results (Figure 5.17) indicate that after 1 h drying time nesquehonite was formed. Gradually as time progressed nesquehonite converted to the unidentified product after 24 h drying time. This conversion corresponds to the earlier observation in Figure 5.12 where nesquehonite converted to the unidentified product when heated at elevated temperatures.

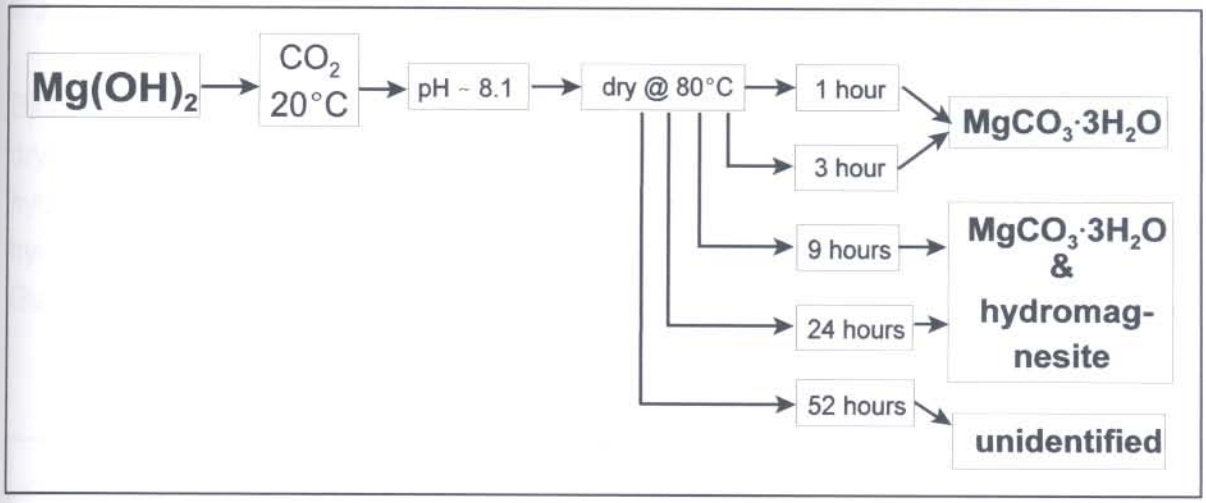

Figure 5.16 Influence of drying time on $Mg(OH)_2$ and CO_2 product obtained at 80°C

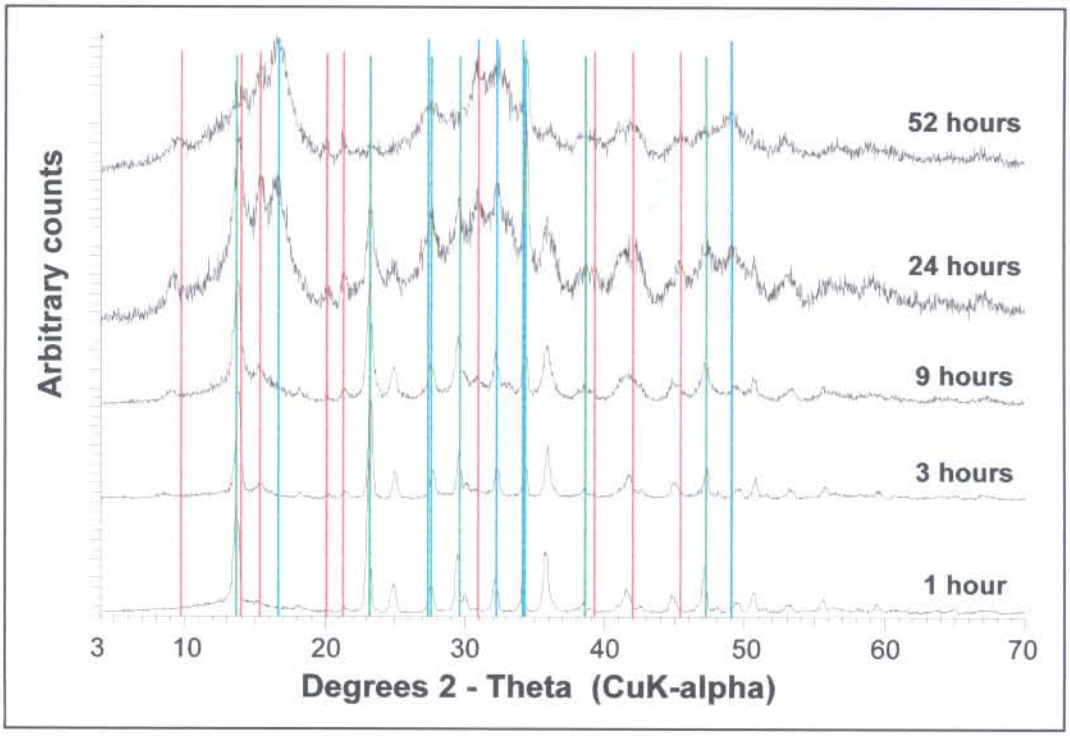

Figure 5.17 XRD patterns of products obtained at different drying times for $Mg(OH)_2$ and CO_2 product obtained at 80°C (— nesquehonite; — hydromagnesite; — unidentified)

5.3.2 $MgCO_3 \cdot 3H_2O$ as reagent

By boiling $MgCO_3 \cdot 3H_2O$, that was formed as depicted in Figure 5.3 (a.iii), in water and drying the solid product at 65°C after filtration (Figure 5.18), it was possible to form hydromagnesite. This approach again confirms the conversion of nesquehonite to hydromagnesite above 55°C. These findings correspond to those of Prakash and Gupta (1987).

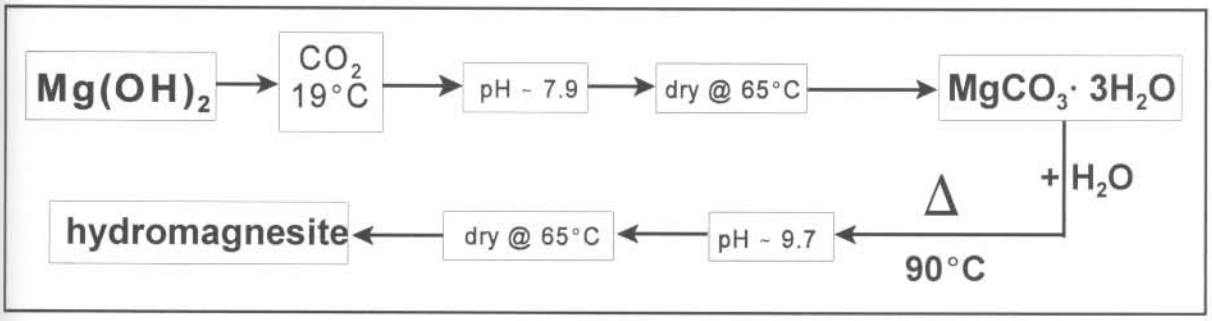

Figure 5.18 Synthesis of hydromagnesite from $MgCO_3 \cdot 3H_2O$

5.3.3 MgO as reagent

The procedure depicted in Figure 5.19, was evaluated in order to determine whether similar results could be obtained to those that were obtained for $Mg(OH)_2$ in Figure 5.10. The results obtained for MgO (Figure 5.20) were different from $Mg(OH)_2$ when the solid products were dried under similar conditions. In this instance the unidentified product was formed from MgO when the solid products were dried at 80 and 120°C respectively. It is possible that the reaction has not gone to completion with respect to MgO. This could explain the absence in the formation of hydromagnesite from MgO when dried at 120°C compared to $Mg(OH)_2$ in Figure 5.10.

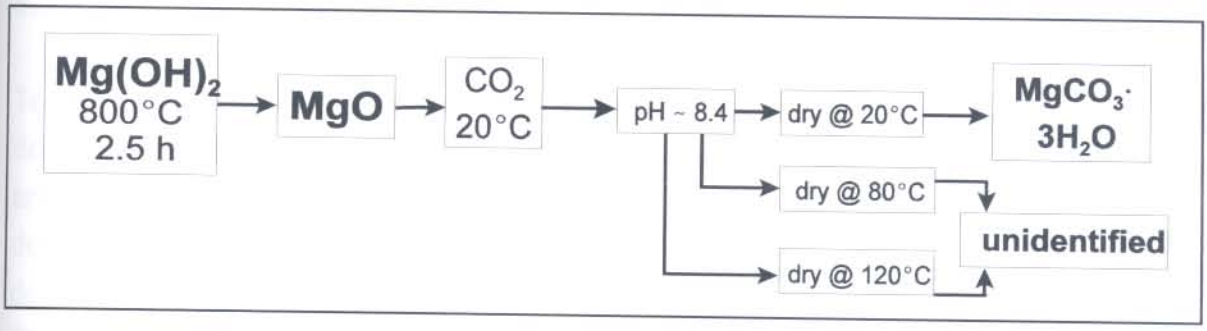

Figure 5.19 Influence of drying temperature on MgO and CO_2 product

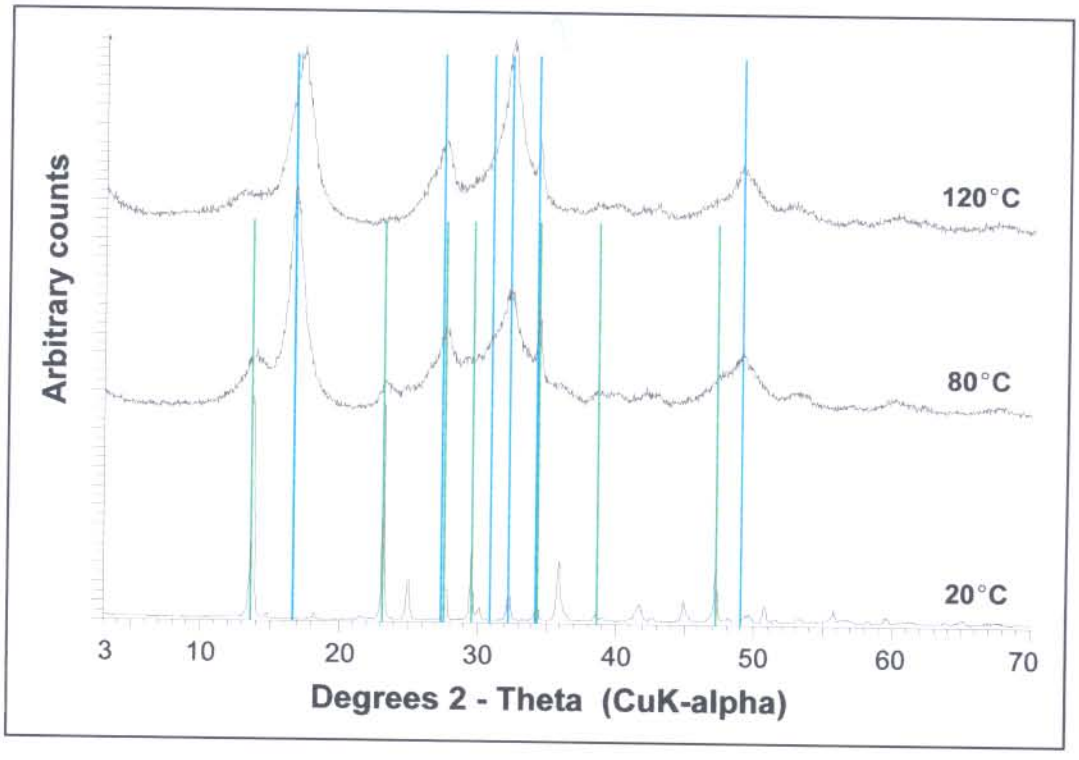

Figure 5.20 XRD patterns of products obtained at different drying temperatures for MgO and CO_2 product (— nesquehonite; — unidentified)

5.3.4 $MgSO_4 \cdot 7H_2O$ and Na_2CO_3 as reagents

To evaluate the synthesised basic magnesium carbonate products above, it was decided to synthesise hydromagnesite by the reaction of a magnesium salt with an appropriate precipitating agent. This approach was subsequently included in the development of a preparation method for a basic magnesium carbonate. The method described by Black and Bergmann (1939) was attempted and is depicted in Figure 5.21. This procedure is based on the addition of a magnesium sulphate solution to a sodium carbonate solution.

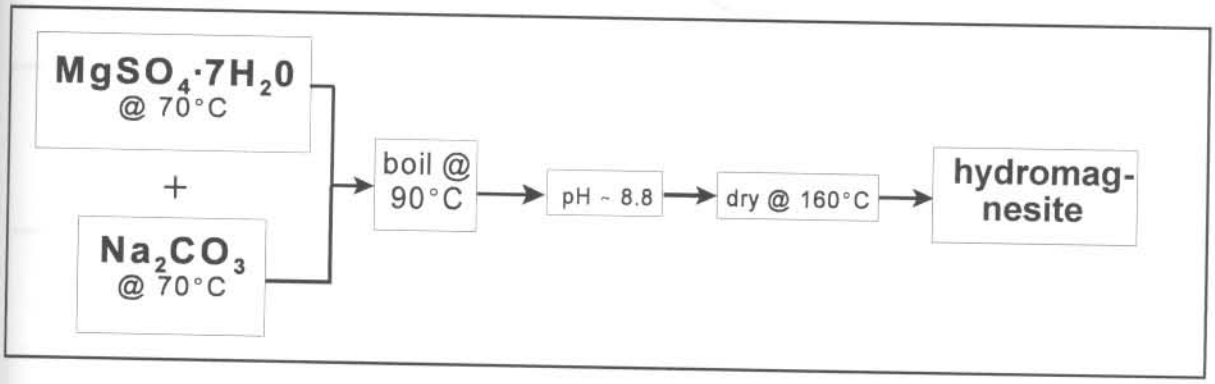

Figure 5.21 Synthesis of hydromagnesite based on $MgSO_4 \cdot 7H_2O$ and Na_2CO_3

The main drawback of this approach is the difficulty in ensuring that the precipitate is free from sulphate. It took a considerable amount of water to wash the precipitate and still the presence of sulphate was visible when testing the filtrate. Despite this drawback, the method seems reliable and delivered hydromagnesite as claimed.

Table 5.1 **Summary of the experimental procedures investigated in the various approaches towards preparing a basic magnesium carbonate**

Reagents	Slurry temperature (°C)	Final pH of slurry before filtration	Drying temperature (°C)	Product formed (confirmed by XRD)
$Mg(OH)_2+CO_2$	20	9.3	60	$Mg(OH)_2$
A	20	8.2	60	$Mg(OH)_2$ + $MgCO_3 \cdot 3H_2O$
	20	7.3	60	$MgCO_3 \cdot 3H_2O$
B	40	8.6	60	$MgCO_3 \cdot 3H_2O$
	65	9.9	60	$Mg(OH)_2$ + (hydromagnesite)
C	65°C + 0.1 M HCl	9.1	60	hydromagnesite
	65°C + 1 M HCl	8.3	60	hydromagnesite
D	19	7.6	90	unidentified
			100	hydromagnesite
E	20	7.8	20	$MgCO_3 \cdot 3H_2O$
			80	unidentified
			120	hydromagnesite
F	20	7.8	65	$MgCO_3 \cdot 3H_2O$
$MgCO_3 \cdot 3H_2O$			80	unidentified
			100	unidentified
			120	unidentified
G	65°C + 1 M HCl	8.3	20	dypingite
			60	hydromagnesite
			120	hydromagnesite

Table 5.2 **Summary of the experimental procedures investigated in the various approaches towards preparing a basic magnesium carbonate (continued)**

Reagents	Slurry temperature (°C)	Final pH of slurry before filtration	Drying temperature (°C)	Product formed (confirmed by XRD)
H	20	8.4	120 - 15 min	$MgCO_3 \cdot 3H_2O$
			120 - 45 min	$MgCO_3 \cdot 3H_2O$ + dypingite
			120 - 1 h	$MgCO_3 \cdot 3H_2O$ + dypingite
			120 - 3 h	hydromagnesite
			120 - 6 h	hydromagnesite
			120 - 24 h	hydromagnesite
I	20	8.1	80 - 1 h	$MgCO_3 \cdot 3H_2O$
			80 - 3 h	$MgCO_3 \cdot 3H_2O$
			80 - 9 h	$MgCO_3 \cdot 3H_2O$ + hydromagnesite
			80 - 24 h	$MgCO_3 \cdot 3H_2O$ + hydromagnesite
			80 - 52 h	unidentified
J	19	7.9	65	$MgCO_3 \cdot 3H_2O$
$MgCO_3 \cdot 3H_2O$	90	9.7	65	hydromagnesite
$MgO + CO_2$	20	8.4	20	$MgCO_3 \cdot 3H_2O$
K			80	unidentified
			120	unidentified
$MgSO_4 \cdot 7H_2O + Na_2CO_3$ L	90	8.8	160	hydromagnesite

5.4 Conclusion

The experimental procedures that were investigated, are summarised in Table 5.3. The procedures for obtaining each product were grouped together so that the various procedures could be compared with one another.

This summary clearly indicates that the experimental conditions which were employed had an important influence on the product that was obtained. The aim of this investigation was to prepare a basic magnesium carbonate. It is evident that only certain experimental procedures were able to deliver a required product. The question which comes to mind, is which procedure would be the best choice when synthesising the basic magnesium carbonate? There are various aspects that influence the choice of a method for the synthesis of a specific product. Time, money and environmental issues are usually at the forefront when making this decision.

Table 5.3 Summary of the products synthesised by the various procedures and the experimental conditions that resulted in the formation thereof

Product formed (confirmed by XRD)		Reagents	Slurry temperature (°C)	Final pH of slurry before filtration	Drying temperature (°C)
$Mg(OH)_2$	(1)	$Mg(OH)_2 + CO_2$	20	9.3	60
	(2)	$Mg(OH)_2 + CO_2$	65	9.9	60
$MgCO_3 \cdot 3H_2O$	(1)	$Mg(OH)_2 + CO_2$	20	8.2	60
	(2)	$Mg(OH)_2 + CO_2$	20	7.3	60
	(3)	$Mg(OH)_2 + CO_2$	40	8.6	60
	(4)	$Mg(OH)_2 + CO_2$	20	7.8	20
	(5)	$Mg(OH)_2 + CO_2$	20	7.8	65
	(6)	$MgO + CO_2$	20	8.4	20

Product formed (confirmed by XRD)	Reagents	Slurry temperature (°C)	Final pH of slurry before filtration	Drying temperature (°C)
hydromagnesite (1)	$Mg(OH)_2 + CO_2$	65°C + 0.1 M HCl	9.1	60
(2)	$Mg(OH)_2 + CO_2$	65°C + 1 M HCl	8.3	60
(3)	$Mg(OH)_2 + CO_2$	65°C + 1 M HCl	8.3	120
(4)	$Mg(OH)_2 + CO_2$	19	7.6	100
(5)	$Mg(OH)_2 + CO_2$	20	7.8	120
(6)	$MgCO_3 \cdot 3H_2O$	90	9.7	65
(7)	$MgSO_4 \cdot 7H_2O + Na_2CO_3$	90	8.8	160
dypingite	$Mg(OH)_2 + CO_2$	65°C + 1 M HCl	8.3	20
unidentified (1)	$Mg(OH)_2 + CO_2$	19	7.6	90
(2)	$Mg(OH)_2 + CO_2$	20	7.8	80
(3)	$MgCO_3 \cdot 3H_2O$			80
				100
				120
(4)	$MgO + CO_2$	20	8.4	80
			8.4	120

Comparing the various procedures that delivered hydromagnesite, indicate advantages and disadvantages for each procedure. The synthesis of hydromagnesite via procedure 1, 2 and 3 included the use of elevated temperatures and additional reagents in order to successfully prepare the required product. The cost of heating the slurry adds to processing costs. The final product also required additional washing to ensure the absence of chloride in the precipitate.

The synthesis of hydromagnesite via procedure 4 and 5 was relatively simple. One drawback which was encountered, was the long reaction time necessary to obtain the desired final pH. In this procedure a constant CO_2 gas flow was employed despite the slurry volume. A constant gas flow was employed due to gas flow measurement equipment limitations. This resulted in increased reaction time required to produce larger amounts of product. This can be overcome by increasing the CO_2 flow when working with larger slurry volumes, thus reducing the reaction time.

Procedures 6 and 7 stipulates a different starting reagent compared to the previous five procedures. It is important to note that the availability of a specific starting reagent might influence the choice of the most appropriate procedure that could be employed. Procedure 6 describes the synthesis of hydromagnesite from $MgCO_3 \cdot 3H_2O$ should this reagent be readily available. The procedure entails the use of elevated temperatures, which is not always desirable when synthesising hydromagnesite.

Procedure 7 is a proven method and has achieved much success in delivering hydromagnesite as product. This method is associated with elevated temperatures and delivers sulphate as effluent which could be undesirable, considering the environmental impact thereof .

Although cost and environmental issues play an important role in the choice of the most appropriate procedure, it is also important to take into account the influence of the method of synthesis on the characteristics of the final product. The possibility exists that the physical and chemical properties of the products could be influenced by the method of synthesis. Since it was not possible to study all the hydromagnesite products that were prepared, only two procedures were chosen and investigated in detail. The decision was based solely on economical and environmental issues. The procedure in which CO_2 is sparged through a $Mg(OH)_2$ slurry at ambient temperature and drying the solid at 80 and 120°C was chosen for further investigation. This procedure is simple, energy efficient and potentially environmentally friendly.

Chapter 6

Characterisation of the basic magnesium carbonates

6.1 Introduction

The following discussion is based on the characterisation of a select group of basic magnesium carbonates synthesised as discussed in chapter 5. The five techniques used in order to study the characteristics of the various compounds were thermogravimetric analysis (TG), differential thermal analysis (DTA), surface area determination, scanning electron microscopy (SEM) and Fourier transform infrared spectroscopy (FT-IR).

The aim of choosing different techniques to characterise the various products, was to obtain information relating to the various aspects that constitute the nature of the products. The use of TG and DTA makes it possible to obtain insight into the thermal decomposition characteristics of a product. Thermal decomposition includes the mass changes that takes place as a function of temperature or time (TG) and the energy changes that occurs as a function of temperature or time (DTA).

Surface area can give an indication of the chemical activity of a solid which relates to its internal area and/or the existence of lattice strain. The surface area properties may reveal itself in the chemical properties of the solid.

SEM is widely used to examine the surfaces of products and to obtain information relating to the morphology of the product.

FT-IR gives information of the dimension and composition of molecules, as well as molecular vibrational, rotational, and electronic states.

The characteristics of the synthetically obtained products were compared to the characteristics of $Mg(OH)_2$, as well as to a commercially available hydromagnesite

compound. Each technique contributed in highlighting the various characteristics of a specific compound. It was possible to distinguish between the physical and chemical properties of the various compounds by combining the results of the respective techniques.

6.2 Experimental

6.2.1 Samples

The procedures that were followed to synthesise the compounds are summarised below. The compounds will be referred to in the discussion by the names/formulas indicated in ***brackets***.

1. $Mg(OH)_2$ (CP from UniLAB, Saarchem (Pty) Ltd) (***$Mg(OH)_2$***) and commercially available hydromagnesite (CP from UniLAB, Saarchem (Pty) Ltd) (***commercial hydromagnesite***).

2. $MgCO_3 \cdot 3H_2O$ (nesquehonite), synthesised by sparging CO_2 gas through a $Mg(OH)_2$ slurry at ambient temperature and drying the solid at 65°C [Chapter 5.2.2.2] (***$MgCO_3 \cdot 3H_2O$***). The unidentified products formed by heating $MgCO_3 \cdot 3H_2O$ at 80°C (***$MgCO_3 \cdot 3H_2O$ 80 °C***) and 120°C (***$MgCO_3 \cdot 3H_2O$ 120 °C***) (DTA only) [Chapter 5.2.2.5 (2)].

3. An unidentified compound and hydromagnesite, synthesised by sparging CO_2 gas through a $Mg(OH)_2$ slurry at ambient temperature, drying half of the solid at 80°C (***unidentified***) and the other half at 120°C (***$Mg(OH)_2$ 120 °C***) respectively [Chapter 5.2.2.5 (1)].

4. Dypingite synthesised by sparging CO_2 gas through a $Mg(OH)_2$ slurry at ambient temperature and drying the solid at 120°C for 3 h (***3 h dypingite***) (SEM only) [Chapter 5.2.2.6].

5. Dypingite synthesised by the addition of 1 M HCl to a $Mg(OH)_2$ slurry that was preheated to 65°C. The solid was filtered and dried at ambient temperature [Chapter 5.2.2.5 (3)] (***1 M HCl dypingite***).

6. Hydromagnesite prepared by the addition of a $MgSO_4 \cdot 7H_2O$ solution to a Na_2CO_3 solution and drying the precipitate at 160°C (***$MgSO_4 \cdot 7H_2O + Na_2CO_3$***) [Chapter 5.2.5].

7. The unidentified compounds synthesised by sparging CO_2 gas through a MgO slurry at ambient temperature, drying half of the solid at 80°C (***MgO 80 °C***) and the other half at 120°C (***MgO 120 °C***) (only DTA and SEM) [Chapter 5.2.4].

6.2.2 Thermogravimetric analysis

Thermogravimetric and calorimetric analyses were performed on a NETZSCH STA 409 simultaneous TG-DTA instrument. Sample sizes varied between 12 and 14 mg. A heating rate of 10°C min^{-1} was used in an air atmosphere. All data was obtained using platinum crucibles. DTA peak maxima were used and compared to each other, as sample sizes and conditions were kept as constant as possible.

6.2.3 Surface area determinations

Surface area determinations were conducted on a Micromeritics FlowSorb II 2300 BET instrument, using nitrogen gas at liquid nitrogen temperature as an adsorptive. Samples of MgO were prepared by heating samples of the various products separately for 15 minutes in a Barnstead Thermolyne laboratory furnace. This procedure was repeated for samples from each product at various temperatures covering the range of 20 to 1000°C. All samples were cooled in a desiccator before the surface area was measured.

6.2.4 Scanning electron microscopy

The surface morphology of the synthesised compounds were analysed on a JEOL 840 scanning electron microscope at an accelerating voltage of 5 kV. The samples were sputter coated with gold in a Polaron E 5200 autocoating unit before viewing.

6.2.5 Infrared analysis

Transmission spectra were recorded using a BRUKER® 113v FTIR spectrometer in the mid-infrared range. All spectra were obtained from KBr discs containing approximately 1 mg of sample and 100 mg of dry KBr. The sample chamber was evacuated (P = 170 mbar) during the recordings.

6.3 Results and Discussion

6.3.1 Thermogravimetric analysis

The TG and DTA results that will be presented, were obtained by simultaneous measurement. Since the heating rate, atmosphere and sampling characteristics were identical for both measurements, it was possible to directly compare and relate the results to each other.

The DTA curves of the various products that were investigated are given in Figure 6.1. Compared to $MgCO_3 \cdot 3H_2O$ and the basic magnesium carbonates which decomposed in multiple steps, $Mg(OH)_2$ decomposed in a single step. All the products decomposed endothermically.

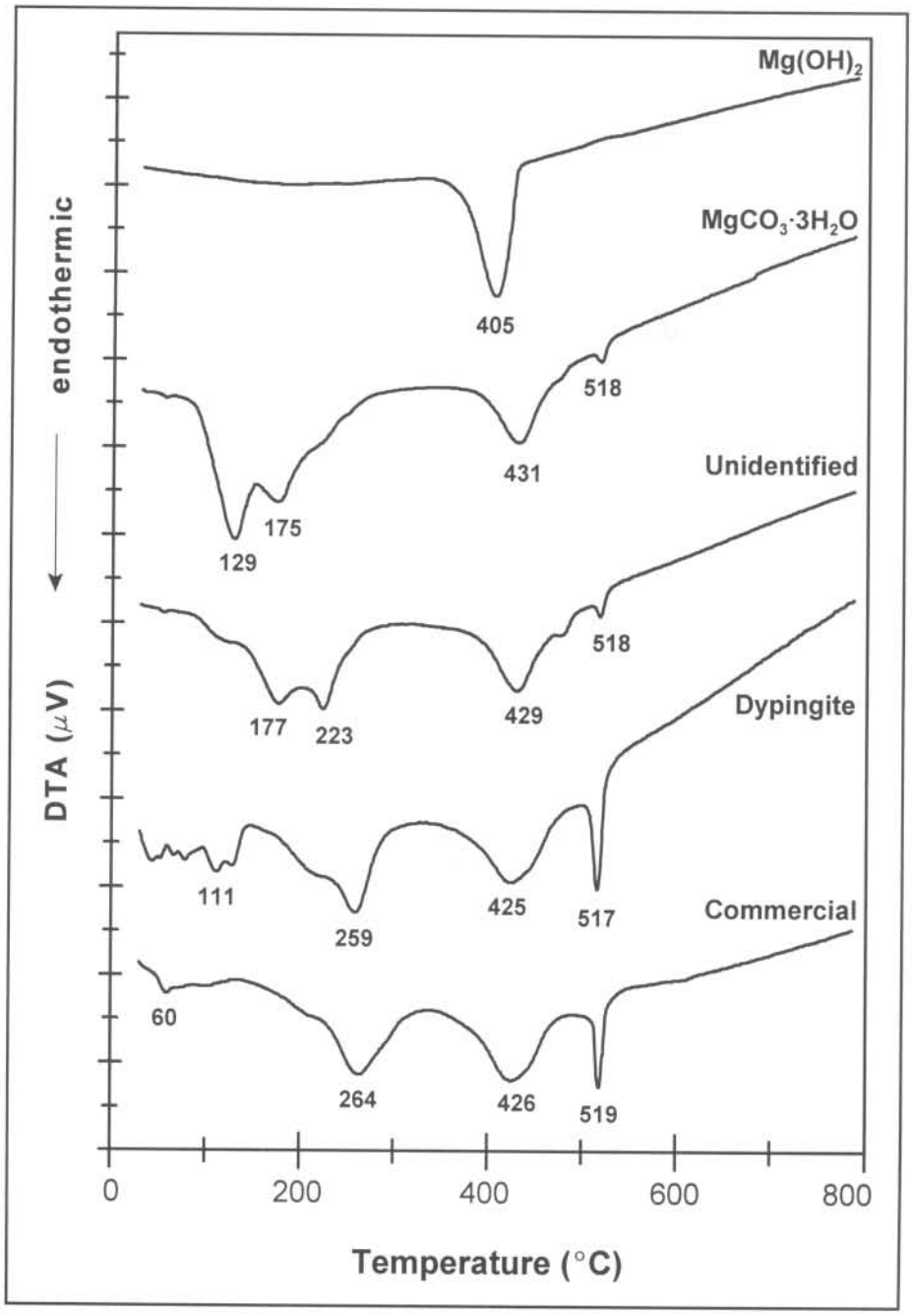

Figure 6.1 DTA curves of the various products

The single endothermic effect observed for $Mg(OH)_2$, is ascribed to the loss of hydroxyl water. This phenomenon occurs typically over the range 350–450°C (Webb, 1970) and can be described by the following reaction:

$$Mg(OH)_{2\,(s)} \rightarrow MgO_{\,(s)} + H_2O_{\,(g)}$$

The decomposition of $MgCO_3 \cdot 3H_2O$ in multiple steps, was due to the fact that it had to undergo both dehydration and decarbonation. These processes require different amounts of energy to take place and were subsequently observed at different temperatures. The endothermic doublet just below 200°C was attributed to the loss of two molecules of water of crystallisation. The remaining molecule of water was expelled between 400–450°C (Webb and Krüger, 1970). Above 500°C, carbonate decomposition took place. These processes can be summarised as follow:

$$MgCO_3 \cdot 3H_2O_{(s)} \rightarrow MgCO_{3\,(s)} + 3\,H_2O_{(g)}$$

$$MgCO_{3\,(s)} \rightarrow MgO_{(s)} + CO_{2\,(g)}$$

The thermal decomposition of hydromagnesite is expected to proceed via dehydration (removal of water of crystallisation) below 250°C, dehydroxylation (decomposition of magnesium hydroxide to MgO) between approximately 250 and 350°C, and decarbonation (decomposition of magnesium carbonate to MgO) above 350°C (Choudhary *et al.*, 1994).

$$4\,MgCO_3 \cdot Mg(OH)_2 \cdot 4H_2O_{(s)} \rightarrow 4\,MgCO_3 \cdot Mg(OH)_{2\,(s)} + 4\,H_2O_{(g)} \quad (<250°C)$$

$$4\,MgCO_3 \cdot Mg(OH)_{2\,(s)} \rightarrow 4\,MgCO_{3\,(s)} + MgO_{(s)} + H_2O_{(g)} \quad (250–350°C)$$

$$4\,MgCO_{3\,(s)} \rightarrow 4\,MgO_{(s)} + 4\,CO_{2\,(g)} \quad (>350°C)$$

These stages of decomposition could be identified for both commercial hydromagnesite and dypingite in the corresponding DTA results (Figure 6.1). It is evident from these results that dypingite and hydromagnesite decomposed similarly. This observation is supported by Raade (1970). The only noticeable difference between the DTA curves of these two compounds, is that dypingite contains loosely bound water that was lost at comparatively low temperatures (50–130°C). The peaks around 100°C for dypingite are similar, though less pronounced than those observed by Raade (1970).

The unidentified compound decomposed similarly to $MgCO_3 \cdot 3H_2O$ and commercial hydromagnesite above 350°C. Below 350°C the differences were more pronounced. The unidentified compound decomposed in a temperature range that was intermediate to the decomposition of $MgCO_3 \cdot 3H_2O$ and commercial hydromagnesite below 350°C. Since the unidentified compound did not undergo any decomposition between

250–350°C, but mainly below 250°C it was concluded that it probably contained mainly water of crystallisation in its structure. It was further concluded that the unidentified compound probably contained less hydroxyl groups than that observed for commercial hydromagnesite.

The occurrence of an exothermic phenomenon that precedes the prominent DTA peak around 518°C has been observed for basic magnesium carbonate (Choudhary *et al.*, 1994; Khan *et al.*, 2001). This phenomenon was not observed during this investigation. There are various aspects that influences the exothermic peak. This includes heating rate, sample size and atmospheric conditions (Khan *et al.*, 2001). Khan *et al.* (2001) showed that either a dry carbon dioxide atmosphere, or a much larger sample size was necessary to obtain the exothermic phenomenon at a 10°C min^{-1} heating rate, as was used for this investigation. The exothermic phenomenon is ascribed to strain within the crystal lattice that is released in the form of heat (Khan *et al.*, 2001) and/or crystallisation of cubic MgO (Raade, 1970).

The TG mass loss curves of the various products are presented in Figure 6.2. The mass losses are given for below 320°C (left of the dotted line) and above 320°C (right of the dotted line). It was difficult to obtain the mass loss for each step during decomposition, since the various decomposition stages overlapped with one another. An attempt was made to separate the various stages, by using a lower heating rate. This approach was not successful since it only resulted in obscured DTA peaks which made it more difficult to distinguish between the various stages. It was decided to distinguish only between the two most distinct stages. From the DTA curves (Figure 6.1) it seemed that the two most distinct stages could be separated at approximately 320°C.

The TG curves clearly indicate a difference in mass loss below 320°C when comparing $MgCO_3 \cdot 3H_2O$ and the basic magnesium carbonate products. It is evident that the larger mass losses below 320°C could be associated with the products containing a larger amount of water of crystallisation with respect to their total mass ($MgCO_3 \cdot 3H_2O$ and dypingite). The TG curves were also characterised by a well defined mass loss above 320°C corresponding to decarbonation. The prominent mass loss at approximately 500°C, observed for commercial hydromagnesite and dypingite, was attributed to the rapid evolution of CO_2 gas.

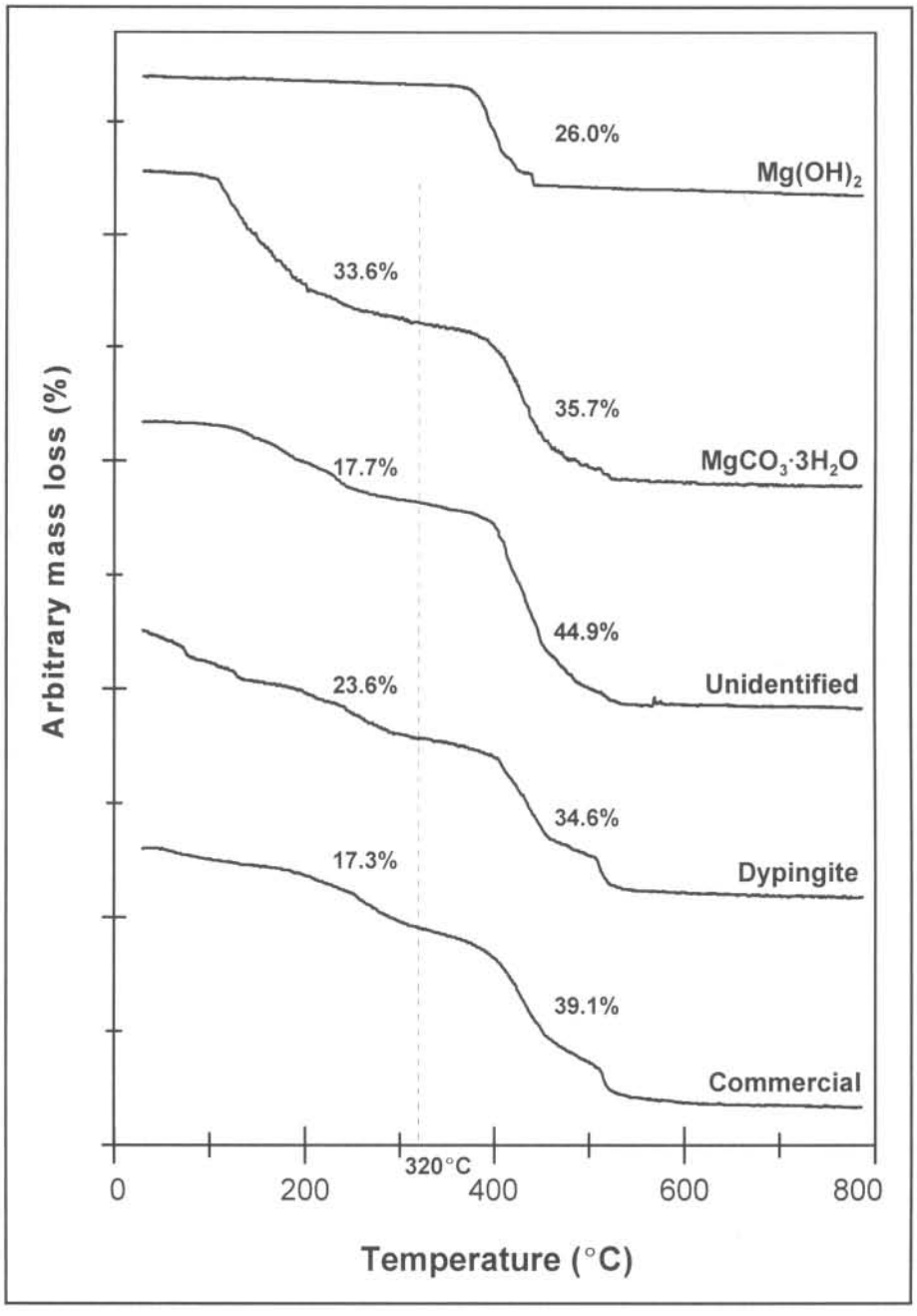

Figure 6.2 TG mass loss curves of the various products

The expected total theoretical mass loss of each product was compared to the total experimental mass loss. This is depicted in Table 6.1. It is evident that the experimental values compared favourably to the expected theoretical values. There is no theoretical value for the unidentified compound, since its molecular formula was unknown. The experimental mass loss for $Mg(OH)_2$ is lower than the expected

theoretical value. It could be possible that there were still traces of water that has not been driven off, since very high temperatures are required to dehydrate $Mg(OH)_2$. This conclusion is supported by Hair (1967) who observed the presence of a free surface hydroxyl grouping at 750°C for $Mg(OH)_2$.

Table 6.1 Comparison of the total theoretical and experimental mass losses (%) of the various products

Product	Total theoretical mass loss (%)	Total experimental mass loss (%)
$Mg(OH)_2$	30.9	26.0
$MgCO_3 \cdot 3H_2O$	70.9	69.3
Unidentified	—	62.6
Dypingite	58.5	58.2
Hydromagnesite (commercial)	56.9	56.4

The DTA curves of the hydromagnesite products that were obtained by different procedures were compared to the commercial product (Figure 6.3). It is evident from these results that the method of synthesis did not influence the decomposition characteristics of the respective products. The possibility does exist that the method by which a product was obtained could influence its decomposition characteristics as indicated by Choudhary *et al.* (1994). The very small endothermic peak at 60°C for each of these products was attributed to hygroscopic water (Raade, 1970).

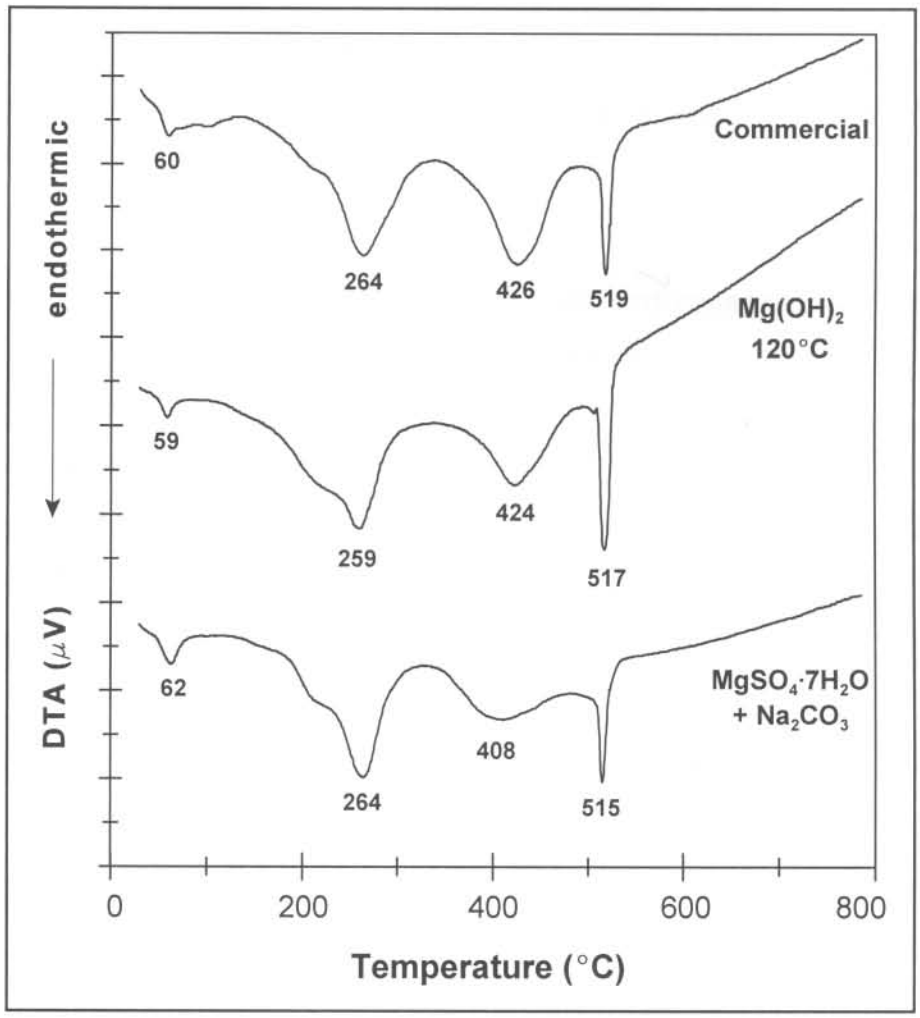

Figure 6.3 DTA curves of the hydromagnesite products that were obtained by different procedures

The mass losses for the hydromagnesite products that were obtained by different procedures were compared to the expected theoretical mass loss of hydromagnesite (Table 6.2). The experimental values compared reasonably well with the theoretical values. The 17% mass loss observed below 320°C for the hydromagnesite products represents approximately 4.5 molecules of water. Since hydromagnesite contains 5 molecules of water (19.3% mass loss), some water must be lost above 320°C. The larger experimental mass losses compared to the theoretical mass losses above 320°C can then be ascribed to 0.5 molecule of water and 4 molecules of CO_2 (for commercial hydromagnesite), 4.2 molecules of CO_2 (for $Mg(OH)_2$ 120°C) and 3.6 molecules of CO_2 (for $MgSO_4 \cdot 7H_2O + Na_2CO_3$). The deviation of the total mass loss of $Mg(OH)_2$ 120°C

and $MgSO_4 \cdot 7H_2O + Na_2CO_3$ from the expected theoretical values, were ascribed to errors in weighing the sample before measurement. Since very small sample masses were used, a small error in weighing could result in a large error when calculating percentage mass loss.

Table 6.2 Comparison of mass losses (%) for hydromagnesite products that were obtained by different procedures

Hydromagnesite	Mass loss < 320°C (%)	Mass loss > 320°C (%)	Total mass loss (%)
Theoretical	19.3	37.6	56.9
Commercial	17.3	39.1	56.4
$Mg(OH)_2$ 120°C	17.1	41.5	58.6
$MgSO_4 \cdot 7H_2O + Na_2CO_3$	17.2	36.2	53.4

The DTA curves of the unidentified compounds that were obtained by various procedures are given in Figure 6.4. The DTA peaks of the unidentified compound ($Mg(OH)_2$ 80°C), $MgCO_3 \cdot 3H_2O$ 80°C and MgO 80°C appeared to be very similar. The DTA curves of the unidentified compounds of $MgCO_3 \cdot 3H_2O$ 120°C and MgO 120°C, were similar to the previous three products with respect to the peaks above 320°C. It is clear though that the doublet peaks that were observed below 320°C for the unidentified compound ($Mg(OH)_2$ 80°C), $MgCO_3 \cdot 3H_2O$ 80°C and MgO 80°C, was replaced by a single peak for the unidentified compounds of $MgCO_3 \cdot 3H_2O$ 120°C and MgO 120°C. This could be ascribed to the higher temperatures at which $MgCO_3 \cdot 3H_2O$ 120°C and MgO 120°C were dried. The higher drying temperatures possibly resulted in driving off the weaker bonded crystallisation water. These results clearly indicated that the temperature at which these products were dried influenced their thermal decomposition, and hence their composition regarding the amount of water molecules either taken up in their structure or attached to the structure.

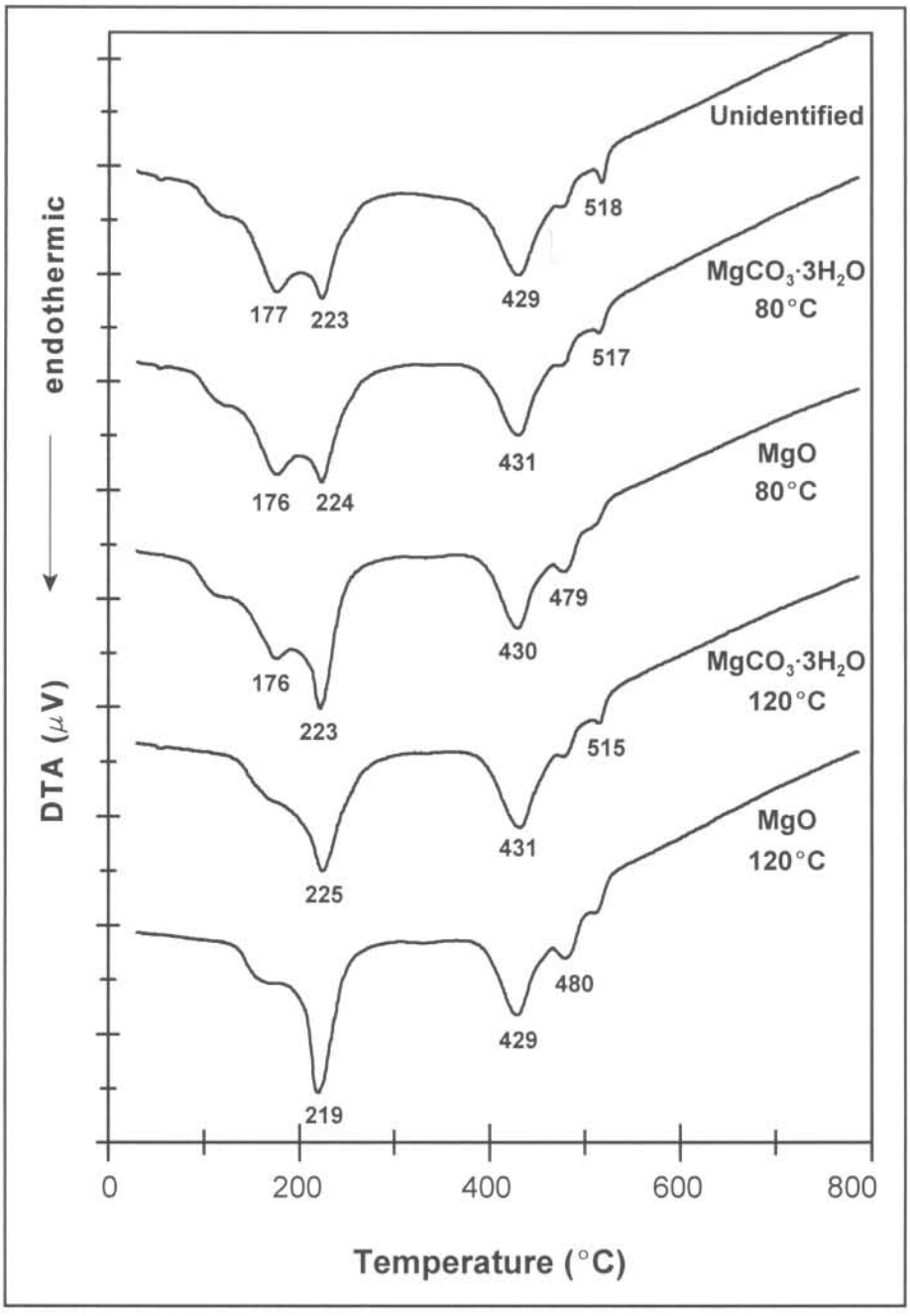

Figure 6.4 DTA curves of unidentified products that were obtained by various procedures

6.3.2 Surface area

When a solid parent material (A) calcines to yield a solid product (B) and a gas (C), it is generally observed that the product is formed with well-developed porosity, and a tremendous increase in surface area. This could happen although the parent solid (A) is nonporous. Examples include calcination of hydroxides, carbonates and oxalates (Mikhail and Robens, 1983). Apart from the development of pores that contributes to increased surface area, another factor also contributes to this phenomenon. The existence of lattice strain, so that some or all of the atoms or ions of the solid are displaced somewhat from the positions they would occupy in the perfect lattice, is also a contributing factor (Gregg, 1953).

The following investigation was based on the determination of the surface area of MgO that was obtained by thermal decomposition of the respective products. The aim of the investigation was to determine whether there were any differences between the surface area of MgO that was obtained from the various products, and relating it to the method of synthesis. Initial investigations were based on the influence of heating time on the surface area profile of MgO obtained by thermal decomposition of $Mg(OH)_2$. The results of heating $Mg(OH)_2$ for respectively 6, 15 and 30 minutes at various temperatures between 20 and 1000°C are given in Figure 6.5.

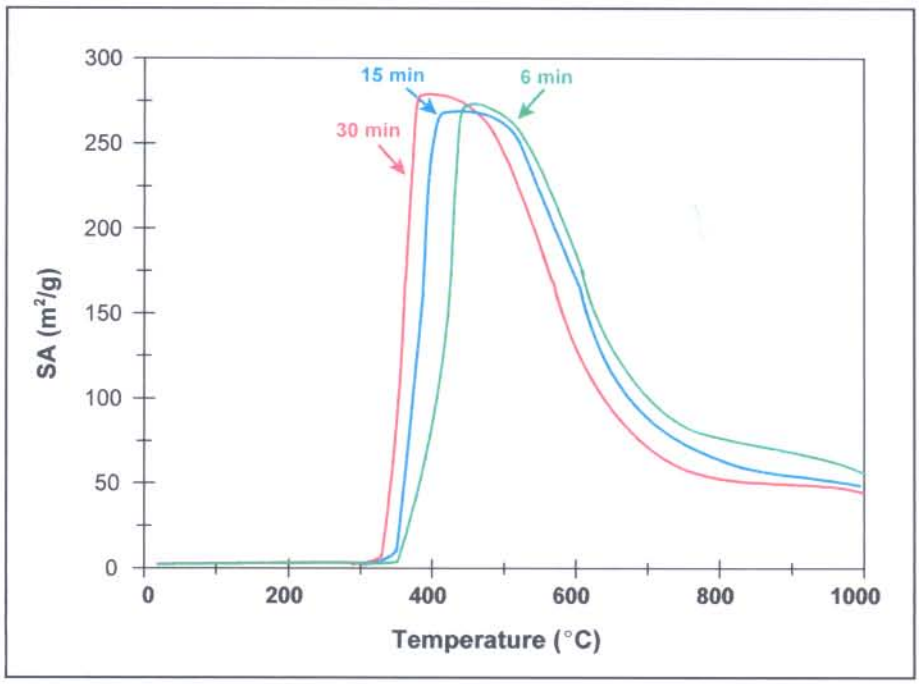

Figure 6.5 Surface area profiles of MgO obtained by decomposition of $Mg(OH)_2$ for different times (6, 15, 30 min) at temperatures between 20 and 1000°C

It is evident that the profiles were influenced by the heating time. For longer heating times, the profile reached a maximum surface area at a lower temperature compared to the shorter heating times. This could be ascribed to the fact that at the longer heating times, a larger amount of decomposition of the solid surface took place compared to less decomposition at the shorter heating times. It was decided that in order to compare the surface area of the various products, the products must be heated for the same time before determining the surface area. For practical reasons a 15 minute heating time was chosen. This allowed enough time for the oven to equilibrate after opening it to place the sample inside.

The surface area profiles that were obtained for the decomposition of the various products are depicted in Figure 6.6. The maximum MgO surface area, in decreasing order, was as follows:

$Mg(OH)_2$ >> unidentified ≈ $Mg(OH)_2$ 120°C > dypingite ≥ $MgSO_4 \cdot 7H_2O + Na_2CO_3$ ≥ commercial hydromagnesite

It is evident that MgO obtained from the decomposition of $Mg(OH)_2$ exhibited the highest surface area. The increase in surface area started at ~350°C which corresponded to the decomposition of $Mg(OH)_2$ ➜ MgO. A maximum surface area was obtained at ~450°C. Above 450°C the surface area decreased.

The large maximum MgO surface area obtained by thermal decomposition of $Mg(OH)_2$, could possibly be explained as follow. According to Green (1983), the thermal decomposition of $Mg(OH)_2$ to MgO occurs topotactically by a mechanism involving the formation of a defect layer of $Mg(OH)_2$, but contracted unit cell dimensions. This structure recrystallises suddenly to the cubic structure characteristic of MgO. If the $Mg(OH)_2$ particles are larger than about 60 nm, recrystallisation will give rise to cracking of the MgO product into particles of about 5 to 10 nm, as the lattice fracture stress is exceeded by the contractional strains. Cracking of the MgO crystallites could then possibly result in an increased MgO surface area (Yoshida *et al.*, 1995). Since most commercially precipitated $Mg(OH)_2$ have crystal sizes above this value, cracking may be expected.

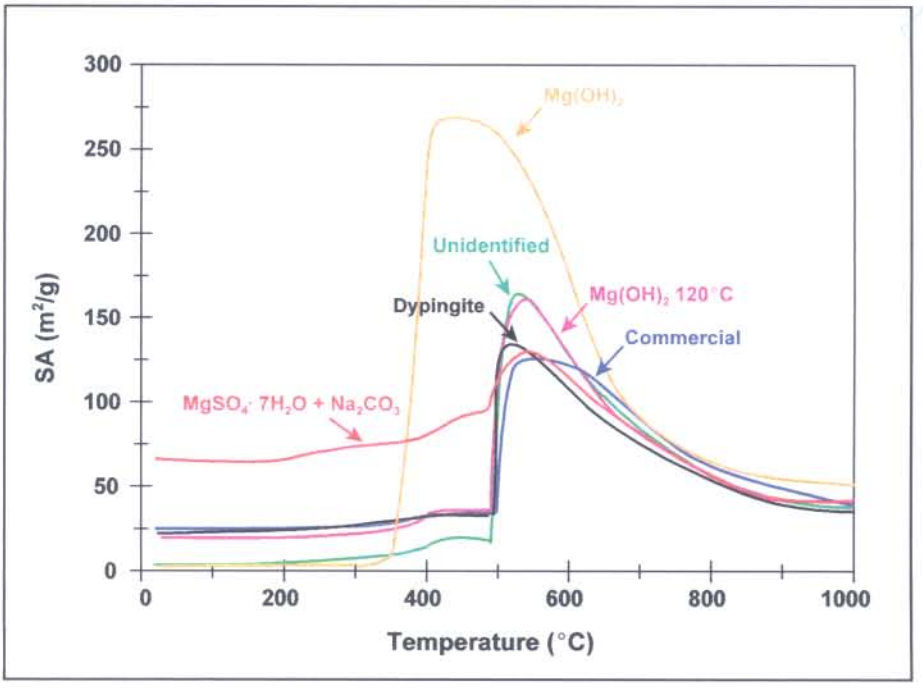

Figure 6.6 Surface area profiles of MgO obtained by decomposition of the various products heated for 15 min at various temperatures between 20 and 1000°C

The surface area profiles of MgO obtained from the other five products, were characterised by a slight increase in surface area at ~400°C, followed by a rapid increase in surface area at ~500°C. The observed increase in surface area of MgO obtained from these products did not correspond to the various stages of decomposition as was expected. This could be ascribed to the fact that at relatively low temperatures (below 250°C), crystallisation water was mainly expelled from the respective products. The removal of the water of crystallisation from the decomposing products, did not seem to result in a prominent change in the surface area of the compounds.

Between 250 and 500°C dehydroxylation and decarbonation took place. Dehydroxylation and decarbonation involved the removal of OH and CO_2 groups from the crystal lattices of the various products. This possibly resulted in a degradation of the respective crystal structures and subsequently an increase in surface area . The rapid increase in surface area at ~500°C was associated with the rapid evolution of CO_2 from the sample matrix. According to Khan *et al.* (2001) at the final stage of CO_2

evolution, mechanical stress in the matrix results in the breakdown of the sample into smaller fragments, which results in an increase of the reaction interface.

Comparison of the surface area profiles of MgO obtained from the respective hydromagnesite products (commercial, $Mg(OH)_2$ 120°C and $MgSO_4 \cdot 7H_2O + Na_2CO_3$) indicated a difference. The maximum surface area decreased for $Mg(OH)_2$ 120°C to $MgSO_4 \cdot 7H_2O + Na_2CO_3$ to commercial. It is evident that the procedure by which the products were obtained had a noteworthy influence on the subsequent MgO surface area. Choudhary *et al.* (1995) showed that the precipitating conditions, among other things, influenced the surface area of MgO obtained from basic magnesium carbonate.

The surface area of MgO obtained from dypingite was comparable to the MgO surface area obtained from the $MgSO_4 \cdot 7H_2O + Na_2CO_3$ and commercial hydromagnesite products. The presence of trace amounts of anions (Cl^-) occluded in the structure of dypingite could be responsible for the surface properties of MgO (Choudhary, 1995). The occlusion of trace amounts of Cl^- in the dypingite structure is possibly the result of inadequate washing of the solid product that was obtained by the addition of HCl during synthesis. This argument also applies to the $MgSO_4 \cdot 7H_2O + Na_2CO_3$ product that could possibly contain trace amounts of SO_4^{2-} ions.

The surface area behaviour of MgO obtained from the unidentified compound and hydromagnesite that were synthesised from $Mg(OH)_2$ and dried at 80 and 120°C respectively, delivered similar results. This was attributed to the similarity in the synthesis procedure. It would seem that the drying temperature did not influence the surface area behaviour of the MgO obtained from these two compounds. A possible explanation why the MgO surface area of these two products were higher than that of dypingite, $MgSO_4 \cdot 7H_2O + Na_2CO_3$ and commercial hydromagnesite, could be their relationship to the precursor $Mg(OH)_2$. The unidentified compound as well as the $Mg(OH)_2$ 120°C product were synthesised from $Mg(OH)_2$, which exhibited a large MgO surface area during decomposition. The surface area characteristics of $Mg(OH)_2$ that results in a large MgO surface area during decomposition, could probably have been retained, to a small extent, in the crystal structures of the newly synthesised products.

In general, the maximum in the surface area profiles versus calcination temperature was the result of the two overlapping processes, activation (decomposition) and sintering (recrystallisation) (Mikhail and Robens, 1983). The decrease in surface area that was observed after maximum MgO surface area was obtained for all the products,

was ascribed to sintering. Sintering occurs as a result of the adhesion of adjacent particles or micelles and is brought about by surface forces. A reduction of surface energy is observed due to the loss of surface area where two particles join. This process occurs at those places where the surfaces of neighbouring micelles are within atomic distance of each other; but the regions immediately adjacent to the area of contact are still within each other's range of attraction, and the forces between them are equivalent to a shearing stress exerted on the two micelles near the region of contact. The adhesion process will continue until it is halted by unfavourable geometry, when surface irregularities are such that areas adjacent to the area of contact and belonging to neighbouring particles are outside the range of each other's attractive forces (Gregg, 1953). Since a rise in temperature reduces the rigidity of solids, adhesion will be promoted by an increase in temperature.

Sintering is a rate determined process, involving an energy barrier, so that the extent of sintering is a function of both temperature and time. The extent of sintering, in this instance, was the result of an increase in temperature for a fixed time. Heating a compound beyond the time at which conversion of the undecomposed phase to the decomposed phase (MgO) was complete, would result in sintering and the activity and correlating surface area would begin to decrease (Gregg, 1953).

6.3.3 Scanning electron microscopy

The morphological and physical characteristics of a compound can be obtained by using SEM. SEM produces images with contrast and a great depth of focus. The initial aim of this investigation was to relate the surface characteristics of the various products under investigation, to the surface area results that were obtained in the previous section. This included identifying the presence of pores and if possible, compare the pore sizes of the products. It was only possible to obtain information regarding to the morphological characteristics at low magnifications. No pores could be observed. It was also difficult to observe any pores at higher magnifications. The information obtained though, contributed significantly in comparing the products with respect to physical appearance with each other.

The crystalline form of $Mg(OH)_2$, with uniaxial hexagonal platelets can be seen in Figure 6.7.

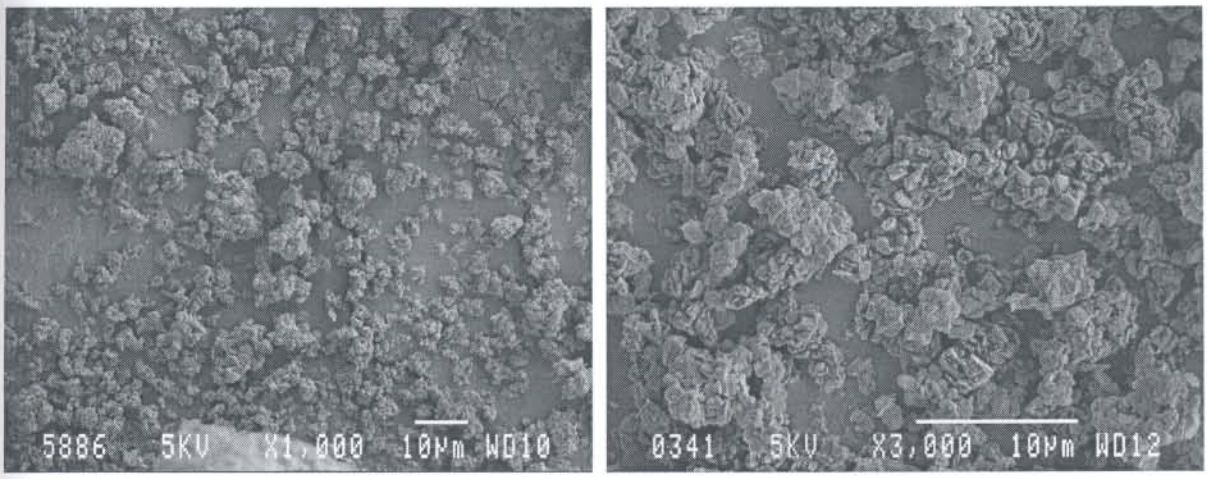

Figure 6.7 SEM image of $Mg(OH)_2$

The $MgCO_3 \cdot 3H_2O$ crystals (Figure 6.8) had a needle-like crystal form. This corresponds to the observations made by Davies and Bubela (1973) and Canterford and Moorrees (1985). The unidentified compound (Figure 6.9) had a similar crystal form to that of $MgCO_3 \cdot 3H_2O$. The presence of an additional possible phase looking like pods of crystals between the needle-like crystals was observed for the unidentified compound (x1000 magnification). This observation corresponds to that observed by Davies and Bubela (1973). In their investigation an intermediate phase was identified, named protohydromagnesite, growing amidst the needle-like crystals of $MgCO_3 \cdot 3H_2O$. The resemblance between the unidentified compound and protohydromagnesite was limited to the SEM images. The TG-DTA results of the unidentified compound and protohydromagnesite were only similar above 350°C with distinct differences below 350°C. An interesting observation was the presence of flake-like crystals on the needle-like crystals of the unidentified compound (x3000 magnification) (Figure 6.9). This resembled the flake-like appearance of the hydromagnesite products.

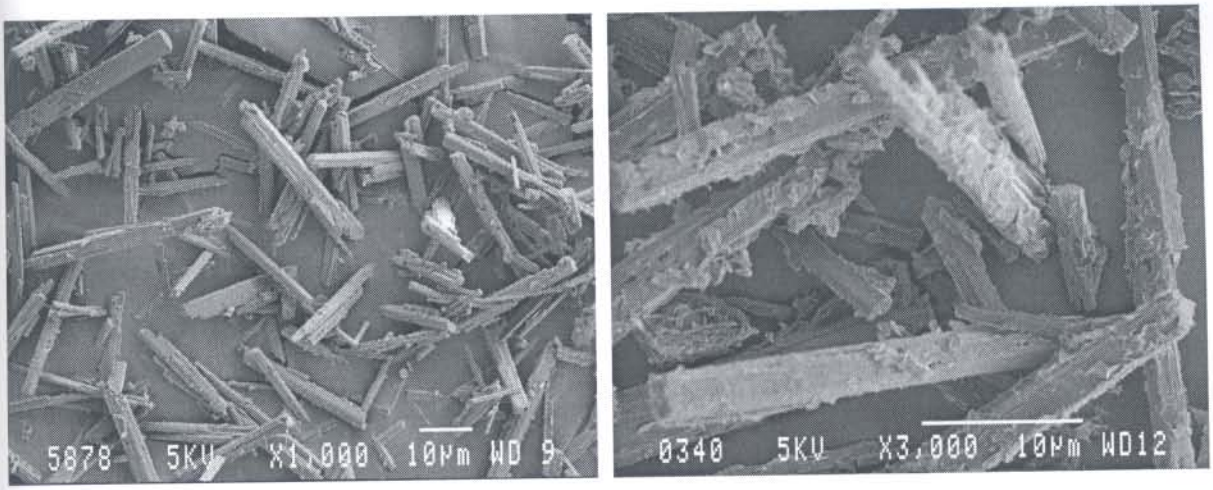

Figure 6.8 SEM image of $MgCO_3 \cdot 3H_2O$

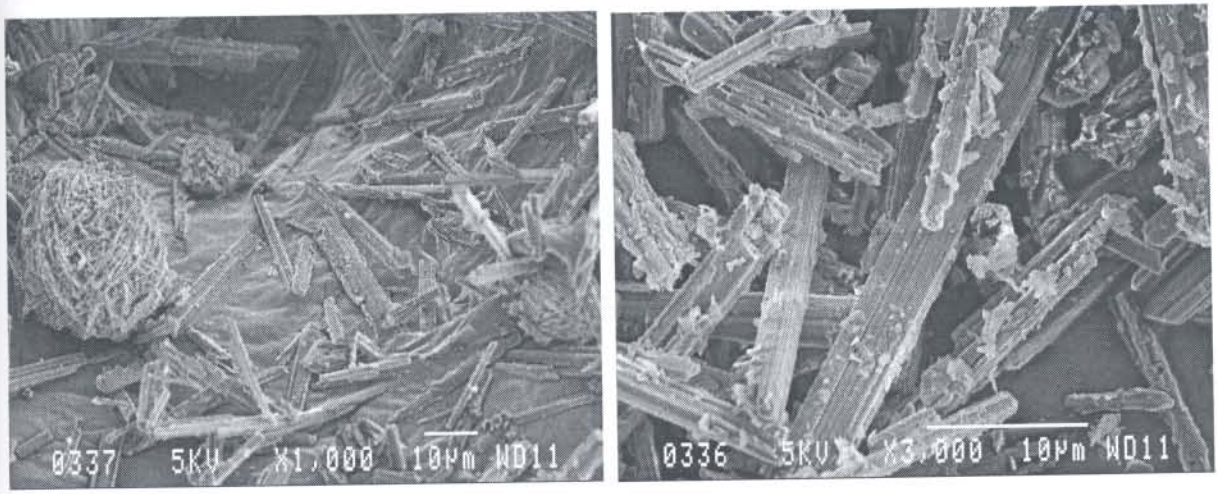

Figure 6.9 SEM image of unidentified compound

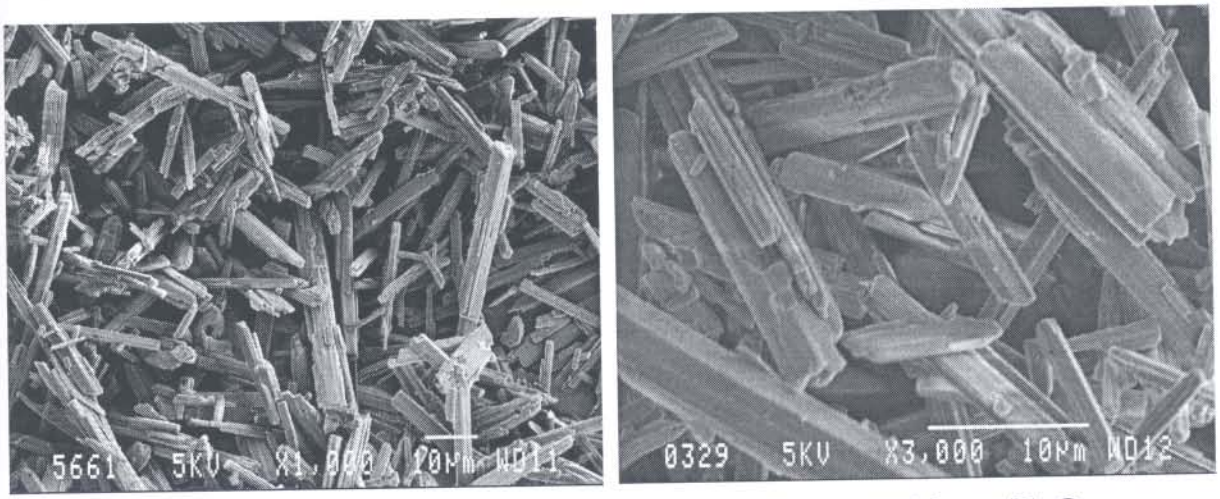

Figure 6.10 SEM image of unidentified compound obtained from MgO

The SEM image of the unidentified compound obtained from MgO (Figure 6.10) resembled that of $MgCO_3 \cdot 3H_2O$ (Figure 6.8). The presence of flake-like crystals growing on the needles were not observed. This is in contrast to that observed for the unidentified compound (Figure 6.9).

Figures 6.11 to 6.13 depict the SEM images of the hydromagnesite products that were obtained by different procedures. The expected physical appearance of hydromagnesite is as sprays, rosettas or crusts. The crystal could be acicular (needle-like) or bladed. It is also described as massive, powdery or chalk like (Roberts *et al.*, 1990). All three products had a flaky appearance that looked like flattened rosettes. Thin flakes of the hydromagnesite products entrap large quantities of air that accounts for its low bulk density (Gloss, 1952). The commercial product had the appearance of an agglomeration of the flakes.

The $Mg(OH)_2$ 120°C product (Figure 6.12) also had the appearance of an agglomeration of flakes, though the agglomeration seemed to be shaped in a needle form. This observation of a possible needle-like form related strongly to the needle shaped crystals observed for $MgCO_3 \cdot 3H_2O$ (Figure 6.8) and the unidentified compound (Figure 6.9). Since $MgCO_3 \cdot 3H_2O$ was observed as an intermediate phase to the formation of the $Mg(OH)_2$ 120°C product, it seemed possible that the original $MgCO_3 \cdot 3H_2O$ crystal form was retained. At a higher magnification it was observed that the flaky needle-like crystal form of the $Mg(OH)_2$ 120°C product was not solid, but it seemed that the needles consisted entirely of an agglomeration of flakes. It could possibly be concluded that the $Mg(OH)_2$ 120°C product crystallised within the needle shaped form.

The $MgSO_4 \cdot 7H_2O + Na_2CO_3$ product (Figure 6.13) also consisted of flakes and rosettes. Some appeared to be an agglomeration of flakes, while others had a bladed appearance.

It is evident from the hydromagnesite images that although the products were obtained by different procedures the general appearance of the crystals, flake-like and rosettes, were alike. The procedure by which these products were synthesised , did seem to influence the packing of the flakes and rosettes, either in an agglomeration or a needle-like/bladed form.

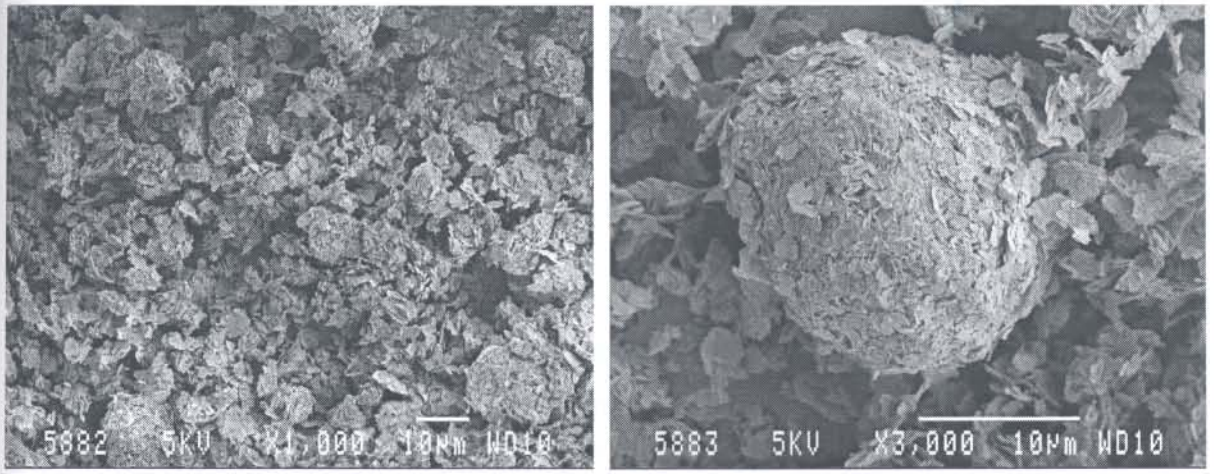

Figure 6.11 SEM image of commercial hydromagnesite

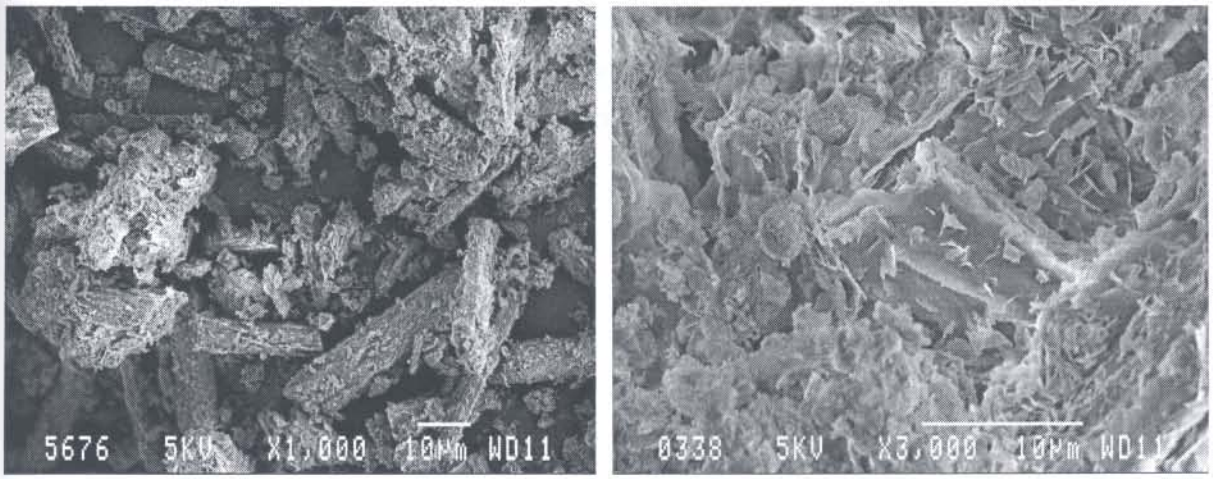

Figure 6.12 SEM image of $Mg(OH)_2$ 120°C

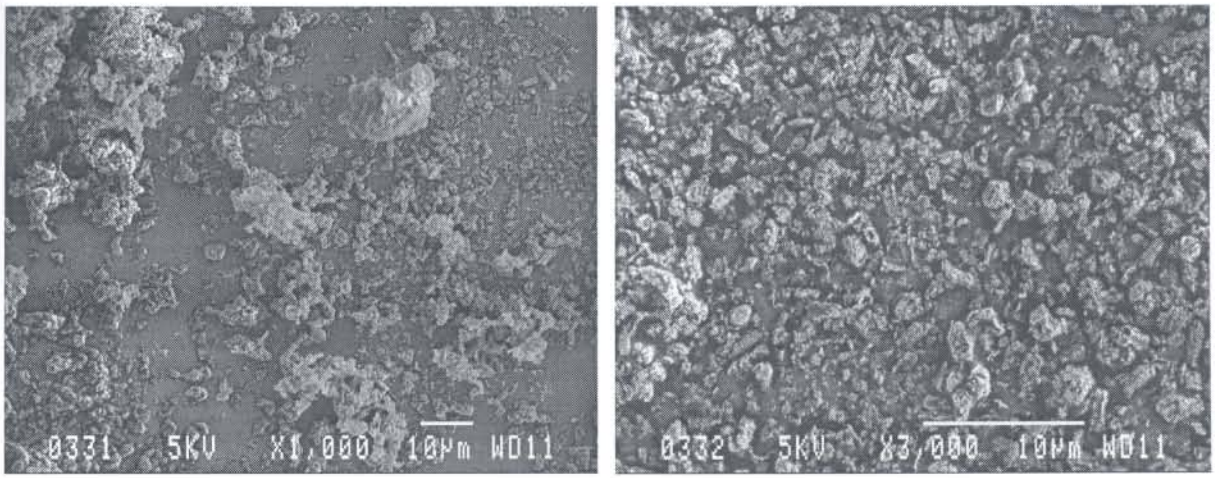

Figure 6.13 SEM image of $MgSO_4 \cdot 7H_2O + Na_2CO_3$

The SEM images of dypingite that was synthesised by different procedures are given in Figure 6.14 and Figure 6.15. In general the products had a flaky and rosette appearance similar to that observed for the hydromagnesite products. The product in Figure 6.14 had a similar appearance to the hydromagnesite product synthesised from $Mg(OH)_2$ 120°C (Figure 6.12). This dypingite product was obtained after approximately 3 h drying time of the $Mg(OH)_2$ 120°C product, compared to 24 h drying time for the $Mg(OH)_2$ 120°C hydromagnesite product (Figure 6.12). It may be expected that since these two products, 3 h and 24 h drying for $Mg(OH)_2$ 120°C, were obtained by the same procedure that the crystal form would be similar. This relates to the observation made from the respective SEM images (Figure 6.12 and Figure 6.14).

The dypingite product synthesised through the addition of 1 M HCl (Figure 6.15), had the appearance of globular aggregates. This corresponds to the observation made by Raade (1970). It is evident that the method of synthesis of dypingite influences the appearance of the crystal form as was observed for the respective hydromagnesite products.

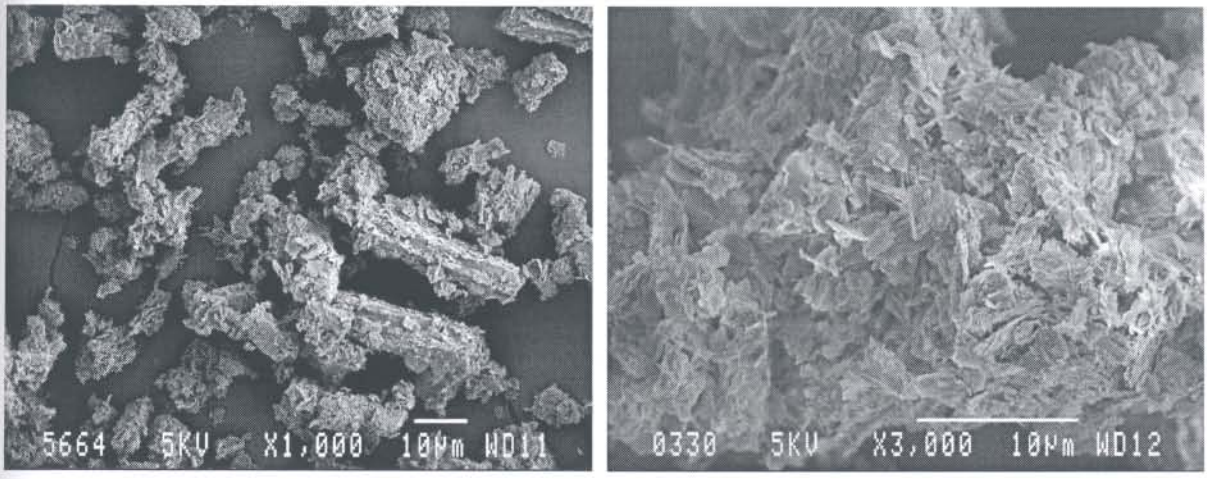

Figure 6.14 SEM image of 3 h dypingite

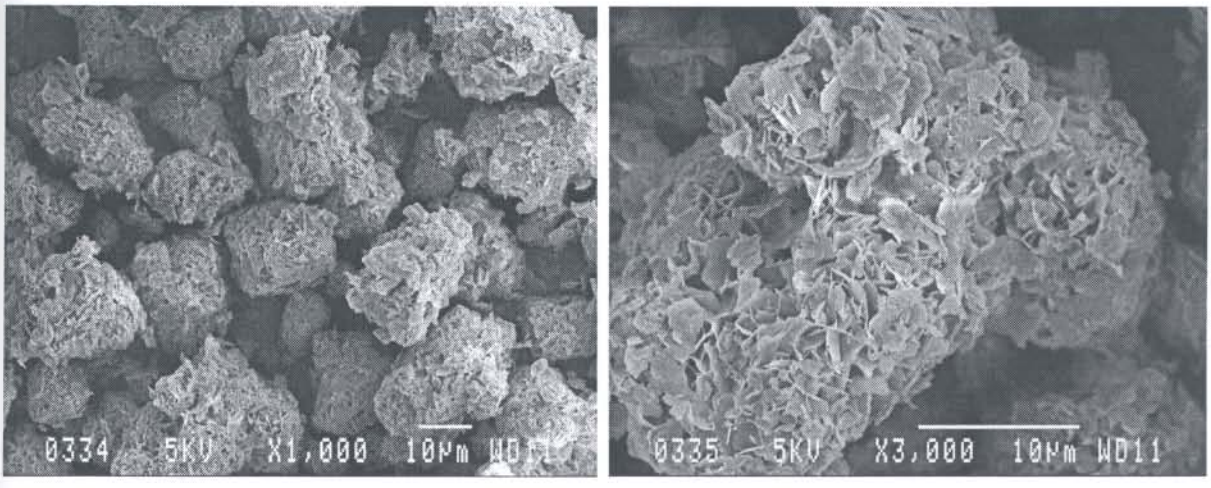

Figure 6.15 SEM image of 1 M HCl dypingite

6.3.4 Infrared analysis

The products that were investigated could be characterised with FT-IR, since each product exhibited characteristic IR bands. Although the products contained similar molecular groups, such as hydroxy, carbonate and/or water, the vibrations of these molecules were influenced by their coordination within the crystal structure of a specific product.

The IR spectra of the various products are given in Figure 6.16. $Mg(OH)_2$ exhibited a strong band at 3700 cm^{-1}, that was attributed to the anti-symmetrical OH stretching vibration of the lattice hydroxide (Hair, 1967).

The presence of carbonate, hydroxy and/or water in $MgCO_3 \cdot 3H_2O$ and the basic magnesium carbonates results in an IR spectrum with distinct characteristics that relates to the structure and composition of each compound. Group theoretical analysis of the carbonate molecule predicts four normal modes. Mode v_1 is associated with the symmetric stretch, v_2 the out-of-plane bend, v_3 the asymmetric stretch and v_4 in-plane bend.

The hydroxyl and water molecule stretching region near 3000 cm^{-1} for most hydrated carbonates, usually consists of one or two broad bands shifted somewhat to lower frequencies due to hydrogen bonding. In addition to the usual broad band, one or more very sharp bands occur for the basic magnesium carbonates. These bands have been interpreted to indicate two kinds of OH groups in the minerals: those that participate in the hydrogen bonding and those that do not. The broad bands occur at lower frequencies because the hydrogen bonding is stronger and causes a greater frequency shift (White, 1974).

$MgCO_3 \cdot 3H_2O$ exhibited a CO_3^{2-} v_1 symmetric stretching vibration at ~1098 cm^{-1} and a CO_3^{2-} bending vibration (v_2) at ~852 cm^{-1}. These bands were sharp and showed no multiplicity. The CO_3^{2-} v_3 asymmetric stretching vibrations at ~1420–1520 cm^{-1} exhibited at least three components. This is inconsistent with the structure that contains a single distinct CO_3^{2-} group (White, 1974). In the region where v_4 was expected, only two broad and ill-defined bands (601 and 701 cm^{-1}) were observed. The broad group of bands in the 3000 cm^{-1} range were attributed to O-H stretching motions of water or hydroxyl. The sharp band at 3568 cm^{-1} implies a longer hydrogen bond length than the hydrogen bond lengths at the lower frequencies (~3136–3463 cm^{-1}) (White, 1971). The H_2O bending vibration band at ~1650 cm^{-1} appeared as a prominent shoulder on the side of the CO_3^{2-} stretching band.

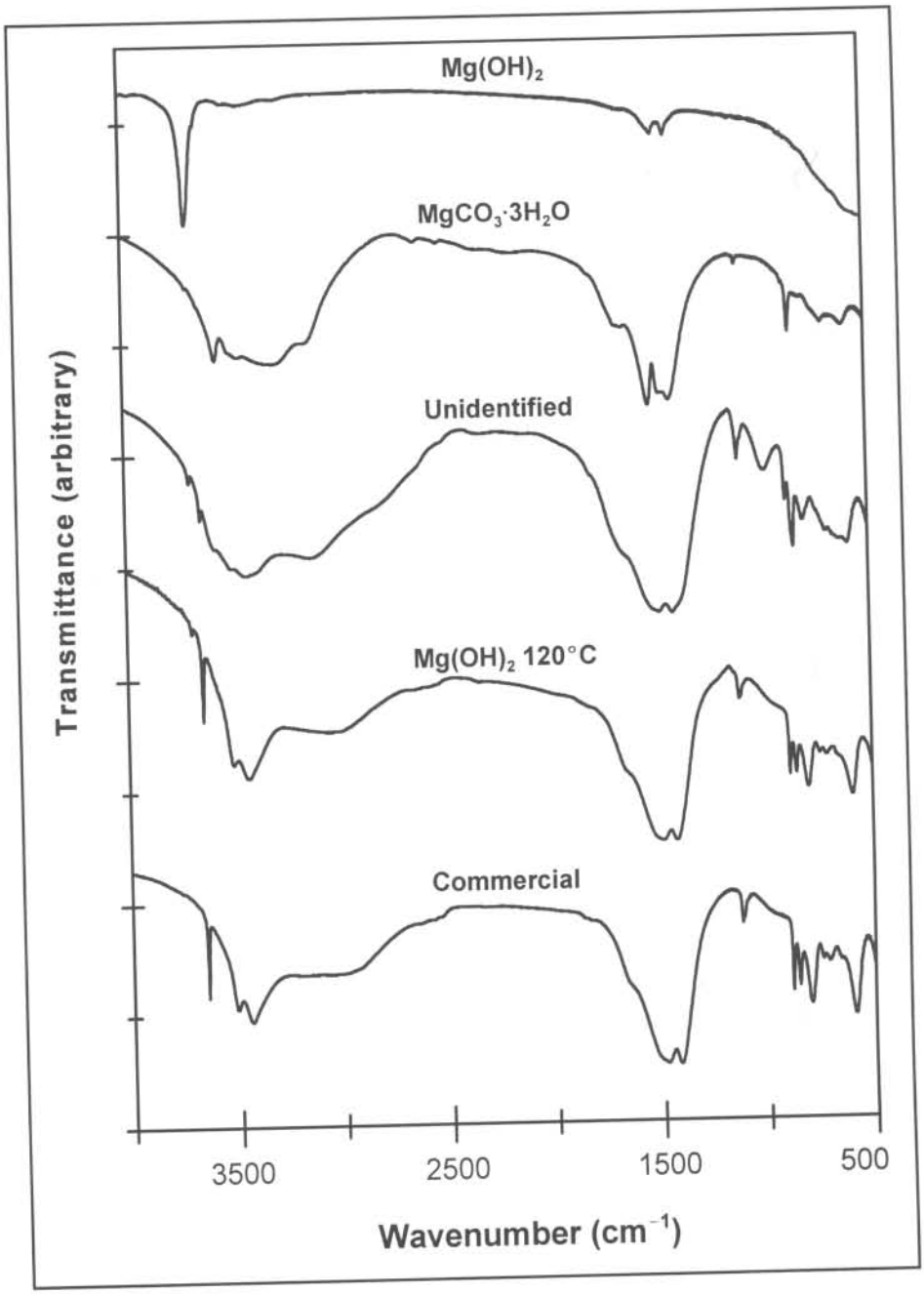

Figure 6.16 IR spectra of the various products

It is evident from Figure 6.16 that the IR spectrum of commercial hydromagnesite was distinctly different from the IR spectrum of $MgCO_3 \cdot 3H_2O$. The internal modes of the carbonate ion are split, indicating site distortion and distinct kinds of carbonate ions. The sharp and well resolved bands indicates the absence of the active participation of the carbonate groups in the bonding (White, 1971). The CO_3^{2-} v_3 asymmetric stretching

vibrations were observed as a strong band split in two at ~1420–1480 cm^{-1} (Sawada *et al.*, 1978). The three bands at ~800 (strongest), 850 and 880 cm^{-1} were assigned to the CO_3^{2-} bending vibrations (Sawada *et al.*, 1978; Raade, 1970). A band at ~1120 cm^{-1} was assigned to the CO_3^{2-} v_1 symmetric stretching vibration (Sawada *et al.*, 1978; Raade, 1970).

The IR spectrum of commercial hydromagnesite was also characterised by an almost free O-H vibration that gave rise to a sharp band at 3650 cm^{-1} (Raade, 1970; White, 1971). Bands resulting from water of crystallisation were observed at 3510 and 3450 cm^{-1} (Raade, 1970; White, 1971). The H_2O bending vibration band at 1650 cm^{-1} was relatively weak and appeared only as a faint shoulder on the side of the CO_3^{2-} stretching band (White, 1971). It was concluded that much of the water that appears in the formula is probably present as OH rather than H_2O.

The IR spectrum corresponding to the $Mg(OH)_2$ 120°C product, was almost identical to that of commercial hydromagnesite. This was expected since the commercial hydromagnesite product and $Mg(OH)_2$ 120°C, were in essence the same product. The only difference between these two spectra was the presence of a small band at ~3700 cm^{-1} in the IR spectrum of $Mg(OH)_2$ 120°C. This band was attributed to the anti-symmetrical OH stretching vibration of the lattice hydroxide corresponding to $Mg(OH)_2$. This band is possibly an indication that a small amount of $Mg(OH)_2$ remained unreacted. A similar observation was made from the IR spectrum of the unidentified compound.

The IR spectrum of the unidentified product indicated several similarities and differences compared to the hydromagnesite products. The band split in two at ~1420–1480 cm^{-1} was similar to the CO_3^{2-} v_3 asymmetric stretching vibration observed for hydromagnesite. This band was broader for the unidentified product which was indicative of its amorphous structure as seen in the XRD. The three bands at ~800, 850 (strongest) and 880 cm^{-1} corresponded to the CO_3^{2-} bending vibrations although the intensity ratio of these bands differed from those observed for hydromagnesite. The band at ~1110 cm^{-1} was assigned to the CO_3^{2-} v_1 symmetric stretching vibration.

It was expected that the unidentified product contained mainly water of crystallisation and to a lesser extent hydroxyl groups. This assumption was confirmed by the IR spectrum, when the bands at 3510 and 3450 cm^{-1}, assigned to water of crystallisation, overshadowed the band at 3658 cm^{-1}, that was associated with an almost free O-H vibration. The band at 3650 cm^{-1} was not nearly as intense as observed for

commercial hydromagnesite and $Mg(OH)_2$ 120°C. A very broad band around 3500 cm^{-1} could be indicative of different types of water of crystallisation as well as corresponding to the amorphous structure of the compound.

The IR spectrum of dypingite was not given here since it was identical to the IR spectrum obtained for hydromagnesite. Raade (1970) found that although the IR spectrum of dypingite was very similar to that of hydromagnesite, two small IR bands could be noticed for dypingite at 1020 and 940 cm^{-1} that were absent in the IR spectrum of hydromagnesite. This though was not observed during this investigation.

6.4 Conclusion

The characterisation of the basic magnesium carbonate products by using various techniques, made it possible to identify similarities and differences between the products. TG-DTA results distinguished between the various stages of decomposition of the respective products. The basic magnesium carbonate products underwent dehydration, dehydroxylation and decarbonation during decomposition. The decarbonation stage was similar for the respective products, with respect to the position of the DTA peak. The dehydration and dehydroxylation stages were though different and characteristic of each product. It seemed that the dehydration and dehydroxylation stages were influenced by the procedure by which a product was obtained.

The surface area results indicated that the procedure by which a product was obtained influenced its surface characteristics. This was evident when different MgO surface areas were obtained for the thermal decomposition of the various hydromagnesite, unidentified and dypingite products. These products, obtained by different procedures, were expected to have similar characteristics. Since surface area relates to the chemical reactivity of a product, it is expected that these results gives a good indication to what is to be expected from the products' chemical properties. The chemical properties of a product relates to the products' reaction rate with reagents, dissolution rate in solvents and adsorptive capacity, to mention a few. The larger MgO surface areas are expected to increase these kinetic properties due to the active condition of the surface.

The SEM images gave a clear indication of the surface morphology of the products. Unfortunately it was not possible to relate the MgO surface area results to the observed

morphology, since the pores that were supposedly formed during decomposition could not be observed. The images contributed in giving valuable information regarding the crystal forms that were obtained by the various procedures. Similarities between the crystal forms observed for some of the products, supported their close structural relationship.

The FT-IR results made it possible to obtain specific information relating to the structure and distinction of molecular groups and their vibrations within the product structure. It was possible to identify the different carbonate vibrations in the various products, due to the differences in bonding of the molecular groups. Some of the products contained mainly water of crystallisation and to a lesser extent hydroxyl groups, while some products contained more distinctly bonded hydroxyl groups and less loosely bonded water. The presence of these different groups inevitably influenced the carbonate vibrations which could be derived from the IR spectra.

It was possible to derive valuable information, by combining the results that were obtained from the respective techniques. It was clear that the basic magnesium carbonate products shared several similarities with respect to their physical and chemical nature. The differences that were observed though, indicated the uniqueness of each product.

Chapter 7

Rehydration characteristics of the basic magnesium carbonates

7.1 Introduction

The rehydration characteristics of the basic magnesium carbonates were investigated in order to obtain insight into the structural changes that characterise the rehydration of these compounds. The basic magnesium carbonates, $Mg(OH)_2$ 120°C and an unidentified compound, that were synthesised as described in Chapter 5, were investigated. The rehydration characteristics of these compounds were compared to a commercially available hydromagnesite. This was done to identify similarities and differences between the rehydration characteristics of the synthesised basic magnesium carbonates and the commercial product. Rehydration was attempted after the basic magnesium carbonate products have been dehydrated and dehydroxylated.

The rehydration characteristics of the various products were investigated by using differential thermal analysis (DTA), Fourier transform infrared spectroscopy (FT-IR) and X-ray diffraction analysis (XRD). Each of these techniques contributed in delivering valuable information relating to the rehydration characteristics of the various basic magnesium carbonates.

The changes observed in the DTA and FT-IR results were correlated with one another in order to identify the changes taking place during rehydration.

By using XRD to investigate the rehydration of the basic magnesium carbonates, it was possible to identify some of the changes that characterised the rehydration processes in the crystal structure of the respective products.

The transmission and reflection spectra of the products at various stages of rehydration were also investigated. The aim was to identify differences between the processes that were taking place on the surface of the rehydrating products (reflection IR spectra) and

in the products itself (transmission IR spectra).

7.2 Experimental

7.2.1 Samples

The products, which rehydration characteristics were investigated, are summarised below. The products will be referred to in the discussion by the names/formulas indicated in ***brackets***.

1. Commercially available hydromagnesite (CP from UniLAB, Saarchem (Pty) Ltd) (***commercial hydromagnesite***).

2. An unidentified compound and hydromagnesite, synthesised by sparging CO_2 gas through a $Mg(OH)_2$ slurry at ambient temperature, drying half of the solid at 80°C (***unidentified***) and the other half at 120°C (***$Mg(OH)_2$ 120 °C***) respectively [Chapter 5.2.2.5 (1)].

7.2.2 Dehydration and rehydration experiments

The basic magnesium carbonate products were dehydrated and dehydroxylated by heating at 325°C for 2.5 h. The treated products were then placed in a sealed humidity cabinet with a saturated water vapour atmosphere at room temperature. At various time intervals, the sample mass was determined for calculation of percentage rehydration. A sample was taken from the rehydrating product at this point for DTA and FT-IR analysis. The remaining sample was returned to the cabinet for the duration of the investigation.

7.2.3 Thermogravimetric analysis

Thermogravimetric and calorimetric analyses were performed on a NETZSCH STA 409 simultaneous TG-DTA instrument. Sample sizes varied between 12 and 14 mg. A heating rate of 10°C min^{-1} was used in an air atmosphere. All data was obtained using platinum crucibles. Only the DTA results will be presented since the changes observed

during DTA were more pronounced than those observed during TG analysis. DTA peak maxima were used and compared to each other, as sample sizes and conditions were kept as constant as possible.

7.2.4 Infrared analysis

Transmission and reflection spectra were recorded using a BRUKER® 113v FTIR spectrometer in the mid-infrared range. All the transmission spectra were obtained from KBr discs containing approximately 1 mg of sample and 100 mg of dry KBr. The reflection spectra were obtained from powdery mixtures containing approximately 5 mg of sample and 300 mg of dry KBr. A Harrick Diffuse Reflectance cell was used to record the reflection spectra. The sample chamber was evacuated (P = 170 mbar) during the recordings.

7.2.5 X-ray diffraction analysis

X-ray powder diffraction analyses were performed on a Siemens D501 diffractometer using Cu K_α radiation. The PDF-2 database from ICDD volume 1–45 was used to analyse the data (JCPDS, 1995). To identify the diffraction pattern of the various basic magnesium carbonate products, the strongest lines for each compound under consideration were used to constitute the XRD pattern of the compound, as discussed in Chapter 5.2.6.

7.3 Results and Discussion

7.3.1 Percentage rehydration as a function of time

It was possible to assess the amount of rehydration by continuously monitoring the products' change in mass as rehydration progressed. By calculating the amount of rehydration, it was possible to determine the degree of rehydration for each product. Figure 7.1 depicts percentage rehydration as a function of time. The results for the hydromagnesite products, commercial and $Mg(OH)_2$ 120°C, indicated a sharp and steady initial increase in rehydration for the first 3 weeks, after which rehydration seemed to stabilise. The amount of rehydration of the $Mg(OH)_2$ 120°C product did not seem to remain stable after 3 weeks, as for the commercial product. The $Mg(OH)_2$ 120°C product underwent a further steady increase in rehydration between 6 and 11 weeks of rehydration.

The hydromagnesite products seemed to rehydrate completely since the percentage rehydration first equaled and then exceeded 100% at approximately 2 weeks rehydration. The observation that complete rehydration was achieved, was supported by the XRD results (Figure 7.5 and 7.6). The amount of rehydration that exceeded total rehydration (100%), was possibly due to surface adsorbed water that covered the rehydrating products. From the larger percentage rehydration between 6 and 11 weeks, it seemed as if the $Mg(OH)_2$ 120°C product contained more adsorbed water compared to the commercial product.

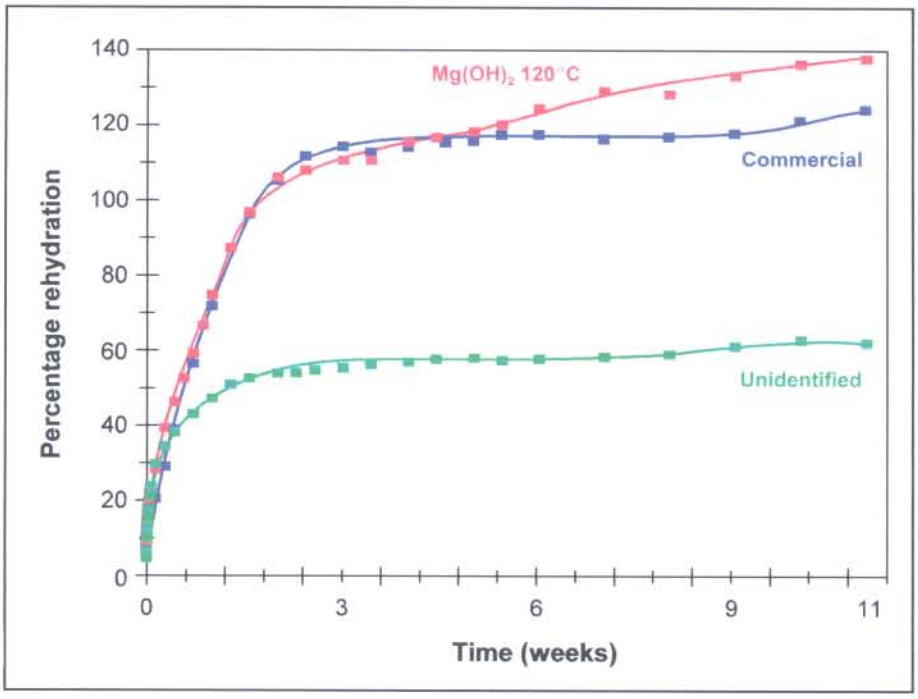

Figure 7.1 Percentage rehydration as a function of time for the respective basic magnesium carbonate products

Up to 2 weeks of rehydration the unidentified product exhibited a steady sharp increase in rehydration, that seemed to remain relatively stable for the remainder of the rehydration process. The unidentified product did not achieve total rehydration as observed for the hydromagnesite products. The unidentified product only rehydrated approximately 60% in total and did not seem to take up additional water for the remainder of the time. Before dehydration the unidentified product exhibited an amorphous structure which persisted after dehydration and during rehydration (Figure 7.7). The lack of a definite crystal structure probably contributed in hindering the uptake of water during rehydration, since no definite crystal structure existed in which the water molecules could be reincorporated into. As a result, complete rehydration could not be achieved.

7.3.2 DTA and FT-IR results for the rehydration of the hydromagnesite products

The discussion of the rehydration of the basic magnesium carbonate products will be structured in three parts. The DTA and FT-IR characteristics of the various products will be discussed for the various stages investigated namely before dehydration, directly after dehydration (0 h rehydration) and during rehydration.

The DTA and FT-IR results corresponding to the various stages of dehydration and rehydration are presented in Figure 7.2 for the commercial hydromagnesite product and in Figure 7.3 for the $Mg(OH)_2$ 120°C hydromagnesite product. The results for the commercial and $Mg(OH)_2$ 120°C products will be discussed together since these two products are essentially the same.

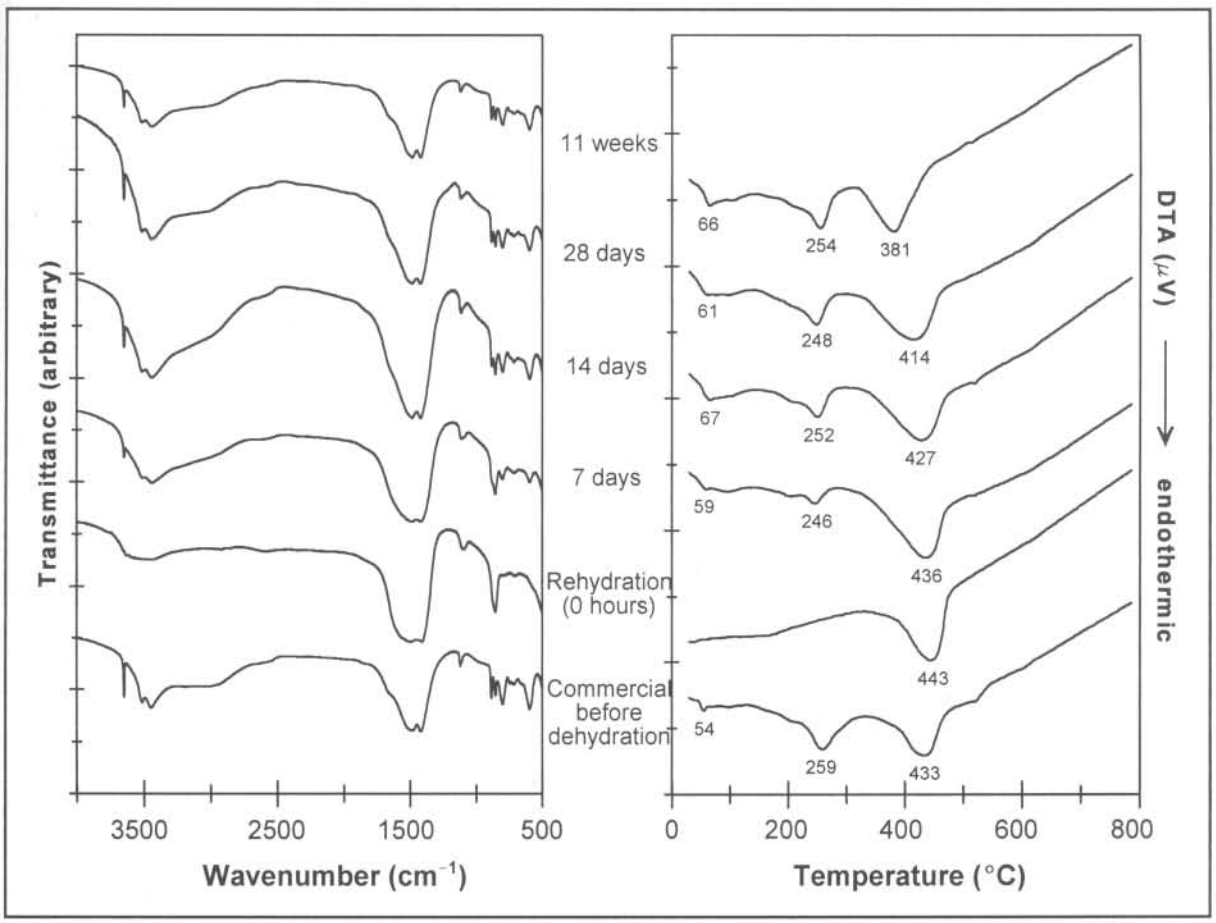

Figure 7.2 FT-IR and DTA dehydration and rehydration results for the commercial hydromagnesite product

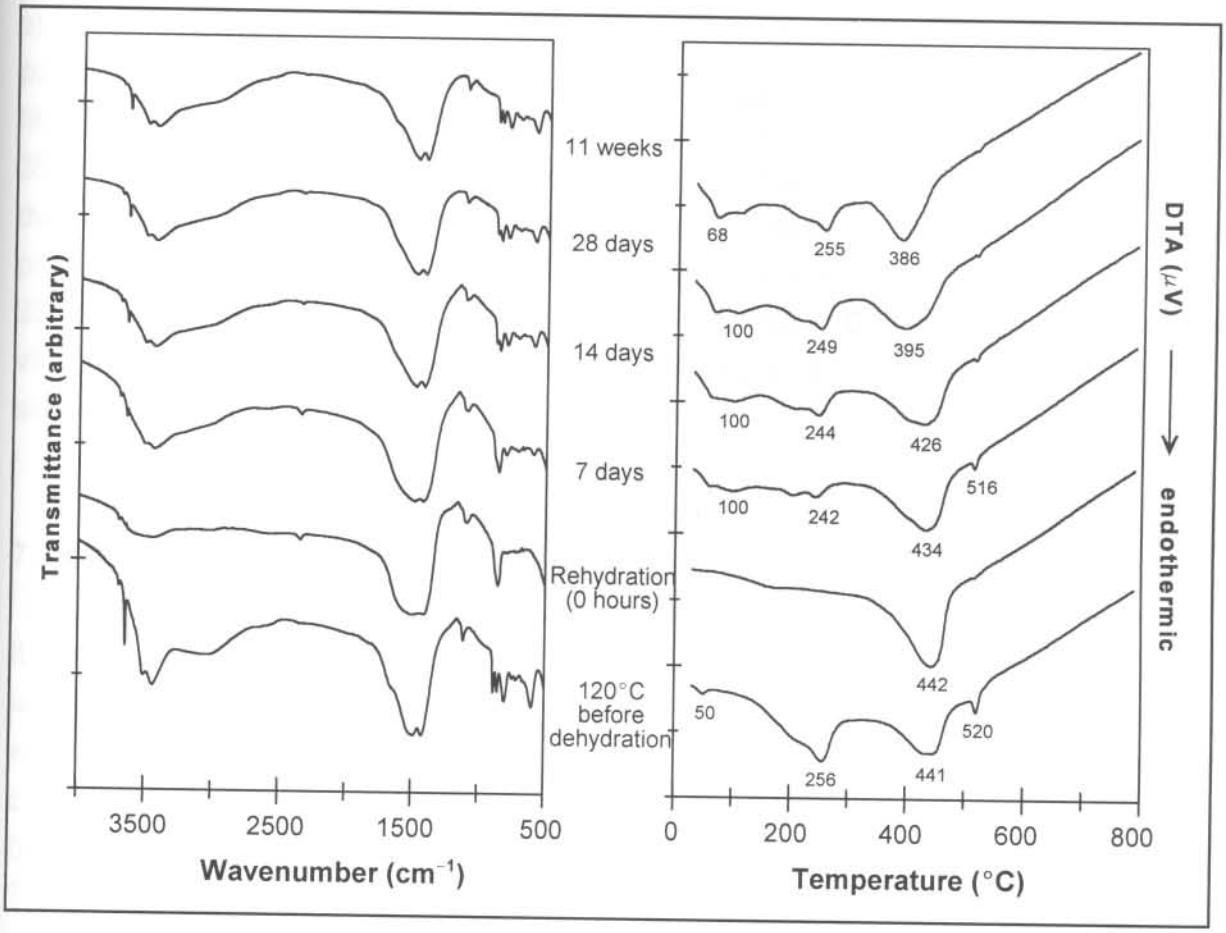

Figure 7.3 **FT-IR and DTA dehydration and rehydration results for the $Mg(OH)_2$ 120°C hydromagnesite product**

7.3.2.1 Before dehydration

Before discussing the IR and DTA results for the rehydration of the hydromagnesite products, it is necessary to take note of the characteristic IR bands and DTA peaks that can be associated with these specific compounds. By observing these bands closely it will be possible to identify any changes resulting from the dehydration and rehydration processes. The CO_3^{2-} v_3 asymmetric stretching vibrations are observed as a strong band split in two at ~1420–1480 cm^{-1} (Sawada *et al.*, 1978). The three bands at ~800 (strongest), 850 and 880 cm^{-1} are assigned to the CO_3^{2-} bending vibrations (Sawada *et al.*, 1978; Raade, 1970). A band at ~1120 cm^{-1} is assigned to the CO_3^{2-} v_1 symmetric stretching vibration (Sawada *et al.*, 1978; Raade, 1970). The DTA peaks corresponding to decarbonation are at 433°C for the commercial product and at 441 and 520°C for the $Mg(OH)_2$ 120°C product. An almost free O-H vibration gives rise to a sharp band

at 3650 cm^{-1} (Raade, 1970; White, 1971). This band can be correlated to the DTA peak at 259°C (dehydroxylation) for the commercial product and at 256°C for the $Mg(OH)_2$ 120°C product. Bands resulting from water of crystallisation are observed at 3510 and 3450 cm^{-1} (Raade, 1970; White, 1971). These bands can be associated with the DTA peak at 54°C for the commercial product and 50°C for the $Mg(OH)_2$ 120°C product (hygroscopic water) and the water of crystallisation that decomposes below 250°C (dehydration) for both products in the respective DTA's. The H_2O bending vibration band at 1650 cm^{-1} is very weak and appears only as a faint shoulder on the side of the CO_3^{2-} stretching band (White, 1971).

7.3.2.2 Directly after dehydration

It is expected that the H_2O and hydroxyl groups would be removed from the crystal lattice during dehydration and dehydroxylation of the hydromagnesite products. This was confirmed by the absence of the IR band corresponding to the water of crystallisation at ~3510 and 3450 cm^{-1} and the absence of the DTA peaks at 54 and 50°C for the commercial and $Mg(OH)_2$ 120°C products respectively, at 0 h rehydration. The sharp O-H vibration band at ~3650 cm^{-1} also disappeared, corresponding to the absence of the DTA peaks at 259 and 256°C for the commercial and $Mg(OH)_2$ 120°C products respectively. Only one of the three bands at 850 cm^{-1} was retained after dehydration which suggested an increase in symmetry in the carbonate radical (Sawada *et al.*, 1978). This change in symmetry was ascribed to the absence of the H_2O and hydroxyl groups that inadvertently influenced the coordination of the carbonate groups. The band at ~590 cm^{-1} also disappeared and the split band at ~1450 cm^{-1} changed into a single band. The change from a split band into a single broader band was associated with the change from crystalline to amorphous phase during dehydration. This change in crystallinity was confirmed by the XRD results (Figure 7.5 and 7.6) at 0 h rehydration.

7.3.2.3 During rehydration

During the initial stages of rehydration, corresponding to the first 7 days of rehydration, water vapour is only taken up as bulk water. This was evident from the development of a broad IR band between 3510 and 3450 cm^{-1} as well as the appearance of the corresponding DTA peaks between 50–100°C. As rehydration progressed during the 11 week rehydration period, the system crystallised out into the hydromagnesite lattice

as the H_2O and hydroxyl groups were taken back into the crystal structure. This was evident from the development of a sharp band at 3650 cm^{-1} and the appearance of the corresponding DTA peak at 254°C for the commercial product and at 255°C for the $Mg(OH)_2$ 120°C product. As the H_2O and hydroxyl groups re-coordinated within the crystal lattice, the symmetry of the carbonate radicals were inadvertently influenced. The single CO_3^{2-} bending vibration at 850 cm^{-1} expressed this change in symmetry as it gradually split to form the original three bands after 11 weeks of rehydration. The single band at 1450 cm^{-1} also split into two bands at 1420–1480 cm^{-1}, as well as becoming progressively narrower as the amorphous structure converted back to the crystalline phase during the 11 week period.

Changes between 14 days and 11 weeks of rehydration were not really noticeable from the IR results. The IR bands only became more pronounced as the original crystal structure was reclaimed during this time. The DTA peaks corresponding to the decarbonation step above 350°C underwent displacement to a lower temperature as rehydration progressed over the 11 week period. The decarbonation peak for the commercial product was displaced from 433°C before dehydration to 381°C after 11 weeks rehydration. The displacement observed for the $Mg(OH)_2$ 120°C product was from 441°C before dehydration to 386°C after 11 weeks rehydration. The displacement of the decarbonation temperature to a lower temperature as rehydration progressed, was attributed to a weakening of the carbonate bonds as the water and hydroxyl groups were taken back up into the hydromagnesite structure.

The only noticeable difference between the rehydration of the commercial product and the $Mg(OH)_2$ 120°C product, was the appearance of a relatively small band at ~2346 cm^{-1} in the IR spectrum of the $Mg(OH)_2$ 120°C product. This band gradually disappeared as rehydration progressed.

It would seem for both the hydromagnesite products that the original orientation and vibrations of the molecules were reclaimed after 11 weeks of rehydration.

7.3.3 DTA and FT-IR results for the rehydration of the unidentified product

The DTA and FT-IR results corresponding to the various stages of dehydration and rehydration are presented in Figure 7.4 for the unidentified product.

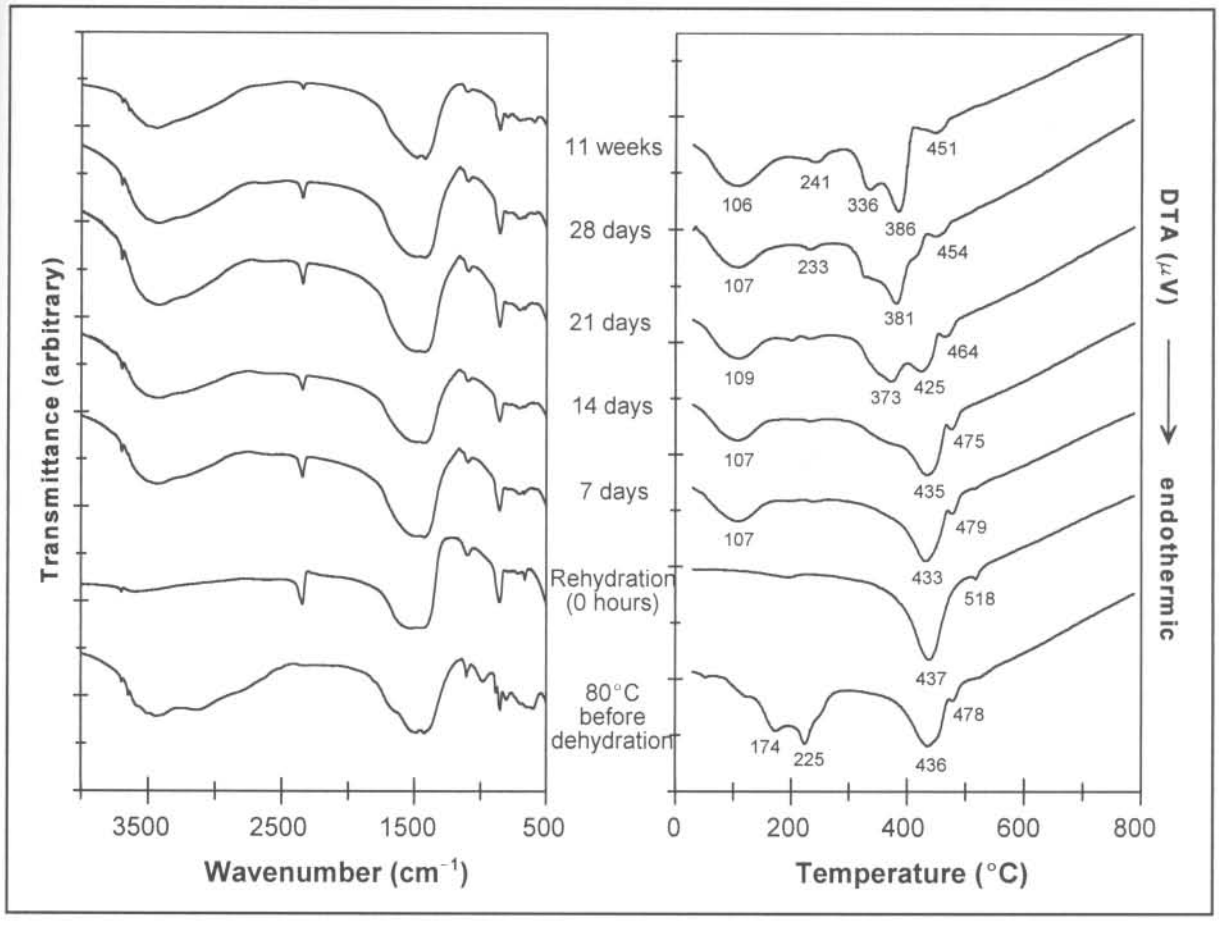

Figure 7.4 FT-IR and DTA dehydration and rehydration results for the unidentified product

7.3.3.1 Before dehydration

The IR spectra and DTA results for the unidentified product indicated several similarities and differences compared to that of the hydromagnesite products. The band split in two at ~1420–1480 cm^{-1} was similar to the CO_3^{2-} v_3 asymmetric stretching vibration observed for hydromagnesite. This band was broader for the unidentified product which was indicative of its amorphous structure as seen in the XRD (Figure 7.7). The three

bands at ~800, 850 (strongest) and 880 cm^{-1} corresponded to the CO_3^{2-} bending vibrations although the intensity ratio of these bands differed from those observed for hydromagnesite. The band at ~1110 cm^{-1} was assigned to the CO_3^{2-} v_1 symmetric stretching vibration. The similarities between the carbonate vibrations of the unidentified product and the hydromagnesite products were also reflected in the position of the DTA peak at 436°C for the unidentified product. This corresponded to the decarbonation step above 350°C for the hydromagnesite products.

It is suspected that the unidentified product contains mainly water of crystallisation and to a lesser extent hydroxyl groups. This was deducted from the DTA results where the peaks at 174 and 225°C should correspond to the loss of water of crystallisation, which is expected to be given off below 250°C. This was confirmed by the absence of a dehydroxylation step between 250 and 350°C in the DTA curve. The IR spectrum also confirmed this assumption when the bands at 3510 and 3450 cm^{-1}, assigned to water of crystallisation, overshadowed the band at 3658 cm^{-1}, that was associated with an almost free O-H vibration. The band at 3650 cm^{-1} was not nearly as intense as observed for the commercial and $Mg(OH)_2$ 120°C products. The very broad band around 3500 cm^{-1} could be indicative of different types of water of crystallisation as well as corresponding to the amorphous structure of the compound.

7.3.3.2 Directly after dehydration

After dehydration the absence of water of crystallisation is expected. This was confirmed in the IR spectrum due to the absence of the corresponding band around 3500 cm^{-1} and the absence of the double DTA peak around 200°C at 0 h rehydration. Both the IR and DTA results at 0 h rehydration for the dehydrated and dehydroxylated unidentified product were almost identical to that of the dehydrated and dehydroxylated hydromagnesite products. The only noticeable difference was the appearance of a very sharp band at 2346 cm^{-1} in the IR spectrum of the unidentified product. This band was more intense in the IR spectrum of the unidentified product compared to the IR spectrum of the $Mg(OH)_2$ 120°C product. The band at 2346 cm^{-1} could be assigned to the formation of CO_2 gas in the structure of the dehydrated-dehydroxylated product, as it corresponds to the position of the v_3 fundamental of CO_2 (Schrader, 1989). Prolonged heating of the product at 325°C did not result in the disappearance of this band, indicating that the band could not be due to CO_2 gas absorption. This band might be the result of an O-H vibration, since in $KHCO_3$ and $NaHCO_3$ strong hydrogen bonds

causes delocalisation of the primary O-H bond (White, 1974).

7.3.3.3 During rehydration

The only changes observed during rehydration as water vapour was taken up as bulk water, was the appearance of the IR bands at 3510 and 3450 cm^{-1}, which coincided with the uptake of water of crystallisation. This was also observed as a DTA peak around 100°C. The band that appeared at 2346 cm^{-1} disappeared as rehydration progressed but to a lesser extent than that observed for the $Mg(OH)_2$ 120°C product.

The changes during rehydration were more evident from the DTA results. During rehydration the peak at 435°C developed a shoulder at 14 days and by 21 days two distinct peaks were noticeable at 373 and 425°C. By 28 days this peak shifted to 381°C with a shoulder at 329°C. By 11 weeks of rehydration the peak at 386°C had a prominent additional peak at 336°C. During peak shifting, no changes could be observed in the IR spectra. The DTA changes were associated with a weakening of the carbonate bonds as rehydration progressed.

The appearance of a DTA peak at 241°C between 28 days and 11 weeks of rehydration was also noted, although the peak was not very prominent. This peak's position differed from the doublet peak around 200°C before dehydration that was associated with the water of crystallisation of the unidentified product. Since the peak at 241°C did not develop much between 28 days and 11 weeks rehydration, it was difficult to come to a conclusion regarding the process that might be responsible for its appearance. The appearance of the DTA peak at 241°C could not be related to any changes in the IR or XRD results.

7.3.4 XRD results of the dehydrated-dehydroxylated and rehydrated products

XRD makes it possible to identify a product, due to the unique nature of the diffraction pattern that is exhibited by a crystalline compound. XRD also gives an indication of the crystalline state of a specific product. Various conclusions were drawn from the IR results of the respective products, regarding the crystallinity of each product at a specific stage of rehydration. By obtaining the XRD patterns it was possible to verify

the conclusions drawn from the IR results.

The XRD patterns of the respective basic magnesium carbonate products before dehydration, directly after dehydration (0 h rehydration) and after 11 weeks of rehydration were obtained. The results are given in Figure 7.5 for the commercial product, Figure 7.6 for the $Mg(OH)_2$ 120°C product and in Figure 7.7 for the unidentified product.

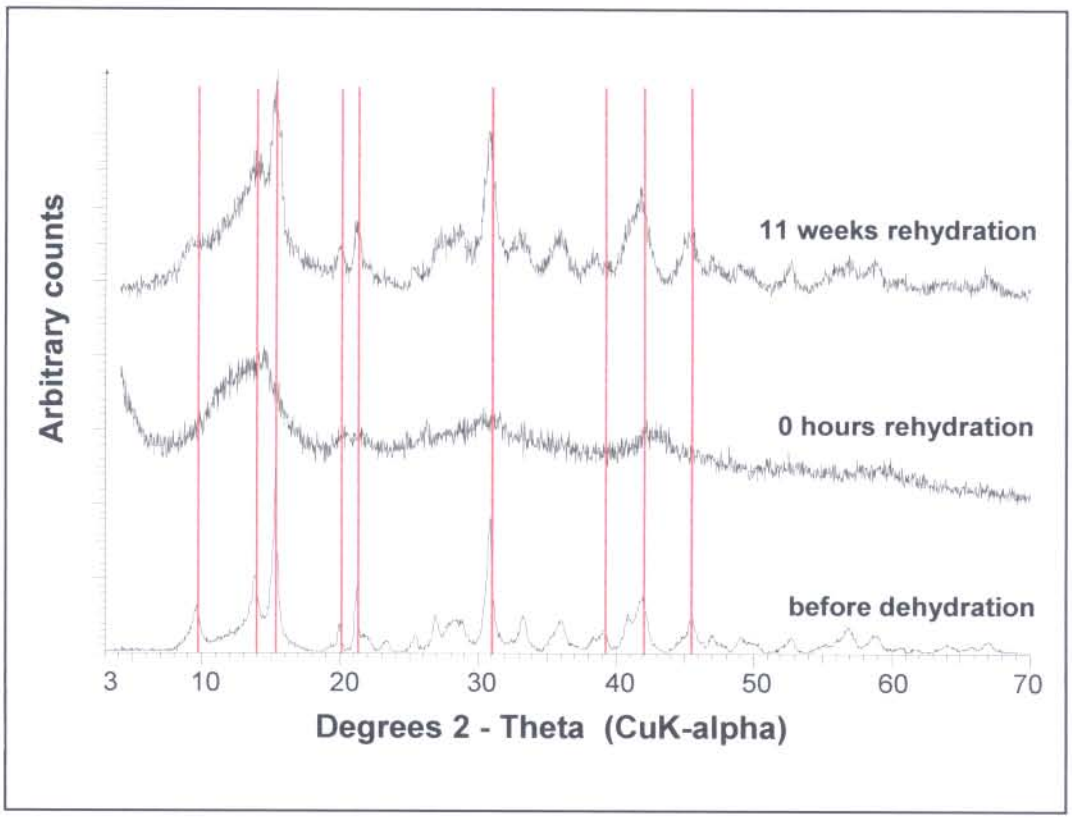

Figure 7.5 XRD pattern of commercial hydromagnesite product during the various stages of rehydration (— hydromagnesite)

It is evident from Figure 7.5 that the commercial product appeared to be crystalline before dehydration. During dehydration the commercial product changed from crystalline to amorphous. This corresponds to the change from crystalline to amorphous during the XRD investigation of the dehydration of hydromagnesite by Sawada *et al.* (1978).

After 11 weeks of rehydration it seemed as if the dehydrated-dehydroxylated commercial product regained the original hydromagnesite crystalline structure. This complies with the DTA and IR results that also indicated that the hydromagnesite structure was reclaimed after 11 weeks of rehydration. The broadness of the XRD pattern after 11 weeks, still seemed to indicate a certain degree of an underlying amorphous structure, but in general the original hydromagnesite product was obtained.

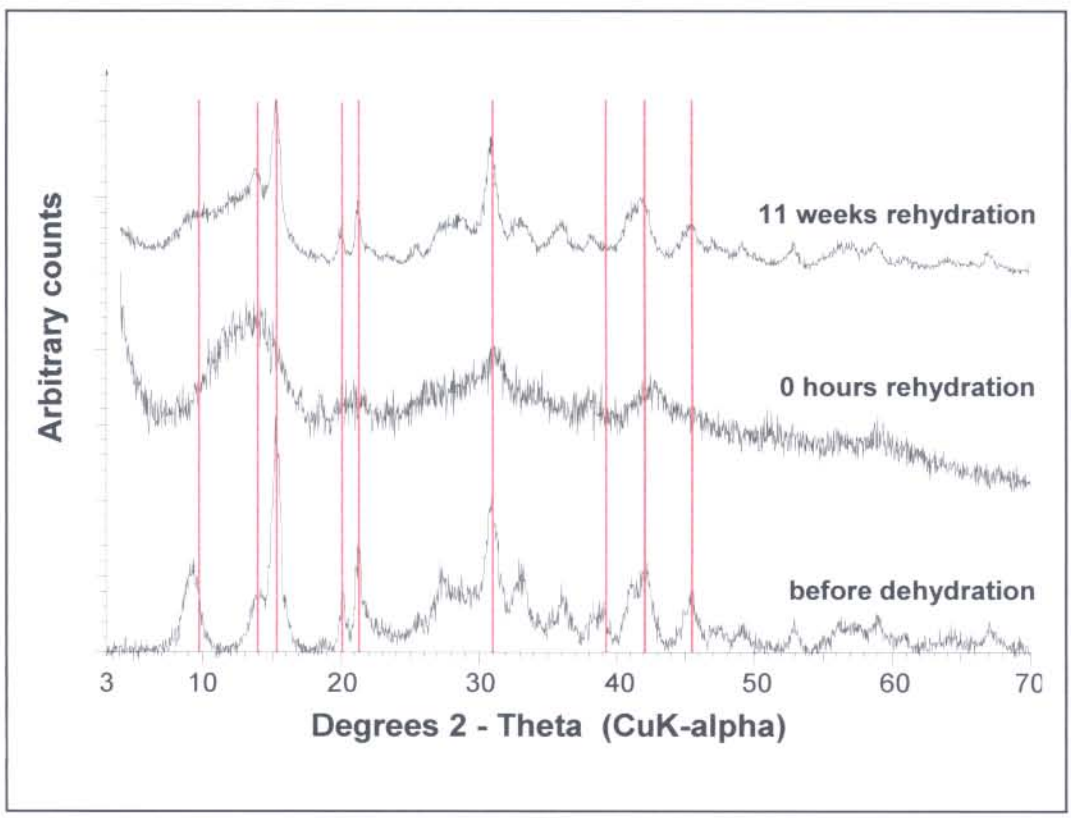

Figure 7.6 XRD pattern of $Mg(OH)_2$ 120°C hydromagnesite product during the various stages of rehydration (— hydromagnesite)

The XRD results of the rehydration of the $Mg(OH)_2$ 120°C product (Figure 7.6) seemed to be similar to the XRD results of the commercial product (Figure 7.5). The $Mg(OH)_2$ 120°C product exhibited a crystalline structure before dehydration that became amorphous after dehydration. The original hydromagnesite crystal structure seemed to have been regained after 11 weeks of rehydration. These results coincided with the conclusions drawn from the DTA and IR results regarding the crystalline characteristics

of the rehydrating product. The broadness of the XRD pattern after 11 weeks of rehydration could still be indicative of an underlying amorphous structure.

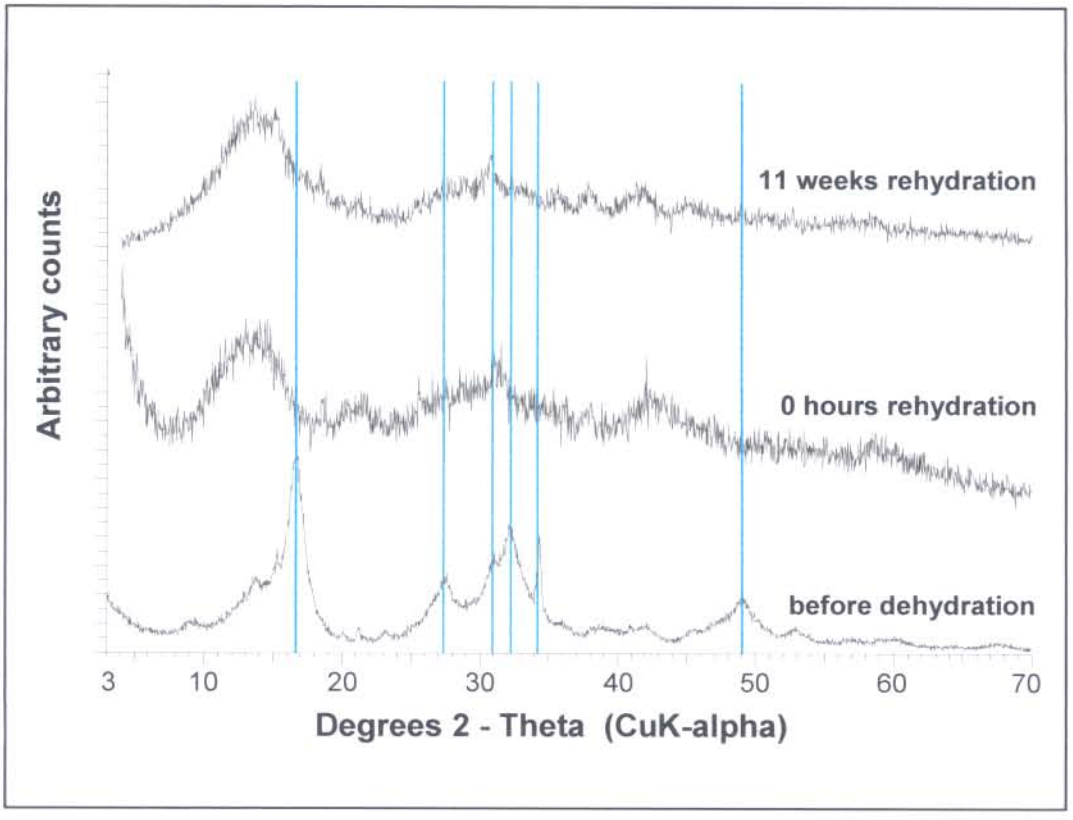

Figure 7.7 XRD pattern of unidentified product during the various stages of rehydration (— unidentified)

The unidentified product (Figure 7.7) exhibited an amorphous structure before dehydration, that could not be matched to any of the known compounds or a combination of them in the XRD database. After dehydration and 11 weeks of rehydration the amorphous structure was retained and virtually no change in the crystal structure could be observed. This observation was supported by the IR results (Figure 7.4). The absence of any noticeable change in the structure during rehydration was attributed to the absence of a definite crystal structure before dehydration.

7.3.5 Comparison of transmission and reflection spectra during rehydration

The transmission and reflection spectra of the rehydration products of the basic magnesium carbonates, were obtained to determine whether there were any differences between the rehydration processes taking place on the surface of the products (reflection spectra) and the inside (transmission spectra). It is well known that transmission and reflection spectra are obtained by different techniques. Transmission spectra are obtained when light that has not been absorbed by a sample, moves through the sample. Reflection spectra are obtained when light is reflected or scattered from the surface of a sample.

The transmission and reflection spectra of the basic magnesium carbonates were compared at three different stages of rehydration: 0 h, 35 days (5 weeks) and 11 weeks rehydration.

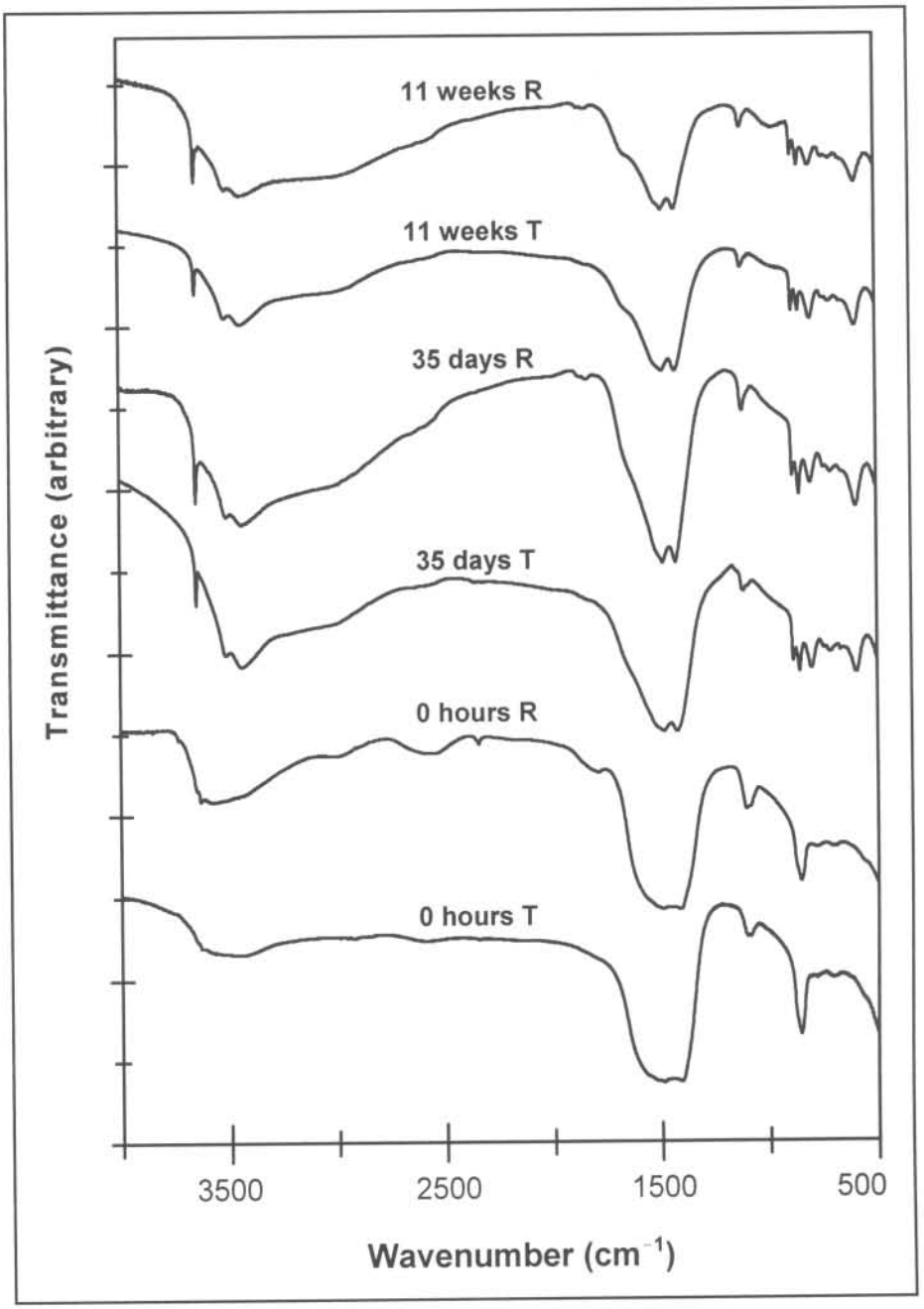

Figure 7.8 **Transmission (T) and reflection (R) spectra for the various stages of rehydration of the commercial hydromagnesite product**

The transmission and reflection spectra for the rehydrating commercial product are given in Figure 7.8. It is evident that the differences between these two spectra were more pronounced at the start of rehydration and that the differences became less

obvious as rehydration progressed. A noticeable difference at 0 h rehydration was the prominence of water of crystallisation observed around 3500 cm^{-1}. This band was stronger in the reflection spectrum compared to the transmission spectrum. This was expected since if a small amount of water was present directly after dehydration, it was expected to be present as adsorbed water on the surface of the dehydrated product which would be more clearly observable on the reflection spectrum.

It was also evident that as rehydration progressed for the commercial product, the transmission and reflection spectra became almost identical. This is indicative of the similarities between the molecular groups on the surface and on the inside of the rehydrating product.

The transmission and reflection spectra for the $Mg(OH)_2$ 120°C product is given in Figure 7.9. The difference between these spectra were more noticeable at 0 h rehydration and became less noticeable as rehydration progressed. At 0 h rehydration the water of crystallisation band around 3500 cm^{-1} was more prominent in the reflection spectrum and much less noticeable in the transmission spectrum. The band at 2346 cm^{-1}, was also more prominent in the reflection spectrum than in the transmission spectrum at 0 h rehydration. These observations clearly indicated that the molecular groups that were responsible for the bands at 3500 and 2346 cm^{-1}, were initially (0 h rehydration) mainly present on the surface of the rehydrating product as observed from the reflection spectrum. As rehydration progressed these groups were probably taken up into the product. This was concluded from the similarities between the transmission and reflection spectra after 11 weeks of rehydration. This is indicative of a kinetic process where the rate of uptake is limited by diffusion of the reacting groups to the inside of the material.

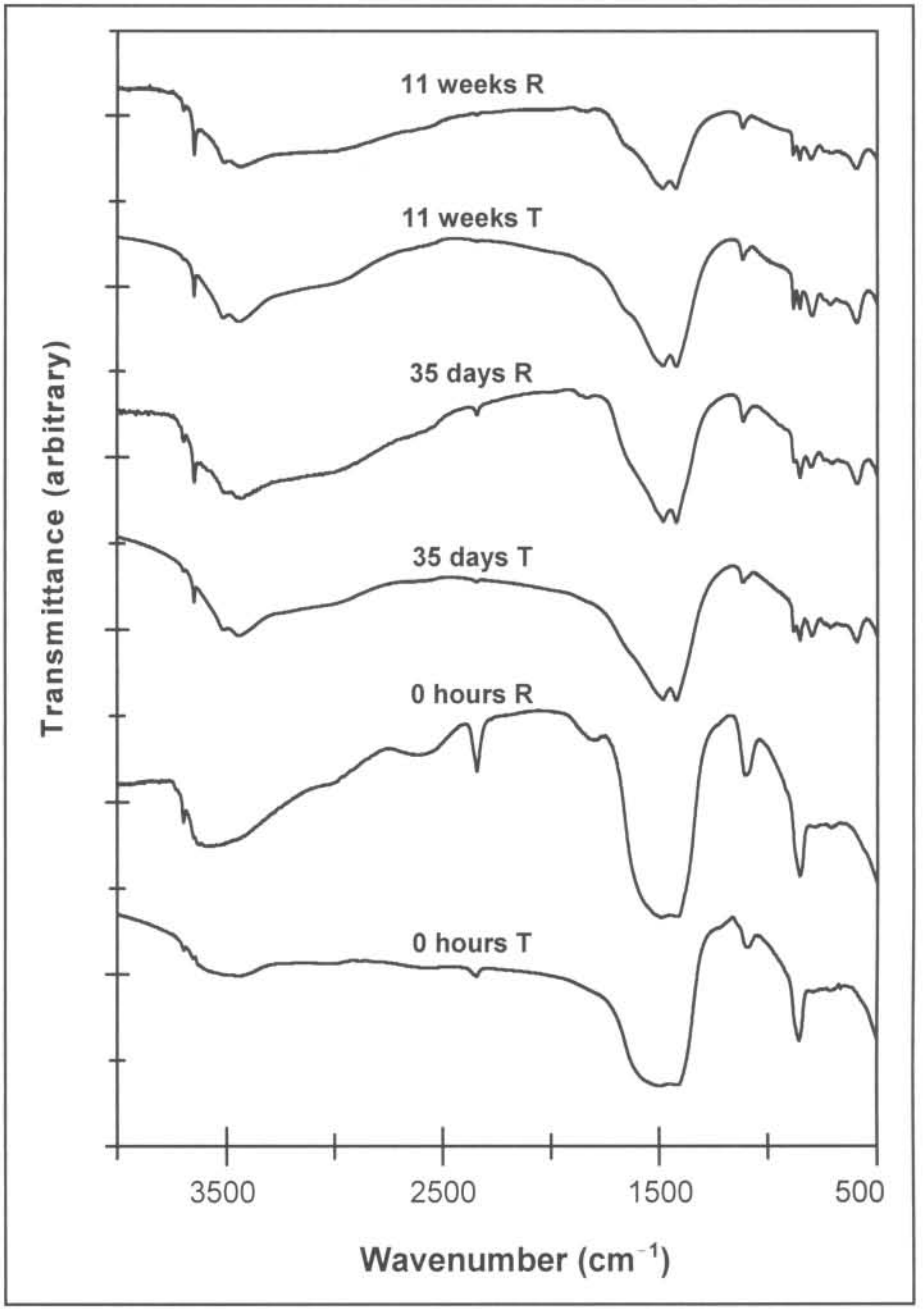

Figure 7.9 Transmission (T) and reflection (R) spectra for the various stages of rehydration of the $Mg(OH)_2$ 120°C hydromagnesite product

The transmission and reflection spectra for the various stages of rehydration for the unidentified product is given in Figure 7.10. The initial differences between the transmission and reflection spectra at 0 h rehydration were noticeable. The reflection

spectrum at 0 h rehydration exhibited stronger bands with respect to the water of crystallisation band around 3500 cm^{-1} and the strong band at 2346 cm^{-1}, compared to the transmission spectrum. As rehydration progressed the differences between the transmission and reflection spectra were less noticeable. This corresponds to the observations made for the similarities between the transmission and reflection spectra of the commercial and $Mg(OH)_2$ 120°C products as rehydration neared 11 weeks.

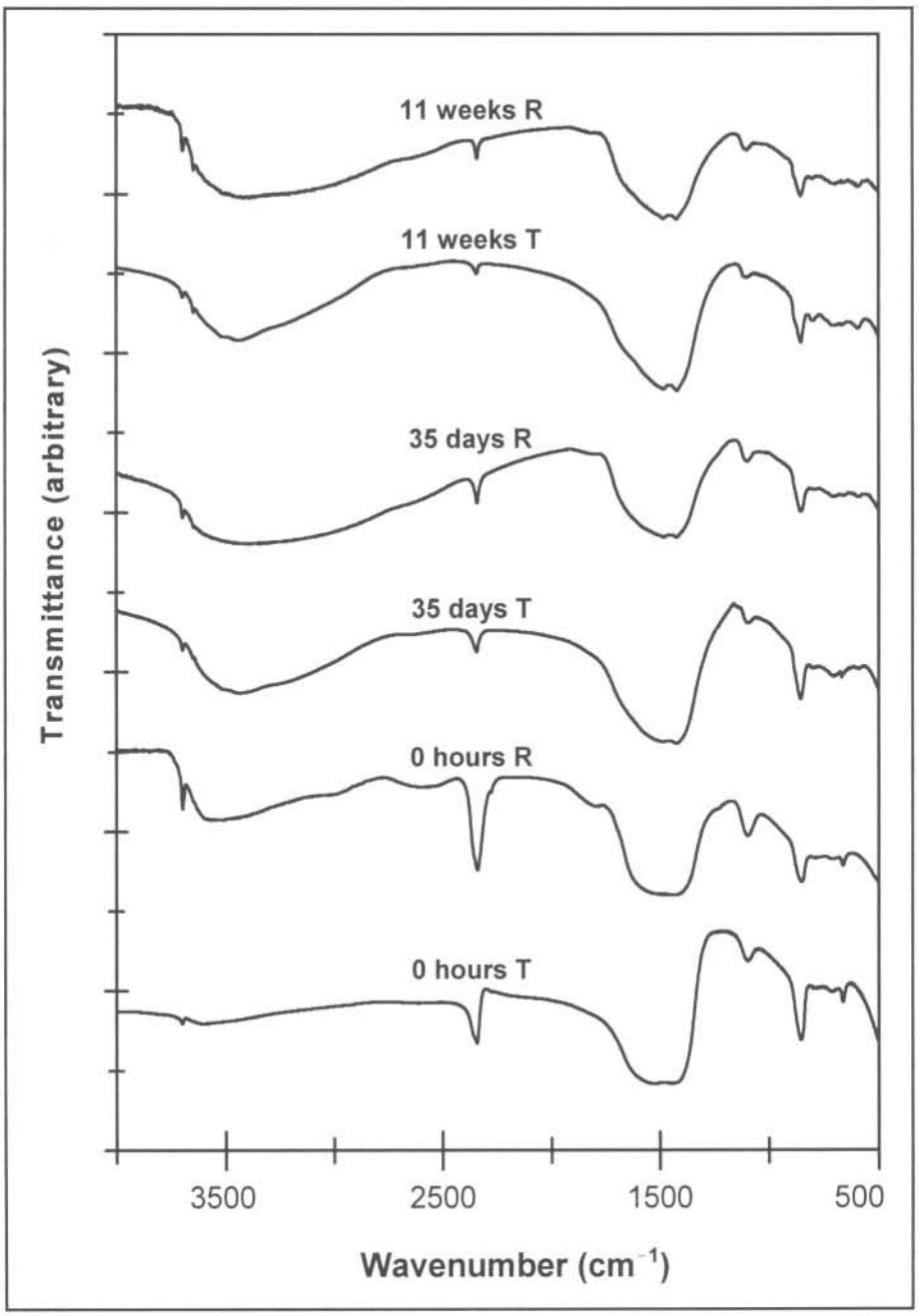

Figure 7.10 Transmission (T) and reflection (R) spectra for the various stages of rehydration of the unidentified product

7.4 Conclusion

The investigation into the rehydration characteristics of a commercial and $Mg(OH)_2$ 120°C hydromagnesite product and an unidentified basic magnesium carbonate, gave insight into the structural changes that takes place during rehydration of the dehydrated and dehydroxylated products. It was evident from the DTA and IR results that the hydromagnesite products seemed to regain the original symmetry of the various groups during an 11 week rehydration period in a water vapour saturated atmosphere at ambient temperature. The unidentified product did not seem to regain its original symmetry. These conclusions were supported by the XRD results which indicated that the hydromagnesite products converted back to a relatively crystalline hydromagnesite product during rehydration. The combined use of DTA and FT-IR made it possible to identify the changes taking place by correlating the respective results.

The correlation between the transmission and reflection spectra gave an indication of the different processes taking place on the surface and inside the rehydrating products at the various stages of rehydration. It was evident that at 0 h rehydration the differences between the transmission and reflection spectra were more pronounced compared to the differences during rehydration. The similarities between the respective spectra were more obvious after prolonged rehydration.

The various techniques that were employed to investigate the rehydration of the basic magnesium carbonates, gave valuable insight into the various processes that characterised their rehydration.

Chapter 8

Evaluation of basic magnesium carbonate as a flame retardant

8.1 Introduction

The aim of this chapter is to determine whether the $Mg(OH)_2$ 120°C hydromagnesite product and the unidentified compound, synthesised in chapter 5, could be applied as flame retardants. The evaluation of a newly synthesised product is necessary in order to determine whether the product could live up to the standards set by other similar products. The inorganic flame retardants, $Mg(OH)_2$ and $Al(OH)_3$, have achieved much success in presenting an alternative choice as flame retardants with respect to the traditionally used halogenated flame retardants (Hornsby and Watson, 1986; Weber, 2000). The application of the basic magnesium carbonates as flame retardants in comparison, have been studied to a lesser extent.

The viability of the $Mg(OH)_2$ 120°C and unidentified products as flame retardants were investigated by conducting a few tests. These tests included determining the influence of the products on the char formation of citrazinic acid and phenolphthalein. The products were also compounded with ethylene-vinyl acetate (EVA) and studied by thermogravimetric (TG) and differential thermal analysis (DTA), limiting oxygen index (LOI) and scanning electron microscope (SEM).

TG-DTA analyses were done to determine if and how the added fillers influenced the thermal degradation of EVA. The addition of a filler could lower the onset temperature at which the polymer would start to degrade. The formation of char during polymer degradation could also be assessed by using TG-DTA.

Since the risk associated with a material is determined by its flammability, it could prove helpful to quantify this parameter. A very reliable quantitative small-scale flammability test is LOI. This test gives the limiting concentration of oxygen in the atmosphere necessary to maintain combustion (Bair, 1997).

The morphology of the EVA composites were investigated with SEM in order to evaluate dispersion of the inorganic fillers within the EVA matrix. Good bonding between the filler surface and polymer is necessary to maximize the mechanical properties of the polymer.

EVA composites containing a commercial $Mg(OH)_2$, $Al(OH)_3$ and hydromagnesite respectively were also studied with TG-DTA, LOI and SEM, in order to effectively evaluate the application of the synthesised products as flame retardants. This investigation aims to highlight the advantages associated with the use of the $Mg(OH)_2$ 120°C and unidentified products as flame retardants.

8.2 Experimental

8.2.1 Samples

8.2.1.1 Inorganic products evaluated

The flame retardant characteristics of the following products were investigated. The products will be referred to in the discussion by the names/formulas indicated in ***brackets***

1. $Mg(OH)_2$ (CP from UniLAB, Saarchem (Pty) Ltd) (***$Mg(OH)_2$***)

2. $Al(OH)_3$ (Acros Organics, New Jersey, USA) (***$Al(OH)_3$***)

3. Commercially available hydromagnesite (CP from UniLAB, Saarchem (Pty) Ltd) (***commercial hydromagnesite***)

4. An unidentified compound and hydromagnesite, synthesised by sparging CO_2 gas through a $Mg(OH)_2$ slurry at ambient temperature, drying half of the solid at 80°C (***unidentified***) and the other half at 120°C (***$Mg(OH)_2$ 120 °C***) respectively [Chapter 5.2.2.5 (1)].

8.2.1.2 Charring compounds

The charring experiments were conducted by using the following compounds:

1. Citrazinic acid, 2,6-dihydroxy pyridine-4-carboxylic acid (Sigma Chemical Co., St. Louis, USA) (***citrazinic acid***)

2. Phenolphthalein (BDH Chemicals Ltd., Poole, England) (***phenolphthalein***)

8.2.1.3 EVA composites

The EVA copolymer with a density of 0.95 g cm^{-3}, melt flow index of 420 g per 10 min at 190°C / 2.16 kg, and a vinyl acetate content of 28% (Evatane) was obtained from Elf Atochem (France).

A series of EVA and approximately 60% (w/w) inorganic filler composites were melt-blended with a Bridge two-roll laboratory compounding mill (England) at approximately 95°C. The composites were then compression moulded into sheets.

1.0 g samples of the composites were ashed at 950°C for 30 minutes. Ashings of the filler alone were also carried out under identical conditions to allow for volatile loss during filler decomposition. The percentage filler was determined by combining these two results.

8.2.2 Charring experiments

The charring experiments were conducted by grinding equal masses (1:1 (w/w) ratio) of citrazinic acid with the inorganic products (8.2.1.1) in a mortar and pestle. Char yields were determined by heating approximately 0.1 g samples in a Barnstead Thermolyne laboratory furnace. This procedure was done at 450 and 520°C and for 15 and 30 minutes at each temperature respectively. The apparent char yields were determined by correcting for the mass loss of the inorganic products at each temperature and heating time. The procedure was repeated for phenolphthalein.

8.2.3 Thermogravimetric analysis

Thermogravimetric and calorimetric analyses were performed on a Mettler Toledo TGA/SDTA 851^e module. Sample sizes varied between 5 and 6 mg. A heating rate of 10°C min^{-1} was used in an air and nitrogen atmosphere respectively (30 ml min^{-1}). All data was obtained using platinum crucibles. DTA peak maxima were used and compared to each other, as sample sizes and conditions were kept as constant as possible.

8.2.4 Limiting oxygen index

Standard test bars (150 x 10 x 4 mm) were employed for determining the minimum oxygen concentration necessary to sustain combustion of the EVA composites. The LOI was measured with a Stanton Redcroft FTA flammability unit according to the standard method described by the American Society for Testing and Materials (ASTM D2863).

8.2.5 Scanning electron microscopy

The test pieces were fractured with a chissel on a copper block in liquid nitrogen. The pieces were mounted on an aluminium stub with fractured faces facing up. The samples were then sputter coated with gold in a Polaron E 5200 autocoating unit before viewing. The surface morphology of the composites were analysed on a JEOL 840 scanning electron microscope at an accelerating voltage of 5 kV.

8.3 Results and Discussion

8.3.1 Influence of inorganic products on char formation

The formation of char when a polymer burns, aids in reducing the volatilisation of active fragments, thus reducing the amount of material that is converted into volatile fuel. The char also aids in the adsorption and dissipation of heat. This char layer forms on the surface of the burning polymer and inhibits further combustion by preventing access of oxygen to the burning substrate. Due to the advantages a char barrier presents during a fire, it is necessary to know the influence a flame retardant might have on the formation of char from a burning substance.

It was decided to investigate the influence the inorganic products might have on char formation, using citrazinic acid and phenolphthalein as measures of char formation. Citrazinic acid and phenolphthalein were chosen as model compounds for the char yield determinations, because depending on the conditions, they may form a considerable amount of char during decomposition.

During this investigation, an attempt was made to relate the surface area of the MgO formed during decomposition of the respective inorganic products, to the amount of char formed during combustion of citrazinic acid and phenolphthalein. This approach was considered, since it was expected that a reactive MgO surface area could result in a decrease in the amount of char formed. The reactive MgO surface is expected to catalyse the char oxidation to a larger extent, compared to a less reactive MgO surface.

Two temperatures, 450 and 520°C, were considered for this investigation. These temperatures coincided with the maximum MgO surface area formed by thermal decomposition of $Mg(OH)_2$ and the basic magnesium carbonates respectively. Since the MgO formed from $Mg(OH)_2$ exhibited the largest surface area at ~450°C, it was expected that less char would be formed in the presence of $Mg(OH)_2$ than for the basic magnesium carbonates. This was expected due to the reactive condition of the MgO surface of $Mg(OH)_2$ at 450°C which was expected to contribute to the oxidation of the char. At 520°C the basic magnesium carbonates exhibited a maximum MgO surface area, although $Mg(OH)_2$ had a larger MgO surface area compared to the basic magnesium carbonates at this temperature (Chapter 6.3.2).

It should be noted that the Al_2O_3 surface area obtained by thermal decomposition of $Al(OH)_3$ has not been studied for this investigation. Hornsby and Watson (1989) has indicated that $Al(OH)_3$ reaches a maximum surface of a similar order than that of $Mg(OH)_2$, but at ~400°C. The Al_2O_3 surface area of $Al(OH)_3$ is thus assumed to be comparable to that of $Mg(OH)_2$. Charring results for citrazinic acid are given in Table 8.1.

Table 8.1 Apparant char yield of 1:1 (w/w) mixtures of citrazinic acid (CA) with the inorganic products

Mixtures	Char yield (%)			
	450°C		520°C	
	15 min	*30 min*	*15 min*	*30 min*
Citrazinic acid	40.9	33.7	23.3	7.3
CA + $Mg(OH)_2$	30.7	19.3	5.3	–
CA + $Al(OH)_3$	32.8	22.5	15.2	3.6
CA + commercial	21.4	10.0	6.5	–
CA + $Mg(OH)_2$ 120°C	23.0	10.8	6.5	0.7
CA + unidentified	28.2	16.2	4.7	0.5

It is evident from these results (Table 8.1) that the inorganic products contributed in reducing the amount of char formed compared to the amount of char formed in the absence of an inorganic additive. This was ascribed to the oxidation of carbon. The oxidation of carbon can be achieved through a number of reactions:

$$2\,C_{(s)} + O_{2\,(g)} \rightleftharpoons 2\,CO_{(g)}$$

$$C_{(s)} + O_{2\,(g)} \rightleftharpoons CO_{2\,(g)}$$

$$C_{(s)} + H_2O_{(g)} \rightleftharpoons CO_{(g)} + H_{2\,(g)}$$

$$C_{(s)} + CO_{2\,(g)} \rightleftharpoons 2\,CO_{(g)}$$

A wide range of metal oxides and related compounds, notably those of the alkali metals, some of the alkaline earths, the transition metals and the noble metals have been shown to catalyse these oxidation reactions (Hornsby and Watson, 1989). Catalytic oxidation of the char barrier is detrimental to flame retardance and can also lead to an "afterglow" effect.

When considering the results at 450°C, it was evident that the char formed in the presence of the various inorganic products did not coincide with the surface area results. $Mg(OH)_2$ which exhibited the largest MgO surface area compared to the basic magnesium carbonates at 450°C, resulted in the largest amount of char formed, next to $Al(OH)_3$, for both heating times. Less char was formed in the presence of the basic magnesium carbonates which exhibited smaller MgO surface areas in contrast to $Mg(OH)_2$ at 450°C.

The unidentified compound, which exhibited the smallest MgO surface area at 450°C, also contributed in increased char formation compared to the $Mg(OH)_2$ 120°C and commercial products. This observation correlated with the expected increase in char formation with a decrease in surface area.

The amount of char formed in the presence of the inorganic products at 520°C (Table 8.1) was similar, except in the case of $Al(OH)_3$ that resulted in the largest amount of char formed. As a result, it was difficult to relate the char results at 520°C to the MgO surface areas of the various inorganic products. The results in Table 8.1 clearly indicated that at increased heating times and temperatures, a decrease in the amount of char formed could be observed. This observation was probably due to carbon destruction at higher temperatures and longer heating times.

The charring results for phenolphthalein are given in Table 8.2.

Table 8.2 Apparant char yield of 1:1 (w/w) mixtures of phenolphthalein (Ph) with the inorganic products

Mixtures	Char yield (%)			
	450°C		520°C	
	15 min	*30 min*	*15 min*	*30 min*
Phenolphthalein	43.4	38.8	18.1	1.5
Ph + $Mg(OH)_2$	12.4	1.9	–	–
Ph + $Al(OH)_3$	50.7	46.7	12.7	0.4
Ph + $Mg(OH)_2$ 120°C	2.7	1.6	–	–

A similar observation to that observed with citrazinic acid, could be made regarding the char formed in the presence of phenolphthalein and $Mg(OH)_2$ at 450°C. Although $Mg(OH)_2$ exhibited the largest MgO surface area at 450°C, it still resulted in a higher char formation compared to the basic magnesium carbonates with lower MgO surface areas. $Al(OH)_3$ again exhibited the largest char formation compared to the other inorganic products at 450 and 520°C. An interesting observation at 450°C was that more char was formed in the presence of $Al(OH)_3$ compared to phenolphthalein with no inorganic additives. Nearly no char formation could be observed for phenolphthalein in the presence of the basic magnesium carbonates at both 450 and 520°C.

It is evident from the results in Table 8.1 and 8.2 that the formation of char was influenced by the compound with which the inorganic products were mixed. Except for $Al(OH)_3$, all other inorganic products experienced more char formation in the presence of citrazinic acid compared to phenolphthalein. This was ascribed to the integral chemical characteristics of the char forming compound. It is not possible to come to a concrete conclusion regarding the influence of the inorganic products on char formation, since this seemed to be influenced by the char forming compounds' characteristics and may therefor vary from compound to compound.

Since a large amount of char was formed in the presence of $Mg(OH)_2$ despite its large MgO surface area, it was concluded that an increase in surface area could probably not be expected to result in decreased char formation during combustion. An alternative mechanism possibly existed that influenced the amount of char formed. Decomposition

of the hydroxides are known to give metallic oxides which are active products. These highly active materials will adsorb a multitude of species in order to reduce their surface energies (Hornsby and Watson, 1989). It could thus be proposed that with larger MgO surface areas and subsequently greater MgO activity, more carbon probably needs to be adsorbed onto the MgO surface to reduce the surface energy. This could result in more char being retained during combustion, as observed for $Mg(OH)_2$ and $Al(OH)_3$. The basic magnesium carbonates that exhibited smaller MgO surface areas, is expected to have smaller surface energies compared to $Mg(OH)_2$. As a result less char probably needed to be adsorbed in order to reduce the surface energy of the MgO formed from the basic magnesium carbonates.

The high surface area of oxides produced by low temperature decomposition of $Mg(OH)_2$, has been related to a reduction in both the rate of evolution of smoke and the volume of smoke produced. This observation was related to the adsorption of considerable quantities of carbon on the active oxides (Hornsby and Watson, 1990). It might be expected that the basic magnesium carbonates could also contribute in reducing smoke evolution during a fire, but to a lesser extent when compared to $Mg(OH)_2$. This is expected since the surface areas of the oxides produced by thermal decomposition of the basic magnesium carbonates were smaller compared to $Mg(OH)_2$.

8.3.2 Thermogravimetric analysis of EVA composites

TG and DTA were used in order to determine whether the addition of fillers to the EVA matrix would have a noticeable influence on its degradation characteristics. It is necessary to study the TG and DTA curves for EVA in the absence of any fillers, to identify any possible changes in the degradation characteristics after the fillers have been added. The TG and DTA curves of EVA in air are given in Figure 8.1.

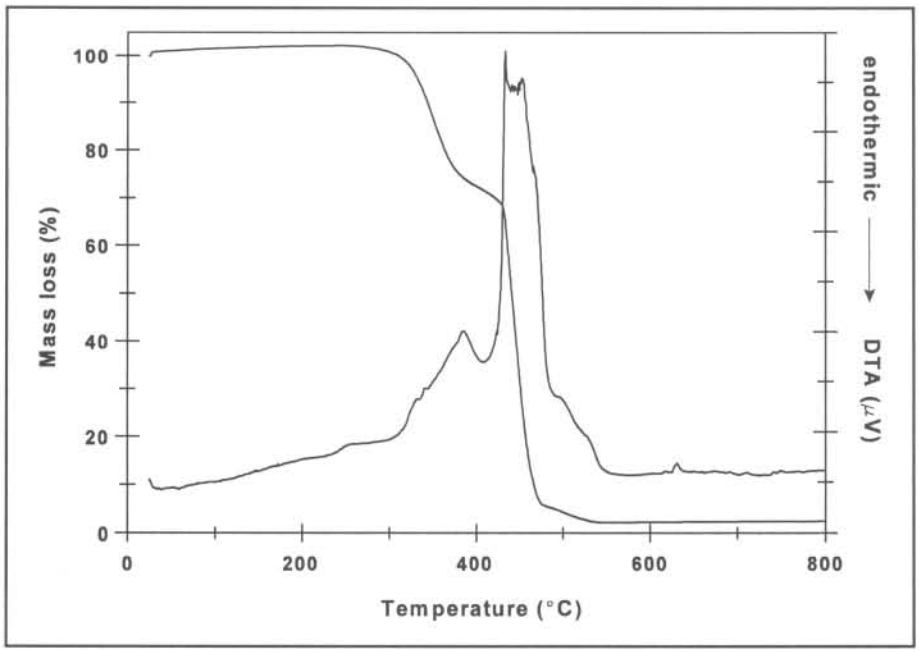

Figure 8.1 TG and DTA curves of EVA in air

The thermal degradation of EVA is characterised by three stages. The first step (250–350°C) is assigned to the evolution of acetic acid due to the decomposition of vinyl acetate groups. Between 425 and 500°C degradation of the polyethylenic chains takes place. The third step (550–600°C) may be assigned to the degradation of carbonaceous residue formed during the degradation of the polyethylenic chains by reacting with the oxygen of the air (Bourbigot *et al.*, 1999). It is evident that these processes are exothermic in air (Figure 8.1).

For the inorganic products to influence the combustion behaviour of EVA, it is assumed that filler decomposition should occur at temperatures below the maximum degradation temperature of EVA. The thermal and decomposition characteristics of the inorganic products that were investigated are summarised in Table 8.3 (also Chapter 6, Figures 6.1, 6.2 and 6.3).

Table 8.3 Thermal properties and decomposition characteristics of selected inorganic products

Inorganic products	Approximate decomposition onset temperature in air (°C)	Total experimental mass loss (%)	Decomposition products	Total reaction enthalpy ($J\ g^{-1}$)
$Mg(OH)_2$	370	26.0	$MgO;H_2O$	1164
$Al(OH)_3$	227	32.7	$Al_2O_3;H_2O$	1225
Commercial	190	56.4	$MgO;H_2O;CO_2$	1114
$Mg(OH)_2$ 120°C	190	58.6	$MgO;H_2O;CO_2$	1173
Unidentified	120	62.6	$MgO;H_2O;CO_2$	1438

It is evident that of all the inorganic products studied in this investigation (Table 8.3), $Mg(OH)_2$ had the highest temperature stability. This is an important parameter to take into account when deciding on the most appropriate filler for flame retardation of a polymer. The lower the decomposition temperature of the inorganic product, the more limited its application range as a flame retardant in polymers. When a polymer is processed at a temperature that is in close proximity to the onset decomposition temperature of the inorganic filler, the inorganic filler could undergo premature decomposition that will ultimately influence is effectiveness as a flame retardant. In this investigation the EVA was processed at ~95°C that was well below that of the onset decomposition temperature of the inorganic fillers. It could be concluded that the commercial and $Mg(OH)_2$ 120°C compounds could only be incorporated into polymers that are processed at temperatures below 190°C, as is the case with $Al(OH)_3$. The unidentified product's application will be severely limited due to its low onset decomposition temperature.

The inorganic products all decomposed to the metallic oxide and water vapour. In addition to metallic oxide and water, the basic magnesium carbonate products also gave off CO_2 gas. The generation of noncombustible gases (H_2O and CO_2) contributes in lowering the oxygen concentration at the flame front that often results in flame snuffing because of the lack of oxygen. This result is transitory because once the material decomposes, the residual matter acts as an incombustible diluent of the

polymer matrix (Sutker, 1988). The decomposition products are non-toxic and non-corrosive in contrast to the halogen flame retardants. The heat capacities of the inert decomposition products also contribute in reducing the thermal energy available to degrade the substrate (Hornsby and Watson, 1990). The oxide residue becomes a conduit through which heat is conveyed away from the flame area, slowing down polymer decomposition (Touval, 1993). Smoke density in a flame is reduced by the oxide residue that adsorbs the soot particles. Oxidation of the adsorbed carbon particles are catalysed by the metal oxide residue due to the oxides' reactive surface characteristics (Hornsby and Watson, 1989).

The mass loss percentages indicated in Table 8.3 showed that the basic magnesium carbonates expelled larger quantities of gases compared to $Mg(OH)_2$ and $Al(OH)_3$. This is expected to contribute in increased dilution of the fuel supply in the gas phase of a fire in the presence of the basic magnesium carbonates, compared to $Mg(OH)_2$ and $Al(OH)_3$.

Another advantage regarding the use of the inorganic products as flame retardants is the endothermic decomposition thereof indicated by the total reaction enthalpy in Table 8.3. Considerable quantities of heat are consumed and hence withdrawn from the combustion of the polymer when the inorganic products decompose. This contributes in retarding the rate of thermal degradation of the burning polymer (Hornsby and Watson, 1986). It is evident from Table 8.3 that $Mg(OH)_2$, $Al(OH)_3$, commercial and $Mg(OH)_2$ 120°C products showed similar total reaction enthalpy values. The unidentified compound indicated a relatively higher value compared to the other inorganic products. It is thus expected that more heat will be withdrawn from a fire in the presence of the unidentified compound as filler, compared to the other inorganic fillers investigated.

The DTA curves of the various EVA composites in nitrogen are compared in Figure 8.2. These results clearly indicated that addition of the inorganic products influenced the degradation of EVA. The peak corresponding to the first stage of decomposition of EVA (~347°C), was displaced to a somewhat lower temperature in the presence of $Mg(OH)_2$ (~337°C) and $Al(OH)_3$ (~297°C). The larger displacement observed for $Al(OH)_3$ was ascribed to its lower decomposition temperature compared to EVA. The position of the EVA peak (~347°C) in the presence of the commercial, $Mg(OH)_2$ 120°C and unidentified products seemed unchanged. It is not possible to say with certainty which processes were responsible for the peak observed at approximately 350°C for

the various composites. This peak could be the combined result of the decomposition of EVA and the inorganic products below 350°C.

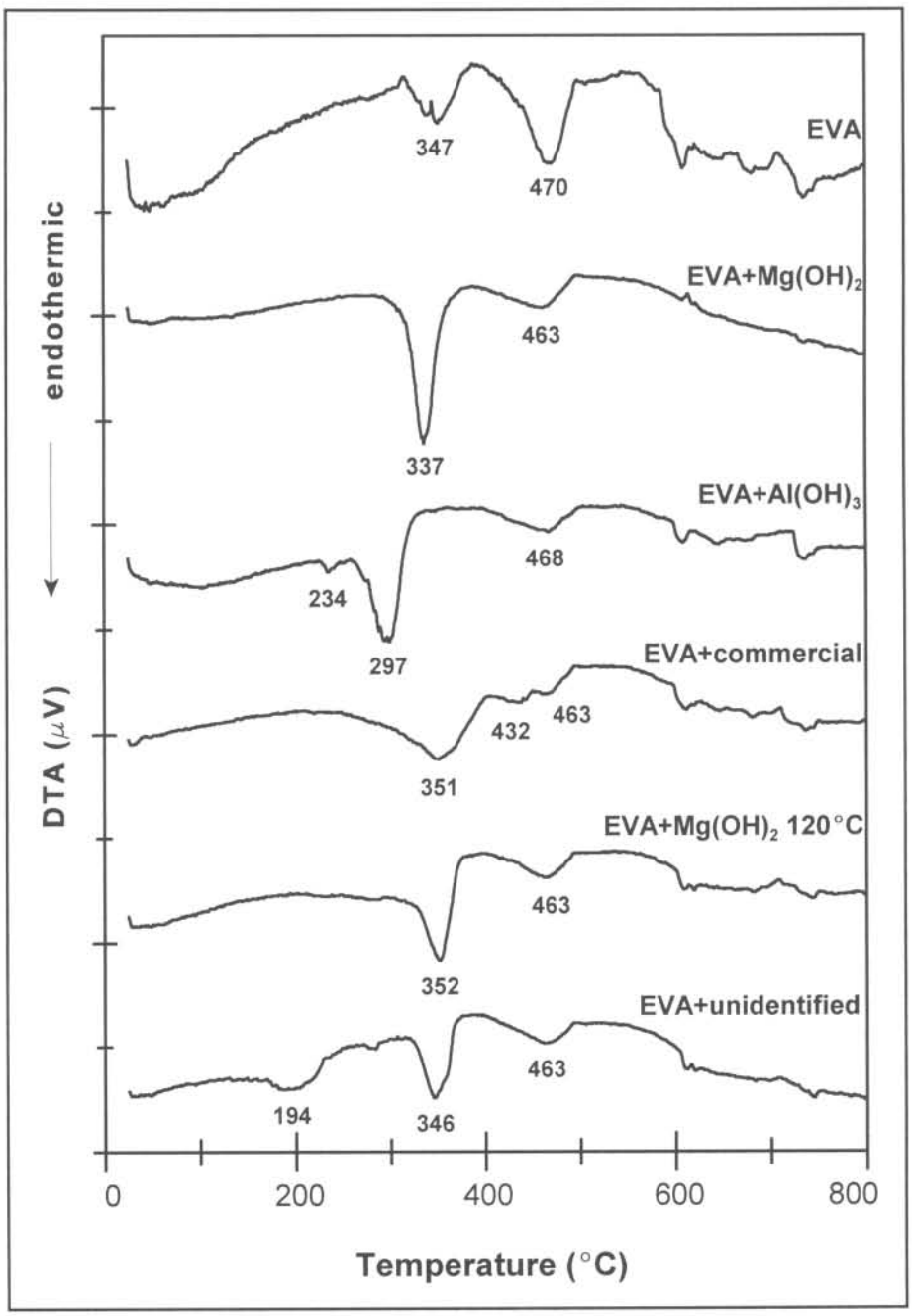

Figure 8.2 Comparison of DTA curves of EVA composites in nitrogen

The DTA peak corresponding to the second stage of EVA degradation (~470°C), seemed larger for pure EVA and noticeably smaller for the inorganic products (Figure 8.2). This observation was probably the result of the change in size ratio between the DTA peak at ~347 and ~470°C for EVA. The contributing endothermic processes of the inorganic products during EVA degradation around ~347°C, probably resulted in enlarging this peak with respect to the peak at ~470°C to the extent that the DTA peak at ~470°C seemed much smaller. The increase in the DTA peak size at ~347°C compared to the DTA peak at ~470°C, is confirmed by the normalised peak integral values depicted in Table 8.4. It is evident from these results, that the peak integral values of the EVA composites remained relatively unchanged at 470°C, while these values increased with respect to pure EVA in the presence of the inorganic products at 347°C.

Table 8.4 DTA normalised peak integrals for EVA composites at ~347 and ~470°C in nitrogen

Composites	Normalised peak integrals (ks°C g^{-1})	
	347°C	470°C
EVA	7.2	15.4
EVA + $Mg(OH)_2$	39.0	15.4
EVA + $Al(OH)_3$	40.9	12.9
EVA + commercial	39.3	8.8
EVA + $Mg(OH)_2$ 120°C	22.6	10.6
EVA + unidentified	19.1	11.3

The DTA curve corresponding to the composite containing unidentified product exhibited a small peak at ~194°C. This peak could possibly be ascribed to decomposition of the unidentified product that occurred below 200°C.

The DTA curves of the EVA composites in air are given in Figure 8.3. It is evident that the reactions that were observed during degradation of EVA and the composites in air, were highly exothermic. The endothermic peak observed at ~346°C for $Mg(OH)_2$ and at ~317°C for $Al(OH)_3$, possibly corresponded to the peaks observed in the DTA curves

in nitrogen (Figure 8.2) in the same temperature range. These peaks seemed to be displaced to a somewhat higher temperature in air compared to nitrogen. It should be noted that the DTA peaks observed in nitrogen (Figure 8.2) are also present in the DTA in air (Figure 8.3). The reason why the reactions in air seem less endothermic compared to the reactions in nitrogen at the same temperature (~347°C), is because of an additional exothermic process taking place in air. A similar observation was made for the $Mg(OH)_2$ 120°C and unidentified products, which exhibited endothermic peaks at ~352 and ~360°C respectively. The peaks previously observed at ~460°C in nitrogen (Figure 8.2) for the respective composites were overshadowed by the exothermic peak in air and were thus not observed (Figure 8.3).

The exothermic phenomenon observed just below 500°C was assigned, in part, to the oxidation of carbon. The exothermic phenomenon observed between 400 and 500°C hinders any possibility of observing the endothermic phenomenon that characterises the decomposition of the basic magnesium carbonate products in this temperature range.

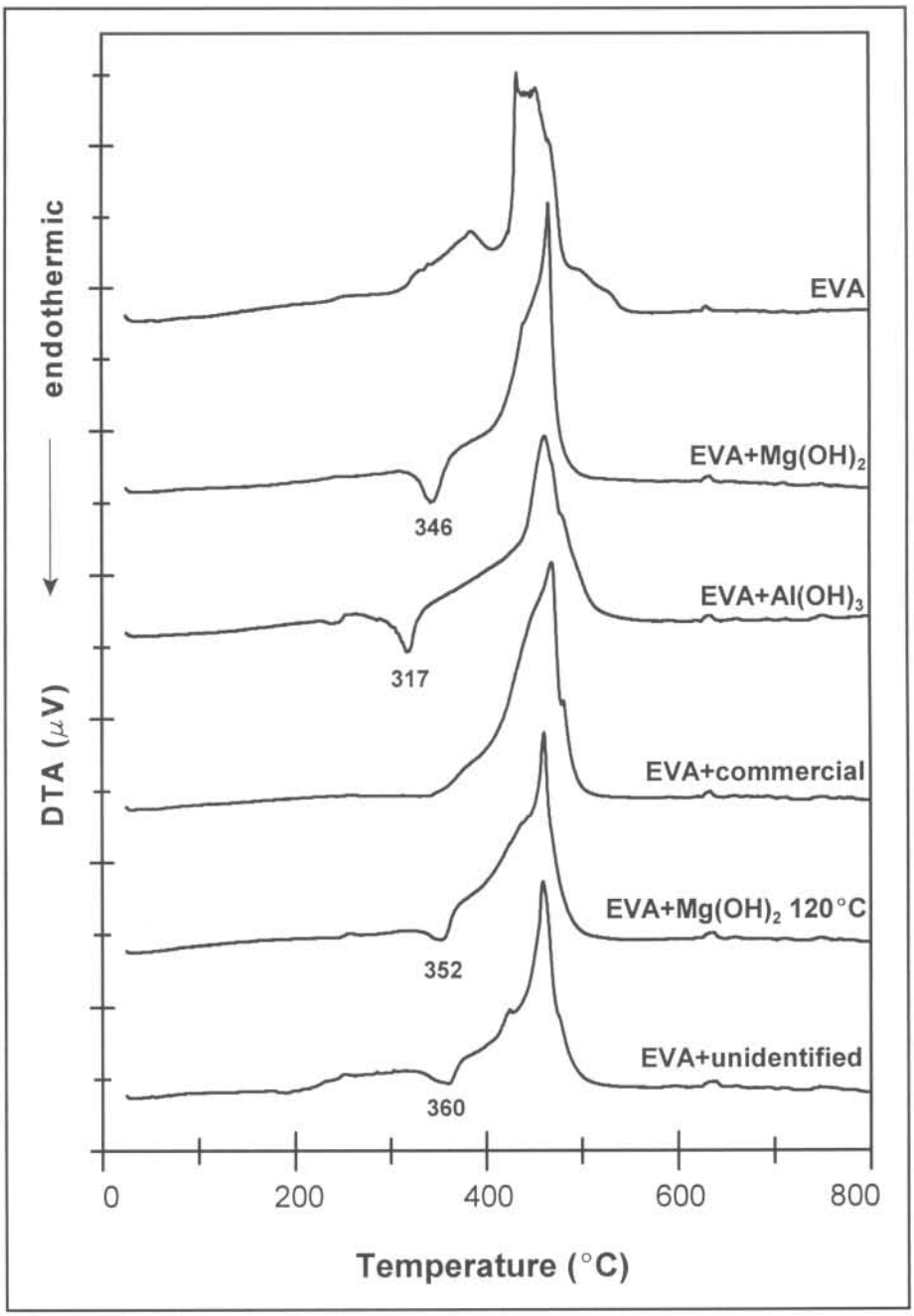

Figure 8.3 Comparison of DTA curves of EVA composites in air

The TG curves of the EVA composites in air are given in Figure 8.4. All the composites, except for the composite filled with the unidentified compound, showed two decomposition stages. The composite filled with the unidentified compound in contrast showed three stages of decomposition. The first stage of decomposition for the

composite filled with unidentified product, possibly corresponded to the dehydration of the unidentified compound below 250 °C, followed by degradation of EVA at 250–350 °C and degradation of both the unidentified compound and EVA at 400–500 °C. The dehydration reactions of $Mg(OH)_2$ and $Al(OH)_3$ and the dehydration, dehydroxylation and decarbonation reactions of the commercial and $Mg(OH)_2$ 120 °C products, were obscured by the simultaneous degradation of EVA.

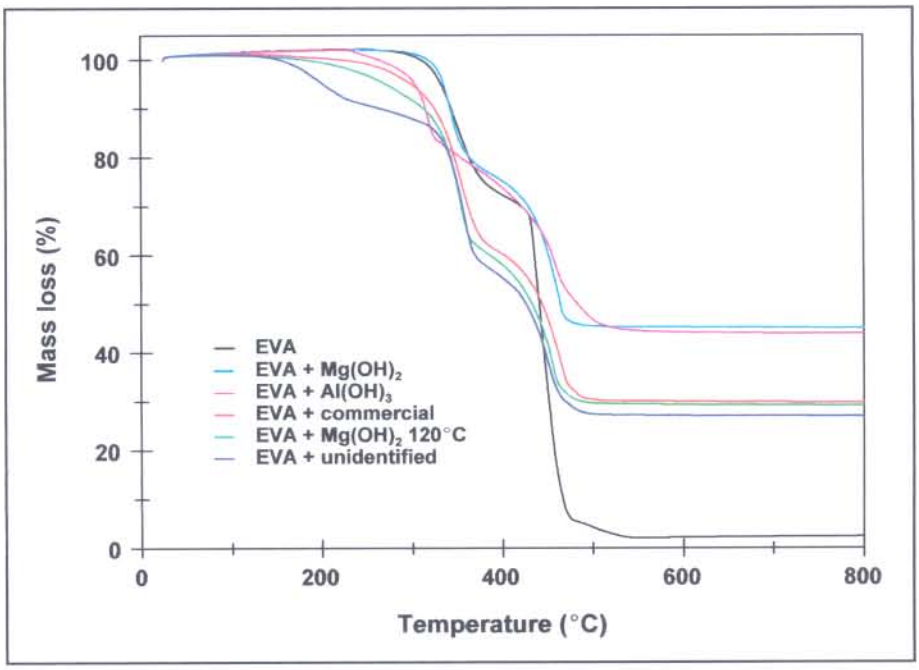

Figure 8.4 Comparison of TG curves of EVA composites in air

The second stage of the EVA degradation seemed to be displaced to a slightly lower temperature for the EVA composites filled with basic magnesium carbonate, compared to pure EVA. The composites filled with $Mg(OH)_2$ and $Al(OH)_3$ started the second decomposition stage at approximately the same temperature as for pure EVA.

The mass of the residue after thermal decomposition of the composites filled with the inorganic products, was similar to the mass of metallic oxide formed as a result of decomposition of the respective inorganic products. This suggests a more complete combustion of EVA with the inorganic products.

Decomposition onset temperatures of the EVA and inorganic product composites in air, are depicted in Table 8.5. It is evident that the decomposition onset temperatures of the composites, excluding that of $Al(OH)_3$ and the unidentified product, were not lowered significantly compared to that of EVA. It was expected that the addition of the inorganic products to EVA would lower the decomposition onset temperature of the EVA due to the lower decomposition temperatures of the inorganic products (Table 8.3). The lower decomposition onset temperature of the unidentified compound did however influence the EVA decomposition onset temperature noticeably.

Table 8.5 Decomposition onset temperatures of EVA and inorganic product composites derived from the TG curves in air

Composites	Decomposition onset temperature (°C)
EVA	316
EVA + $Mg(OH)_2$	321
EVA + $Al(OH)_3$	292
EVA + commercial	311
EVA + $Mg(OH)_2$ 120°C	318
EVA + unidentified	148

8.3.3 Limiting oxygen index (LOI) results for EVA composites

The limiting oxygen index is one of several test methods for evaluating the burning behaviour of polymers. This test illustrates the relative flammability of materials. The oxygen index or limit oxygen index test determines the oxygen concentration at which sustained combustion occurs using a vertically mounted specimen ignited at the upper end (Sutker, 1988). This test is simple and reproducible and is used to guide development work. Conclusions about fire performance in an actual fire should not be made based on results from the oxygen index test though. Results of this test are expressed as (Sutker, 1988):

$$LOI = \frac{\text{volume of } O_2}{\text{volume of } O_2 + \text{volume of } N_2} \times 100\ \%$$

A LOI of 30 means that a material will burn in an atmosphere of 30% oxygen.

An attempt was made to obtain composites with the same amount of filler for this investigation. The amount of filler was kept constant since LOI is a function of the amount of filler. Delfosse *et al.* (1989) and Rigolo and Woodhams (1992) observed an increase in LOI when the amount of filler was increased. The amount of filler obtained during compounding and the LOI results for the various composites are given in Table 8.6.

Table 8.6 Filler content and LOI results for the respective EVA composites

Composite	% Filler (w/w)	LOI (%)
EVA	–	28.4
EVA + $Mg(OH)_2$	60.7	29.2
EVA + $Al(OH)_3$	60.7	38.9
EVA + commercial	62.0	29.5
EVA + $Mg(OH)_2$ 120°C	61.6	30.2
EVA + unidentified	60.5	34.3

The aim was to obtain a filler loading of approximately 60%. To achieve adequate flame retardancy a filler loading of 50–100 parts by weight of the inorganic products are required per 100 parts of polymer (Sutker, 1988). The high filler content acts as a solid phase diluent (Hornsby and Watson, 1990), thus reducing the total quantity of combustible matter. It is evident from the results in Table 8.6, that the compounding procedure produced composites with the filler levels required.

It is evident from the LOI results, that the inorganic fillers succeeded in increasing the pure polymers' flame resistance. The respective inorganic product composites resisted burning in the following decreasing order,

$$Al(OH)_3 > \text{unidentified} > Mg(OH)_2\ 120°C \geq \text{commercial} \geq Mg(OH)_2$$

It seemed that the hydromagnesite products (commercial and $Mg(OH)_2$ 120°C) gave similar results than $Mg(OH)_2$. Rigolo and Woodhams (1992) also noticed a slightly better performance, based on the LOI results, from the basic magnesium carbonates compared to $Mg(OH)_2$ when compounded with polypropylene. As with the charring experiments, $Al(OH)_3$ excelled above the other inorganic products. Delfosse *et al.* (1989) also noticed a higher LOI value for $Al(OH)_3$ compared to $Mg(OH)_2$ when compounded with EVA. An interesting observation was the LOI result obtained for the unidentified compound, that seemed to perform better than its basic magnesium carbonate counterparts and $Mg(OH)_2$. It has been suggested (Hornsby and Watson, 1990) that LOI might be related to the structure of the parent $Mg(OH)_2$.

According to an LOI classification (Schmidt, 1999), the composites filled with the $Mg(OH)_2$, commercial and $Mg(OH)_2$ 120°C products are classified as flame resistant (LOI 29–34). The unidentified product could also be classified as flame resistant since its LOI value is just slightly greater than 34. The composite filled with $Al(OH)_3$, is classified as extra flame resistant (LOI > 34).

During the LOI experiments the behaviour of the samples were observed. The pure polymer burned with a blue flame and flowed down the sides of the sample. During the test, the polymer caved in. After the flame was extinguished a sticky residue remained.

With the composites containing inorganic filler, a red-yellow flame was observed. The formation of black char on the edges of the burning polymer with incandescence also appeared. Of all the composites, the formation of the least char was observed for $Al(OH)_3$. The char did not form on the edges of the burning polymer, as was observed for the other composites, but between the burning white composite. The char that formed on the edges of the burning composite filled with the unidentified compound, was observed to fold in towards the burning plastic resulting in extinction of the flame. This was in contrast to the composites filled with $Mg(OH)_2$, commercial and $Mg(OH)_2$ 120°C products in which the char folded outwards from the burning plastic.

The composites containing $Mg(OH)_2$ and $Al(OH)_3$ did not remain rigid during the test. The plastic caved in after a short time of burning. The composites containing the basic magnesium carbonates remained rigid the entire time of burning. The burning composites were also characterised by dripping char and dripping burning plastic. After extinction of the flame, a sticky residue remained for the $Mg(OH)_2$ and $Al(OH)_3$ filled composites. This residue was less sticky for the basic magnesium carbonate filled composites.

8.3.4 Scanning electron microscopy of EVA composites

When high loadings of fillers are used, as in this investigation, dispersion is difficult and the effect on polymer physical properties is significant. Fillers with surface treatments of organotitanate or organosilicon coupling agents are useful to overcome the dispersion and physical property loss problems (Sutker, 1988). If the material that is added to a polymer behaves as a filler, it is important to consider how to obtain good bonding between the filler surface and the polymer so that mechanical properties can be maximised. These properties will usually show increased modulus and perhaps an increase in tenacity but usually a decrease in elongation and impact strength. Melt viscosity will usually increase (Pearce, 1986).

The SEM images of the various composites were obtained to determine whether homogeneous dispersion has been achieved. Two magnifications (x500 and x2000) were used in order to study the surface morphology of the EVA composites. The x500 magnification gave an overall impression regarding the dispersion of the inorganic products in the various composites. The x2000 magnification gave an in depth view of agglomeration where it could not be distinguished from the x500 magnification. Figure 8.5 gives an image of the unfilled polymer. It is evident that the polymer exhibited a clear smooth surface.

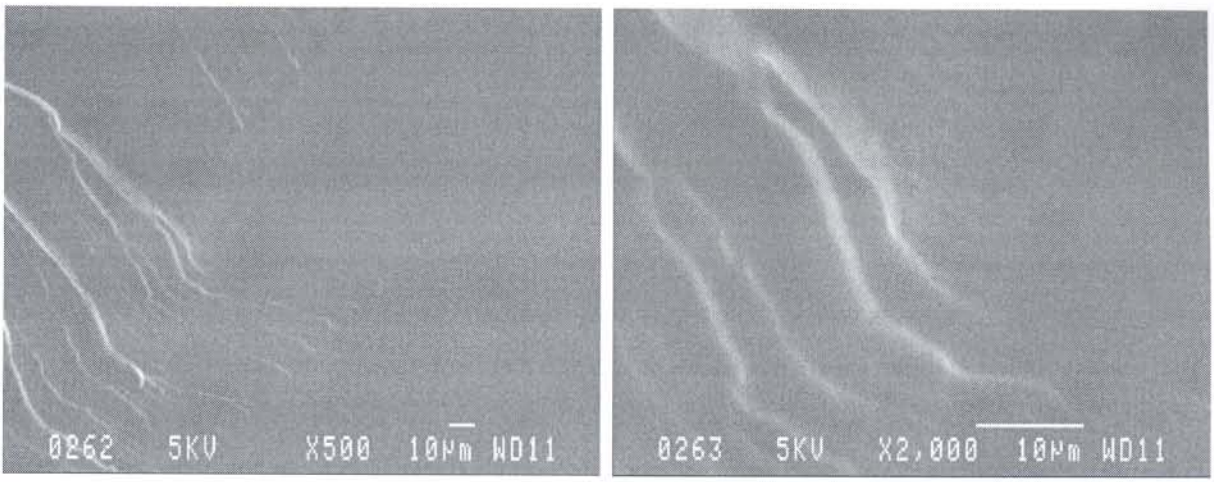

Figure 8.5 SEM image of unfilled EVA

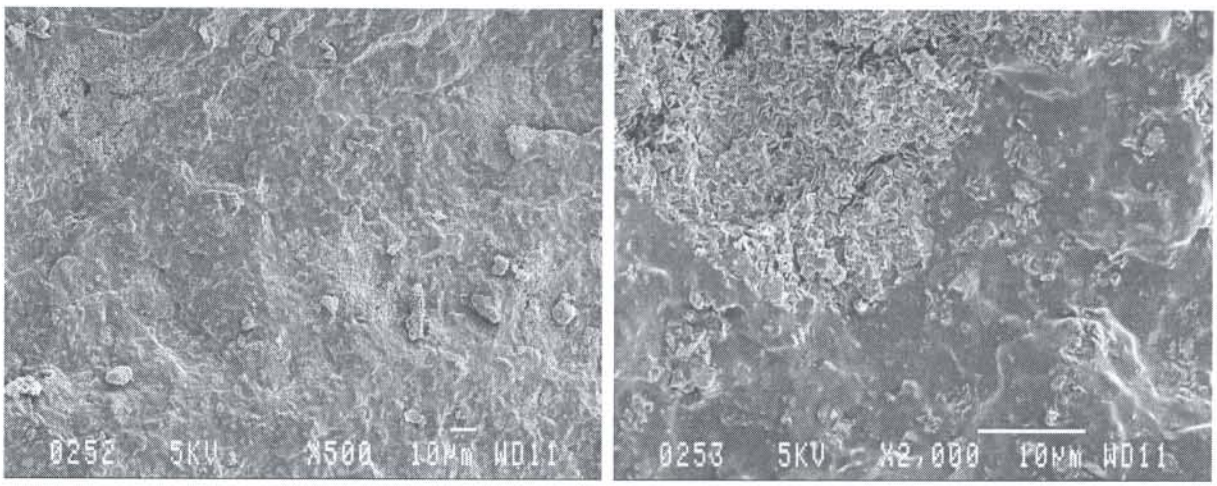

Figure 8.6 SEM image of $Mg(OH)_2$ composite

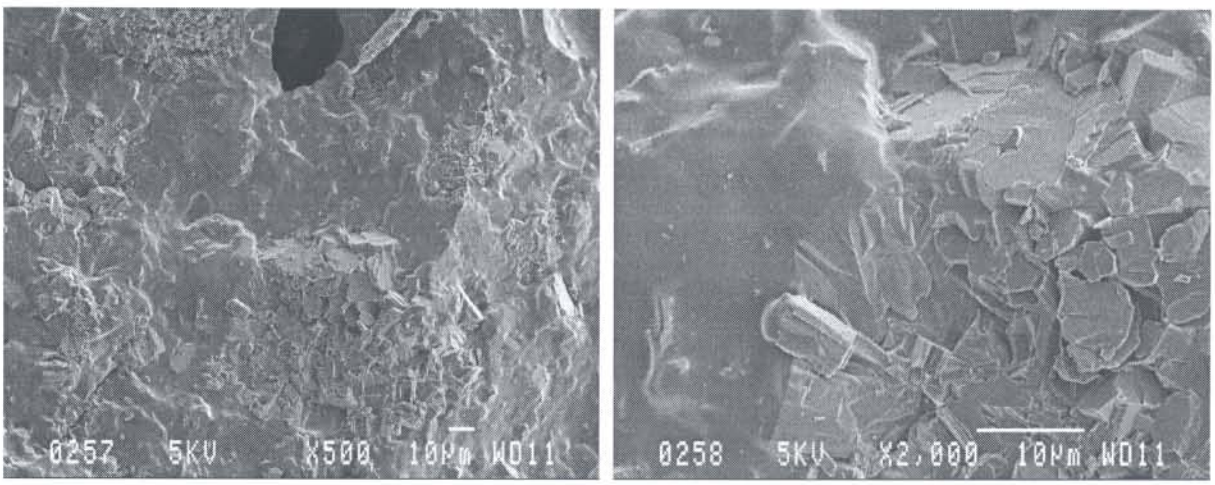

Figure 8.7 SEM image of $Al(OH)_3$ composite

It is evident from Figure 8.6 that the addition of $Mg(OH)_2$ did not result in an even dispersion. In the x500 magnification the lighter contrasts were an indication of the agglomeration of the $Mg(OH)_2$ particles. The agglomeration of the hexagonal platelets were more evident from the x2000 magnification.

The EVA composite containing $Al(OH)_3$ also had an uneven distribution of the inorganic product. The agglomeration of the particles is very clear from the x500 magnification of Figure 8.7, and even more evident from the x2000 magnification.

The SEM images of the EVA composites containing the commercial and $Mg(OH)_2$ 120°C products are given in Figure 8.8 and Figure 8.9 respectively. It seemed as if an even dispersion of the product particles were achieved within the polymer matrix for both products. This homogeneous morphology could possibly be ascribed to the uniform distribution of the hydromagnesite particles within the polymer matrix. Agglomeration of the inorganic particles could though be observed. This observation was more evident for the $Mg(OH)_2$ 120°C filled composite (x2000 magnification, Figure 8.9).

The unidentified filled composite (Figure 8.10) seemed to have a homogeneous morphology. A small amount of agglomeration could though be observed (x500 magnification).

Agglomeration of the inorganic particles was ascribed to inadequate dispersion in the polymer matrix. High loadings of the inorganic product was in part responsible for this effect. This can be overcome through the addition of a dispersing agent that aids dispersion and promotes wetting of the inorganic particles. Rigolo and Woodhams (1992) achieved wetting and dispersion of basic magnesium carbonate filler particles dispersed in polypropylene, through the addition of maleated polypropylene wax.

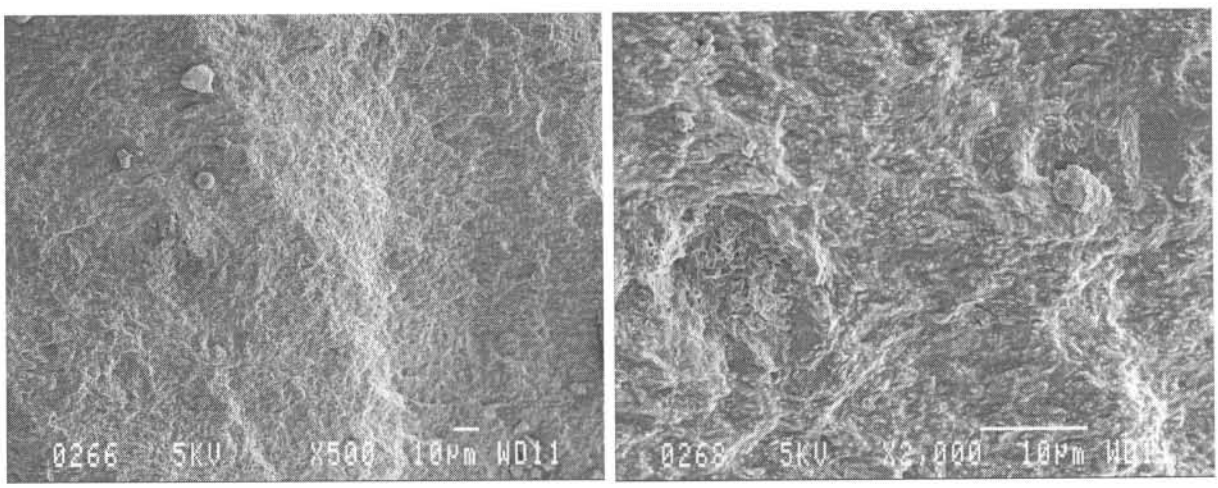

Figure 8.8 SEM image of commercial composite

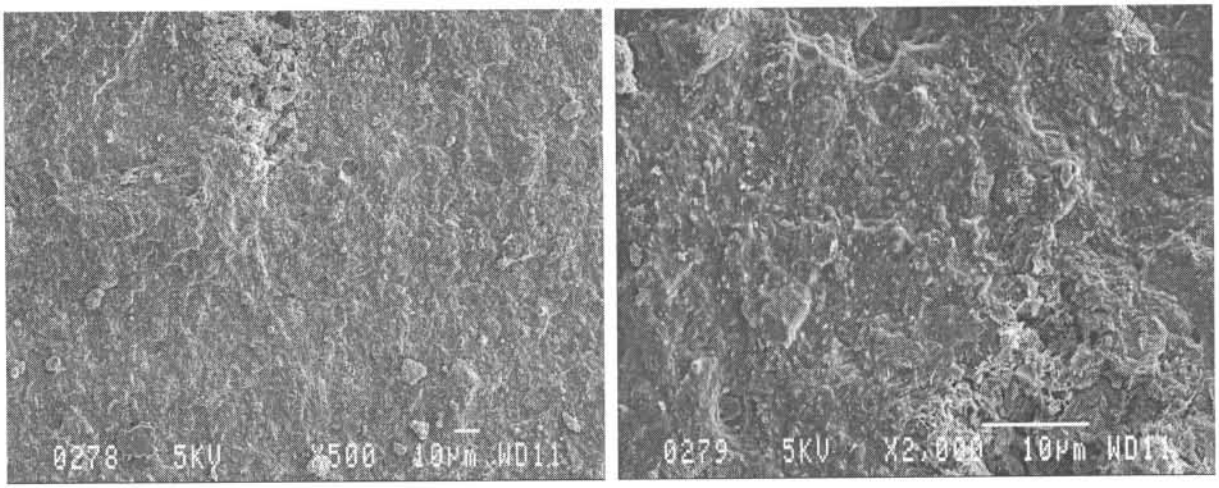

Figure 8.9 SEM image of $Mg(OH)_2$ 120°C composite

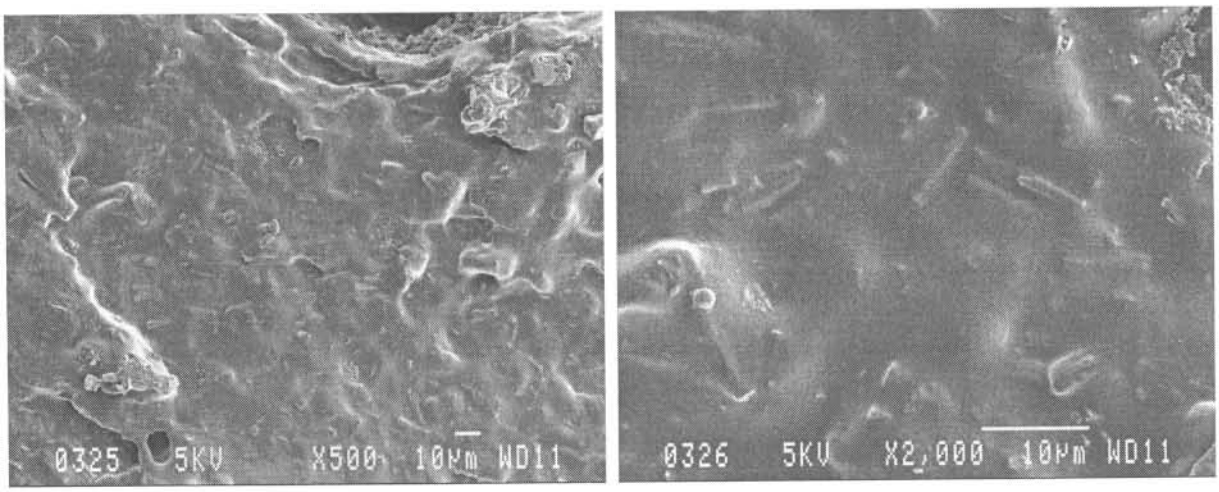

Figure 8.10 SEM image of unidentified composite

The composites were also studied after the LOI tests were conducted. The aim was to identify changes that possibly occurred during burning by comparing the SEM images of the EVA composites after burning, with the SEM images before burning.

Very few changes could be observed in the various burnt composites compared to the unburnt composites. An interesting observation in the SEM images of the burnt composites was the formation of a phase separation between the unburnt composite and what seemed to be the molten polymer phase. This was only observed for the $Mg(OH)_2$ (Figure 8.12), commercial (Figure 8.14) and $Mg(OH)_2$ 120°C (Figure 8.15) filled composites. This observation coincides with a visual observation made from the burnt plastic. When the burnt plastic was viewed, a yellowish molten plastic covering the white molten composite, was observed. No changes were observed in the unburnt parts of the plastic and seemed to be similar to the composites before heat treatment.

The molten polymer phase was not observed for the burnt $Al(OH)_3$ filled composite (Figure 8.13) after an extensive study of the surface morphology. This correlates with the visual inspection of the burnt plastic in which no molten plastic, covering the white molten composite, could be observed. Only the white molten composite could be identified.

The phase separation between the molten polymer and the unburnt plastic was not observed in the SEM image of the composite filled with unidentified product (Figure 8.16). There were though shattered molten polymer pieces on the unburnt surface (x500 magnification) that were probably obtained when the plastic was fractured during preparation of the sample for SEM. The molten plastic that covered the white molten composite was observed during the visual inspection of the burnt plastic.

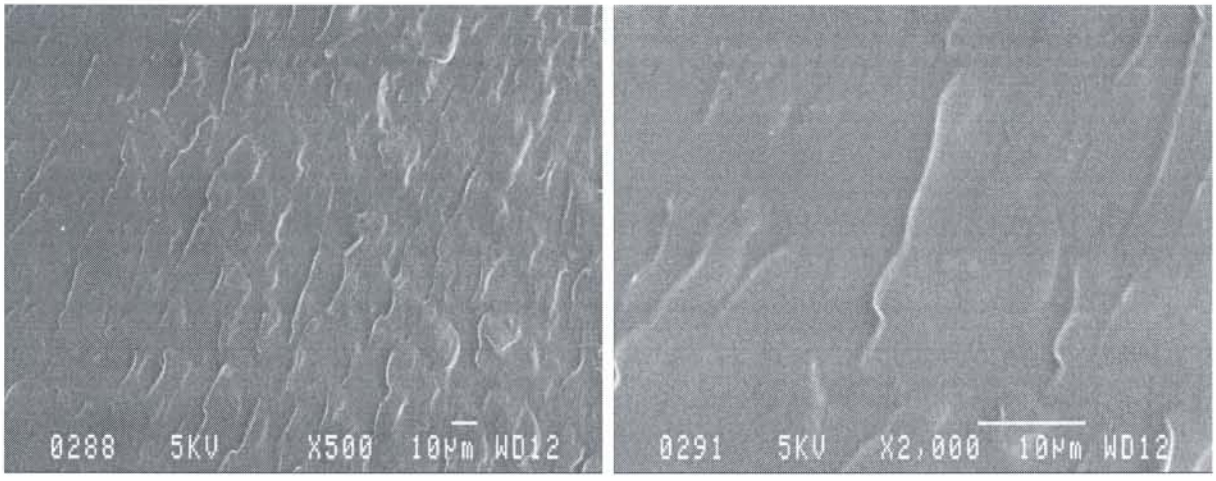

Figure 8.11 SEM image of unfilled EVA after being burned

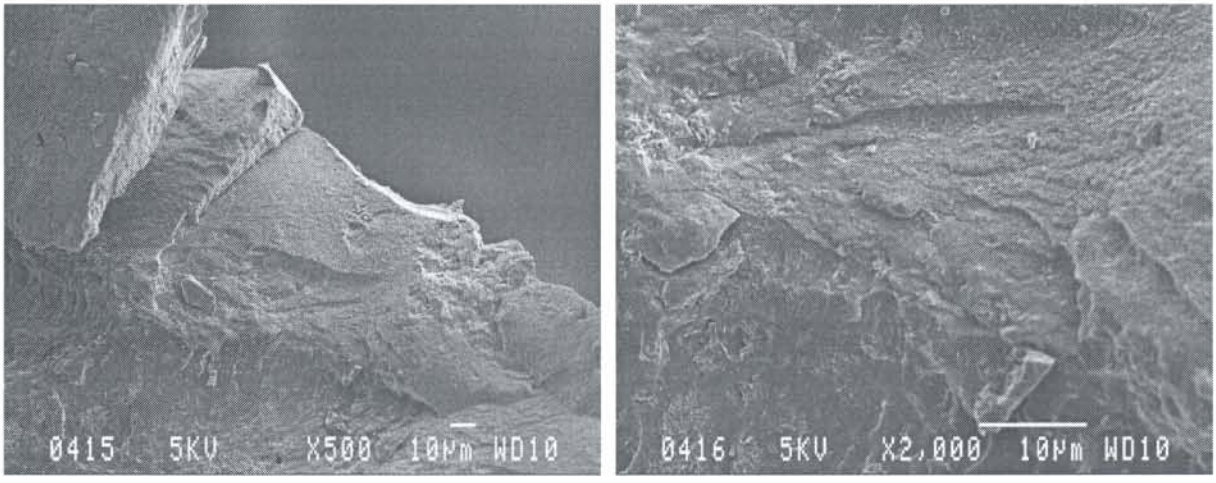

Figure 8.12 SEM image of $Mg(OH)_2$ composite after being burned

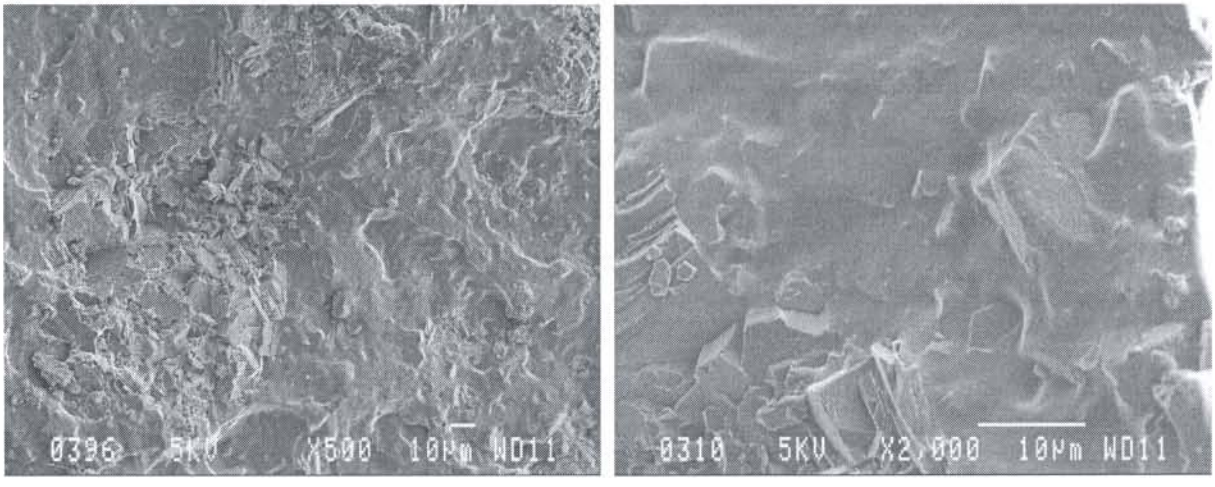

Figure 8.13 SEM image of $Al(OH)_3$ composite after being burned

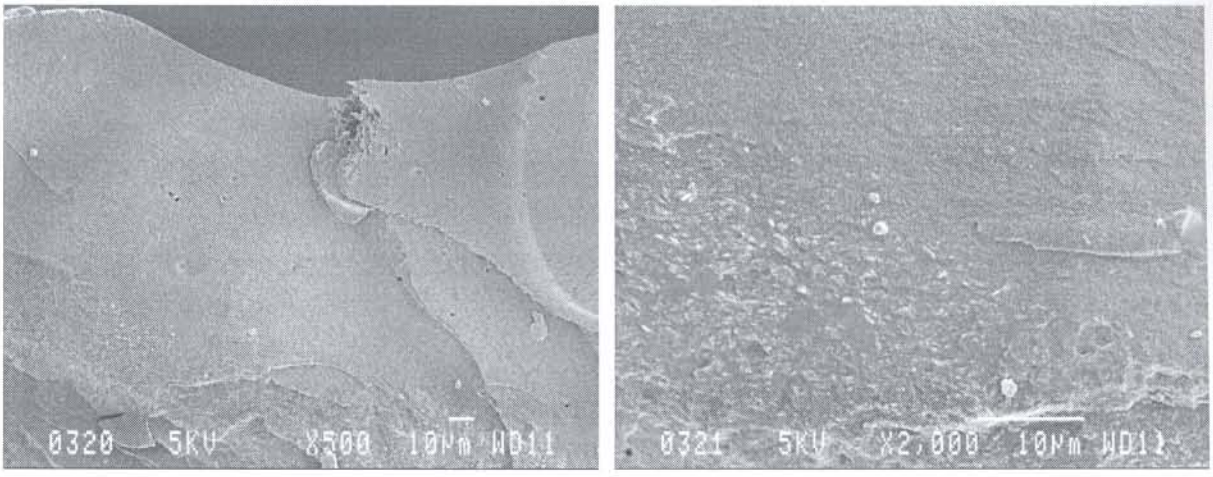

Figure 8.14 SEM image of commercial composite after being burned

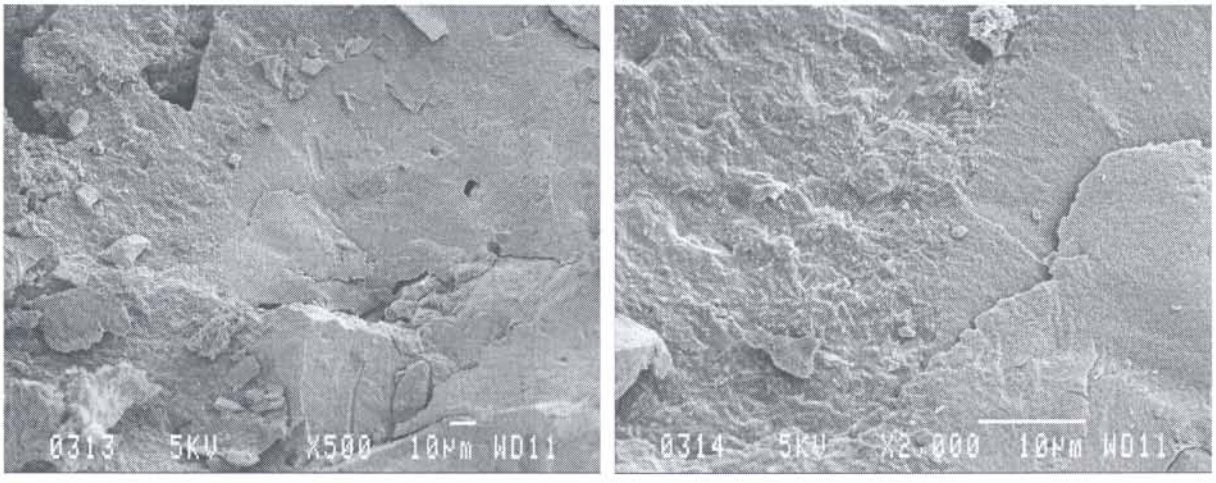

Figure 8.15 SEM image of $Mg(OH)_2$ 120°C composite after being burned

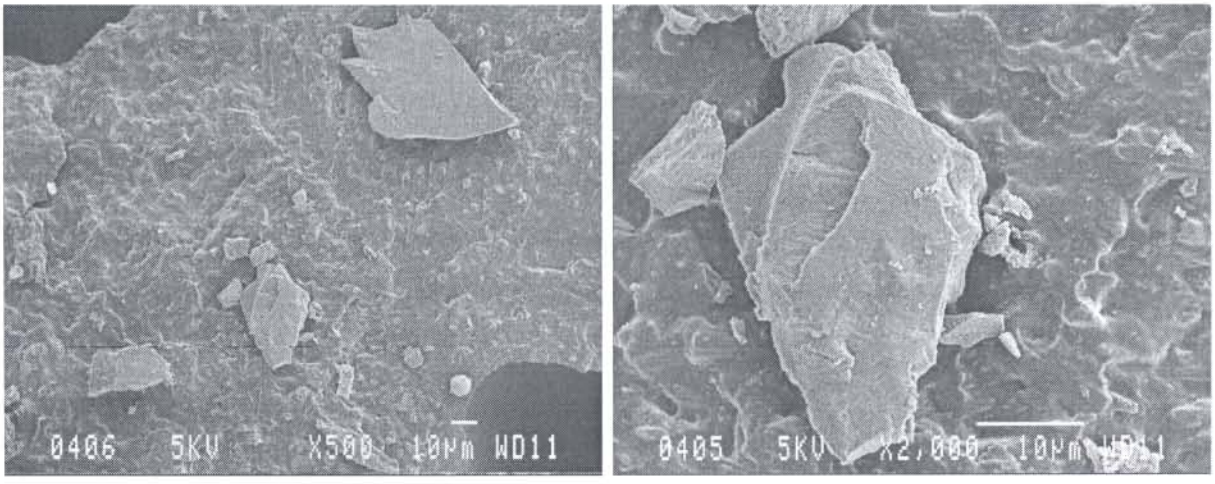

Figure 8.16 SEM image of unidentified composite after being burned

8.4 Conclusion

The flame retardant properties of the $Mg(OH)_2$ 120°C and unidentified product containing composites, compared favourably to that of commercial $Mg(OH)_2$, $Al(OH)_3$ and hydromagnesite. The tests that were done were on a small scale and care needs to be taken when extrapolating these results to the results that could be expected from full scale fire tests.

It was evident from the charring experiments, that the amount of char formed and the influence of the inorganic additive on char formation was dependant on the inherent characteristics of the char forming compound. Results obtained for one char forming compound could not be extrapolated to another compound. The increased char formation that was observed for the higher surface area MgO formed from $Mg(OH)_2$, was probably the result of the adsorption of char to reduce the high surface energy of MgO.

The TG-DTA, LOI and SEM results obtained for the various composites is dependent on the polymer type used. That is, the results obtained for EVA during this investigation, are not necessarily what could be expected by compounding the inorganic products with other types of polymers. The choice of polymer is very important in order to receive required performance of the inorganic flame retardant. The tests however highlighted the possibilities which the inorganic products present as flame retardants, by compounding the inorganic products with EVA.

The TG and DTA results indicated that the lower decomposition temperatures of the $Mg(OH)_2$ 120°C and unidentified products compared to $Mg(OH)_2$, could possibly cause problems when processing a polymer. This restricts the application range of the synthesised products as flame retardants in polymers. The volume of H_2O and CO_2 expelled during decomposition is expected to contribute in diluting the fuel supply in the gas phase of a fire, compared to the lower volume of gas expelled by $Mg(OH)_2$ and $Al(OH)_3$. The $Mg(OH)_2$ 120°C product exhibited a total reaction enthalpy comparable to that of $Mg(OH)_2$ and $Al(OH)_3$. The unidentified compound exhibited a relatively larger reaction enthalpy compared to the other inorganic products investigated. It is expected that the unidentified compound would have a more pronounced influence in reducing the thermal energy available to degrade the burning substrate.

The LOI results showed that the $Mg(OH)_2$ 120°C and unidentified products were able to increase the flame resistance of EVA. These results were comparable to that of $Mg(OH)_2$ and $Al(OH)_3$. The unidentified compound performed better than $Mg(OH)_2$ and the hydromagnesite products in the LOI tests and gave the best results next to $Al(OH)_3$.

The SEM images indicated that additional additives were necessary in order to promote wetting of the filler particles and to possibly contribute in maximizing the polymers' mechanical properties. Further research is necessary to assess the influence of the synthesised products on the polymers' mechanical properties.

It is evident from the results presented, that the $Mg(OH)_2$ 120°C and unidentified products, that were synthesised and tested in this investigation, holds much promise as fillers for flame retardant applications.

Chapter 9

Conclusion

9.1 Synthesis

The development of a new procedure of synthesis for a specific product, had to be preceded by a detailed assessment of the need for such a study. The compound that was under consideration in this study was basic magnesium carbonate. This compound could be obtained either by mining or by synthetic preparation. When mining basic magnesium carbonate, various additional minerals are obtained with it. This influences the purity of the basic magnesium carbonate and requires separation processes to isolate the required product. By synthesising the basic magnesium carbonate from relatively pure starting reagents, a purer product could be obtained. Since the experimental conditions are controllable, it seemed possible to obtain the required product that complied to the set requirements.

In order to plan a strategy for synthesising the basic magnesium carbonate, it was necessary to obtain information relating to the various procedures that have been developed up to date for the synthetic preparation thereof. The synthetic procedures of preparation of the basic magnesium carbonate (or hydromagnesite) was discussed extensively in Chapter 3. The information that was obtained indicated that a number of procedures were available for the synthesis of hydromagnesite. These procedures were summarised in four categories with respect to the starting materials used ($Mg(OH)_2$, MgO, $MgCO_3 \cdot 3H_2O$ and the addition of a precipitating agent to a magnesium salt solution). Some of these procedures presented several disadvantages that needed to be avoided in order to obtain an environmentally safe and cost effective procedure. After a detailed study of the available procedures, it was decided on building upon the procedure suggested by Pond and Heneghan (1965), who used $Mg(OH)_2$ as starting material. The lack of information relating to the synthesis of basic magnesium carbonate from $Mg(OH)_2$ prompted this approach.

The procedure suggested by Pond and Heneghan (1965), excluded the use of reagents that could contribute to environmentally damaging effluents. The procedure seemed

simple without the use of high pressures or excessively high temperatures, which could contribute to a costly procedure, for obtaining basic magnesium carbonate. Their procedure was based on forming a slurry of magnesium hydroxide in water. CO_2 was introduced into the slurry until the pH thereof was between 7.5 and 9.0 (more specifically between 8.0 and 8.6). At this point the solid portion of the slurry was separated from the liquid portion and dried below 75°C.

Initial attempts to synthesise a basic magnesium carbonate by following the exact procedure as suggested by Pond and Heneghan (1965) failed. The result was that various experimental parameters had to be investigated until a combination could be obtained that resulted in the successful synthesis of a basic magnesium carbonate. The parameters that were investigated included:

- variation of slurry pH
- variation of slurry temperature
- addition of HCl at elevated temperatures
- variation of drying temperature
- variation of drying time
- $Mg(OH)_2$, $MgCO_3 \cdot 3H_2O$ and MgO as reagents respectively

Table 9.1 summarises the various basic magnesium carbonate products that were obtained for various combinations of the experimental parameters. It was possible to identify the products that were obtained in the various experiments, with relative accuracy, by using XRD. By using this technique it was possible to match the diffraction patterns of the synthesised products, to the diffraction patterns of a vast range of known compounds in the XRD database.

Table 9.1 Summary of basic magnesium carbonate products and the experimental conditions that resulted in the formation thereof

Product formed (confirmed by XRD)		Reagents	Slurry temperature (°C)	Final pH of slurry before filtration	Drying temperature (°C)
hydromagnesite	(1)	$Mg(OH)_2 + CO_2$	65°C + 0.1 M HCl	9.1	60
	(2)	$Mg(OH)_2 + CO_2$	65°C + 1 M HCl	8.3	60
	(3)	$Mg(OH)_2 + CO_2$	65°C + 1 M HCl	8.3	120
	(4)	$Mg(OH)_2 + CO_2$	19	7.6	100
	(5)	$Mg(OH)_2 + CO_2$	20	7.8	120
	(6)	$MgCO_3 \cdot 3H_2O$	90	9.7	65
	(7)	$MgSO_4 \cdot 7H_2O + Na_2CO_3$	90	8.8	160
dypingite		$Mg(OH)_2 + CO_2$	65°C + 1 M HCl	8.3	20
unidentified	(1)	$Mg(OH)_2 + CO_2$	19	7.6	90
	(2)	$Mg(OH)_2 + CO_2$	20	7.8	80
	(3)	$MgCO_3 \cdot 3H_2O$			80
					100
					120
	(4)	$MgO + CO_2$	20	8.4	80
				8.4	120

Procedures that were based on starting materials other than $Mg(OH)_2$ were also investigated in this study, in order to evaluate the relationship between the starting material and the products obtained for different experimental conditions. The synthesis of hydromagnesite from $MgCO_3 \cdot 3H_2O$, confirmed the conversion of $MgCO_3 \cdot 3H_2O$ to

hydromagnesite. The procedure with MgO as starting material was investigated to determine whether the same results as $Mg(OH)_2$ could be obtained. This proved to be unsuccessful. It seemed as if the MgO approach followed a different reaction route than $Mg(OH)_2$. The synthesis of hydromagnesite from $MgSO_4 \cdot 7H_2O$ and Na_2CO_3, which is a proven method for the synthesis thereof, was investigated for comparative reasons.

The synthesis of hydromagnesite (Table 9.1) via procedure 1, 2 and 3 delivered chloride as an unwanted effluent and required elevated slurry temperatures as well as additional reagents. Procedure 6 and 7 also required elevated slurry temperatures and did not make use of $Mg(OH)_2$ as the starting material. Procedure 7 delivered sulphate as an undesirable effluent. The synthesis of hydromagnesite via procedure 4 and 5 seemed to present the most viable approach to obtaining the required product.

The various products obtained by changing the experimental parameters during this investigation, were either hydromagnesite, dypingite, $MgCO_3 \cdot 3H_2O$ or an unidentified compound (which could not be matched to any of the compounds in the XRD database). The close phase relations between hydromagnesite, dypingite and $MgCO_3 \cdot 3H_2O$ is indicated in Chapter 3. It is evident that any changes in the experimental conditions could result in a different magnesium carbonate phase being obtained. The importance of controlled experimental conditions is vital for obtaining the required product, namely hydromagnesite.

The formation of an unidentified product was an intriguing phenomenon. A decision was made to further investigate the unidentified product together with the synthesised hydromagnesite product during this study. It was thought that the unidentified product could possibly be an intermediate phase.

The procedure that was selected for the synthesis of a basic magnesium carbonate, after weighing up the advantages and disadvantages associated with each procedure investigated, was as follows. The procedure was based on the formation of a slurry of magnesium hydroxide in water. CO_2 was introduced into the slurry until the pH thereof was between approximately 7.5 and 8.5. At this point the solid portion of the slurry was separated from the liquid portion. The solid was divided in half of which one half was dried at 80°C and the other half at 120°C to deliver an unidentified basic magnesium carbonate and hydromagnesite respectively. This procedure was chosen due to its simplicity, energy efficiency and the potentially environmentally friendly advantages thereof.

9.2 Characterisation

The next step in this investigation was to characterise the synthesised products obtained. The techniques that were chosen to assist in the characterisation procedure included: thermogravimetric analysis (TG), differential thermal analysis (DTA), surface area determination, scanning electron microscopy (SEM) and Fourier transform infrared spectroscopy (FT-IR). The characteristics of a select group of the products that were synthesised, were compared to the characteristics of $Mg(OH)_2$ as well as a commercially available hydromagnesite product. Differences and similarities between the various synthesised products (hydromagnesite, dypingite, $MgCO_3 \cdot 3H_2O$ and the unidentified product) and the hydromagnesite and unidentified products obtained by different procedures, were highlighted. It was possible to obtain valuable information relating to the inherent physical and chemical characteristics of the respective products, by combining the information that was obtained from the respective techniques.

9.2.1 Thermogravimetric and Differential thermal analysis

Since the products were to be tested for flame retardant application, the thermal decomposition characteristics thereof were very important. By knowing the degradation profile of the intended flame retardant, it is possible to determine whether it will be able to survive the temperature of any of the processing steps of the polymer. It is necessary to match thermogravimetric analysis curves of the flame retardants and the polymer to ensure that the flame retardant degrades just before the polymer that is being flame retarded. If the flame retardant possesses too low a thermal stability compared to that of the polymer, it will be lost before its function is needed. If it has greater thermal stability, it may remain intact at the time its function is needed (Pearce, 1986).

TG and DTA were used to investigate the thermal decomposition behaviour of the various products. TG records the mass changes as a function of temperature, while DTA records the energy changes as a function of temperature as the products are subjected to a controlled heating programme. The mass changes observed, could be correlated to the various molecular groups expelled from the crystal structures of the products at various temperatures. The processes that accompanied the decomposition reactions, whether endothermic or exothermic, could be identified with DTA. During decomposition, the basic magnesium carbonate products underwent dehydration,

dehydroxylation and decarbonation. The DTA peak position corresponding to decarbonation was similar for all the respective products. The dehydration and dehydroxylation stages differed due to the difference in the amount of water of crystallisation and hydroxyl groups in the respective products.

9.2.2 Surface area

The mineral flame retardants are known for their extensive contribution in the reduction of smoke in a fire, due to the oxides produced by low temperature decomposition of the parent hydroxide. The oxides formed are active materials of high surface area that will readily adsorb many species. Carbon is deposited on residual ash during combustion of polymers and volatilises on exposure to oxygen (Hornsby and Watson, 1990). This contributes to smoke suppression effects. By determining the MgO surface area that is formed during decomposition of the respective products, it might be possible to relate the surface area to the ability of the various products to reduce smoke in a fire. It is expected that the higher the MgO surface area of the decomposing products, the greater the smoke suppression effect could be.

The "active" condition of a solid relates to its internal area and/or the existence of lattice strain. It was possible to assess the activity of the various solid products, by determining the surface area thereof at various temperatures. The results indicated that the procedure by which a product was synthesised, had a noticeable influence on its surface area profile. The surface area profiles obtained for the respective products could be correlated to the change in the crystal structure as decomposition progressed. The maximum MgO surface area, in decreasing order, was as follow:

$Mg(OH)_2$ >> unidentified $\approx$ $Mg(OH)_2$ 120°C > dypingite $\geq$ $MgSO_4 \cdot 7H_2O$+Na_2CO_3 $\geq$ commercial hydromagnesite

Since the basic magnesium carbonate products exhibited smaller maximum MgO surface areas compared to $Mg(OH)_2$ during decomposition, the smoke suppression effect of the former is expected to be inferior to that of the latter.

9.2.3 Scanning electron microscopy

Next the surface characteristics of the products were studied by using SEM. Information relating to the morphology of the products could be obtained this way. It was not possible to relate the observed surface area results to the surface morphological characteristics of the respective products, since no pores could be observed. The physical appearance of hydromagnesite, dypingite and $MgCO_3 \cdot 3H_2O$, compared favourably to the documented physical appearance thereof. Products that were synthesised by different procedures appeared similar but with noticeable differences in the physical appearance of the respective crystal forms. An attempt was made to correlate the physical appearance of the unidentified product with that of the other products. This correlation was expected to indicate that the unidentified product could possibly be an intermediate phase of the other products. The physical characteristics of the unidentified product seemed to be intermediate to that of hydromagnesite and $MgCO_3 \cdot 3H_2O$.

9.2.4 Fourier transform infrared spectroscopy

FT-IR was used to obtain information relating to the functional groups present in the respective products. The IR spectra obtained gave an indication of the orientation of the molecular groups and their vibrational modes within the various product structures. It was possible to conclude that the unidentified product contained mainly loosely bound water and water of crystallisation and to a lesser extent hydroxyl groups, compared to the hydromagnesite products that contained very distinct hydroxyl groups and water of crystallisation and to a lesser extent loosely bound water. The carbonate vibrations in the respective products were noticeably influenced by the amount and mode of bonding of the water and hydroxyl groups present in each product.

9.2.5 Rehydration

The rehydration characteristics of the synthesised hydromagnesite as well as the unidentified products were investigated next. The rehydration characteristics of the commercial hydromagnesite product was investigated for comparison. DTA, FT-IR and XRD were used to follow the rehydration processes. By obtaining insight into the dehydration and rehydration characteristics of these products, insight could be obtained

relating to the differences in bonding of the water, hydroxyl and carbonate groups of the respective products. It was clear from the results obtained, that the crystal structure of the unidentified product was much less defined compared to that of the hydromagnesite products. This was concluded from the fact that the unidentified product did not regain its original orientation of the various molecular groups during rehydration. The hydromagnesite products did regain the original orientation of the various molecular groups, after 11 weeks rehydration in a water vapour saturated atmosphere at ambient temperature, as confirmed by both the XRD, DTA and FT-IR results. The synthesised hydromagnesite product exhibited dehydration and rehydration characteristics that were nearly identical to that of the commercial hydromagnesite product.

Calculation of the percentage rehydration indicated that the hydromagnesite products rehydrated completely. The amount of rehydration exceeded 100% possibly as a result of surface adsorbed water. The unidentified product only rehydrated approximately 60%. Since the unidentified product did not have a well defined crystal structure before dehydration, the water molecules could not be reincorporated into the structure during rehydration.

The transmission and reflection spectra were also correlated during rehydration. Initially the differences were pronounced since the processes were taking place mainly on the surface and to a lesser extent on the inside of the rehydrating products. The similarities between the spectra were nearly identical after 11 weeks of rehydration, as the adsorbed surface moieties were taken up into the crystal structures.

9.3 Flame retardant application

The final objective of this study, was to investigate the possible application of the synthesised products ($Mg(OH)_2$ 120°C hydromagnesite and the unidentified product) as flame retardants. This decision was prompted by the increasing demand for non-toxic, low smoke and environmentally friendly flame retardants. The halogenated flame retardants have been shown to be extremely efficient for flame retardant applications. The disadvantages associated with the use thereof, such as toxicity, corrosivity and increased smoke, limits the use thereof in situations where human life is directly threatened in a fire or where property damage can occur.

The mineral flame retardants, $Mg(OH)_2$ and $Al(OH)_3$, have been shown to provide a safer alternative to the halogenated flame retardants. This includes non-toxic and non-corrosive decomposition products and contributions to suppressing the emission of smoke in a fire. There seemed to be a shortage of mineral flame retardants with a relatively high temperature stability. $Al(OH)_3$ decomposes at a relatively low temperature (~200°C). This subsequently prevents the use thereof in polymers which are processed at high temperatures, since it decomposes before it can be incorporated into the polymer. The modern trend towards faster, more economic processing of all polymers creates compounding situations in which polymers, that were usually processed at relatively low temperatures, need to be processed at temperatures exceeding the decomposition temperature of $Al(OH)_3$. Under such circumstances $Mg(OH)_2$, that decomposes at ~340°C, offers an alternative. Since there are very few mineral flame retardants that can compete at this level with $Mg(OH)_2$, the need exists for the development of suitable alternatives. The high cost of $Mg(OH)_2$ necessitates the move towards more cost-effective mineral flame retardants that delivers comparable flame retardation results and exhibits a relatively high temperature stability.

The decomposition characteristics exhibited by hydromagnesite seemed to present a suitable alternative. As a result, the efficiency of the synthesised hydromagnesite and unidentified basic magnesium carbonate products, were subsequently investigated for flame retardant application. The evaluation of the synthesised products were attempted in order to determine whether the products could live up to the standards set by other similar products. The products were compounded with ethylene-vinyl acetate (EVA) and studied by TG-DTA, limiting oxygen index (LOI) and SEM. The results for the synthesised products compared favourably to that of commercial $Mg(OH)_2$, $Al(OH)_3$ and hydromagnesite that were investigated for comparative reasons.

The influence of the respective products on char formation of citrazinic acid and phenolphthalein were firstly investigated. It was observed that in the presence of the inorganic compounds, the amount of char formed was less than in the absence thereof. This was attributed to the oxidation of carbon due to the reactive oxide surface formed during decomposition of the various products. An attempt was made to correlate the amount of char formed to the surface area of the MgO formed during decomposition of the respective products. The products that formed larger MgO surface areas during decomposition, did not seem to contribute in increased oxidation of the char compared to the less reactive MgO surfaces, as expected. Instead it seemed as if more char was formed in the presence of the products that formed larger MgO surface areas. It was

proposed that for larger oxide surface areas and greater oxide activity, more carbon needed to be adsorbed onto the oxide surface to reduce the high surface energy associated with the high MgO surface area. This could result in more char being retained during combustion. It was also concluded that the amount of char formed was influenced by the integral chemical characteristics of the char forming compound with which the inorganic products were mixed.

It could be concluded from the TG-DTA results that the hydromagnesite and unidentified products exhibited relatively lower temperature stabilities compared to $Mg(OH)_2$. This would indicate that their application would be limited to polymers that are processed at relatively low temperatures, especially the unidentified product. In this study the lower decomposition temperature of the hydromagnesite products did not seem to alter the onset decomposition temperature of the EVA composites significantly. The unidentified products' lower decomposition temperature did however lower the EVA composites onset decomposition temperature.

The larger quantities of gas expelled by the basic magnesium carbonates compared to $Mg(OH)_2$ and $Al(OH)_3$ is expected to contribute in increased dilution of the fuel supply in the gas phase of a fire. The total reaction enthalpy of the hydromagnesite products were similar to that of $Mg(OH)_2$ and $Al(OH)_3$, whereas the total reaction enthalpy of the unidentified product was relatively higher than the other products. It is expected that more heat will be consumed and hence withdrawn from a fire in the presence of the unidentified product. This could possibly be assessed by further testing.

The LOI tests conducted were aimed at indicating the relative flammability of the EVA composites. The composites contained approximately the same amount of filler, which was a prerequisite for comparison of the LOI results. This is due to the fact that the LOI results are influenced by the amount of filler. $Al(OH)_3$ and the unidentified product performed the best in the LOI tests. The synthesised hydromagnesite product ($Mg(OH)_2$ 120°C) performed very similar to the commercial product. In all instances, the mineral flame retardants increased the flame resistance of the EVA polymer. It was evident from a visual observation of the EVA composites during burning, that the basic magnesium carbonate filled composites remained rigid during burning, while the $Mg(OH)_2$ and $Al(OH)_3$ filled composites and the pure EVA polymer caved in after a short time of burning.

SEM images of the EVA composites gave an indication of the dispersion of the filler particles inside the polymer matrix. It was evident that the $Mg(OH)_2$ and $Al(OH)_3$ particles were not evenly distributed within the polymer matrix, whereas it seemed as if the synthesised and commercial hydromagnesite products and the unidentified product were more evenly distributed. A small amount of agglomeration could be observed for the latter. This can be overcome through the addition of a dispersing agent that could aid in dispersion and promote wetting of the filler particles. The EVA composites were also viewed after being burnt. The difference between the burnt and unburnt composites were limited.

It is evident from the flame retardant evaluation of the synthesised products, that they present several advantages for flame retardant application. The tests that were conducted cannot be extrapolated to what could be expected in a real fire situation. Further testing is necessary to accurately access the flame retardant effect of the synthesised products. It will be advantageous to identify other applications of the synthesised products for flame retardation and adapt the products in terms of market needs.

Appendix A

References

ADAMSON, A.W. (1990), "Physical Chemistry of Surfaces", 5th ed., John Wiley & Sons Inc., New York, pp. 561, 591-614.

AMERICAN SOCIETY FOR TESTING AND MATERIALS (2000), "Standard Test Method for Measuring the Minimum Oxygen Concentration to Support Candle-Like Combustion of Plastics (Oxygen Index)", ASTM D2863.

BAIR, H.E. (1997), "Thermal Analysis of Additives in Polymers", In: Turi, E.A. (Ed.), Thermal characterization of polymeric materials, vol. 2, 2nd ed., Academic Press, San Diego, pp. 2355-2372.

BLACK, I. and BERGMANN, T. (1939), "Basische Magnesiumcarbonate", In: Pietsch, E. (Ed.), Gmelins Handbuch der Anorganischen Chemie, vol. 27, Verlag Chemie, Berlin, pp. 321-324.

BOTHA, A. and STRYDOM, C.A. (2001), "Preparation of a magnesium hydroxy carbonate from magnesium hydroxide", *Hydrometallurgy*, **62**, 175-183.

BOURBIGOT, S., LE BRAS, M., LEEUWENDAL, R., SHEN, K.K. and SCHUBERT, D. (1999), "Recent advances in the use of zinc borates in flame retardancy of EVA", *Polymer Degradation and Stability*, **64**, 419-425.

CÁCERES, P.G. and ATTIOGBE, E.K. (1997), "Thermal decomposition of dolomite and the extraction of its constituents", *Minerals Engineering,* **10(10)**, 1165-1176.

CANTERFORD, J.H. and MOORREES, C. (1985), "Magnesia from magnesite by calcination/carbonic acid leaching: precipitation from solution and final product recovery", *Bull. Proc. Austras. Inst. Min. Metall.*, **290(8)**, 67-70.

CHOUDHARI, B.P., VAIDYA, M.C. and DATAR, D.S. (1972), "Physico-chemical Studies on Basic Magnesium Carbonates", *Indian Journal of Chemistry*, **10**, 731-733.

CHOUDHARY, V.R., PATASKAR, S.G., GUNJIKAR, V.G. and ZOPE, G.B. (1994), "Influence of preparation conditions of basic magnesium carbonate on its thermal analysis", *Thermochimica Acta*, **232**, 95-110.

CHOUDHARY, V.R., PATASKAR, S.G., ZOPE, G.B and CHAUDHARI P.N. (1995), "Surface Properties of Magnesium Oxide Obtained from Basic Magnesium Carbonate: Influence of Preparation Conditions of Magnesium Carbonate", *J. Chem. Tech. Biotechnol.*, **64**, 407-413.

COSIC, M., BUREVSKI, D. and MILKOVIC, M. (1994), "Hydrated magnesium carbonates, their transformations and thermal decomposition to give magnesium oxide", *Kem. Ind.*, **43(2)**, 41-48.

DAVIES, P.J. and BUBELA, B. (1973), "The transformation of nesquehonite into hydromagnesite", *Chemical Geology,* **12**, 289-300.

DELFOSSE, L., BAILLET, C., BRAULT, A. and BRAULT, D. (1989), "Combustion of Ethylene-Vinyl Acetate Copolymer Filled with Aluminium and Magnesium Hydroxides", *Polymer Degradation and Stability*, **23**, 337-347.

DODD, J.W. and TONGE, K.H. (1987), "Thermal Methods", John Wiley & Sons, London, pp. 1-160.

FERNÁNDEZ, A.I., CHIMENOS, J.M., SEGARRA, M., FERNÁNDEZ, M.A. and ESPIELL, F. (2000), "Procedure to Obtain Hydromagnesite from a MgO-Containing Residue. Kinetic Study", *Ind. Eng. Chem. Res.*, **39**, 3653-3658.

GAINES, R.V., SKINNER, H.C.W., FOORD, E.E., MASON, B. and ROSENZWEIG, A. (1997), "Dana's New Mineralogy: The System of Mineralogy of James Dwight Dana and Edward Salisbury Dana", 8th ed., John Wiley & Sons, New York, pp. 490-515.

GANN, R.G. (1993), "Flame retardants overview", In: Kroschwitz, J.I. and Howe-Grant, M. (Eds.), Kirk-Othmer Encyclopedia of Chemical Technology, vol. 10, 4th ed., John Wiley & Sons, New York, pp. 930-935.

GEORGE, W.O. and MCINTYRE, P.S. (1987), "Infrared Spectroscopy", John Wiley & Sons, London, pp. 1-201.

GLOSS, G.H. (1952), "Magnesium compounds", In: Kirk, R.E. and Othmer, D.F. (Eds.), Kirk-Othmer Encyclopedia of Chemical Technology, vol. 8, The Interscience Encyclopedia, Inc., New York, pp. 595-599.

GOLDSTEIN, J.I., NEWBURY, D.E., ECHLIN, P., JOY, D.C., ROMIG, A.D. (jr.), LYMAN, C.E., FIORI, C. and LIFSHIN, E. (1992), "Scanning Electron Microscopy and X-Ray Microanalysis: A Text for Biologists, Materials Scientists, and Geologists", 2nd ed., Plenum Press, New York, pp. 1-4, 21-24.

GREEN, J. (1983), "Review: Calcination of precipitated $Mg(OH)_2$ to active MgO in the production of refractory and chemical grade MgO", *Journal of Materials Science*, **18**, 637-651.

GREGG, S.J. (1953), "The Production of Active Solids by Thermal Decomposition. Part I. Introduction", *Journal of the Chemical Society*, 3940-3944.

GREGG, S.J. and SING, K.S.W. (1982), "Adsorption, Surface Area and Porosity", 2nd ed., Academic Press Inc., London, pp. 1-73.

GREMLICH, H.U. (1994), "Infrared and Raman Spectroscopy", In: Elvers, B., Hawkins, S. and Russey, W. (Eds.), Ullmann's Encyclopedia of Industrial Chemistry, vol. B 5, 5th ed., VCH Verlagsgesellschaft, Weinheim, pp. 429-439, 453-459.

HAINES, P.J. (1995), "Thermal Methods of Analysis: Principles, Applications and Problems", Blackie Academic & Professional, London, pp. 11-31, 161-163.

HAIR, M.L. (1967), "Infrared Spectroscopy in Surface Chemistry", Marcel Dekker, Inc., New York, pp.1-55, 198-200.

HILL, R.J., CANTERFORD, J.H. and MOYLE, F.J. (1982), "New data for lansfordite", *Mineralogical Magazine*, **46**, 453-457.

HORNSBY, P.R. and WATSON, C.L. (1986), "Magnesium hydroxide - a combined flame retardant and smoke suppressant filler for thermoplastics", *Plastics and Rubber Processing and Applications*, **6**, 169-175.

HORNSBY, P.R. and WATSON, C.L. (1989), "Mechanism of smoke suppression and fire retardancy in polymers containing magnesium hydroxide filler", *Plastics and Rubber Processing and Applications*, **11**, 45-51.

HORNSBY, P.R. and WATSON, C.L. (1990), "A Study of the Mechanism of Flame Retardance and Smoke Suppression in Polymers Filled with Magnesium Hydroxide", *Polymer Degradation and Stability*, **30**, 73-87.

HTTP://mineral.galleries.com/minerals/carbonat/hydromag/hydromag.htm

JACKSON, L.C., LEVINGS, S.P., MANIOCHA, M.L., MINTMIER, C.A., REYES, A.H., SCHEERER, P.E., SMITH, D.M., WAJER, M.T., WALTER, M.D. and WITKOWSKI, J.T. (1995), "Magnesium compounds", In: Kroschwitz, J.I. and Howe-Grant, M. (Eds.), Kirk-Othmer Encyclopedia of Chemical Technology, vol. 15, 4th ed., John Wiley & Sons, New York, pp. 680-684.

JCPDS (1995), Powder Diffraction File (PDF2, Sets 1–45), International Centre for Diffraction Data, Newton Square, PA, USA.

JONES, P. (1998), "New Threat from Toxic Flame Retardants?", *Marine Pollution Bulletin*, **36(9)**, 653.

KHAN, N., DOLLIMORE, D., ALEXANDER, K. and WILBURN, F.W. (2001), " The origin of the exothermic peak in the thermal decomposition of basic magnesium carbonate", *Thermochimica Acta*, **367-368**, 321-333.

KIRSCHBAUM, G.S. (1999), "The Benefits of using Huntite/Hydromagnesite in Plastics", *Minerals in Compounding '99*, **November**, 1-10.

KRAMER, D.A. (1998), "Mg compounds in the USA. More than magnesia", *Industrial Minerals*, **December**, 45-53.

LANGMUIR, D. (1965), "Stability of carbonates in the system $MgO-CO_2-H_2O$", *Journal of Geology*, **73**, 730-754.

McMICHAEL, B. (1989), "Pyroprocessing techniques: The fiery world of industrial minerals", *Industrial Minerals*, **August**, 54-69.

MICROMERITICS INSTRUCTION MANUAL (1985), "Instruction manual, Flowsorb II 2300 for determining single point and multipoint surface area, Total pore volume and Pore area and volume distribution", Micromeritics Instrument Corporation, Norcross, Georgia, USA, pp. 2.1-3.8, A1-A3.

MIKHAIL, R.S. and ROBENS, E. (1983), "Microstructure and Thermal Analysis of Solid Surfaces", John Wiley & Sons, New York, pp. 11, 76-89.

MORIE, T., KUROKI, T. and MATSUMOTO, Y. (1986), "Manufacture of porous spherical basic magnesium carbonate with narrow particle size", JP86-235240.

NETZSCH-GERÄTEBAU, "Netzsch STA 409 EP Computer version, Operating Instructions", 1st ed., Netzsch-Gerätebau GmbH, Bayern, Germany, pp. 5-16.

PAULUS, E.F. and GIEREN, A. (1994), "Structure Analysis by Diffraction", In: Elvers, B., Hawkins, S. and Russey, W. (Eds.), Ullmann's Encyclopedia of Industrial Chemistry, vol. B 5, 5th ed., VCH Verlagsgesellschaft, Weinheim, pp. 341-353.

PEARCE, E.M. (1986), "Flame retardants for polymer systems", *Pure & Appl. Chem.*, **58(6)**, 925-930.

PETRELLA, R.V. (1992), "Combustibility", In: Gum, W.F., Riese, W. and Ulrich, H. (Eds.), Reaction Polymers: Polyurethanes, Epoxies, Unsaturated Polyesters, Phenolics, Special Monomers, and Additives; Chemistry, Technology, Applications, Markets, Oxford University Press, New York, pp. 802-826.

PETTIGREW, A. (1993), "Halogenated flame retardants", In: Kroschwitz, J.I. and Howe-Grant, M. (Eds.), Kirk-Othmer Encyclopedia of Chemical Technology, vol. 10, 4th ed., John Wiley & Sons, New York, pp. 954-958.

PIERANTOZZI, R. (1993), "Carbon dioxide", In: Kroschwitz, J.I. and Howe-Grant, M. (Eds.), Kirk-Othmer Encyclopedia of Chemical Technology, vol. 5, 4th ed., John Wiley & Sons, New York, p. 37.

POND, R.L. and HENEGHAN, L.F. (1965), "Method of preparing a hydrated magnesium carbonate", US Patent 3 169 826.

POPE, M.I. and JUDD, M.D., (1977), "Differential Thermal Analysis", Heyden & Son Ltd., London, pp. 22-29.

POSTEK, M.T., HOWARD, K.S., JOHNSON, A.H. and M^{c}MICHAEL, K.L. (1980), "Scanning Electron Microscopy: A Student's Handbook", pp. 7-9, 115-168.

PRAKASH, S. and GUPTA, K.N. (1987), "Commercial production of Magnesium Chemicals from Industrial Waste Dust and Fines", *Chem. Eng. World*, **22(1)**, 39-41.

RAADE, G. (1970), "Dypingite, a new hydrous basic carbonate of magnesium, from Norway", *The American Mineralogist*, **55(9-10)**, 1457-1465.

RAJESWARA RAO, T. and CHOHAN, V.S. (1995), "Kinetics of Thermal Decomposition of Hydromagnesite", *Chem. Eng. Technol.*, **18**, 359-363.

REYNOLDS, J.E.F., PARFITT, K., PARSONS, A.V. and SWEETMAN, S.C. (Eds.) (1993), "Martindale. The Extra Pharmacopoeia", 30th ed., The Pharmaceutical Press, London, p. 889.

RIGOLO, M. and WOODHAMS, R.T. (1992), "Basic Magnesium Carbonate Flame Retardants for Polypropylene", *Polymer Engineering and Science*, **32(5)**, 327-334.

ROBERTS, W.L., CAMPBELL, T.J. and RAPP, G.R. (jr.) (1990), "Encyclopedia of Minerals", 2nd ed., Van Nostrand Reinhold, New York, pp. 385-386.

ROSA, R. (1996), "Procédé de production de dérivés du magnesium", EP0732304A1.

SAWADA, Y., UEMATSU, K., MIZUTANI, N. and KATO, M. (1978), "Thermal decomposition of hydromagnesite $4MgCO_3 \cdot Mg(OH)_2 \cdot 4H_2O$ under different partial pressures of carbon dioxide", *Thermochimica Acta*, **27**, 45-59.

SCHMIDT, R. (1999), "In the line of fire. Flame retardants overview", *Industrial Minerals*, **February**, 37-41.

SCHRADER, B. (1989), "Infrared and raman spectroscopy: methods and applications", John Wiley & Sons, London.

SMITH, A.L. (1979), "Applied infrared spectroscopy", John Wiley & Sons, New York, pp. 8-15.

SMITHSON, G.L. and BAKHSHI, N.N. (1973), "Kinetics and Mechanism of Carbonation of Magnesium Oxide Slurries", *Ind. Eng. Chem. Process Des. Develop.*, **12(1)**, 99-106.

SUTKER, B.J. (1988), "Flame retardants", In: Gerhartz, W., Yamamoto, Y.S., Elvers, B., Rounsaville, J.F. and Schulz, G. (Eds.), Ullmann's Encyclopedia of Industrial Chemistry, vol. A 11, 5th ed., VCH Verlagsgesellschaft, Weinheim, pp. 123-139.

TOUVAL, I. (1993), "Antimony and other inorganic flame retardants", In: Kroschwitz, J.I. and Howe-Grant, M. (Eds.), Kirk-Othmer Encyclopedia of Chemical Technology, vol. 10, 4th ed., John Wiley & Sons, New York, pp. 936, 943-944.

VERRYN, S. (2000), "Introduction to X-Ray Powder Diffraction", Course notes, University of Pretoria, pp. A17-A18, B1-B3, C1.

VOGEL, A.I. (1961), "A Text-Book of Quantitative Inorganic Analysis Including Elementary Instrumental Analysis", 3rd ed., Longmans, Green and Co. Ltd., London, pp. 826-835.

WARRINGTON, S.B. and HÖHNE, G.W.H. (1994), "Thermal Analysis and Calorimetry", In: Elvers, B., Hawkins, S. and Russey, W. (Eds.), Ullmann's Encyclopedia of Industrial Chemistry, vol. B 6, 5th ed., VCH Verlagsgesellschaft, Weinheim, pp. 1-7.

WEBB, T.L. (1970), "Oxides and Hydroxides of Monovalent and Divalent Metals", In: Mackenzie, R.C. (Ed.), Differential Thermal Analysis, vol.1, Academic Press, London, p. 246.

WEBB, T.L. and KRÜGER, J.E. (1970), "Carbonates", In: Mackenzie, R.C. (Ed.), Differential Thermal Analysis, vol.1, Academic Press, London, pp. 314-316.

WEBER, M. (2000), "Mineral flame retardants: Overview & future trends", *Industrial Minerals*, **February**, 19-27.

WHISTON, C. (1987), "X-ray Methods", John Wiley & Sons, London, pp. 1-33, 45-112.

WHITE, W.B. (1971), "Infrared characterization of water and hydroxyl ion in the basic magnesium carbonate minerals", *The American Mineralogist*, **56**, 46-53.

WHITE, W.B. (1974), "The carbonate minerals", In: Farmer, V.C. (Ed.), The infrared spectra of minerals, Mineralogical Society, London, pp. 261-267.

YOSHIDA, T., TANAKA, T., YOSHIDA, H., FUNABIKI, T., YOSHIDA, S. and MURATA, T. (1995), "Study of Dehydration of Magnesium Hydroxide", *J. Phys. Chem.*, **99**, 10890-10896.